# HUMAN CORONAVIRUS RESEARCH: 20 YEARS SINCE THE SARS-COV OUTBREAK

EDITED BY: Burtram Clinton Fielding, Rosemary Ann Dorrington, Sunil Kumar Lal and Patrick C. Y. Woo
PUBLISHED IN: Frontiers in Microbiology

**frontiers** Research Topics

## About Frontiers

Frontiers is more than just an open-access publisher of scholarly articles: it is a pioneering approach to the world of academia, radically improving the way scholarly research is managed. The grand vision of Frontiers is a world where all people have an equal opportunity to seek, share and generate knowledge. Frontiers provides immediate and permanent online open access to all its publications, but this alone is not enough to realize our grand goals.

## Frontiers Journal Series

The Frontiers Journal Series is a multi-tier and interdisciplinary set of open-access, online journals, promising a paradigm shift from the current review, selection and dissemination processes in academic publishing. All Frontiers journals are driven by researchers for researchers; therefore, they constitute a service to the scholarly community. At the same time, the Frontiers Journal Series operates on a revolutionary invention, the tiered publishing system, initially addressing specific communities of scholars, and gradually climbing up to broader public understanding, thus serving the interests of the lay society, too.

## Dedication to Quality

Each Frontiers article is a landmark of the highest quality, thanks to genuinely collaborative interactions between authors and review editors, who include some of the world's best academicians. Research must be certified by peers before entering a stream of knowledge that may eventually reach the public - and shape society; therefore, Frontiers only applies the most rigorous and unbiased reviews.
Frontiers revolutionizes research publishing by freely delivering the most outstanding research, evaluated with no bias from both the academic and social point of view. By applying the most advanced information technologies, Frontiers is catapulting scholarly publishing into a new generation.

## What are Frontiers Research Topics?

Frontiers Research Topics are very popular trademarks of the Frontiers Journals Series: they are collections of at least ten articles, all centered on a particular subject. With their unique mix of varied contributions from Original Research to Review Articles, Frontiers Research Topics unify the most influential researchers, the latest key findings and historical advances in a hot research area! Find out more on how to host your own Frontiers Research Topic or contribute to one as an author by contacting the Frontiers Editorial Office: frontiersin.org/about/contact

# HUMAN CORONAVIRUS RESEARCH: 20 YEARS SINCE THE SARS-COV OUTBREAK

Topic Editors:

**Burtram Clinton Fielding,** University of the Western Cape, South Africa
**Rosemary Ann Dorrington,** Rhodes University, South Africa
**Sunil Kumar Lal,** Monash University Malaysia, Malaysia
**Patrick C. Y. Woo**, The University of Hong Kong, Hong Kong, SAR China

# Table of Contents

Check for updates

# Editorial: Human coronavirus research: 20 years since the SARS-CoV outbreak

Burtram C. Fielding*

Department of Medical Biosciences, Faculty of Natural Sciences, University of the Western Cape, Bellville, South Africa

Editorial on the Research Topic
Human coronavirus research: 20 years since the SARS-CoV outbreak

This Editorial introduces 10 articles published in a Special Issue highlighting human coronavirus (hCoV) research on the twentieth anniversary of the outbreak of severe acute respiratory syndrome (SARS) in late 2002. Only with the SARS outbreak was the pandemic potential of hCoVs acknowledged. HCoV-OC43 (Tyrrell and Bynoe, 1966), HCoV-229E (Hamre and Procknow, 1966), HCoV-NL63 (Van Der Hoek et al., 2004), and HCoV-HKU1 (Woo et al., 2005) are endemic in the human population and are mainly associated with mild, self-limiting "common cold" illnesses annually. The burden of respiratory tract infections, caused by the four "common-cold" hCoVs, is increased in patients with chronic co-morbidities or clinical risk factors including young children, the elderly and immunocompromised (Van Der Hoek, 2007). On the other hand, the three know pathogenic hCoVs, SARS-CoV (Drosten et al., 2003; Peiris et al., 2003), Middle East Respiratory Syndrome CoV (MERS-CoV) (Zaki et al., 2012), and SARS-CoV-2 (Zhou et al., 2020a,b), cause severe respiratory syndromes and result in high morbidities and mortalities, especially in the elderly (Chen et al., 2020).

The current pandemic has shown that we have not effectively used the vast knowledge gained from decades of HCoV research in studying and fighting SARS-CoV-2; this has often resulted in delays in reporting on therapeutics, control measures, etc. For this Special Issue we invited contributions of human coronavirus research, with particular focus on, but not limited to, morbidity and mortality numbers, genomic differences, their distinct immune evasion mechanisms, viral-host interactions, the development of potential broad-spectrum antiviral or therapeutics.

In the first article, Teng et al. sets out to identify the aetiological agent of respiratory infections in a herd of nine dromedary camel calves in the United Arab Emirates. Using cell culture and molecular biology techniques, they identify that MERS-CoV and a dromedary camel bovine parainfluenza virus 3 (DcPIV3), a novel species of the genus *Respirovirus*, are co-circulating in this herd. This is the first report of a novel respirovirus in sick dromedaries.

**FIGURE 1**
Timeline of human coronavirus discovery, with total reported infections and deaths shown. # https://www.cdc.gov/sars/about/fs-sars.html; + reported numbers as of July 2022 (http://www.emro.who.int/health-topics/mers-cov/mers-outbreaks.html); * reported numbers as of 2 September 2022 (worldometers.info/coronavirus/). Created with BioRender.com.
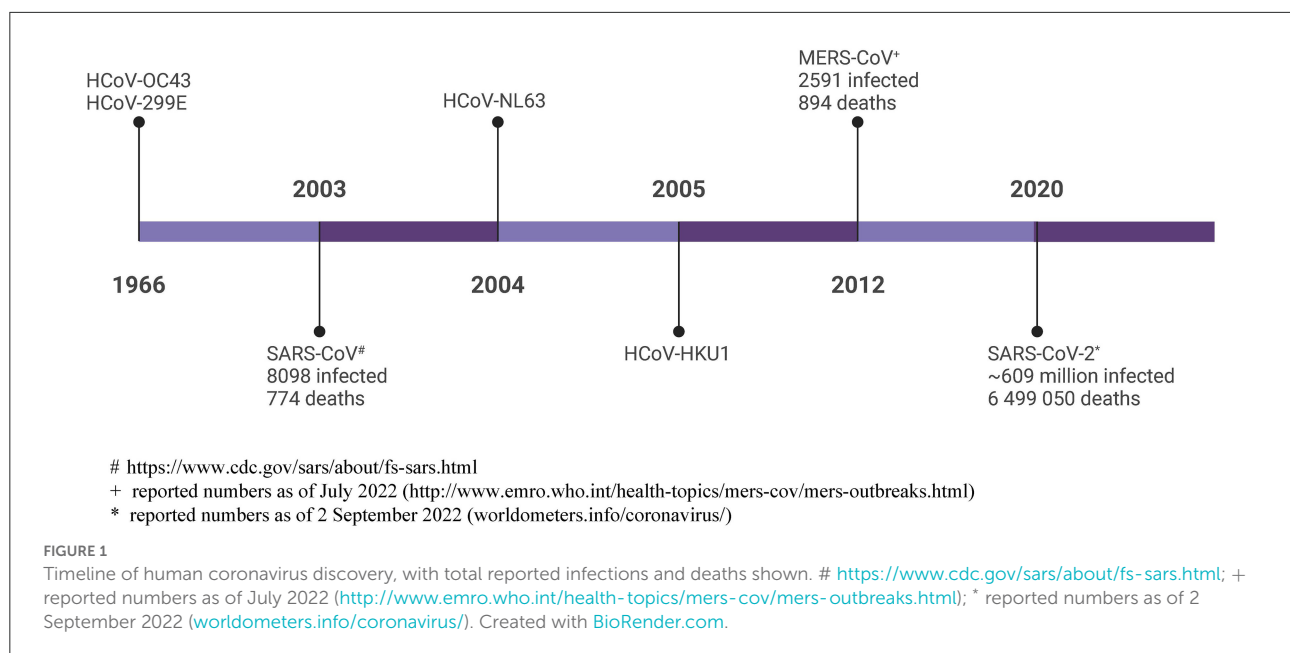
In the second article, Blumenthal et al. report an observational study of adults admitted to a public hospital in South Africa during June to August 2020 tested for SARS-CoV-2 infection. The authors also measure Kaposi's sarcoma-associated herpesvirus (KSHV) serology, as well as Epstein-Barr virus (EBV) and KSHV viral load in peripheral blood, and relates it to COVID-19 prognosis. Even though the study design does not allow the authors to conclude that disease synergy exists between COVID-19 and KSHV, their data allude to a relationship between KSHV infection and COVID-19 outcome, as well as SARS-CoV-2 infection and KSHV reactivation. These findings warrant further study in countries with high disease burdens. In the article by Lau et al., a case of fatal primary pneumonia in a 75-year old patient, with good past health, is linked to a novel HCoV-OC43. With fatal primary pneumonia due to HCoV-OC43 infection rarely reported (Van Der Hoek, 2007), the authors report high HCoV-OC43 loads in the lower respiratory tract throughout the illness of the patient. They hypothesize that a four-amino-acid insertion in the immediate downstream region of the S1/S2 cleavage site is linked to the hypervirulence of this novel genotype.

In a small cohort study, using sera collected during, as well as post-, HCoV-HKU1 infection, Sechan et al. report that a substantial portion of people infected with HCoV-HKU1 display no rise in viral-specific antibodies. This finding differs from previous reports for HCoV-OC43, HCoV-NL6 and HCoV-229E, that show more typical antibody dynamics (Sastre et al., 2011). The authors hypothesize that this difference is a result of the lower disease severity of HCoV-HKU1 infections. In another antibody study, this time for SARS-CoV-2, Ren et al. look at the kinetics of secretory IgA in the mucosa of the respiratory system and non-secretory IgA in the blood of 28 COVID-19 patients and 55 COVID-19-vaccine recipients. The authors suggest that anti-NP IgA detection in sputum and throat swabs could have diagnostic value for COVID-19 prevention and control. Interestingly, in their article, Irungbam et al. report evaluating the diagnostic efficacy of rapid IgM and IgG chemiluminescence kits targeting the receptor-binding domain (RBD) of the SARS-CoV-2 spike protein in a real-world hospital setting in India. They conclude that SARS-CoV-2 diagnostic tools using the detection of anti-RBD IgM are less effective than diagnostic tools using anti-RBD IgG in a real-world hospital setting.

Xie et al. report the generation of a mouse-adapted HCoV-OC43 strain, VR-1558, that is effective and reproducible for anti-HCoV-OC43 drug studies. Following an antiviral drug screen, they report that arbidol hydrochloride and Qingwenjiere Mixture decrease symptoms and improve the survival rate of infected mice. The authors report that the two compounds result in a measurable decrease in the expression of N, the inflammatory response and pathological changes. In another article, reporting the database screening of more than 3,400 compounds, Matos et al. identify Hypericin as one of the top candidates with high binding affinity to viral Mpro and RdRp. With Mpro and RdRp known to be critical for coronavirus replication (Stobart et al., 2012), the authors then use cell culture studies to show that Hypericin has anti-SARS-CoV-2 properties. This study is the first step in establishing the suitability of Hypericin as an anti-SARS-CoV-2, and possibly a broad-spectrum anti-coronaviral, drug. Zhang et al. report in their article that the SARS-CoV-2 nucleocapsid protein (N) melts double-stranded DNA (dsDNA)

in the 5′-3′ direction. Moreover, the authors hypothesize that the protein's ssDNA binding and dsDNA unwinding activity show that the N binds to the host's genomic ssDNA during replication and affects host cell replication. These findings could also inform the future development of broad-spectrum anti-coronaviral agents.

In the final article, showing the multidisciplinary approach needed to understand and fight coronavirus pandemics, Mehta et al. review recent studies to understand the interplay of nutrition and psychoneuroendocrineimmune (PNEI) modulation, and its impact on the prognosis and convalescence of COVID-19. The authors report that large population sizes, high prevalence of undernourishment, and high incidence of mental health issues increase the risk for COVID-19. They conclude that the monitoring of these factors will assist in designing complimentary pandemic interventions through medical nutrition therapy and psychopsychiatric management.

The COVID-19 pandemic has showed us that the human coronaviruses pose a real threat. It has taken us 56 years since the discovery of the first human coronaviruses, and millions of deaths (Figure 1) to develop the first human coronavirus vaccine. This Special Issue provides a platform to share the work done on the known hCoVs, and should provide us with a better research foundation when the next pathogenic hCoV is identified.

## Author contributions

This editorial was written solely by the one guest editor.

## Acknowledgments

## Conflict of interest

The author declares that the research was conducted in the absence of any commercial or financial relationships that could be construed as a potential conflict of interest.

## Publisher's note

All claims expressed in this article are solely those of the authors and do not necessarily represent those of their affiliated organizations, or those of the publisher, the editors and the reviewers. Any product that may be evaluated in this article, or claim that may be made by its manufacturer, is not guaranteed or endorsed by the publisher.

## References

Chen, B., Tian, E. K., He, B., Tian, L., Han, R., Wang, S., et al. (2020). Overview of lethal human coronaviruses. *Signal. Transduct. Target Ther.* 5, 89. doi: 10.1038/s41392-020-0190-2

Drosten, C., Gunther, S., Preiser, W., Van Der Werf, S., Brodt, H. R., Becker, S., et al. (2003). Identification of a novel coronavirus in patients with severe acute respiratory syndrome. *N. Engl. J. Med.* 348, 1967–1976. doi: 10.1056/NEJMoa030747

Hamre, D., and Procknow, J. J. (1966). A new virus isolated from the human respiratory tract. *Proc. Soc. Exp. Biol. Med.* 121, 190–193. doi: 10.3181/00379727-121-30734

Peiris, J. S., Lai, S. T., Poon, L. L., Guan, Y., Yam, L. Y., Lim, W., et al. (2003). Coronavirus as a possible cause of severe acute respiratory syndrome. *Lancet* 361, 1319–1325. doi: 10.1016/S0140-6736(03)13077-2

Sastre, P., Dijkman, R., Camunas, A., Ruiz, T., Jebbink, M. F., Van Der Hoek, L., et al. (2011). Differentiation between human coronaviruses NL63 and 229E using a novel double-antibody sandwich enzyme-linked immunosorbent assay based on specific monoclonal antibodies. *Clin. Vaccine Immunol.* 18, 113–118. doi: 10.1128/CVI.00355-10

Stobart, C. C., Lee, A. S., Lu, X., and Denison, M. R. (2012). Temperature-sensitive mutants and revertants in the coronavirus nonstructural protein 5 protease (3CLpro) define residues involved in long-distance communication and regulation of protease activity. *J. Virol.* 86, 4801–4810. doi: 10.1128/JVI.06754-11

Tyrrell, D. A., and Bynoe, M. L. (1966). Cultivation of viruses from a high proportion of patients with colds. *Lancet* 1, 76–77. doi: 10.1016/S0140-6736(66)92364-6

Van Der Hoek, L. (2007). Human coronaviruses: what do they cause? *Antivir. Ther.* 12, 651–658. doi: 10.1177/135965350701200S01.1

Van Der Hoek, L., Pyrc, K., Jebbink, M. F., Vermeulen-Oost, W., Berkhout, R. J., Wolthers, K. C., et al. (2004). Identification of a new human coronavirus. *Nat. Med.* 10, 368–373. doi: 10.1038/nm1024

Woo, P. C., Lau, S. K., Chu, C. M., Chan, K. H., Tsoi, H. W., Huang, Y., et al. (2005). Characterization and complete genome sequence of a novel coronavirus, coronavirus HKU1, from patients with pneumonia. *J. Virol.* 79, 884–895. doi: 10.1128/JVI.79.2.884-895.2005

Zaki, A. M., Van Boheemen, S., Bestebroer, T. M., Osterhaus, A. D., and Fouchier, R. A. (2012). Isolation of a novel coronavirus from a man with pneumonia in Saudi Arabia. *N. Engl. J. Med.* 367, 1814–1820. doi: 10.1056/NEJMoa1211721

Zhou, P., Yang, X. L., Wang, X. G., Hu, B., Zhang, L., Zhang, W., et al. (2020a). Addendum: a pneumonia outbreak associated with a new coronavirus of probable bat origin. *Nature* 588, E6. doi: 10.1038/s41586-020-2951-z

Zhou, P., Yang, X. L., Wang, X. G., Hu, B., Zhang, L., Zhang, W., et al. (2020b). A pneumonia outbreak associated with a new coronavirus of probable bat origin. *Nature* 579, 270–273. doi: 10.1038/s41586-020-2012-7

# Co-circulation of a Novel Dromedary Camel Parainfluenza Virus 3 and Middle East Respiratory Syndrome Coronavirus in a Dromedary Herd With Respiratory Tract Infections

*Jade Lee Lee Teng[1†], Ulrich Wernery[2*†], Hwei Huih Lee[1†], Joshua Fung[1], Sunitha Joseph[2], Kenneth Sze Ming Li[1], Shyna Korah Elizabeth[2], Jordan Yik Hei Fong[1], Kwok-Hung Chan[1], Honglin Chen[1], Susanna Kar Pui Lau[1] and Patrick Chiu Yat Woo[1*]*

[1]Department of Microbiology, Li Ka Shing Faculty of Medicine, The University of Hong Kong, Hong Kong, Hong Kong SAR, China, [2]Central Veterinary Research Laboratory, Dubai, United Arab Emirates

Since the emergence of Middle East Respiratory Syndrome (MERS) in 2012, there have been a surge in the discovery and evolutionary studies of viruses in dromedaries. Here, we investigated a herd of nine dromedary calves from Umm Al Quwain, the United Arab Emirates that developed respiratory signs. Viral culture of the nasal swabs from the nine calves on Vero cells showed two different types of cytopathic effects (CPEs), suggesting the presence of two different viruses. Three samples showed typical CPEs of Middle East respiratory syndrome (MERS) coronavirus (MERS-CoV) in Vero cells, which was confirmed by partial RdRp gene sequencing. Complete genome sequencing of the three MERS-CoV strains showed that they belonged to clade B3, most closely related to another dromedary MERS-CoV isolate previously detected in Dubai. They also showed evidence of recombination between lineages B4 and B5 in ORF1ab. Another three samples showed non-typical CPEs of MERS-CoV with cell rounding, progressive degeneration, and detachment. Electron microscopy revealed spherical viral particles with peplomers and diameter of about 170 nm. High-throughput sequencing and metagenomic analysis showed that the genome organization (3'-N-P-M-F-HN-L-5') was typical of paramyxovirus. They possessed typical genome features similar to other viruses of the genus *Respirovirus*, including a conserved motif [323]FAPGNYALSYAM[336] in the N protein, RNA editing sites 5'-[717]AAAAAAGGG[725]-3', and 5'-[1038]AGAAGAAAGAAAGG[1051]-3' (mRNA sense) in the P gene with multiple polypeptides coding capacity, a nuclear localization signal sequence [245]KVGRMYSVEYCKQKIEK[261] in the M protein, a conserved sialic acid binding motif [252]NRKSCS[257] in the HN protein, conserved lengths of the leader (55 nt) and trailer (51 nt) sequences, total coding percentages (92.6–93.4%), gene-start (AGGANNAAAG), gene-end (NANNANNAAAAA), and trinucleotide intergenic sequences (CTT, mRNA sense). Phylogenetic analysis of their complete genomes showed that they were most closely related to bovine parainfluenza virus 3 (PIV3) genotype C strains. In the phylogenetic tree constructed using the complete L protein, the branch length between dromedary camel

PIV3 (DcPIV3) and the nearest node is 0.04, which is >0.03, the definition used for species demarcation in the family *Paramyxoviridae*. Therefore, we show that DcPIV3 is a novel species of the genus *Respirovirus* that co-circulated with MERS-CoV in a dromedary herd in the Middle East.

Keywords: camel calves, metagenomics, Middle East respiratory syndrome coronavirus, novel species, dromedary camel parainfluenza virus 3, respiratory tract infections

# INTRODUCTION

Camels are one of the most unique mammals on earth that have shown adaptation to desert life. There are three surviving Old World camel species, namely, *Camelus dromedarius* (dromedary or one-humped camel), which inhabits the Middle East, North, and Northeast Africa; *Camelus bactrianus* (Bactrian or two-humped camel) and *Camelus ferus* (the wild camel), both, inhabitants of Central Asia. Among the 20 million camels on earth, 90% are dromedaries. Before the emergence of the Middle East Respiratory Syndrome (MERS) in 2012, viruses of at least eight families, including *Paramyxoviridae*, *Flaviviridae*, *Herpesviridae*, *Papillomaviridae*, *Picornaviridae*, *Poxviridae*, *Reoviridae*, and *Rhabdoviridae*, were known to infect dromedaries (Yousif et al., 2004; Wernery et al., 2008; Intisar et al., 2009; Khalafalla et al., 2010; Ure et al., 2011; Al-Ruwaili et al., 2012; Wernery et al., 2014). Subsequently, Middle East respiratory syndrome (MERS) coronavirus (MERS-CoV) was confirmed to be the causative agent of MERS (Lau et al., 2016a, 2017; El-Kafrawy et al., 2019; Al-Shomrani et al., 2020). In the last few years, we have discovered a number of novel viruses in dromedaries, including another coronavirus, named dromedary camel coronavirus UAE-HKU23, two novel genotypes of hepatitis E virus, a novel genus of enterovirus, a novel astrovirus, two novel bocaparvoviruses, and novel picobirnaviruses and circoviruses in dromedaries (Woo et al., 2014, 2015a,b, 2016, 2017; Sridhar et al., 2017). In addition, we have also described the first isolation of Newcastle disease virus and West Nile virus from dromedaries (Joseph et al., 2016; Teng et al., 2019).

In 2015, a herd of dromedaries consisting of nine camel calves from Umm Al Quwain, the United Arab Emirates, developed respiratory signs. Viral culture of the respiratory samples showed two different types of cytopathic effects (CPEs), suggesting the presence of two different viruses. To confirm the identities of these viruses, complete genome sequencing, phylogenetic, and comparative genome analyses were conducted.

# MATERIALS AND METHODS

## Sample Collection and Viral Culture

In May 2015, nine camel calves (4–8 months old) of the same herd developed respiratory signs with clear nasal discharge and fever. Nasal swab samples were collected and sent to the Central Veterinary Research Laboratory in Dubai, the United Arab Emirates for investigations. Nasal swab samples from the nine camel calves were inoculated into Vero cells, respectively, for isolation of MERS-CoV as previously described

(Wernery and Zachariah, 1999; Wernery et al., 2015). Briefly, the samples were diluted 10-fold with viral transport medium and filtered. Two hundred microliters of the filtrate were inoculated into 200 μl of minimum essential medium (Gibco, United States). Four hundred microliters of the mixture were added to 24-well tissue culture plates with Vero cells by adsorption inoculation. After 1 h of adsorption, excess inoculum was discarded, the wells were washed twice with phosphate-buffered saline, and the medium was replaced with 1 ml of minimum essential medium (Gibco, United States) supplemented with 1% fetal bovine serum (Gibco, United States). Culture was incubated at 37°C with 5% $CO_2$ and inspected daily for CPEs for 7 days by inverted microscopy. Two different types of CPEs were observed. All cultures with CPEs were screened for the presence of MERS-CoV using RT-PCR assay as described below.

## RNA Extraction

Viral RNA was extracted from the nine nasal swab samples and the corresponding culture samples using EZ1 Virus Mini Kit v2.0 (Qiagen, Hilden, Germany). RNA was eluted in 60 μl of AVE buffer (Qiagen, Hilden, Germany) and was used as template for RT-PCR.

## RT-PCR for MERS-CoV

Screening of MERS-CoV was performed by amplifying a 440-bp fragment of the RdRp gene of CoVs using conserved primers (5'-GGTTGGGACTATCCTAAGTGTGA-3' and 5'-ACCATC ATCNGANARDATCATNA-3') as described previously (Lau et al., 2016a).

## Complete Genome Sequencing of MERS-CoVs Detected From the Camel Calves

Three MERS-CoVs (D1189.1, D1189.5, and D1189.6), which showed typical CPE in Vero cells, isolated from three nasal swab samples from three dromedary calves were included in this study. One complete genome of MERS-CoV strain D1189.1 was sequenced in our previous study (Lau et al., 2016a). The complete genomes of the other two MERS-CoVs strains, D1189.5 and D1189.6, were sequenced in this study as previously described (Lau et al., 2016a). Briefly, the RNA extracted from the two MERS strains was converted to cDNA by a combined random-priming and oligo(dT) priming strategy. The cDNA was amplified by primers designed based on multiple sequence alignments of available MERS-CoV genome sequences using previously described strategies (Lau et al., 2016a). Primers used for PCR amplification and DNA sequencing were shown in

## Recombination Analysis

Bootscan analysis was performed to detect possible recombination by using the complete nucleotide alignment of the genome sequences of MERS-CoV and Simplot version 3.5.1, as previously described (Woo et al., 2006; Lau et al., 2011). The analysis was conducted using model F84, a sliding window of 1,500 nucleotides moving in 200 nucleotide steps with complete genome sequences D1189.1, D1189.5, and D1189.6, respectively, as the query. Possible recombination sites suggested by the bootscan analysis were confirmed through multiple sequence alignments.

## Sample Preparation for Illumina Sequencing

Three culture isolates (D1189.2, D1189.4, and D1189.8), which showed non-typical CPE in Vero cells, isolated from three nasal swab samples from three dromedary calves were negative for MERS-CoV using RT-PCR assay and subjected to further investigation by deep sequencing and microscopic analysis as described below. RNA was individually extracted from the three cultures, and the RNA samples were subjected to library preparation and Illumina sequencing, respectively, using NovaSeq 6000 (Pair-End sequencing of 151 bp) at University of Hong Kong, Centre for Genomic Sciences (HKU, CGS), as described previously (Joseph et al., 2016).

## Sequence Analysis and *de novo* Assembly of Reads From Viruses of Interest

Illumina sequence raw reads were quality and adapter trimmed using Trimmomatic-0.4.3 with Nextera-PE FASTA sequences (Illumina, San Diego, CA, United States). Trimmed paired-end reads were analyzed as described previously (Joseph et al., 2016). The taxonomical content of the dataset was visualized by a phylogenetic tree computed using MEtaGenome ANalyzer (MEGAN) version 6.20.14, which assigned each sequence according to its taxonomical identity that are based on NCBI database (Huson et al., 2016). Once viruses of interest were found in the phylogenetic tree by MEGAN analysis, sequenced reads from the corresponding virus family, genus, or species were extracted. The extracted paired-end reads were *de novo* assembled into contigs using MIRA version 4.9.6 in accurate mode (Chevreux et al., 1999). The assembled contigs were subjected to further genome analysis by comparing with their corresponding closest relatives.

## Genome and Phylogenetic Analyses

The putative open reading frames (ORFs) and their deduced amino acid sequences of the assembled genomes were predicted using ORF Finder.[1] The nucleotide sequences of the genomes

---

[1]https://www.ncbi.nlm.nih.gov/orffinder/

and the deduced amino acid sequences of the ORFs were compared to those of other known viruses using ClustalOmega by multiple sequence alignment (Sievers and Higgins, 2014). MEGAX was used for the phylogenetic analyses of MERS-CoV (complete genome sequence) and dromedary camel parainfluenza virus 3 (DcPIV3; complete genome sequence, partial and complete amino acid sequence of L protein, and complete nucleotide sequences of L gene; Kumar et al., 2018). To minimize the potential loss of phylogenetic information in the trees constructed based on the amino acid sequences, both amino acid and nucleotide sequences were used for analyses. Maximum-likelihood method was used because it can apply a model of sequence evolution, representing a more accurate method than distance-based method for building a phylogeny using sequence data. The best substitution model for each alignment was predicted using the function "Find best DNA/Protein Model (Maximum-Likelihood)" implemented in MEGAX. Sequences of MERS-CoV were aligned using default parameter in MUSCLE. Phylogenetic tree of MERS-CoV was built with the model Tamura-Nei (TN93) + G + I where all sites were used for gaps and missing data. All the respective DcPIV3 sequences were aligned using MUSCLE with gap-opening penalty of five and gap extension penalty of one. Phylogenetic analyses of DcPIV3 were constructed using MEGAX with substitution model Jukes and Cantor (JC) with uniform rates for complete genome, Jones Taylor Thornton (JTT) with uniform rates for both partial and complete L proteins, and General Time Reversible (GTR) + G where all sites were used for gaps and missing data for complete L gene. Bootstrap analysis was performed for the assessment of confidence level of the observed clades in the inferred phylogenetic trees, in which 1,000 pseudoreplicates were used due to restrictions imposed by computational demand.

## Electron Microscopy

Dromedary camel parainfluenza virus 3 isolated from the sample D1189.8 was subjected to negative-contrast electron microscopy analysis as described previously (Lau et al., 2012; Lau et al., 2016b). Briefly, tissue culture cell extracts infected with DcPIV3 were centrifuged at $5,000 \times g$ at 4°C, after which the solution was fixed with GTA at a final concentration of 2.5% overnight. The sample was mounted into a carbon-formvar coated copper grid and stained with 3% urabyl acetate. The grid was then dried and irradiated with UV (1,250 mW) for 15 min with a Philips CM100 transmission electron microscope (Eindhoven, Netherlands).

## Nucleotide Sequence Accession Numbers

The nucleotide sequences of the two dromedary MERS-CoV genomes and the three DcPIV3 genomes sequenced in this study have been submitted to GenBank sequence database under accession numbers MW545527, MW545528, MW504257, MW504258, and MW504259. Raw data have been submitted to Sequence Read Archive (SRA) under accession numbers SRR13442189, SRR13442188, and SRR13442187.
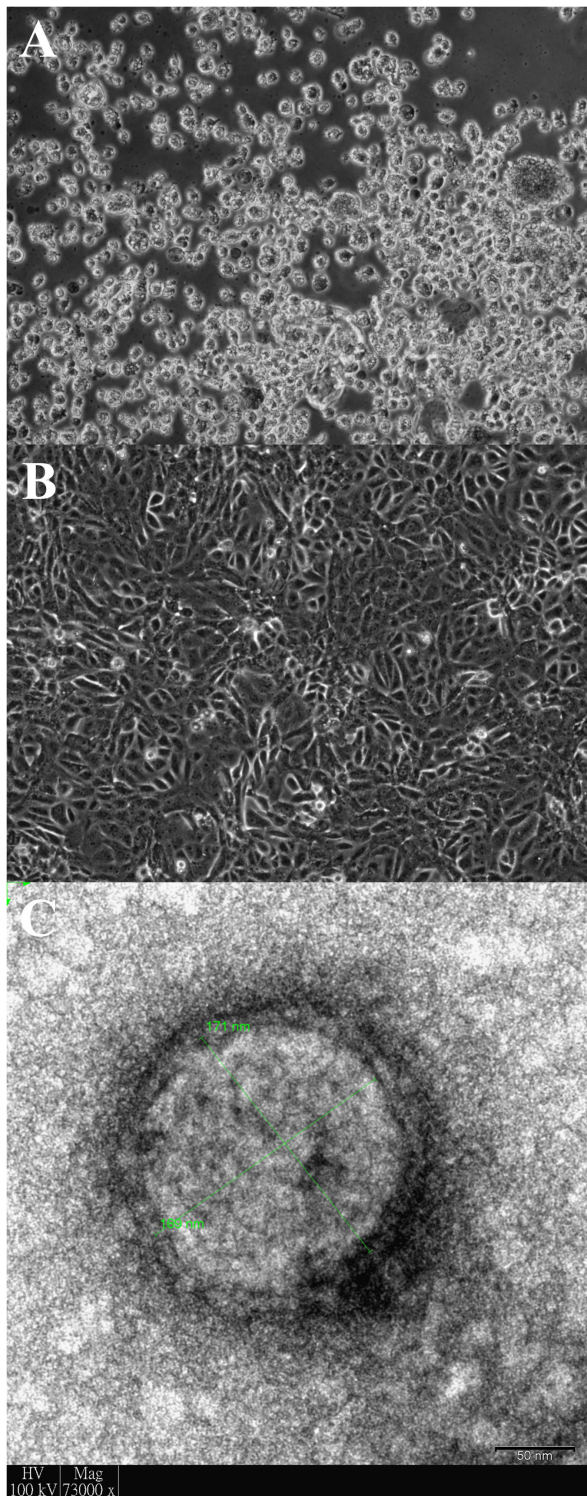
**FIGURE 1** | Vero cells infected with dromedary camel parainfluenza virus 3 (DcPIV3; D1189.8). Light micrograph showing cytopathic effects (CPEs) of D1189.8 culture isolate from the camel calf of a dromedary on **(A)** Vero cells; **(B)** Uninfected control of Vero cells. Magnification: ×100 and **(C)** DcPIV3 (D1189.8) viral particle stained with phosphotungstic acid under transmission electron microscope. The size of the displayed viral particle is about 170 nm. Scale bar represents 50 nm.

# RESULTS

## RT-PCR, Virus Culture, and Electron Microscopy

Nasal swab samples from nine camel calves of the same herd were collected and cultured on Vero cells for MERS-CoV screening. Three samples, D1189.1, D1189.5, and D1189.6, showed typical CPEs of MERS-CoV in Vero cells on day 4. RT-PCR targeting the 440-bp fragment of the RdRp gene confirmed the presence of MERS-CoV in these three nasal swab samples and their corresponding culture samples.

Another three cultures inoculated with samples D1189.2, D1189.4, and D1189.8 showed non-typical CPEs of MERS-CoV on day 4 with cell rounding, progressive degeneration, and detachment (**Figures 1A,B**). Electron microscopy of one of the three culture samples D1189.8 showed spherical viral particles with peplomers and diameter of about 170 nm (**Figure 1C**). The CPE, morphology, and size of the virus were inconsistent with those of MERS-CoV. These three unknown culture isolates were subjected to high-throughput sequencing to confirm the presence of other viruses. The remaining three samples did not show any CPE in Vero cells. Therefore, further investigation on these samples was not proceeded.

## Complete Genome Sequencing and Phylogenetic Analysis of MERS-CoV

Analysis of the complete genomes of the three isolated dromedary MERS-CoV strains (D1189.1, D1189.5, and D1189.6) showed that these sequences were 30,103 bases in length with G + C content of 41.1%. The size, G + C content, and genome structure of the three isolated dromedary MERS-CoV strains are similar to other dromedary MERS-CoVs. The genome sequence analysis showed that the three MERS-CoV isolates were closely related among each other, sharing 99.88–99.95% nucleotide identities. Phylogenetic analysis of the complete genomes of the three MERS-CoV isolates showed that they belonged to clade B3, being most closely related to another dromedary isolate, D1271 (GenBank accession number KX108945), which was previously detected in Dubai and they shared 99.84–99.93% nucleotide identities (**Figure 2**). Comparison of deduced amino acid sequences of proteins among the three MERS-CoV isolates showed only 8–17 amino acid substitutions along the whole-genome sequences, most occurring in the membrane protein (M; **Table 1**), while 5–21 substitutions compared to other clade B3 strains (**Figure 2**).

## Recombinant Analysis

Bootscan analysis showed high bootstrap frequencies (80–100%) for clustering between the three strains and lineage 4 MERS-CoV in their genomes (position 1–14,000); but for position 15,000–24,000, bootscan analysis showed high bootstrap frequencies (75–100%) for clustering between the three strains and lineage 5 MERS-CoV (**Figure 3A**). Additional multiple sequence alignment using the three strains, a lineage 4 MERS-CoV and a lineage 5 MERS-CoV indicated that upstream of position 13,407, the three strains possessed nucleotides identical to

**FIGURE 2 |** Maximum-likelihood phylogeny based on the complete genome sequences of the three isolated dromedary Middle East respiratory syndrome coronavirus (MERS-CoV) strains (D1189.1, D1189.5, and D1189.6) and those of other closely related MERS-CoV strains. Phylogenetic tree was generated using the TN93 model and a discrete Gamma distribution with 1,000 bootstrap pseudoreplicates. Thirty thousand three hundred thirty nucleotide positions of the complete genome were included in the analyses. The tree with the highest log likelihood (−48750.09) is shown. Bootstrap values are shown next to the branches. The scale bar indicates the number of nucleotide substitutions per site. The three MERS-CoV strains sequenced and analyzed in the present study are shown in red triangular. All the accession numbers are given as cited in GenBank.

lineage 4 MERS-CoV; but from position 16,187–23,825, the three strains possessed nucleotides similar to lineage 5 MERS-CoV (**Figure 3B**).

## Metagenomics Analysis of the Three Unknown Culture Isolates

The three culture isolates (D1189.2, D1189.4, and D1189.8) showed non-typical CPEs of MERS-CoV on Vero cells were subject to high-throughput sequencing, respectively, generating 5,621,614–6,500,327 paired-end 151-bp reads. After trimming adapter sequences and filtering the rRNA sequences, bacterial, and host genomes, a total of 4,377,997–5,432,096 clean reads remained and were used for downstream BLASTx analysis.

Among these clean reads, 82,373–94,948 reads matched to viruses. The largest portion of these viral sequences was assigned to the family *Paramyxoviridae* ($n = 54,570-94,941$). *De novo* assembly of reads of *Paramyxoviridae* revealed a complete genome of parainfluenza virus 3 (PIV3) of the genus *Respirovirus* in all three samples, tentatively named dromedary camel parainfluenza virus 3 (DcPIV3), where DcPIV3-1189.2, DcPIV3-1189.4, and DcPIV3-1189.8 represented the parainfluenza virus 3 discovered in the sample D1189.2, D1189.4, and D1189.8, respectively. RT-PCR targeting 400-bp fragment of the F gene confirmed the presence of DcPIV3 in these three nasal swab samples and their corresponding culture samples.
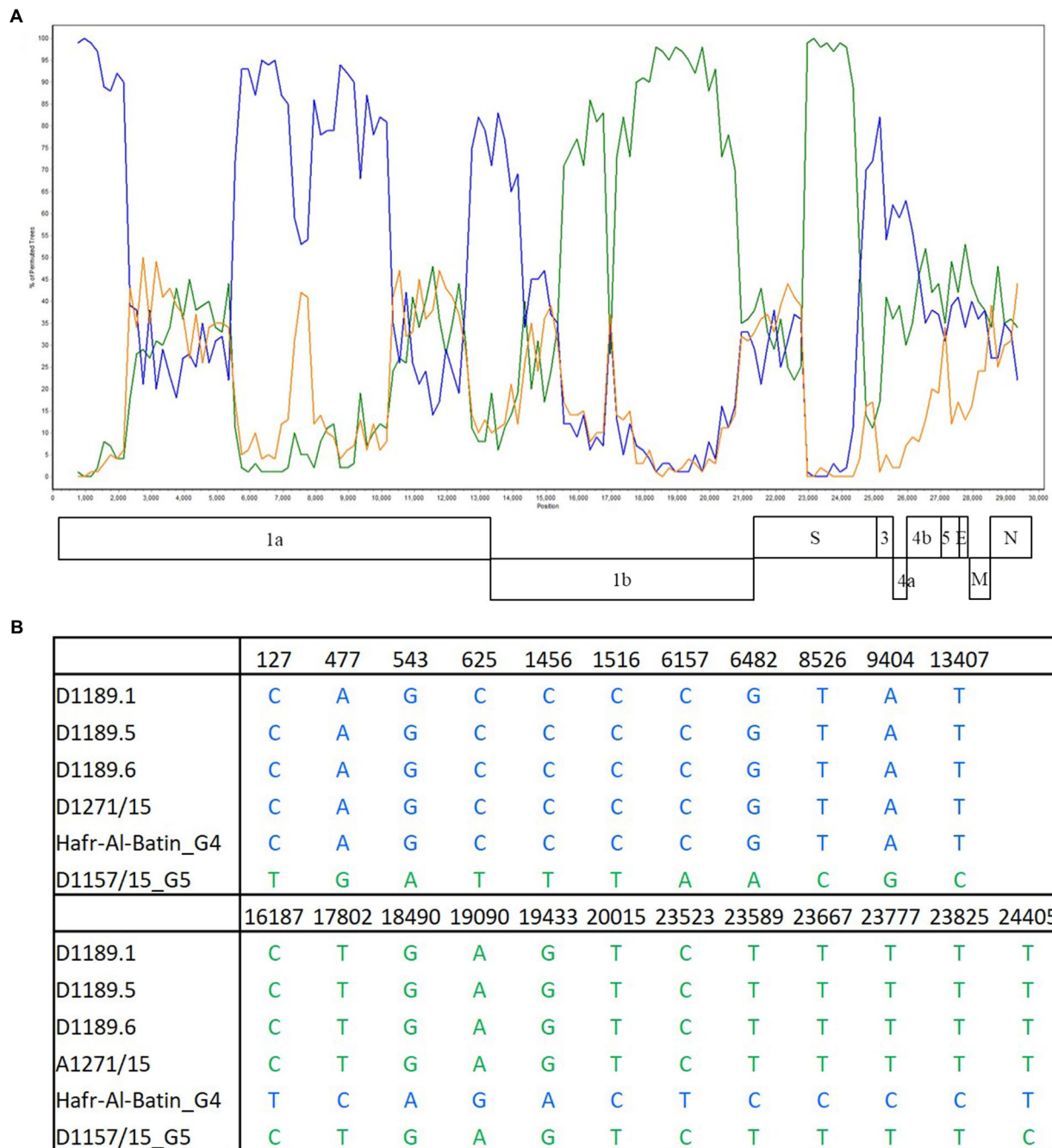
**FIGURE 3** | Detection of potential recombination by **(A)** bootscan analysis and **(B)** multiple sequence alignment. Bootscan analysis was conducted with Simplot version 3.5.1 (Maximum-likelihood; F84 model; window size 1,500 bp; and step 200 bp) on a gapless nucleotide alignment. D1189.1, D1189.5, D1189.6, and D1271 were selected as the query sequences and compared with the genome sequences of a lineage 4 MERS-CoV strain Hafr-Al-Batin (blue, KF600628), a lineage 5 MERS-CoV strain D1157/15 (green, KX108944), and a lineage 1 MERS-CoV strain UAE/Abu Dhabi_UAE_9 (orange, KP209312).

## Genome and Phylogenetic Analysis of DcPIV3

Analysis of the complete genome of the three DcPIV3 strains showed that these sequences ranged from 15,474–15,498 bases in length, which conformed to the paramyxovirus rule of six,

and had an overall G + C content of 34.6–34.8% (**Table 2**). They were highly similar and shared 98.8% nucleotide identities among each other (**Table 3**). Comparison of deduced amino acid sequences of proteins among the three DcPIV3 strains showed only 8–22 amino acid substitutions along the

**TABLE 1** | Comparison of amino acid substitutions among the three DcMERS-CoV isolates in this study.

| Protein | Position (aa) | Strain | | |
|---|---|---|---|---|
| | | D1189.1 | D1189.5 | D1189.6 |
| ORF1a | 1,578 | V | L | V |
| | 1,666 | M | M | I |
| | 2,123 | V | A | A |
| | 2,241 | S | S | P |
| | 2,702 | Q | H | Q |
| ORF1b | 1,573 | Q | Q | H |
| | 1,934 | C | Y | C |
| Spike (S) | 1,188 | G | G | S |
| | 1,251 | F | S | S |
| ORF4a | 22 | C | C | F |
| Membrane (M) | 67 | S | N | S |
| | 77 | Q | H | Q |
| | 84 | A | N | A |
| | 85 | A | G | A |
| | 86 | V | A | V |
| | 127 | T | N | T |
| | 129 | V | L | V |
| | 136 | S | F | S |

whole-genome sequences (**Table 4**). Overall, the genome organization of the three DcPIV3 strains was typical of paramyxovirus, with six genes 3′-N-P-M-F-HN-L-5′ encoding the nucleocapsid protein (N), phosphoprotein (P), matrix protein (M), fusion protein (F), hemagglutinin neuraminidase (HM), and large polymerase (L), respectively (**Table 2; Figure 4**). They possessed typical genome features similar to other viruses of the genus *Respirovirus*, including a conserved motif $^{323}$FAPGNYALSYAM$^{336}$ in the N protein, RNA editing sites 5'–$^{717}$AAAAAAGGG$^{725}$–3' and 5'-$^{1038}$AGAAGAAAGAAAGG$^{1051}$-3' (mRNA sense) in the P gene with multiple polypeptides coding capacity, a nuclear localization signal sequence $^{245}$KVGRMYSVEYCKQKIEK$^{261}$ in the M protein, a conserved sialic acid binding motif $^{252}$NRKSCS$^{257}$ in the HN protein, conserved lengths of the leader (i.e., 55 nt) and trailer (i.e., 51 nt) sequences, total coding percentages (92.6–93.4%), gene-start (consensus: AGGANNAAAG), gene-end (consensus: NANNANNAAAAA), and trinucleotide intergenic sequences (i.e., CTT, mRNA sense; **Table 2; Figure 4**). Similar to P genes of respiroviruses, the P gene of DcPIV3 encodes for three overlapping polypeptides, including a non-structural C protein (203 aa utilizing +1 frame), a cysteine-rich V protein (158 aa + 1G), and a D protein (131 aa + 2G).

Phylogenetic analysis of the complete genome of the three sequenced DcPIV3 strains and representative viruses of the genus *Respirovirus* showed that they were most closely related to BPIV3 genotype C (BPIV3c) strains, being most closely related to BPIV3c strain TVMDL20 (GenBank accession number KJ647287), sharing 85.2–85.5% nucleotide identities (**Table 3; Figure 5A**). They shared 83.7–84.4, 83.1–83.8, and 84.8–85.5% nucleotide identities to other BIV3 strains of genotype A, B, and C, respectively (**Table 3**). Further sequence analysis of the L protein revealed that the three DcPIV3 strains shared 98.0% amino acid identities to the partial L protein (1,525

aa) of a PIV3 strain previously discovered from a MERS-CoV-positive dromedary camel in Abu Dhabi, the UAE (GenBank accession number MF593477; **Figure 5B**). Phylogenetic tree constructed based on the complete L protein showed that the branch length between the three DcPIV3 strains and the nearest node, BPIV3, was >0.03 (**Figure 5C**), and it showed similar topology as the trees constructed based on the whole-genome sequence (**Figure 5A**) and the nucleotide sequence of the complete L gene (**Figure 5D**). The pairwise amino acid identities of N, P, M, F, HN, and L of the three DcPIV3 strains and other virus strains of BPIV3 genotypes were shown in **Table 5**.

# DISCUSSION

In this study, we showed that both MERS-CoV and DcPIV3 co-circulated in a dromedary herd in the Middle East. Since the emergence of MERS epidemic in human in 2012, detection of MERS-CoV and its antibodies has been reported in dromedaries in various countries in the Middle East and North Africa (Lau et al., 2016a). We have also detected MERS-CoV neutralizing antibodies in Bactrian and hybrid camels from Dubai (Lau et al., 2020), suggesting that camel is probably the reservoir for MERS-CoV. In this study, the herd was from a dromedary farm in Umm Al Quwain, the UAE. When the dromedaries in the herd developed respiratory signs that were not specific for a particular respiratory infection, nasal swabs were collected from them for viral culture, of which one form of CPE developed in samples from three dromedaries and another kind of CPE was observed in specimens of another three dromedaries. In the first three samples (D1189.1, D1189.5, and D1189.6), MERS-CoV was detected by RT-PCR using virus-specific primers, consistent with the typical CPE for MERS-CoV on Vero cells. Complete genome sequencing and phylogenetic analysis revealed that D1189.1, D1189.5, and D1189.6 were clustered (**Figure 2**), indicating that the virus had probably been transmitted from one camel to another within the herd. They belonged to clade B3 and were most closely related to another dromedary isolate D1271 previously detected in Dubai (**Figure 2**). Similar to D1271, bootscan analysis and multiple alignment revealed evidence of recombination for the three B3 strains, with the potential recombination site detected in ORF1ab (**Figure 3**). Although several studies have reported recombination among MERS-CoVs from different countries (Huang et al., 2016; Sabir et al., 2016), we could not exclude the possibility that the apparent recombination events may have been resulted from individual nucleotide mutations. Such recombination analyses are particularly complicated in RNA viruses, including MERS-CoV, which are known to have high mutation rate. The high frequency of mutations will increase the likelihood of convergent mutations, causing sequence similarities in divergent virus strains that can be misinterpreted as recombination events. Furthermore, most recombination analysis tools may not be able to distinguish between recombined and rapidly evolving sequences. Therefore, one should be cautious when determining whether phylogenetic

**TABLE 2 |** Genomic features and coding potential of the three DcPIV3 strains isolated from dromedary nasal samples.

| DcPIV3 strain | | | ORF features | | | | | | | | |
|---|---|---|---|---|---|---|---|---|---|---|---|
| | Length (nt) | G+C content (%) | Protein | Location (nt) | Length (nt) | Length (aa) | Frame | mRNA insertion | Gene-start | IGR | Gene-end |
| D1189.2 | 15,474 | 34.8 | Nucleoprotein (N) | 112–1,659 | 1,548 | 516 | | | AGGATTAAAG | CTT | GAGTAAGAAAAA |
| | | | Phosphoprotein (P) | 1,785–3,587 | 1,803 | 601 | | | AGGATTAAAG | CTT | TAATAATAAAAA |
| | | | C protein (C) | 1,795–2,403 | 609 | 203 | +1 | | | | |
| | | | D protein (D) | 1,785–2,178 | 393 | 131 | | +2G | | | |
| | | | V protein (V) | 1,785–2,259 | 474 | 158 | | +1G | | | |
| | | | Matrix (M) | 3,748–4,803 | 1,056 | 352 | | | AGGACAAAG | CTT | AAAAATCAAAAA |
| | | | Fusion (F) | 5,096–6,718 | 1,623 | 541 | | | AGGATCAAAG | CTT | AAGTATAAAAAA |
| | | | Hemagglutinin neuraminidase (HN) | 6,830–8,548 | 1,719 | 573 | | | AGGAACAAAG | CTT | GAAAATAAAAAA |
| | | | Large (L) | 8,670–15,371 | 6,702 | 2,234 | | | AGGAGAAAAG | CTT | AAATAAGAAAAA |
| D1189.4 | 15,498 | 34.8 | Nucleoprotein (N) | 111–1,658 | 1,548 | 516 | | | AGGATTAAAG | CTT | GAGTAAGAAAAA |
| | | | Phosphoprotein (P) | 1,784–3,586 | 1,803 | 601 | | | AGGATTAAAG | CTT | GATTAAGAAAAA |
| | | | C protein (C) | 1,794–2,403 | 609 | 203 | +1 | | | | |
| | | | D protein (D) | 1,784–2,177 | 393 | 131 | | +2G | | | |
| | | | V protein (V) | 1,784–2,258 | 474 | 158 | | +1G | | | |
| | | | Matrix (M) | 3,747–4,802 | 1,056 | 352 | | | AGGACAAAG | CTT | AAAAATCAAAAA |
| | | | Fusion (F) | 5,108–6,730 | 1,623 | 541 | | | AGGATCAAAG | CTT | AAGTATAAAAAA |
| | | | Hemagglutinin neuraminidase (HN) | 6,842–8,560 | 1,719 | 573 | | | AGGAACAAAG | CTT | TAAAATAAAAAA |
| | | | Large (L) | 8,694–15,395 | 6,702 | 2,234 | | | AGGAGAAAAG | CTT | AAATAAGAAAAA |
| D1189.8 | 15,480 | 34.6 | Nucleoprotein (N) | 111–1,658 | 1,548 | 516 | | | AGGAGAAAAG | CTT | GAGTAAGAAAAA |
| | | | Phosphoprotein (P) | 1,784–3,586 | 1,803 | 601 | | | AGGATTAAAG | CTT | TACTATGAAAAA |
| | | | C protein (C) | 1,794–2,403 | 609 | 203 | +1 | | | | |
| | | | D protein (D) | 1,784–2,177 | 393 | 131 | | +2G | | | |
| | | | V protein (V) | 1,784–2,258 | 474 | 158 | | +1G | | | |
| | | | Matrix (M) | 3,747–4,802 | 1,056 | 352 | | | AGGAGAAAAG | CTT | AAAAATCAAAAA |
| | | | Fusion (F) | 5,102–6,724 | 1,623 | 541 | | | AGGATCAAAG | CTT | AAATATAAAAAA |
| | | | Hemagglutinin neuraminidase (HN) | 6,836–8,554 | 1,719 | 573 | | | AGGAACAAAG | CTT | GAAAATAAAAAA |
| | | | Large (L) | 8,676–15,377 | 6,702 | 2,234 | | | AGGAGAAAAG | CTT | AAATAAAAAAAA |

15

| PIV3 strain (GenBank accession no.) | Pairwise identity (%) | | |
|---|---|---|---|
| | D1189.2 | D1189.4 | D1189.8 |
| *Dromedary parainfluenza virus 3 (DcPIV3)* | | | |
| Camel D1189.2 (MW504257) | | 98.4 | 98.9 |
| Camel D1189.4 (MW504258) | 98.4 | | 97.9 |
| Camel D1189.8 (MW504259) | 98.9 | 97.9 | |
| *Bovine parainfluenza virus 3 (BPIV3)* | | | |
| *Genotype A* | | | |
| *Sub-genotype A1* | | | |
| Bovine TVMDL24 (KJ647288) | 83.9 | 84.3 | 83.7 |
| Bovine 910 N (D84095) | 84.3 | 84.3 | 83.7 |
| *Sub-genotype A2* | | | |
| Bovine 15,626 (AF178654) | 84.1 | 84.4 | 83.8 |
| Bovine Shipping fever (AF178655) | 83.7 | 84.4 | 83.9 |
| *Sub-genotype A3* | | | |
| Bovine TVMDL60 (KJ647289) | 83.9 | 84.2 | 83.6 |
| Cattle NM09 (JQ063064) | 83.9 | 84.1 | 83.6 |
| *Genotype B* | | | |
| Bovine Q5592 (EU277658) | 83.2 | 83.6 | 83.1 |
| Bovine TVMDL15 (KJ647284) | 83.4 | 83.7 | 83.2 |
| Bovine TVMDL17 (KJ647286) | 83.5 | 83.8 | 83.3 |
| *Genotype C* | | | |
| Cattle 12Q061 (JX969001) | 84.8 | 85.1 | 84.8 |
| Cattle SD0835 (HQ530153) | 85.2 | 85.4 | 84.9 |
| Bovine TVMDL16 (KJ647285) | 85.1 | 85.5 | 84.9 |
| Bovine TVMDL20 (KJ647287) | 85.2 | 85.5 | 85.0 |



FIGURE 4 | Schematic diagram of a DcPIV3 genome with the transcriptional gene-start, intergenic, and gene-end sequences. The gene sizes are shown as boxes that are drawn to approximate scale. The positions of the extragenic 3' leader, 5' terminal trailer, and gene junctions are shown as horizontal lines. The conserved gene-start and gene-end transcription regulatory sequences at the boundaries between genes are indicated.

discordant regions are attributable to recombination or to convergent mutations. Overall, comparative genome analysis showed that the amino acid of the three MERS-CoV isolates differed by 8–17 amino acids with the highest amino acid substitutions at M protein (**Table 1**). Notably, in two of the three MERS-CoV strains (D1189.1 and D1189.6), their M protein sequences were identical, but they differed from the third one (D1189.5) by eight amino acids (**Table 1**). However, for the other parts of the genome (ORF1a, ORF1b, ORF4a, and S), which showed variations among the three strains, there were seven amino acid differences between D1189.1 and D1189.6, five amino acid differences between D1189.1 and D1189.5, and eight amino acid differences between D1189.5 and D1189.6 (**Table 1; Figure 2**).

**FIGURE 5** | Phylogenetic analyses of **(A)** the complete genome, the amino acid sequences of **(B)** partial L protein and **(C)** complete L protein, and **(D)** the nucleotide sequences of the complete L gene of the three DcPIV3 strains discovered in the present study. Phylogenetic trees were generated using Jukes and Cantor (JC) model (complete genome), Jones Taylor Thornton (JTT) model (partial L and complete L protein), and General Time Reversible (GTR) + G model (complete L gene) with 1,000 bootstrap pseudoreplicates. Nineteen thousand and fifty-four nucleotide positions of the complete genome, 1,635 and 2,428 amino acid positions of the partial and complete L protein, and 5,861 nucleotide positions of the complete L gene were included, respectively, in the analyses. Trees with the highest log likelihood (−181887.15 for the complete genome, −17365.96 for the partial L protein, −27636.23 for the complete L protein, and −53701.29 for the complete L gene) are shown. Bootstrap values are shown next to the branches. The scale bar indicates the number of nucleotide or amino acid substitutions per site. The three DcPIV3 strains sequenced and analyzed in the present study are shown in red triangular and black spade for MF593477. All the accession numbers are given as cited in GenBank.

In the other three samples that showed CPE atypical for MERS-CoV, DcPIV3 was detected. Antibodies against PIV3 have been detected in dromedaries for a few decades (Van der Maaten, 1969; Nawal et al., 2003; Shaker et al., 2003). In 2009, a PIV3 was first described in the respiratory samples of dromedaries (Intisar et al., 2010). In that study, two lung specimens from dromedaries in slaughterhouses from Sudan with pneumonia outbreak were found to be RT-PCR positive for PIV3, although no sequencing results were described. Virologists have speculated that this PIV3 detected in dromedaries could be BPIV3 (Van der Maaten, 1969; Nawal et al., 2003; Shaker et al., 2003). In 2017, PIV3 sequences were found in

the nasopharyngeal swabs of healthy dromedaries by metagenomic sequencing (Li et al., 2017). However, only one partial L sequence from this study was uploaded in GenBank. In the present study, for the three samples (D1189.2, D1189.4, and D1189.8) that showed CPE on Vero cells but were RT-PCR negative for MERS-CoV, the viral isolates were subjected to next-generation sequencing, using a strategy we previously employed for the detection of West Nile virus in a dromedary (Joseph et al., 2016). Overall, comparative genome analysis showed that the concatenated amino acids of the three DcPIV3 isolates differed by 8–22 amino acids (**Table 4**). They possessed typical genome features similar to other viruses of the genus

**TABLE 4 |** Comparison of amino acid substitutions among the three DcPIV3 isolates in this study.

| Protein | Position (aa) | Strain | | |
|---|---|---|---|---|
| | | D1189.2 | D1189.4 | D1189.8 |
| P gene | 530 | K | E | E |
| | 756 | R | G | G |
| | 793 | N | S | N |
| M gene | 1,463 | K | K | E |
| F gene | 1,470 | I | F | I |
| | 1,476 | I | V | I |
| | 1,479 | I | V | I |
| | 1,693 | T | K | K |
| | 1,732 | V | F | V |
| | 1,734 | D | V | D |
| | 1,736 | D | Y | D |
| | 1,739 | D | E | D |
| | 1,788 | F | F | S |
| | 1,830 | R | K | I |
| HN gene | 2,198 | V | A | A |
| | 2,203 | N | H | N |
| | 2,260 | K | K | R |
| | 2,336 | N | K | N |
| L gene | 4,426 | S | L | S |
| | 4,441 | Q | L | Q |
| | 4,442 | I | L | I |
| | 4,446 | V | E | V |
| | 4,451 | N | S | N |
| | 4,461 | N | I | N |

*Respirovirus*, including a conserved motif in the N protein, RNA editing sites in the P gene, a nuclear localization signal sequence in the M protein, a conserved sialic acid binding motif in the HN protein, conserved lengths of the leader and trailer sequences, total coding percentages, gene-start and gene-end, and trinucleotide intergenic sequences (**Table 2, Figure 4**). Phylogenetic analysis revealed that the three strains were clustered (**Figure 5**), indicating that they were also a result of inter-camel transmission within the herd. Phylogenetic trees constructed using complete genome or L protein showed that although DcPIV3 is most closely related to the other three genotypes of BPIV3, it forms a cluster distinct from BPIV3 (**Figure 5**).

Complete genome sequencing and phylogenetic and comparative genome analysis showed that DcPIV3 is a novel species of the genus *Respirovirus*. According to the ICTV definition, in the genus *Respirovirus* under the subfamily *Orthoparamyxovirinae* of the *Paramyxoviridae* family, there are six species, namely, BPIV3, human parainfluenza virus 1 and 3 (HPIV1 and HPIV3), porcine parainfluenza virus 1 (PPIV1), caprine parainfluenza virus 3 (CPIV3), and Sendai virus (SeV; Rima et al., 2019). For the BPIV3 species, the members were further sub-classified into three genotypes; most of them were from cattle, although there is no concrete definition on the criteria for genotype demarcation. In the present study, although our results showed that DcPIV3 is most closely related to BPIV3c strains, DcPIV3 constitutes a new species in the genus *Respirovirus* because in the phylogenetic tree constructed using the complete L protein,

**TABLE 5 |** Comparison of amino acid identities between the predicted open reading frames (ORFs) of three DcPIV3 strains and the corresponding proteins of other representative PIV3 strains.

| Representative member | | | Pairwise amino acid identity (%) | | | | | | | | | | | | | | | | | | |
|---|---|---|---|---|---|---|---|---|---|---|---|---|---|---|---|---|---|---|---|---|---|
| | | | D1189.2 | | | | | | D1189.4 | | | | | | D1189.8 | | | | | | |
| Genotype | Strain | Accession no. | N | P | M | F | HN | L | N | P | M | F | HN | L | N | P | M | F | HN | L |
| **Dromedary parainfluenza virus 3 (DcPIV3)** | | | | | | | | | | | | | | | | | | | | | |
| NA | D1189.2 | MW504257 | | | | | | | 100.0 | 99.5 | 100.0 | 97.6 | 99.5 | 99.3 | 100.0 | 99.8 | 99.7 | 99.4 | 99.3 | 100.0 |
| NA | D1189.4 | MW504258 | 100.0 | 99.7 | 99.7 | 97.6 | 99.5 | 99.3 | | | | | | | 100.0 | 99.7 | 99.7 | 97.6 | 99.1 | 99.3 |
| NA | D1189.8 | MW504259 | 100.0 | 99.8 | 99.7 | 99.4 | 99.3 | 100.0 | 100.0 | 99.7 | 99.7 | 97.6 | 99.1 | 99.3 | | | | | | |
| **Bovine parainfluenza virus 3 (BPIV3)** | | | | | | | | | | | | | | | | | | | | | |
| A | 15,626 | AF178654 | 89.7 | 67.0 | 95.4 | 85.7 | 81.5 | 91.0 | 89.7 | 67.3 | 95.4 | 84.4 | 81.3 | 90.3 | 89.7 | 67.1 | 95.2 | 85.7 | 81.5 | 91.0 |
| B | Q5592 | EU277658 | 89.3 | 68.7 | 94.3 | 82.4 | 80.4 | 91.5 | 89.3 | 69.2 | 94.3 | 82.0 | 80.2 | 90.9 | 89.3 | 68.8 | 94.0 | 82.4 | 80.4 | 91.5 |
| C | 12Q061 | JX969001 | 91.5 | 70.5 | 95.7 | 85.2 | 83.0 | 90.9 | 91.5 | 71.0 | 95.7 | 84.4 | 83.0 | 90.2 | 91.5 | 70.7 | 95.4 | 85.2 | 82.7 | 90.9 |
| C | SD0835 | HQ530153 | 90.3 | 71.8 | 97.2 | 84.8 | 83.2 | 91.6 | 90.3 | 72.3 | 97.2 | 84.1 | 83.2 | 91.0 | 90.3 | 72.0 | 96.9 | 84.8 | 82.9 | 91.6 |
| C | TVMDL16 | KJ647285 | 91.1 | 71.3 | 97.2 | 85.8 | 83.2 | 92.0 | 91.1 | 71.8 | 97.2 | 84.8 | 83.2 | 91.3 | 91.1 | 71.5 | 96.9 | 85.8 | 82.9 | 92.0 |
| C | TVMDL20 | KJ647287 | 91.5 | 72.0 | 97.2 | 85.6 | 82.7 | 92.0 | 91.5 | 72.5 | 97.2 | 84.6 | 82.7 | 91.3 | 91.5 | 72.2 | 96.9 | 85.6 | 82.3 | 92.0 |

the branch length between DcPIV3 and the nearest node is 0.04, which is more than 0.03, the definition used for species demarcation in the family *Paramyxoviridae*.

## CONCLUSION

Collectively, our results showed that both MERS-CoV and DcPIV3 co-circulated in a dromedary herd in the Middle East and DcPIV3 is a novel species of the genus *Respirovirus*. The present study is the first that demonstrated isolation of a novel respirovirus in sick dromedaries, further expanding the host range for respiroviruses. Future studies are warranted to improve our understanding of DcPIV3 evolution and ecology, as well as its pathogenicity in camels.

## DATA AVAILABILITY STATEMENT

The datasets presented in this study can be found in online repositories. The names of the repository/repositories and accession number(s) can be found at: https://www.ncbi.nlm.nih.gov/genbank/, MW545527; https://www.ncbi.nlm.nih.gov/genbank/, MW545528; https://www.ncbi.nlm.nih.gov/genbank/, MW504257; https://www.ncbi.nlm.nih.gov/genbank/, MW504258; https://www.ncbi.nlm.nih.gov/genbank/, MW504259; https://www.ncbi.nlm.nih.gov/genbank/, SRR13442189; https://www.ncbi.nlm.nih.gov/

genbank/, SRR13442188; and https://www.ncbi.nlm.nih.gov/genbank/, SRR13442187.

## AUTHOR CONTRIBUTIONS

JT, UW, and PW conceived and designed the experiment. JT, HL, JF, SJ, KL, SE, and K-HC performed the experiment. JT, UW, HL, JYHF, HC, SL, and PW contributed to analysis. JT, UW, HL, and PW drafted the manuscript. All authors reviewed and revised the first and final drafts of this manuscript. PW and UW are co-corresponding authors who contributed equally to this article.

## FUNDING

## SUPPLEMENTARY MATERIAL

The Supplementary Material for this article can be found online at: https://www.frontiersin.org/articles/10.3389/fmicb.2021.739779/full#supplementary-material

## REFERENCES

Al-Ruwaili, M. A., Khalil, O. M., and Selim, S. A. (2012). Viral and bacterial infections associated with camel (Camelus dromedarius) calf diarrhea in North Province, Saudi Arabia. *Saudi J. Biol. Sci.* 19, 35–41. doi: 10.1016/j.sjbs.2011.10.001

Al-Shomrani, B. M., Manee, M. M., Alharbi, S. N., Altammami, M. A., Alshehri, M. A., Nassar, M. S., et al. (2020). Genomic sequencing and analysis of eight camel-derived Middle East respiratory syndrome coronavirus (MERS-CoV) isolates in Saudi Arabia. *Viruses* 12:611. doi: 10.3390/v12060611

Chevreux, B., Wetter, T., and Suhai, S. (1999). Genome sequence assembly using trace signals and additional sequence information. *German Conf. Bioinform.* 99, 45–56.

El-Kafrawy, S. A., Corman, V. M., Tolah, A. M., Al Masaudi, S. B., Hassan, A. M., Müller, M. A., et al. (2019). Enzootic patterns of Middle East respiratory syndrome coronavirus in imported African and local Arabian dromedary camels: a prospective genomic study. *Lancet Planet. Health* 3, e521–e528. doi: 10.1016/S2542-5196(19)30243-8

Huang, C., Liu, W. J., Xu, W., Jin, T., Zhao, Y., Song, J., et al. (2016). A bat-derived putative cross-family recombinant coronavirus with a Reovirus Gene. *PLoS Pathog.* 12:e1005883. doi: 10.1371/journal.ppat.1005883

Huson, D. H., Beier, S., Flade, I., Górska, A., El-Hadidi, M., Mitra, S., et al. (2016). MEGAN community edition-interactive exploration and analysis of large-scale microbiome sequencing data. *PLoS Comput. Biol.* 12:e1004957. doi: 10.1371/journal.pcbi.1004957

Intisar, K. S., Ali, Y. H., Khalafalla, A. I., Mahasin, E. R., and Amin, A. S. (2009). Natural exposure of dromedary camels in Sudan to infectious bovine rhinotracheitis virus (bovine herpes virus-1). *Acta Trop.* 111, 243–246. doi: 10.1016/j.actatropica.2009.05.001

Intisar, K. S., Ali, Y. H., Khalafalla, A. I., Rahman, M. E. A., and Amin, A. S. (2010). Respiratory infection of camels associated with parainfluenza virus 3 in Sudan. *J. Virol. Methods* 163, 82–86. doi: 10.1016/j.jviromet.2009.08.017

Joseph, S., Wernery, U., Teng, J. L., Wernery, R., Huang, Y., Patteril, N. A., et al. (2016). First isolation of West Nile virus from a dromedary camel. *Emerg. Microb. Infect.* 5, 1–12. doi: 10.1038/emi.2016.53

Kearse, M., Moir, R., Wilson, A., Stones-Havas, S., Cheung, M., Sturrock, S., et al. (2012). Geneious basic: an integrated and extendable desktop software platform for the organization and analysis of sequence data. *Bioinformatics* 28, 1647–1649. doi: 10.1093/bioinformatics/bts199

Khalafalla, A. I., Saeed, I. K., Ali, Y. H., Abdurrahman, M. B., Kwiatek, O., Libeau, G., et al. (2010). An outbreak of peste des petits ruminants (PPR) in camels in the Sudan. *Acta Trop.* 116, 161–165. doi: 10.1016/j.actatropica.2010.08.002

Kumar, S., Stecher, G., Li, M., Knyaz, C., and Tamura, K. (2018). MEGA X: molecular evolutionary genetics analysis across computing platforms. *Mol. Biol. Evol.* 35, 1547–1549. doi: 10.1093/molbev/msy096

Lau, S. K. P., Lee, P., Tsang, A. K. L., Yip, C. C., Tse, H., Lee, R. A., et al. (2011). Molecular epidemiology of human coronavirus OC43 reveals evolution of different genotypes over time and recent emergence of a novel genotype due to natural recombination. *J. Virol.* 85, 11325–11337. doi: 10.1128/JVI.05512-11

Lau, S. K. P., Li, K. S. M., Luk, K. H., He, Z., Teng, J. L. L., Yuen, K. Y., et al. (2020). Middle East respiratory syndrome coronavirus antibodies in Bactrian and hybrid camels from Dubai. *mSphere* 5, e00898–e00819. doi: 10.1128/mSphere.00898-19

Lau, S. K. P., Wernery, R., Wong, E. Y. M., Joseph, S., Tsang, A. K. L., Patteril, N. A. G., et al. (2016a). Polyphyletic origin of MERS coronaviruses and isolation of a novel clade A strain from dromedary camels in the United Arab Emirates. *Emerg. Microb. Infect.* 5:e128. doi: 10.1038/emi.2016.129

Lau, S. K. P., Wong, A. C. P., Lau, T. C. K., and Woo, P. C. Y. (2017). Molecular evolution of MERS coronavirus: dromedaries as a recent intermediate host or long-time animal reservoir? *Int. J. Mol. Sci.* 18:2138. doi: 10.3390/ijms18102138

Lau, S. K. P., Woo, P. C. Y., Li, K. S. M., Zhang, H.-J., Fan, R. Y. Y., Zhang, A. J. X., et al. (2016b). Identification of novel Rosavirus species That infects

diverse rodent species and causes multisystemic dissemination in mouse model. *PLoS Pathog.* 12:e1005911. doi: 10.1371/journal.ppat.1005911

Lau, S. K. P., Woo, P. C. Y., Yip, C. C., Fan, R. Y. Y., Huang, Y., Wang, M., et al. (2012). Isolation and characterization of a novel Betacoronavirus subgroup A coronavirus, rabbit coronavirus HKU14, from domestic rabbits. *J. Virol.* 86, 5481–5496. doi: 10.1128/JVI.06927-11

Li, Y., Khalafalla, A. I., Paden, C. R., Yusof, M. F., Eltahir, Y. M., Al Hammadi, Z. M., et al. (2017). Identification of diverse viruses in upper respiratory samples in dromedary camels from United Arab Emirates. *PLoS One* 12:e0184718. doi: 10.1371/journal.pone.0190108

Nawal, M. A. Y., Gabry, G. H., Hussien, M., and Omayma, A. A. S. (2003). Occurrence of parainfluenza type-3 (PI-3) and bovine herpes virus type-1 (BHV-1) viruses (mixed infection) among camels. *Egypt. J. Agric. Res.* 81, 781–791.

Rima, B., Balkema-Buschmann, A., Dundon, W. G., Duprex, P., Easton, A., Fouchier, R., et al. (2019). ICTV virus taxonomy profile: *Paramyxoviridae*. *J. Gen. Virol.* 100, 1593–1594. doi: 10.1099/jgv.0.001328

Sabir, J. S., Lam, T. T., Ahmed, M. M., Li, L., Shen, Y., Abo-Aba, S. E., et al. (2016). Co-circulation of three camel coronavirus species and recombination of MERS-CoVs in Saudi Arabia. *Science* 351, 81–84. doi: 10.1126/science. aac8608

Shaker, E.I., Saber, M.S., and Ali, N.M. (2003). Virological and serological studies on viruses associated with respiratory infection in camels. MVSc Thesis. Faculty of Veterinary Medicine, University of Cairo, Egypt.

Sievers, F., and Higgins, D. G. (2014). Clustal omega. *Curr. Protoc. Bioinformatics* 48, 3–13. doi: 10.1002/0471250953.bi0313s48

Sridhar, S., Teng, J. L., Chiu, T. H., Lau, S. K., and Woo, P. C. (2017). Hepatitis E virus genotypes and evolution: emergence of camel hepatitis E variants. *Int. J. Mol. Sci.* 18:869. doi: 10.3390/ijms18040869

Teng, J. L. L., Wernery, U., Lee, H. H., Joseph, S., Fung, J., Elizabeth, S. K., et al. (2019). First isolation and rapid identification of Newcastle disease virus from aborted Fetus of dromedary camel using next-generation sequencing. *Viruses* 11:810. doi: 10.3390/v11090810

Ure, A. E., Elfadl, A. K., Khalafalla, A. I., Gameel, A. A. R., Dillner, J., and Forslund, O. (2011). Characterization of the complete genomes of Camelus dromedarius papillomavirus types 1 and 2. *J. Gen. Virol.* 92, 1769–1777. doi: 10.1099/vir.0.031039-0

Van der Maaten, M. J. (1969). Immunofluorescent studies of bovine Para-influenza 3 virus I. cell cultures and experimentally infected hamsters. *Can. J. Comp. Med.* 33:134.

Wernery, U., Corman, V., Wong, E., Tsang, A., Muth, D., Lau, S., et al. (2015). Acute Middle East respiratory syndrome coronavirus infection in livestock dromedaries, Dubai, 2014. *Emerg. Infect. Dis.* 21, 1019–1022. doi: 10.3201/eid2106.150038

Wernery, U., Kinne, J., and Schuster, R. K. (2014). *Camelid Infectious Disorders.* Paris: OIE (World Organisation for Animal Health).

Wernery, U., Knowles, N. J., Hamblin, C., Wernery, R., Joseph, S., Kinne, J., et al. (2008). Abortions in dromedaries (Camelus dromedarius) caused by equine rhinitis A virus. *J. Gen. Virol.* 89, 660–666. doi: 10.1099/vir.0.82215-0

Wernery, U., and Zachariah, R. (1999). Experimental camelpox infection in vaccinated and unvaccinated dromedaries. *J. Veterinary Med. Ser. B* 46, 131–135. doi: 10.1111/j.0931-1793.1999.00250.x

Woo, P. C., Lau, S. K., Fan, R. Y., Lau, C. C., Wong, E. Y., Joseph, S., et al. (2016). Isolation and characterization of dromedary camel coronavirus UAE-HKU23 from dromedaries of the Middle East: minimal serological cross-reactivity between MERS coronavirus and dromedary camel coronavirus UAE-HKU23. *Int. J. Mol. Sci.* 17:691. doi: 10.3390/ijms17050691

Woo, P. C., Lau, S. K., Li, T., Jose, S., Yip, C. C., Huang, Y., et al. (2015a). A novel dromedary camel enterovirus in the family *Picornaviridae* from dromedaries in the Middle East. *J. Gen. Virol.* 96, 1723–1731. doi: 10.1099/vir.0.000131

Woo, P. C., Lau, S. K., Teng, J. L., Tsang, A. K., Joseph, M., Wong, E. Y., et al. (2014). Metagenomic analysis of viromes of dromedary camel fecal samples reveals large number and high diversity of circoviruses and picobirnaviruses. *Virology* 471, 117–125. doi: 10.1016/j.virol.2014.09.020

Woo, P. C., Lau, S. K., Teng, J. L., Tsang, A. K., Joseph, S., Xie, J., et al. (2015b). A novel astrovirus from dromedaries in the Middle East. *J. Gen. Virol.* 96, 2697–2707. doi: 10.1099/jgv.0.000233

Woo, P. C., Lau, S. K., Tsoi, H. W., Patteril, N. G., Yeung, H. C., Joseph, S., et al. (2017). Two novel dromedary camel bocaparvoviruses from dromedaries in the Middle East with unique genomic features. *J. Gen. Virol.* 98, 1349–1359. doi: 10.1099/jgv.0.000775

Woo, P. C. Y., Lau, S. K. P., Yip, C. C., Huang, Y., Tsoi, H. W., Chan, K. H., et al. (2006). Comparative analysis of 22 coronavirus HKU1 genomes reveals a novel genotype and evidence of natural recombination in coronavirus HKU1. *J. Virol.* 80, 7136–7145. doi: 10.1128/JVI.00509-06

Yousif, A. A., Braun, L. J., Saber, M. S., Aboellail, T. A., and Chase, C. C. L. (2004). Cytopathic genotype 2 bovine viral diarrhea virus in dromedary camels. *Arab J. Biotechnol.* 7, 123–140.

# Interplay of Nutrition and Psychoneuroendocrineimmune Modulation: Relevance for COVID-19 in BRICS Nations

Arundhati Mehta[1], Yashwant Kumar Ratre[1], Krishna Sharma[2], Vivek Kumar Soni[1], Atul Kumar Tiwari[3], Rajat Pratap Singh[1], Mrigendra Kumar Dwivedi[4], Vikas Chandra[1], Santosh Kumar Prajapati[5], Dhananjay Shukla[1]* and Naveen Kumar Vishvakarma[1]*

[1]Department of Biotechnology, Guru Ghasidas Vishwavidyalaya, Bilaspur, India, [2]Department of Psychology, Government Bilasa Girls Post Graduate Autonomous College, Bilaspur, India, [3]Department of Zoology, Bhanwar Singh Porte Government Science College, Pendra, India, [4]Department of Biochemistry, Government Nagarjuna Post Graduate College of Science, Raipur, India, [5]Department of Botany, Guru Ghasidas Vishwavidyalaya, Bilaspur, India

The consequences of COVID-19 are not limited to physical health deterioration; the impact on neuropsychological well-being is also substantially reported. The inter-regulation of physical health and psychological well-being through the psychoneuroendocrineimmune (PNEI) axis has enduring consequences in susceptibility, treatment outcome as well as recuperation. The pandemic effects are upsetting the lifestyle, social interaction, and financial security; and also pose a threat through perceived fear. These consequences of COVID-19 also influence the PNEI system and wreck the prognosis. The nutritional status of individuals is also reported to have a determinative role in COVID-19 severity and convalescence. In addition to energetic demand, diet also provides precursor substances [amino acids (AAs), vitamins, etc.] for regulators of the PNEI axis such as neurotransmitters (NTs) and immunomodulators. Moreover, exaggerated immune response and recovery phase of COVID-19 demand additional nutrient intake; widening the gap of pre-existing undernourishment. Mushrooms, fresh fruits and vegetables, herbs and spices, and legumes are few of such readily available food ingredients which are rich in protein and also have medicinal benefits. BRICS nations have their influences on global development and are highly impacted by a large number of confirmed COVID-19 cases and deaths. The adequacy and access to healthcare are also low in BRICS nations as compared to the rest of the world. Attempt to combat the COVID-19 pandemic are praiseworthy in BRICS nations. However, large population sizes, high prevalence of undernourishment (PoU), and high incidence of mental health ailments in BRICS nations provide a suitable landscape for jeopardy of COVID-19. Therefore, appraising the interplay of nutrition and PNEI modulation especially in BRICS countries will provide better understanding; and will aid in combat COVID-19. It can be suggested that the monitoring will assist in designing adjunctive interventions through medical nutrition therapy and psychopsychiatric management.

Keywords: BRICS, COVID-19, immunity, nutrition, neuropsychology

# INTRODUCTION

The ongoing COVID-19 pandemic affected the various dimensions of well-being in all parts of the globe. As of August 2021, over 216 million diagnosed cases and approximately 4.4 million people have lost their life due to this panic disease worldwide (WHO, 2021). The BRICS countries comprise a wide range of territory cover and substantially share the population, economy, and development at the global level (Jakovljevic, 2014). A significant share in world gross domestic product (GDP) and unique socioeconomic population structure has been linked with essential consideration of BRICS, while designing policies at the global level (Jakovljevic, 2014). These nations are also affected by the severity of COVID-19. The COVID-19 pandemic was originated in one of the member countries of BRICS. Out of the remaining four member countries, three (India, Brazil, and Russia) are among the top five affected countries with the highest number of confirmed cases, along with South Africa in the top 20 (WHO, 2021). Unique socioeconomic, and demographic status of BRICS countries and comparative differences between country members of different economic groups like BRICS, group of seven (G7), emerging seven markets (EM7), and The Organization for Economic Co-operation and Development (OECD) can be linked with their medical preparedness (Jakovljevic, 2014, 2016; Jakovljevic et al., 2020; Carvalho et al., 2021) The rapid increase in affected individuals warrants proactive pharmaceutical solutions and natural remedies to cope up with this ongoing pandemic. The deteriorating effect of COVID-19 is not limited to physical health; it also affected the lifestyle, work culture, and financial welfare (HLPE, 2020; Huang et al., 2020; Soni et al., 2020d). The state of nutrition and neuropsychological well-being has been bilaterally linked with COVID-19 severity. The well-being of physical and psychological health is connected through *Psychoneuroendocrineimmune* (PNEI) system (Soni et al., 2020d; Mehta et al., 2021). Undernourishment has negatively impacted the disease prognosis of COVID-19 (Briguglio et al., 2020; Calder, 2020). On the other hand, pathological manifestations [respiratory distress, gastrointestinal (GI) complications, loss of appetite, and deficient nutrient absorption] caused malnutrition in COVID-19 patients (Zvolensky et al., 2020) Nutritional deficiencies, mainly in protein and vitamin uptake, can have a negative impact on immunity against infections including COVID-19. The unexpected epidemiological burden and post-COVID consequences are disrupting the nutritional status and survival especially those from low- and middle-income countries, and of young age (Rodriguez-Leyva and Pierce, 2021). At the global level, the Committee on World Food Security High Level Panel of Experts on Food Security and Nutrition in its 2020 report discussed the COVID-19 consequences on various dimensions of food availability through initial to long-term effects. In their deliberations, they also pressed the need of considering the complex interaction of nutritional deficiency with outcome including health, society, and psychological well-being (HLPE, 2020). The State of Food Security and Nutrition in the World 2021 report documented a marked escalation in the number of people not having access to adequate food (2.37 billion; 320 million more than that 2019) and facing hunger (811 million; 161 million more than that of 2019; FAO, IFAD, UNICEF, WFP, and WHO, 2021). The prevalence of undernourishment (PoU) among BRICS nations is quite alarming (FAO, IFAD, UNICEF, WFP, and WHO, 2021), India and South Africa have high undernourishment prevalence in their population than the world average. Although. Russia, Brazil, and China have low PoU, these nations share a large undernourished population. Benefits of nutritional supplementation in COVID-19 are speculated as well reported in various investigations (Rodriguez-Leyva and Pierce, 2021). Effector and regulator molecules of psycho-physiological homeostasis are ultimately derived from the diet components. Therefore, the supply of adequate nutrients stands pivotal to fuel the immune system to its optimum as required in abnormal health conditions. Reports indicate that an ample intake of nutrients plays a defensive role against viral infection (Calder, 2020). Elevated consumption of immunity boosters has been reported (Godman et al., 2020; Soni et al., 2021). However, the instability of prices for antimicrobials and vitamins amid the COVID-19 pandemic is a concern to be addressed (Godman et al., 2020). Nevertheless, the hindrance in the immune response can be brought up by common deficiencies and inadequacy of micro- as well as macro-nutrients (Elmadfa and Meyer, 2019; Rodriguez-Leyva and Pierce, 2021). Moreover, bilateral dependency of immunity and psychological status also play a critical role in overall well-being (Soni et al., 2020b).

Neuropsychological consequences and correlation with COVID-19 have surfaced through various reports (Abers et al., 2014; Calder, 2020; García et al., 2020). Nutritional deficiency and exaggerated immune response in COVID-19 patients can invite psychological consequences (Ambrus and Ambrus, 2004; Calder, 2020; Mehta et al., 2021). Moreover, perceived fear, state of uncertainty, and financial crisis amid COVID-19 pandemic effects contribute to such mental distorts. Depressive disorders are quite prevalent in BRICS nations (Ritchie and Roser, 2018).

BRICS nations have a unique state at various global fronts; and hold diversity in economic development, social composition, healthcare practices, food habit, nutritional state, and priority for mental health management (Jakovljevic, 2015, 2016; Jakovljevic et al., 2017; Reshetnikov et al., 2020; Awe et al., 2021; Dash et al., 2021; de Almondes et al., 2021; Popkova et al., 2021; Rababah et al., 2021; Zhu et al., 2021). These nations have distinctive influences of COVID-19 pandemic on society, medical system, and economics (Dash et al., 2021; de Almondes et al., 2021; Rababah et al., 2021; Zhu et al., 2021). BRICS nations are among the countries facing the highest number of confirmed cases of COVID-19 (WHO, 2021) and are affected by associated consequences of malnutrition, and psychological disorders among their population. Members of BRICS have taken measures as a country as well as a group of nations to contribute to combating the COVID-19 pandemic (Reshetnikov et al., 2020; Chattu et al., 2021; Ranabhat et al., 2021). COVID-19 not only affected physical health but also affected mental well-being (Soni et al., 2020d; Mehta et al.,

2021). Moreover, the impact of COVID-19 pandemic effects severely affects the production and distribution equilibrium including those of essential items and medicines (Godman et al., 2020; Carvalho et al., 2021; Chattu et al., 2021; Ranabhat et al., 2021). Therefore, deliberations on the association of nutrition, immunity, and neuropsychological state are expected to uncover the potential point in combating COVID-19. As per the unique socioeconomic and healthcare level, the BRICS nations should be especially considered in designing global policies to combat the current pandemic of COVID-19. Existing strategies under practice are advised along with integrated psychiatric interventions (Holmes et al., 2020; Steardo and Verkhratsky, 2020; Tandon, 2020). Nutritional sufficiency through supplementation has been observed to refute the neuropsychiatric altercations in infected patients as well as in post-COVID recuperation. Moreover, nutritional supplements, as well as bioactive components of food items including those rich in nutrition and vested medicinal properties, offer benefits against detrimental manifestations in human diseases including COVID-19 (Singh et al., 2020; Soni et al., 2021). Maintaining the sufficiency of nutrients in affected and susceptible patients will have not only have clinical benefits but can also have preventive advantages (Soni et al., 2021). Moreover, pandemic effects including distorted lifestyle, food habits and stay home measures heavily affect the neuropsychological behavior acting through the PNEI axis. As nutrition is key to maintaining a healthy life and its importance in COVID-19, measures, and guidelines released by authorities at national as well international levels recommend maintaining a good nutritional state and incorporating "immunity boosters" in the daily regimen (Bennett et al., 2020; Khanna et al., 2020; Soni et al., 2020a, 2021). In the time of "COVID-Infodemic," the overabundance of COVID-related information, the scientific awareness and the spread of reliable information will adjunct the combating approaches. Collectively, it can be suggested that the interplay of nutrition, immunity, and mental health have compounded effects through the PNEI axis; and strategies against pandemic effects must involve these concerns.

## PREVALENCE IN BRICS COUNTRIES: DRAWING AN EPIDEMIOLOGICAL PICTURE

BRICS nations share a large fraction of world territory, economics, and population in the world (Godman et al., 2020). They belong to various demographic regions and have diverse ethnicity among their population. The rate of economic growth of these nations surpasses the rest of the world (Jakovljevic, 2014). Further, better forbearance against crisis was reported for Emerging Market Seven (EM7) countries as compared to G7 countries (Jakovljevic et al., 2020). Interestingly, Brazil, China, India, and Russia are common in EM7 and BRICS nations, reflecting the potential of these nations. However, many other factors including climate, culture, and lifestyle affect the transmission and management of infectious health conditions.

Despite being among the few largest economies, none of the BRICS nations are in the current member list of organizations for Economic Co-operation and Development (OECD). A comparison of nations from Asia reflects that OECD member countries have better healthcare performance indicators as compared to non-OECD BRICS nations (India and China). The healthcare disparity prevalent in India and China was correlated with heterogeneity among their population at the socioeconomic level (Jakovljevic et al., 2020). Comparing the G7 and BRICS nations, current rate predictions suggest that later groups will surpass in *per capita* growth of the OECD average (Jakovljevic, 2016). However, health disparity, increasing expenses affecting healthcare affordability are among major concerns in BRICS nations (Jakovljevic, 2016). The prevalence of COVID-19 is quite high in these nations. The SARS-CoV-2 was originated in one of the BRICS countries, China, in late 2019, and subsequently affected each part of the globe. The BRICS nations share a large fraction of confirmed COVID-19 cases in the world (**Figure 1**). As per an estimate, the collective share of BRICS nation COVID-19 cases is approximately 30% (WHO, 2021). Among the top five nations with most cases of COVID-19, BRICS counties India, Brazil, and Russia are standing at 2nd, 3rd, and 4th rank, respectively. South Africa is also among the top 20 nations affected by the most cases of COVID-19.

COVID-19 deaths are also high in these nations having Brazil, India, and Russia in the top six affected counties and South Africa among the top 20. About 1.3 million deaths occurred in BRICS nations which accounts for more than 28% of death worldwide (**Figure 2**). This indicates the severity of COVID-19 in the group of these countries with emerging economies. The healthcare system available in these countries is among the major key factors affecting the COVID-19 outcome. The sufficient number of healthcare individuals, timely diagnosis, and therapeutic interventions along with efficient measures to counter the spread of SARS-CoV-2 infection plays a determinative role in combating the COVID-19 pandemic. The Universal health coverage (UHC) effective coverage index indicates that none of the BRICS nations hold the position among the top 50 countries having good healthcare system (Fullman et al., 2018). China, Russia, and Brazil hold 58th, 63rd, and 74th rank with their UHC effective coverage index (70, 69, and 65, respectively) slightly better than the global average of 60.3. The UHC effective coverage index of South Africa (60) is slightly lower than the global average and ranked 98. Lowest among BRICS nations, India has a UHC effective coverage index of 47, and ranked on 162 among 204 countries assessed. Low access to healthcare will hinder the combat of COVID-19. It will be noteworthy to mention that countries with a good UHC effective coverage index are also impacted by COVID-19; however, the ease and access to healthcare will aid in the management of the COVID-19 pandemic. Through a humanitarian approach, and balancing of social as well as political context the UHC spirit can be achieved in combating the COVID-19 (Jakovljevic, 2015; Ranabhat et al., 2021). Further, the need for intensive promotion of scientific perspective and morality is also pressed to overcome challenges associated with the COVID-19 pandemic (Ranabhat
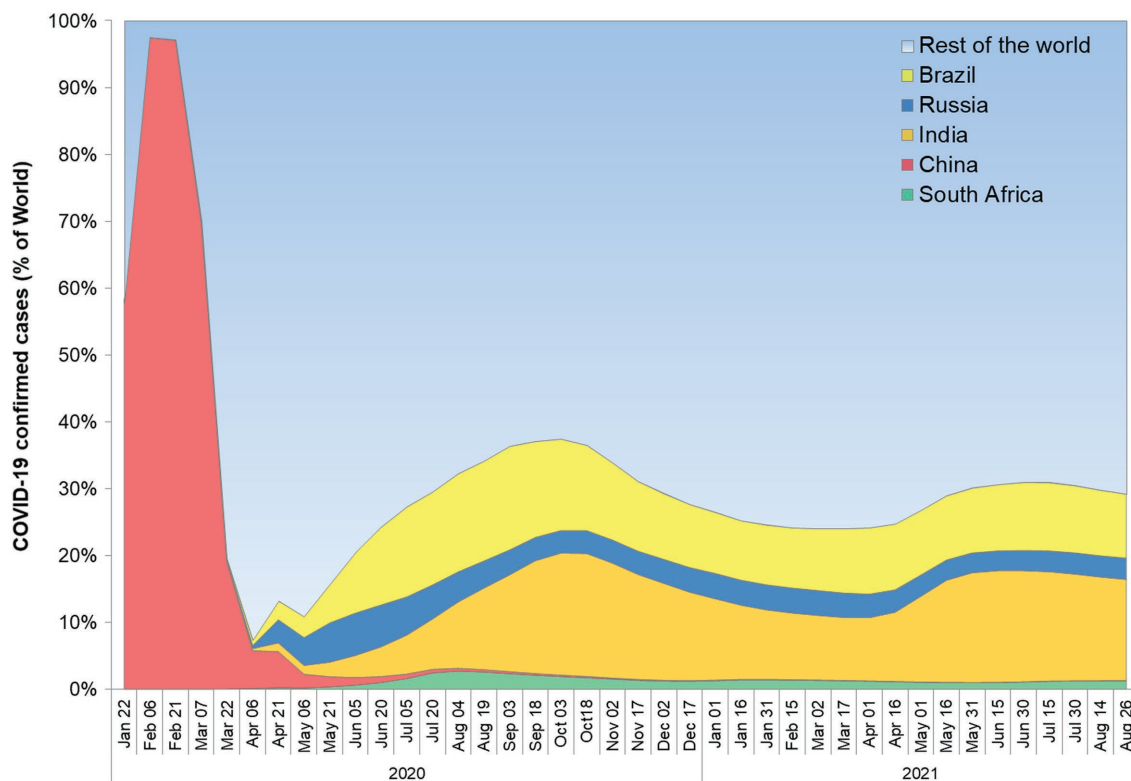
**FIGURE 1 |** BRICS nations share in confirmed cases worldwide.
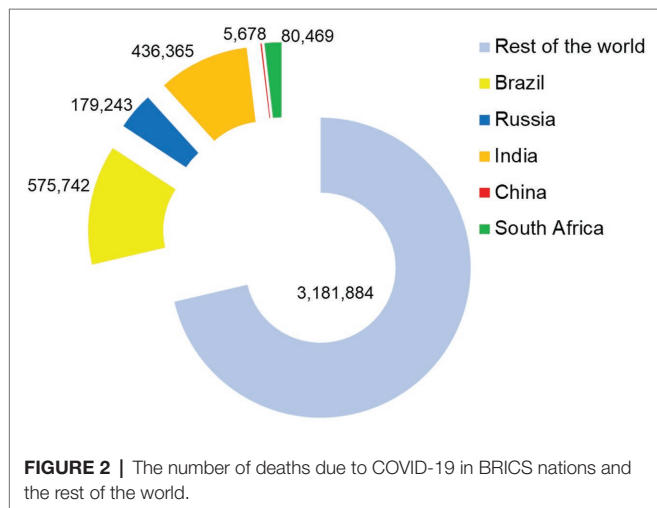


**FIGURE 2 |** The number of deaths due to COVID-19 in BRICS nations and the rest of the world.

et al., 2021). Moreover, effective utilization and strategic planning can aid the optimal management of COVID-19. As per an estimate, Brazil and South Africa will have a health expenditure, 10.0 and 10.5% of their GDP, comparable with the world average of 10.4% GDP in the year 2025 (Jakovljevic et al., 2017). India's national health expenditure (<4%) is the lowest among the BRICS nations; however, it is expected to surpass the 4% of GDP in 2025. The projected national health expenditure

of Russia (8% of GDP) and China (7% of GDP) are also expected to lag behind the world average (Jakovljevic, 2015; Jakovljevic et al., 2017). The affordability of healthcare and medicine also depends on purchase power parity. However, the privileged vulnerable socioeconomic groups are supported through various government-led schemes for their healthcare (Gauttam et al., 2021). Amid the COVID-19 pandemic, the government of nations including those of the BRICS group offered indiscriminate support to all affected individuals. The insufficiency of the healthcare system has been lessened by public-driven initiatives and volunteer contributions in many countries. Nevertheless, diversity among BRICS nations exists in it is a substantial proportion of the rural population; the public health system is predicted to be effective in nations (Gauttam et al., 2021). Public health expenditure of BRICS countries impacted public health at the world level as well. The promotion of a healthy lifestyle, awareness, and physical activities (including sports activities) can adjunct the other attempts of health maintenance (Jakovljevic et al., 2019). This can be suggested to counter the COVID-19-associated physical and mental health problem.

Among BRICS countries PoU of Brazil, Russia, China (all 2.5), and South Africa (5.7) is low as compared to its global value (8.9; FAO, IFAD, UNICEF, WFP, and WHO, 2021). India has a very high PoU of 14. As PoU is weighted values against population size, these countries share a large number of individuals facing undernourishment. The undernourishment

**FIGURE 3** | Prevalence of undernourishment (PoU) in BRICS nations.
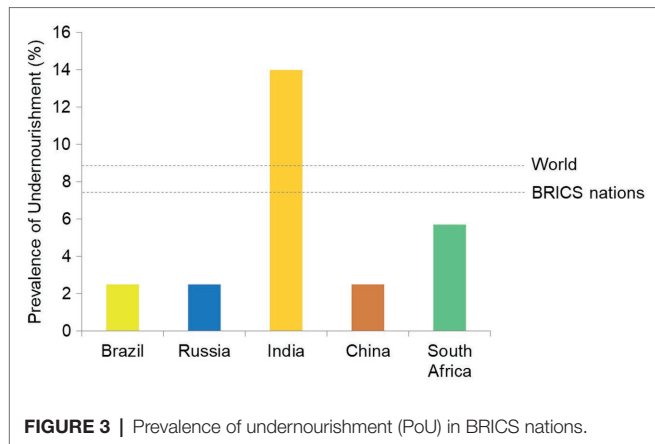
and nutritional deficiencies have wrecking consequences on health, both physically and mentally. The low nourishment state prevalent in BRICS nations (**Figure 3**) can be suggested as a driving force in COVID-19 morbidities.

Neuropsychological manifestations were also linked with the manifestations of COVID-19 and their severity. The collective prevalence of depressive disorders in BRICS nations (4.09%) is higher than the global average (3.91%; **Figure 4**). In absolute numbers, India, China, Brazil, and Russia share the 1st, 2nd, 4th, and 6th highest number of individuals affected with depression. BRICS nations collectively account for approximately 44% global burden of depression-affection individuals. Other mental health disorders also show a similar trend (Ritchie and Roser, 2018).

Owing to performances in nourishment status, healthcare access, mental health level, as well as distribution of population, BRICS nations individually as well as collectively plot a landscape for the menace in COVID-19 pandemic. The BRICS nations applied the measures suggested by WHO and acted promptly to prevent the transmission of COVID-19 through various measures including preventive and diagnostic strategic plans (Reshetnikov et al., 2020; Chattu et al., 2021; Gauttam et al., 2021). The diet habits, lifestyle, level of scientific awareness, and use of immunity boosters/supplements in these regions will have enduring consequences on the COVID-19 pandemic (Roser and Ritchie, 2019). However, the exertions in COVID-19 pandemic management (implementing WHO guidelines, preventive and curative management), and development and use of vaccines against COVID-19 reflect the efforts of these nations (**Table 1**). To prevent the hindrance in the development and distribution of vaccines, India and South Africa jointly appealed to the world trade organization (WTO) to waive off the trade and intellectual property-related issues to establish global health diplomacy (Chattu et al., 2021). The use of the digital platform for the spread of information and awareness was also observed in BRICS nations. Moreover, digital methods, computation strategies, and artificial intelligence can aid in predictions. Strategies including artificial neural networks have demonstrated effectiveness in predicting the propagation of COVID-19 and vaccination drive outcome in France, Germany, the United Kingdom, Portugal, and Italy (Carvalho et al., 2021). Similar approaches are being

utilized in BRICS countries, however, apart from many other factors; the accuracy of data is a major concern.

## VIRAL MANIFESTATIONS

SARS-CoV-2 infection is associated with complex viral illnesses that range from asymptomatic to severe symptomatic complications. The most critical manifestation is abnormal respiratory health which promotes respiratory disease such as acute respiratory distress syndrome (ARDS), among many other clinical features along with disease progression. The most common manifestations among these clinical features are fever, acidosis, cough, dyspnea, headache, myalgia, nausea, diarrhea, loss of smell and taste, coagulation dysfunction, organ failure, and ultimately death (Guang et al., 2021; Zhu et al., 2021).

About 20% of cases have severe complications such as dyspnea, hypoxia, and >50% lung infection observed in high-resolution-computed tomography (HR-CT) imaging require hospital admission. Among hospital admitted COVID-19 patients, about 5% develop critical disease and need intensive care for the management of hypoxemic respiratory failure or hypotension (CDC, 2021). SARS-CoV-2 severity is also age-dependent, and severity of illness is more frequent in patients of old age as compared to children younger than 10 years (Shi et al., 2020). Nevertheless, many other factors also influence the severity including pre-existing comorbidities. The case fatality rate (CFR) was significantly higher in the older population reported as 14%, whereas lower to approximately 2.3% in general individuals (Amore et al., 2021).

Till now, several general characteristics and diseased elements such as sex, age, high blood pressure, diabetes, chronic lung infection, dermatologic infection, endocrine and hepatobiliary complications, and cardiovascular manifestation are considered among the main risk factor observed during clinical managements of COVID-19 (Jordan et al., 2020; Yang et al., 2020; Jamshidi et al., 2021).

The spectrum of clinical cardiac presentations in COVID-19 patients includes acute coronary syndrome, myocardial injury, cardiac arrhythmias, cardiomyopathy, and cardiac shock, and thromboembolic complications. Some cardiac tests displayed an elevated level of troponin with the more lethal condition of patients (Guo et al., 2020; Shi et al., 2020). Recent reports indicate that immunological manifestations play a potential role in COVID-19 severity *via* promoting the development of extra-pulmonary features (Gupta et al., 2020). These features include thromboembolic complications, arrhythmia, GI symptoms, renal dysfunction, liver dysfunction, diabetic ketosis, and neurological deficits (Gupta et al., 2020; Soni et al., 2020d; Sahu et al., 2021). In addition, some patients can develop an aggressive hyper-inflammatory response, known as cytokine release syndrome, caused by an excessive reaction due to impaired IFN-1 response and transcription factor NF-κB with elevated TNF and IL-6 production (Hadjadj et al., 2020).

Apart from cardiac manifestations, abnormal digestive symptoms were also associated with disease severity and worst outcomes. GI complications include appetite loss [81 (79%)

**FIGURE 4 |** Prevalence of individuals with depression among the population of BRICS nations.
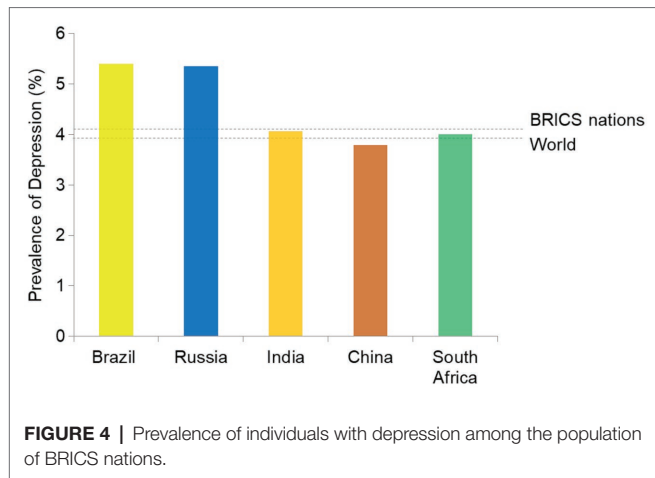
cases], diarrhea [35 (34%) cases], and vomiting [4 (4%) cases] on their clinical data with 204 COVID-19 patients (Pan et al., 2020; Sahu et al., 2021). Therefore, dysregulated GI function became more identifiable as the severity of the disease increased. GI dysregulations also affect the uptake and absorption of nutrients and provoke deficiencies (Sahu et al., 2021). Nutritional defects as a repercussion of anatomical and physiological damages caused by the systemic spread of SARS-CoV-2.

Neurological and psychiatric manifestations are also being observed in many severe COVID-19 patients (Mao et al., 2020). Neuropsychiatric consequences including episodes of anxiety, depression-associated disorders and mood distort were observed in a significantly large fraction of infected patients (Abers et al., 2014; Alpert et al., 2020; Tandon, 2020; Mehta et al., 2021). Notably, clinical data indicated that about 80% of infected cases have a mild infection and/or asymptomatic which can be managed without admission to hospitals with proper monitoring of physicians. However, these asymptomatic patients or those with mild symptoms pose a threat of onward transmission and spread of the pandemic. Nosophobia and uncertainty about treatment outcomes among these patients attract other psychological defects and warrant regular monitoring and counseling. Zubair et al. (2020) indicated that SARS-CoV-2 infection can affect the nervous system *via* several routes such as trans-synaptic transfer across infected neurons, olfactory nerve, infection of vascular endothelium, or leukocyte migration across the blood-brain barrier. According to a recent finding by three neuroscience bodies in the United Kingdom, the neuro-invasion of viruses develop dysphagia after their first acute ischemic stroke in the brain (Aoyagi et al., 2021). The severity of symptoms in COVID-19 patients is also a product of physical and mental health, nourishment, strain of SARS-COV-2, and timely diagnosis of infection.

# EQUATION OF COVID-19 AND MALNUTRITION

Incidence and progression of several illnesses including those of infectious mature largely depend on the nutritional profile of

the host and have a key influence on the outcome of therapeutic interventions. The global 2015 famine trend, indicated by the incidence of malnutrition, reversed since decades of consistent declines and has been stabilizing little below ~11% over the preceding 3 years (Ribeiro-Silva et al., 2020). However, a rise in the proportion of individuals suffering from starvation has been observed. As per an estimate one in every nine people across the globe was struggling with hunger in 2018. A recent appraisal in 2020 suggests that a population of 130 million has fallen in this struggle including a large proportion of 44 million minors (HLPE, 2020; Ribeiro-Silva et al., 2020). The socioeconomic distort brought by associated with public heath emergencies cannot be denied to aid in food unavailability to the large section of the population. Even, it is estimated that the current pandemic has the potential to push 49 million people into severe economic distress. Such distresses are forcing the unavailability of nutritive meals, leading to food insecurity and highlighting the enormous difficulty of achieving the Null Hunger objective by 2030~2050 (Prosekov and Ivanova, 2018; Ribeiro-Silva et al., 2020; UNICEF, 2020). Social restrictions and the potential risk of the contract with COVID-19 also hinder the aids from public initiatives feeding hungry people. These public group-driven initiatives of food donations also dribble due to their impeding financial condition in pandemic-driven economic load. On the communal level, this load decreases productivity, especially food production, and maintains the vicious circle of increased hunger, infection, disease, poverty, and socioeconomic and political instability (Silverio et al., 2021). Hyper infectious nature of SARS-CoV-2, especially it is few variants, countries including BRICS territories have taken unrivaled initiatives to combat COVID-19 transmission, ranging from the limited social exposure, revocation of public transit to social isolation (Zhao et al., 2020; Dash et al., 2021; Popkova et al., 2021; Rababah et al., 2021). Distinct nutrient deficiency or protein-energy deprivation has been shown to detrimentally affect the infection combating prospects along with diminished immunity level (Ambrus and Ambrus, 2004; Silverio et al., 2021).

COVID-19 exhibited a multitude of manifestations, spanning asymptomatic to the severe (Soni et al., 2020a; Silverio et al., 2021). Nutritional deficiencies especially protein-energy malnutrition, body profile, and hyperalimentation (over-nutrition) are among the major risk factors of deterioration, contributing to SARS-CoV-2 response (Cava and Carbone, 2021; Silverio et al., 2021). The risk is accelerated in COVID patients as stirring respiratory illness marked with hypercatabolism and inflammation syndrome, raises energy demands associated with ventilation effort (Thibault et al., 2021). The COVID-19 infection can also affect the assimilation of nutrients as the manifestations include the loss of appetite (Rao et al., 2008). Moreover, COVID-19-driven defects in the expression profile of nutrient-absorbing molecules in the GI tract of patients contribute to nutritional deficiencies (Sahu et al., 2021). These deficiencies culminate in the declined level of neurotransmitters (NTs) essential for mental well-being (França and Lotti, 2017; Amruta et al., 2021). The anxious and depressogenic events in infected patients further strengthen the consequences culminating in malnutrition (Fedotova et al., 2017). Possible routes of COVID-19-associated nutritional deficiencies are illustrated in **Figure 5**.

**TABLE 1 |** COVID-19 vaccine being used in BRICS nations.

| Country | Vaccines | Vaccine type | Route | Developer | Manufacturer/Importer | Approval |
|---|---|---|---|---|---|---|
| Brazil | Sputnik V | Adenovirus viral vector, RNA | IM | Gamaleya Research Institute of Epidemiology and Microbiology | | Restricted use |
| | BNT162b1 | RNA | IM | Pfizer Inc., BioNTech | | Under trial (III) |
| | BNT162b2 | RNA | IM | Pfizer Inc., BioNTech | | Approved |
| | Ad26.COV2.S | Non-replicating viral vector | IM | Johnson & Johnson (Janssen) | | Approved |
| | Covishield | Non-replicating viral vector | IM | Oxford University, Astrazeneca, Serum Institute of India | | Approved |
| | Oxford/Astrazeneca formulation | Non-replicating viral vector | IM | Oxford University + Astrazeneca + Coalition for Epidemic Preparedness Innovations | | Approved |
| | CoronaVac | Inactivated | IM | Sinovac Biotech | | Emergency use |
| | BBIBP-CorV | Inactivated | IM | China National Pharmaceutical Group (Sinopharm) and Beijing Institute of Biological Products | | Emergency use |
| Russia | EpiVacCorona | Protein subunit | IM | Vector Centre of Virology | | Approved |
| | KoviVac | Inactivated | IM | Chumakov Center | | Approved |
| | Sputnik V | Adenovirus viral vector, RNA | IM | Gamaleya Research Institute of Epidemiology and Microbiology | | Approved (Emergency) |
| | Sputnik light | Non-replicating viral vector | IM | Gamaleya Research Institute of Epidemiology and Microbiology | | Emergency use |
| | Convidecia/Ad5-nCoV | Non-replicating viral vector | IM, IN | CanSino Biologics | | Under trial (III) |
| India | Covishield | Non-replicating viral vector | IM | Oxford University, Astrazeneca, Serum Institute of India | | Approved |
| | Covaxin | Inactivated | IM | Bharat Biotech, Indian Council of Medical Research and National Institute of Virology | | Approved |
| | Sputnik V | Adenovirus viral vector, RNA | IM | Gamaleya | Panacea Biotech | Emergency approval |
| | mRNA-1273 (Spikevax) | RNA | IM | Moderna + NIAID + BARDA | Cipla (filed application) | Emergency approval |
| | Pfizer | RNA | IM | Pfizer Inc. | | Under approval |
| | Janssen COVID-19 | Viral vector | IM | Johnson & Johnson (Janssen) | | Emergency approval |
| | Covovax | Protein-based | IM | Novovax | Serum Institute of India | Under trial (III) |
| | ZyCoV-D | DNA (Plasmid expressing SARS-CoV-2 protein) | ID | Cadila Healthcare + Biotechnology Industry Research assistance Council (BIRAC) | | Awaiting approval |
| | BBV154 | Viral vector | IN | Bharat Biotech + American company Precision virologics + Washington University School of Medicine | | Under trial (II) |
| | Corbevax/BECOV2D/BioE COVID-19 | Protein-subunit (Antigen) | IM | Biological E. Limited (BioE), the Baylor College of Medicine in Houston, United States, and American company Dynavax Technologies (DVAX) | | Under trial (II) |
| | HGC019 | mRNA | IM | Gennova Biopharmaceuticals and HDT Biotech Corporation with active support from Department of Biotechnology, India | | Under trial (I) |
| China | BBIBP-CorV | Inactivated | IM | China National Pharmaceutical Group (Sinopharm) and Beijing Institute of Biological Products | | Approved |
| | Convidecia/Ad5-nCoV | Non-replicating viral vector | IM, IN | CanSino Biologics | | Approved |
| | SARS-CoV-2 Vaccine (Vero Cells) | Inactivated | IN | Shenzhen Kangtai Biological Products Co. Ltd., and Minhai Biotechnology Co. Ltd. | | Approved |
| | CoronaVac | Inactivated | IM | Sinovac Biotech | | Approved |
| | Inactivated (Vero Cells) | Inactivated | IM | China National Pharmaceutical Group (Sinopharm) and its Wuhan Institute of Biological Products. | | Approved |
| | ZF2001/RBD-Dimer | Protein subunit | IM | Anhui Zhifei Longcom in collaboration with the Institute of Microbiology at the Chinese Academy of Sciences. | | Emergency use |
| | SCB-2019 | Protein subunit | IM | Clover Biopharmaceuticals using an adjuvant from Dynavax | | Under trial (III) |
| | INO-4800 | DNA | IM | Inovio Pharmaceuticals | | Under trial (III) |
| | BNT162b1 | RNA | IM | Pfizer Inc. + BioNTech | | Under trial (I) |
| | BNT162b2 | RNA | IM | Pfizer Inc. + BioNTech | | Under trial (II) |
| | Recombinant (Sf9 cell) | Protein subunit | IM | West China Hospital of Sichuan University | | Under trial (II) |
| South Africa | BNT162b1 | RNA | IM | Pfizer Inc. + BioNTech | | Under trial (III) |
| | BNT162b2 | RNA | IM | Pfizer Inc. + BioNTech | | Emergency use |
| | Ad26.COV2.S | Non-replicating viral vector | IM | Johnson & Johnson (Janssen) | | Approved |
| | Covishield | Non-replicating viral vector | IM | Oxford University, Astrazeneca, Serum Institute of India | | Approved |
| | CoronaVac | Inactivated | IM | Sinovac Biotech | | Emergency use |

*ID, intradermal; IM, intramuscular; and IN, intranasal.*

**FIGURE 5 |** Nutritional deficiency triggered by the COVID-19 pandemic can affect physical and mental health through psychoneuroendocrineimmune (PNEI) modulation.
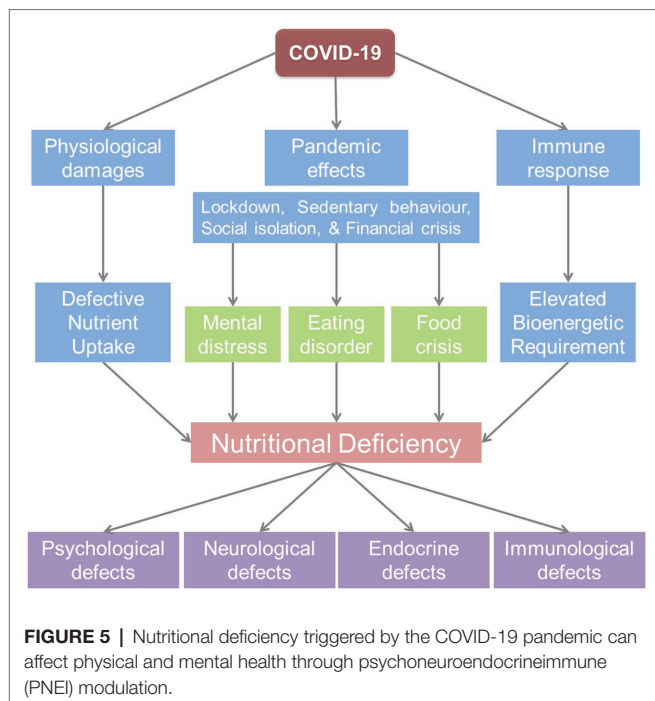
Protein Energy Malnutrition is a specific single nutrient deficiency, a frequent etiology of acquired immunodeficiency (SID, Secondary Immuno-Deficiency), and vulnerability to infections (Ambrus and Ambrus, 2004; Ulrich and Kaufmann, 2007). Immune cells have significant calorie consumption and in the events of response such as during infection, these energy and nutrient requirements significantly enhance (Cutrera et al., 2010). An elevation in basic metabolic rate (BMR) observed during fever owing to the activation of the inflammatory response can be attributed to meeting such requirements (Childs et al., 2019). Systemic consequences of lung infection such as cytokine storm and spread of SARS-CoV-2 can invite anatomical damages in multiple organs affecting vital functions. The GI cells (intestinal epithelium) also express ACE2 receptor in abundance, which serves as an anchor for SARS-CoV-2 to infect the host cells. As a result, SARS-CoV-2 infection could impair the digestive function resulting in GI problems (nausea, anorexia, diarrhea, etc.) and a reduction in patients' nutritional-metabolic status (Huang et al., 2020). Anorexia combined with diarrhea was indicated to add in nutritional disequilibrium resulting in the lag phase of recuperation (Mobarhan and DeMeo, 1995). Therefore, it is clear that SARS-CoV-2 infection will provide a landscape for malnutrition to manifest through direct anatomical and physiological damages leading to deficient absorption of nutrients. Nevertheless, the nutrient requirement in infected patients is higher to meet the demand of responding immune system components (cells and organs). Moreover, the nutrient deprivation and inflammatory consequences in infected patients attract the neuropsychiatric ailments causing stress-driven loss of appetite. The perceived fear of COVID-19 contraction and therapeutic outcome also pour into psychiatric distort in both normal and SARS-CoV-2-infected individuals.

The pre-existing malnutrition or deficiencies in specific nutrient have compounded effect with SARS-CoV-2 infection in engaging COVID-19-associated malnutrition and negatively affect the therapeutic outcome. Considering the nutritional deficit and its role in aggravated manifestation of clinical symptoms, food and food supplements able to replenish the calorie requirements can be of immense help. Additional medicinal benefits associated with food ingredients will be of added advantages in many human disorders including COVID-19 (Soni et al., 2020a; Singh et al., 2021). Mushroom is of such ingredients rich in protein content which fulfills energy requirements and also aids in curative as well as preventive measures against various human health anomalies (Singh et al., 2021). The medicinal benefits of mushrooms encompass the antioxidant, anti-inflammatory, anti-infective as well as anticancer activities (Singh et al., 2021).

## THE INTERPLAY OF NUTRITION AND PNEI MODULATION IN COVID-19

The significant loss of muscle mass as well as a deterioration of immunological defenses, which collectively add to the gravity of COVID-19, would thus be linked with the chronic malnutrition driven by SARS-CoV-2 infection (Thibault et al., 2021). Various regulators of immune response and neuroendocrine system (NTs, etc.) are derived from dietary components [amino acids (AAs), etc.]. Moreover, the interdependency of the neuroendocrine and immune system affects both of them even in the circumstances directly deteriorative only for one. Therefore, optimal dietary nutrition is a key to maintain immunity as well mental well-being; undernourishment damages folk's psychological health, emotional resilience affecting their capability to cherish life and deal with pain, deception, and grief (Ferguson et al., 1999). Intervened regulatory network and interdependency significantly affect the immunological responses under neuropsychological defects. Through PNEI regulatory elements, immunological events/mediators prevailing in the body of the host shake the neuroendocrine processes systemically. The possible triggers of homeostatic imbalance by neuropsychological abnormalities through PNEI modulation are presented in **Figure 6**. This cross-talk across systems is meticulously pruned by feedback threads that operate in tandem to preserve homeostasis balance (França and Lotti, 2017).

### Metabolic Deficiency as an Induction Loophole

Acute respiratory distress syndrome, PNA inflammation, hyperthermia, consumption coagulopathy (intravascular disseminated coagulation), multi-organ dysfunction, and GI impairment are only a few of the clinical symptoms of COVID-19 (Mitchell, 2020; Soni et al., 2020a; Fedele et al., 2021; Sahu et al., 2021) Among COVID-19 patients, metabolic linkage of psychiatric problems are also invariably mentioned (Mohan et al., 2020; Tandon, 2020). Exposure and risk of contraction with SARS-CoV-2 are majorly governed by lifestyle, presence at public places, and chance incidental acquaintance with

**FIGURE 6 |** Neuropsychological abnormalities can adjunct the COVID-19 pathophysiology.
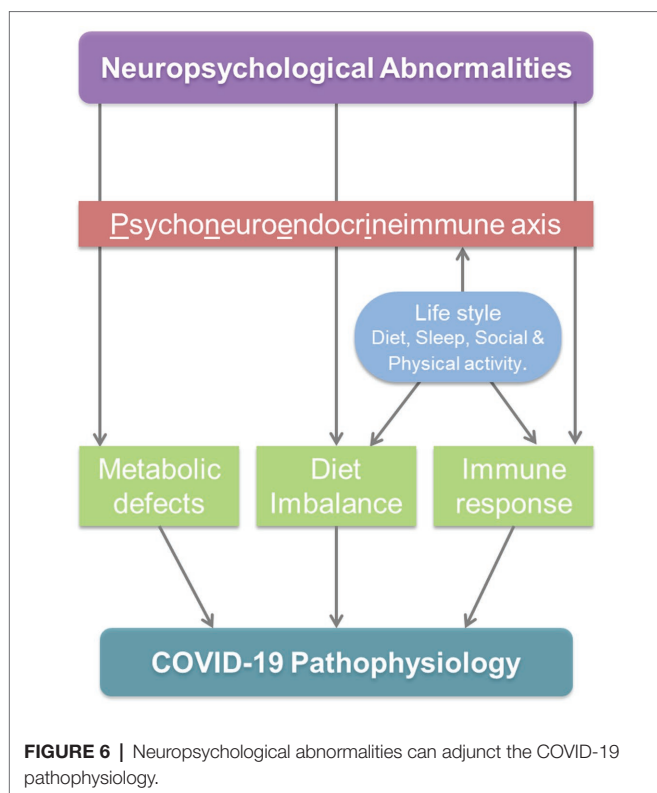
infected individuals. However, the establishment of infection and degree of symptom severity is largely affected by nutritional state. Deficiency of nutrients, especially of those which serve as the precursors for immunological or neuroendocrine regulators or mediators, is associated with undesirable disease progression and treatment outcome (Mehta et al., 2021). Therefore, along with attempts to improve the immune response, medical nutrition treatment (MNT) for severely sick COVID-19 patients is being considered against the critical issue of malnutrition-driven complications (Rozga et al., 2021). The absence or deficiency of metabolites deregulates the gradient and availability and creates a shift in homeostasis leading to the manifestation of ill effects. Among many, AAs and vitamins provide crucial mediators of the PNEI regulatory network; and deficiencies of these will negatively affect the strength of infected individuals to withstand mental distorts as well as dampen the immunity level.

## Amino Acid Deficiency

The deficiency of amino acids has been linked with various pathological conditions. Moreover, the deficiency of this nutrient correlates with severity as well as manifestation of a few exclusive symptoms associated with diseases (Elmadfa and Meyer, 2019; Chen et al., 2020c). COVID-19 is no exception for this. Interestingly, pathological manifestations associated with COVID-19 also pave the path for deficiencies of these critical nutritional components mediating diverse biochemical events. In a systemic spread of SARS-CoV-2 infection, physiological and anatomical damages in the GI tract culminate into impaired absorption of nutrients leads to nutritional deficiency (Sahu

et al., 2021). The molecular linkage between SARS-COV-2 infection and amino acid deficiencies is also explored in various investigations. The sodium-dependent neutral amino-acid transporters ($B^0AT1$) expression level is suppressed by the aberrant form of SARS-CoV-2 entry gate enzyme, angiotensin-converting enzyme-2 (ACE-2; Warner et al., 2020). The diminished expression of nutrient transporters including $B^0AT1$ impairs the absorption of AAs (Huang et al., 2020; Wang et al., 2021). The resultant imbalance in the amino acid pool leads to diverse pathophysiological consequences both on physical and mental health (Carnegie et al., 2020). The expression of flawed $B^0AT1$ in COVID-19 patients is correlated with psychiatric signs similar to those in Hartnup disorder, which also shares defective expression of amino acid transporters (Soni et al., 2020d; Mehta et al., 2021). Moreover, anorexia in COVID-19 also contributes to the deficiencies of nutrients including amino acids. Anorexia is induced by secondary clinical manifestations in COVID-19 like GI issues; and physiological impairment triggered by viral infection impedes nutrition intake, resulting in nutrient mal-absorption. Pre-existing amino acid deficiencies are also speculated to enforce the severity of ill effects associated with COVID-19 (Bedock et al., 2020; Rozga et al., 2021). Through potentiation of anti-infective immune response, dietary nutrients keep immune response optimal to prevent establishment of any invading pathogen in the host body. Although contrasting links were observed between malnutrition and clinical signs associated with SARS-CoV-2 infection, studies found a positive correlation between poor prognosis, severity, and mortality with deprived nutritional state (Nicolau et al., 2021). Early nutritional profiling of infected patients is suggested to favor better clinical outcomes through supplement or diet management (Bedock et al., 2020). Though nourishment therapy delivers necessary nutrients, it is feasible that supplementing regular nutrition support with conditional amino acids may result in a greater capacity for recuperation and nutritional stability (Rozga et al., 2021).

Amino acids are not just the architectural element of proteins, they are also essential in the homeostasis of emotional and neuropsychiatric wellness. Disturbances *via* dietary shortfalls cause mood swings as they serve as precursors for various NTs and hormones regulating the psychological consequences and its interrelation with PNEI (Slominski et al., 2002; Mehta et al., 2021). Such detrimental consequences aid up in the deteriorative effects of COVID-19 (Zubair et al., 2020). The biosynthesis of 5-hydroxytryptamine, 5-HT (Serotonin) requires Tryptophan, an essential AA; and the deficiency of tryptophan lowers the serum concentration of serotonin (Bjork et al., 2000). Pioneer investigations have revealed that the lower levels of tryptophan in plasma are linked to a greater likelihood of aggression, anxiety, and depressive disorders (Bjork et al., 2000; Von Polier et al., 2014). Psychological resilience and neuroticism are dictated by metabolic derivatives of amino acids (including tryptophan catabolites; TRYCAT). Numerous NTs including GABA, dopamine (DA), epinephrine, and norepinephrine are deduced from a diverse spectrum of amino acids (including glycine, tyrosine, phenylalanine, glutamate, etc.; Rao et al., 2008; Carnegie et al., 2020; Mehta et al., 2021). Amino acid

anomalies in COVID-19 are anticipated to influence both physiological and mental well-being. Supplementation of conditional amino acid and/or incorporating food items rich in protein/amino acid contents can be expected to not only overcome the bioenergetics deficiencies but will also provide benefits in maintaining the psychosomatic homeostasis.

## Vitamin Paucity

Vitamins have their role in preventing infection through strengthening the anti-infective immunity. Since the onset of the pandemic, the immuno-nutritive potency of vitamins, especially Vitamin C and D, has gained much attention. Accumulating findings have begun to give greater weight to possible links between the prevalence and severity of COVID-19 with vitamin levels of the infected patient (Lanham-New et al., 2020; Lordan, 2021). Vitamin D has also been shown to affect the pathological consequences of many other diseases. In obese persons with relation to geography and age, the prevalence of vitamin D (Vit D or calciferol) inadequacy is 35 times greater (Holick, 2017). Vit D, a fat-soluble secosteroid hormone, can act as an immunomodulator as well as antioxidant (Lee et al., 2018; Lanham-New et al., 2020). Moreover, it has historically been linked with altered hematopoiesis and PNEI reactions to optimize immunity and cognitive health (Fedele et al., 2021; Mehta et al., 2021).

Vitamin D enhances the synthesis of respiratory epithelial antimicrobial peptides (such as human β-defensin-2 and cathelicidin) and therefore reduces the frequency of disease onset and COVID-19 effects (Mitchell, 2020; Hernández et al., 2021). As the twin response, it is also engaged in the prophylaxis of viral respiratory tract infections (RTIs) and acute lung damage, as documented in ARDS condition, where lung permeability diminishes due to modification of ACE-2 expression and renin-angiotensin system interaction (Mitchell, 2020; Fedele et al., 2021). Calciferol deficiency has also been aligned to neuropsychiatric afflictions such as Autism and major depressive disorder (MDD). Furthermore, in COVID-19, a decreased serum 25-hydroxyvitamin D level has been related to psychological distress signs (Basheer et al., 2017; Lordan, 2021). The levels of serotonin (5-HT), DA, and estradiol (E2) in the brain are all affected by vitamin D deficiency as it activates neuronal activity by triggering vitamin D receptors (VDR) in the central nervous system (Di Nicola et al., 2020; Mehta et al., 2021).

Other players of the vitamin bandwagon, like Vitamin A, B, and E, are also playing a significant role in combatting COVID-19 infection and their deficiency may too result in crisis. Vitamin A and B are shown to be critical for maintaining gut integrity; and deficiency will lead to impairment in barrier function (Yoshii et al., 2019; Calder, 2020). In asymptomatic individuals without chronic pulmonary problems, vitamin A depletion is linked to a minimal forced vital capacity FVC (FVC). A low FVC is an indicator of airway blockage and a substantial marker of fatality. Functional maturation of phagocytes neutrophils and macrophages are also affected by Vitamin A depletion leading to impaired ability of these cells to kill pathogens (Calder, 2020). Among the vitamin B family, Vitamin

B1, B3, and B5 are majorly involved in the regulation of phagocytosis and inflammatory cytokine production by macrophages (Yoshii et al., 2019). As B3 can resist the production of inflammatory cytokine (Lipszyc et al., 2013) and favors the differentiation of regulatory cells through GPR109a signaling (Lipszyc et al., 2013; Yoshii et al., 2019), its deficiency is suggested to exaggerate the inflammatory consequences and cytokine storm in COVID-19. Along with innate immune responses, Vitamin D also supports acquired immunity by driving the proliferation and functionality of B and T lymphocytes. Similarly, vitamin C also protects cells from oxidative stress as well as acts as an immune system regulator suppressing the release of pro-inflammatory cytokines (Elmadfa and Meyer, 2019). According to a recent comprehensive analysis, intravenous (IV) vitamin C treatment might minimize the need for mechanized ventilation presumably by curbing lung damage, without influencing the overall risk of death (Zhang and Jativa, 2018).

Vitamin A deficiency can negatively affect the optimal formation of specific antibodies after immunization attempts (Penkert et al., 2019). Moreover, vitamin D deficiency deteriorates the seroprotection after vaccination against respiratory viral disease (Lee et al., 2018). Deficiencies of different vitamins are prevalent in BRICS countries (Awe et al., 2021), and are anticipated to hinder the optimum effectiveness of COVID-19 vaccination drives in these parts of the globe. Various publications have advocated for the supplementation of vitamins in SARS-COV-2 infected patients as well as to the individuals receiving COVID-19 vaccines for better recovery and immune response (Calder, 2020; Shakoor et al., 2020).

Despite the role in immune response modulation, vitamins also affect the psychoneurological inter-regulation (Soni et al., 2020b; Mehta et al., 2021). Nevertheless, vitamin deficiency-induced defects in immune response also affect psychosomatic well-being through PNEI modulation (Cornish and Mehl-Madrona, 2008; Calder, 2020; Soni et al., 2020b). The positive correlation between the severity of COVID-19 symptoms and undesirable clinical outcome with vitamin deficiencies (Mohan et al., 2020) can be suggested to have a contribution in frequent psychiatric manifestations in infected patients. Moreover, the restriction measures at the social and occupational level along with uncertainty about health, perceived fear, and associated factors act as additional factors contributing to deficiencies of these psycho-immune active vitamins. The most notable vitamin in the linkage of COVID-19 and depressive disorders is vitamin D (Shakoor et al., 2020; Ceolin et al., 2021). Vitamin D plays a critical role in the maintenance of the chronobiological rhythms through Vitamin D binding protein and VDR (Jones et al., 2017; Ceolin et al., 2021). Vitamin D also acts as an antidepressant; upholds serotonergic neurotransmission through induction of tryptophan hydroxylase 2 gene expression (Ceolin et al., 2021).

Unique prevalence status of psycho-neurological disorders in parts of BRICS countries (Charlson et al., 2016) and deficiencies of nutrients (Awe et al., 2021) can be suggested to have a causal association. These deficiency frequencies in BRICS countries will have additional contributions in defective immune

response and associated neuropsychological consequences in the COVID-19 pandemic dissimilar to other parts of the world. The paucity of medicines including nutritional supplements and vitamins in parts of the world including BRICS nations affect the optimal management of the COVID-19 pandemic (Jakovljevic, 2015; Godman et al., 2020). Although countries of the BRICS group have taken quite similar measures to prevent the spread of SARS-CoV-2, the preparedness and attempts to prevent psychological ailments seem to be different (de Almondes et al., 2021).

## Role of Altered Immune Response

In many contexts, malnutrition has been associated with immunological dysfunction, notably hunger and cachexia. It has been confirmed with investigations both in human and animal models. Nevertheless, starvation also hampers T cell cytokine synthesis along with significantly decreasing T cell counts (Mengheri et al., 1992). A cumulative rise in the generation of pro-inflammatory cytokines and an infantile inflammatory reaction is attributed to an elevation in fat saturated with N-6/N-3 PUFAs (Teasdale et al., 2019). The systemic energy equilibrium including glucose and lipid metabolism is governed by a variety of PUFAs operating as natural ligands for PPARs and SREBP (Muralikumar et al., 2017). Consequently, an imbalanced n-6/n-3 PUFA ratio in serious mental illness (SMI) patients may add to hyperglycemia, dyslipidemia, and obesity risk indirectly *via* PPAR and SREBP transcriptional activation. This theory may be relevant to COVID-19 since persons with such conditions have a higher risk of catastrophic consequences (Choi et al., 2020; Zhou et al., 2020).

The investigators hypothesized a link between ingesting foods with high anti-ACE activity and having a low COVID-19 mortality rate (Nadalin et al., 2021). Few of the countries with low mortality rates such as Bulgaria, Greece, and Turkey record for consumption of fermented milk, which is known to be an organic ACE inhibitor. These observations might be explained by a decrease in angiotensin II (Ang II) synthesis, and preventing the pro-inflammatory state and subsequent acute lung damage leading to more drastic consequences COVID-19 embodiment (Warner et al., 2020). According to research from China, individuals with progressed COVID-19 had remarkably accelerated inflammatory indices in their bloodstream, and plasma ferritin, C-reactive protein, and IL-6 levels were considerably enhanced in non-survivors than veterans (Chen et al., 2020b; Zhou et al., 2020).

Further, bioenergetics requirements during immune responses in COVID-19 are heightened leading to utilization of available nutrient resources. It will be noteworthy to mention here that owing to social distancing measures and restricted outdoor activities, the nutritional imbalance prevails in large geographical areas of the world including those of BRICS countries (Zhu et al., 2021). This is linked with health vulnerability in the region with the incidence rate of infections (Zhu et al., 2021). The activation of immune response and associated energy demand can cumulatively shore up the nutrient deprivation worsening the PNEI response. The severity of COVID-19

symptoms and cytokine storm has been linked with incidences of depression episodes in patients. Molecular events of inflammatory immune responses like the stimulation of NLRP3 inflammasome have been linked with neuro-invasion and onset of neuropsychiatric disorders (Ribeiro et al., 2021). Moreover, anxiety about treatment outcome along with other depressive disorders leads to loss of appetite. Depression itself has been shown as an inducer of an inflammatory immune response. Low food intake and mal-absorption can expectedly hamper the optimal immune response as well as neuropsychological well-being.

## Dietary Restriction as a Triggering Agent

Diseases triggered by nutritional imbalance, as well as other dietary ailments, have been considerably reduced in populations in developed countries. This is owing to an upgraded insight of the priority of nourishment, augmentation of specific food items, and rapid substantial improvements in the standard of living (Childs et al., 2019). However, dietary restrictions are prevalent in parts of the globe, which can be suggested to be an underlying cause of nutritional imbalance. The factors influencing the diet restrictions range from non-availability of specific food items, preferential choice due to customary dietary habits and religious beliefs (Persynaki et al., 2017). These dietary restrictions practiced among diverse socioeconomic and religious groups have both beneficial and harmful health consequences (Persynaki et al., 2017; Pourabbasi et al., 2021). Such dietary restrictions may lead to nutritional insufficiency that attracts various health conditions. The diverse religious groups and climatic conditions in BRICS countries affect the diet practices and can be suggested to influence the COVID-19 consequences. Although socio-scientific links can be traced to the climate and agricultural practices in the region of origin for the specific religion or practice, a customary adaptation of such food habits/restrictions exists (Tan et al., 2013). The copious presence of groups practicing fasting, for a specific time or food items, can be seen in the territories of BRICS countries. Preventive measures associated with the COVID-19 pandemic also differentially influenced the dietary habits of various groups of the population (Bennett et al., 2020). Moreover, food allergies and intolerance compel absentees from certain food items (HLPE, 2020). The pandemic also affected the availability of safe food items to these allergic patients which further increases the risk of deficiencies (Mack et al., 2020). Psychological manifestation linked with a pandemic is also suggested flaring the food allergic response in individuals. Nutritional inadequacies can bring up temporal immunodeficiencies and have neuropsychological consequences (Sarris et al., 2015). Dietary restrictions-led deficiencies in either physical or mental health will be prompting the defect in others through mediators of the PNEI axis (Bennett et al., 2020; Mehta et al., 2021). It will be noteworthy to mention that scientifically planned diet restrictions have health benefits even in COVID-19 (Ambrus and Ambrus, 2004; Rozga et al., 2021; Silverio et al., 2021). Recently gaining a diverse form of vegetarianism including vegan, lacto-vegetarian diets, etc., may lead to deficiencies of some nutritional elements. Such specific diet habit-driven

deficiencies can be replenished with conditional supplementation (Soni et al., 2020b; Mehta et al., 2021; Rozga et al., 2021). Many of the COVID-19 patients under recuperation have preferential food habits due to lifestyle and religious practices, and these supplementations may aid the convalescence in these patients. One of the sought strategies to supplement the essentials is probiotics (Mack et al., 2020; Mak et al., 2020). While probiotics supplementation has demonstrated direct association with the immune system and may avoid many kinds of infections, delusional use of standard probiotics for combating COVID-19 is not advised until understanding its influence on the intestinal microbiota and SARS-CoV-2 pathogenesis (Mak et al., 2020). The optimal dietary approach in the management of COVID-19 patients relies on the individual's health status (Childs et al., 2019; Rozga et al., 2021; Sahu et al., 2021). For the patients with COVID-19 consumption issues, whey protein fortification and a supplement that combines vitamins and minerals covering daily requirements are suggested (Hernández et al., 2021). Conversely, regimens with meals of various textures and consistence, readily digested (e.g., yogurt or custard, fruit mousse, fruit slices, and soft cheese), of at least 25–30 kcal/day, are advised for individuals that are not in a severe condition (Yamamoto et al., 2020). The general method for handling COVID-19 people from the ICU to the clinical ward is comprised of dietary interventions, medical nourishment treatment, careful supervision, and prompt follow-up. Optimal nutritional interventions, particularly in the fragile aged, immuno-compromised, and those with dysthymia who may be undernourished or at the nutrition risk can assure longevity along with a healthier and faster recuperation from this condition (Barazzoni et al., 2020). The dietary restriction-associated neuroimmunological consequences can be averted by surveillance and information management of nutritional status and dietary monitoring.

## Influences of Activity Deprivation

COVID-19 pandemic affected the various dimensions of life. The measures taken to counter the rapid spread of SARS-CoV-2 distorted the lifestyle and work practices (Soni et al., 2020b). The lockdown and work-form-home adaptations restricted the outdoor activities. This distorts put an unprecedented and unwelcomed but compelling alteration in daily routine culminating into changes in diurnal activities (Hammami et al., 2020; Kumar and Nayar, 2021). These deviations in routine physical activity, outdoor movements, and social interactions create a depressogenic state conducive for medium and long-term psychological consequences (Holmes et al., 2020). Stay at home condition is an oddity that compels individuals to change regular lives and everyday routines. Behavioral adaptations to these activity-restricted conditions in ongoing pandemic hamper the desire to do feasible work (Girdhar et al., 2020). This confining situation triggers mental pathologies of psychosomatic origins like anxiety issues, frustration, shifts of circadian rhythm, insomnia, impulsiveness, hypervigilance, etc (Clemente-Suárez et al., 2020; Kumar and Nayar, 2021). Episodes of PTSD and major depression disorder (MDD) have been observed to increase with the periods of isolation and confinement (Soni et al., 2020b). Among many, age has been a critical factor affecting the manifestations of these psychiatric conditions (Soni et al., 2020d; Steardo and Verkhratsky, 2020). Physical activity restrictions have detrimental consequences on the qualitative and quantitative magnitude of immune response including those in COVID-19 (Hammami et al., 2020). The onset of psychiatric disorders can also be suggested as a maneuvering force for wrecked immunity (Clemente-Suárez et al., 2020). Through the modulation in the PNEI network, fluctuations in the immune system, psychological state, and neuroendocrine coordination are conveyed to each component (França and Lotti, 2017; Soni et al., 2020b; Steardo and Verkhratsky, 2020). Social distancing measures have a detrimental influence on physical activity and had prolonged the hours of sitting and lying (Hammami et al., 2020). Moreover, COVID-19 patients with prolonged lying on bed and artificial ventilation usually incur deep muscular weakness, decubitus ulceration (bedsores), dysautonomia, and respiratory dysfunction (Yamamoto et al., 2020). These conditions evoke a stringent pulmonary illness balancing abnormalities, post-intubation regurgitation, postural hypotension, deep venal thrombosis (DVT), joint contractures, etc. (Yamamoto et al., 2020), and thus, need extra care and rehabilitation. Given the necessity of physical fitness maintenance, concepts of home-based workout with physical performance assessments tailored as in-house fitness alternatives are propagated for the amid the COVID-19 outbreak (Chen et al., 2020a; Clemente-Suárez et al., 2020). Suggestive performance checks on daily basis and application of practical residence practices can offset the deleterious repercussions of the passive lifestyle during solitary confinement (Chen et al., 2020a; Clemente-Suárez et al., 2020; Hammami et al., 2020). Alleviating the physical health through these modalities during COVID-19 pandemic can also be suggested to improve the digestion, nutrient balance, and immunity along with improved neuropsychological health.

## Perceived Nosophobia and Psychiatric Link

COVID-19-related neuropsychiatric problems, including depression, anxiety, traumatic stress disorder, and so on, tend to be prevalent, and cover a broad variety of fractious phenotypes that have a detrimental influence on the quality of life (Ribeiro et al., 2021). Social distancing measures, isolation, and quarantine, and uncertainty are among plausible reasons for the discontent observed in service users seeking psychiatric treatment for personal well-being and emotional resilience (Barazzoni et al., 2020; Tandon, 2020). Unfortunately, this epidemic has led to a rise in maladaptive survival strategies such as the use of materials as well as suicide (Czeisler et al., 2020; Amruta et al., 2021). In the last couple of years, the involvement of the immune interface with the CNS framework in psychiatric health and stress response has been the focus of extensive investigations (Calder, 2020; Aoyagi et al., 2021), which uncovered many conventions facilitating neuropsychiatric comorbidities by immune stimulation (i.e., by viral infection; Steardo and Verkhratsky, 2020).

Symptoms of PTSD are being observed in SARS-CoV-2 infected patients as well as among those who have not contracted the COVID-19 (Lai et al., 2020; Mao et al., 2020; Aoyagi et al., 2021). Nosophobia of COVID-19 and uncertainty of subsequent treatment outcomes have also contributed to these observed neuropsychiatric consequences (França and Lotti, 2017; Soni et al., 2020d; Steardo and Verkhratsky, 2020; Mehta et al., 2021). Bilateral contributions from immune stimulation and psychological distress through PNEI regulation also exist (França and Lotti, 2017; Steardo and Verkhratsky, 2020; Mehta et al., 2021). Prolonged distress boosts the level of pro-inflammatory chemokines like TNF-α, interleukins (IL-1, IL-6) and stimulates activation of indolamine-2,3-dioxygenase (IDO). IDO triggers the generation of tryptophan catabolites (TRYCATs) which are psychoactive. Under the homeostatic state, the levels of neurotoxic and neuroprotective TRYCATs are balanced; and any imbalance can be sought to elicit PNEI disturbances (França and Lotti, 2017; Steardo and Verkhratsky, 2020). In the pandemic, TRYCATs have established a health degradation anxiety-immune-neuropsychiatric-immune cycle (Soni et al., 2020b). The patients admitted to the intensive care unit (ICU) are frequently stressed; feel mental health burden frequently observed in severely affected by COVID-19 (Yamamoto et al., 2020). In addition to infected patients, medical professionals working at the forefront also have fairly high emotional and physical strain and develop signs of anxiety, sadness, sleeplessness, and discomfort in their working environment, particularly in high-risk regions (Lai et al., 2020; Yamamoto et al., 2020). Long working hour demand in management of pandemic restricts their dietary routines. The inadequacy of medical professionals in parts of globe including those in BRICS countries also contributes to demand of long working hours without any resting periods. This can be suggested as underlying factor driving the physical, psychological, and nutritional stress. These stresses make healthcare professional more susceptible in their work environment. Therefore, it can be suggested that prevailing dietary restrictions are affecting the COVID-19 risk and severity; and the contractions of infection and measures to combat pandemic may also drive the constraint on diet practices. The monitoring and maintaining the diet as per guidelines and medical conditions can have an adjunct effect in alleviating the ill effects of on-going pandemic.

# THERAPEUTIC MEASURES AND REMEDIAL PLAN

Until recently, there is no proven and effective antiviral treatment exists to mitigate the COVID-19 infection. The current treatment guidelines and management strategies vary between countries worldwide. The inclusion and weightage on the management of psychological manifestation and their influences through nutrition and immune response also varies in different countries. The bidirectional cooperation between COVID-19 and psychiatric disorders is being reported (Wang et al., 2020). The PNEI mediators are also suggested to deteriorate the immune responses through this linkage of COVID-19: psychiatric consequences.

Owing to the crucial role of nutrition in both immune response and mental health, dietary management holds a good place in the therapeutic regimen against COVID-19. Therefore, the recommendation of one approved guideline at a global scale might be highly appreciated in all aspects of treatment planning. However, the rapidly growing evidence in SARS-CoV-2 research provides a significant number of sites for potential drug targeting. Currently, some conditional solutions and psychological canceling are available for the clinical management of the ongoing viral outbreak. In the current scenario, the vaccination program is on the high priority to break the chain of infection to prevent further transmission of COVID-19.

## Conditional Treatment

To date, there is no specific and effective antiviral treatment established to fight COVID-19. Although there are many antiviral drugs under initial investigation and clinical trial phase which may hold promise against coronavirus-2.[1] Repurposing clinically evaluated old drugs are the major available therapeutic candidates that come from established clinical pieces of evidence from the previous pandemic such as SARS-CoV, MERS-CoV, and other influenza virus outbreak (Ratre et al., 2020). These conditional options are the only available cure for identification, mitigation, and deployment of treatment of COVID-19-associated pathological manifestations. Toward this end, some previously approved antiviral therapies including the HIV-1 protease inhibitors lopinavir (LPV) and ritonavir, the hepatitis C protease inhibitor danoprevir, and the influenza virus RNA-dependent RNA polymerase inhibitor (RdRp) favipiravir are under clinical investigation (Cao et al., 2020).

Lopinavir is a clinically tested agent, against HIV-1 and influenza viruses, approved for combinational treatment with fix dose of ritonavir (Chu et al., 2004). A review of studies reveals that investigations observing the effectiveness of combination therapy of lopinavir/ritonavir are clinical case reports, small retrospective; nonrandomized cohort studies (Yao et al., 2020). This makes it more challenging to ascertain the straightforward benefits of these potential agents. Nevertheless, a recent randomized clinical trial of lopinavir/ritonavir (400/100 mg, twice-daily for 14 days) in 199 hospitalized patients with severe COVID-19 and found no significant effect with lopinavir/ritonavir treatment compared with standard therapy (Cao et al., 2020). In addition, Deng et al. (2020) reported that combination therapy of LPV-r and arbidol was associated with improved lung morphology observed by pulmonary computed tomography images. Favipiravir is an RdRp inhibitor that blocks the replication of a virus *via* acting as a prodrug of a purine nucleotide (Sanders et al., 2020). This agent has significant antiviral activity ($EC_{50} = 61.88\,\mu M/L$) against SARS-CoV-2 (Wang et al., 2020). However, the limited number of clinical data is supporting the use of favipiravir for COVID-19. A randomized clinical trial-based study with 120 moderate and severe SARC-CoV-2 patients demonstrated the administration of favipiravir compared with Arbidol and found

[1]https://clinicaltrials.gov

that there is no clinically significant difference in recovery at day 7 with both drugs (71.4% favipiravir and 55.9% Arbidol, $p = 0.019$). Therefore, further investigation of favipiravir is recommended for the treatment of COVID-19 (Chen et al., 2020d). Ribavirin, another antiviral agent has been considered as a hopeful therapy for the management of COVID-19 owing to its effectiveness against previously existing SARS-CoVs. Wang et al. (2020) demonstrated its extensive *in vitro* potential against COVID-19 (strain WIV04). In addition, a retrospective study in the city of Wuhan, China with 134 clinically approved severe COVID-19 patients was conducted (Tong et al., 2020). However, due to unfavorable reactions pattern, the proper dose of ribavirin in the clinical application should be standardized; and be given with proper monitoring according to the patient's severity. US-FDA granted the emergency use of remdesivir in the second wave of COVID-19. Remdesivir, a viral RNA polymerase inhibitor; and in investigations including a clinical trial, it showed significant antiviral activity ($EC_{50} = 0.77 \mu M$; $EC_{90} = 1.76 \mu M$) against several coronaviruses including novel COVID-19 (Wang et al., 2020; Kalil et al., 2021). Therefore, this agent is a highly recommended therapy for COVID-19 at the early stage of infection (Al-Tawfiq et al., 2020; Wang et al., 2020). More recently, a cocktail of remdesivir with Baricitinib was found to significantly reduce the recovery time and drive improved outcomes in those COVID-19 patients receiving high-flow oxygen or noninvasive ventilation (Kalil et al., 2021). However, remdesivir is only available as an intravenous fluid (IVF), and the effectively of the drug is yet to be established for critically ill ICU patients. Other FDA approved antiviral remedies such as penciclovir, Oseltamivir, etc. are under experimental phase for possible antiretroviral management of COVID-19.

Besides drugs with established antiviral activity, other agents 19 are also considered for their effectiveness against COVID-19. Among these, chloroquine and hydroxychloroquine have a long-standing history in the prevention and treatment of malaria and autoimmune diseases (Savarino et al., 2003). However, chloroquine has been previously reported to possess broad-spectrum antiviral effects (Savarino et al., 2003; Gao et al., 2020). Interestingly, it was previously known for its potent inhibitory action against SARS-CoV *via* blocking the ACE2 receptor (Savarino et al., 2003; Warner et al., 2020). Furthermore, clinical shreds of evidence demonstrated that the COVID-19 virus enters the epithelial cells of mucosa *via* ACE2 receptor, and chloroquine can act at both entry and post-entry levels of COVID-19 infection (Gao et al., 2020; Wang et al., 2020). One recent study depicted that hydroxychloroquine is more effective and acts even at lower concentrations compared to chloroquine against SARC-CoV-2. Further, its immunomodulatory action has also been noted that could synergistically accelerate the antiviral potential *in vivo* (Yao et al., 2020). During previous virus outbreaks including the SARS pandemic, interferons were extensively used as treatment measures. IFN-$\beta$ inhibits the *in vitro* replication of viruses including SARS-CoV (Hensley et al., 2004). Therefore, IFN-$\beta$ was proposed as a choice of candidate for COVID-19 treatment. One of the studies found that Type I IFN significantly declines

the viral protein load and replication of SARS-CoV-2 (Lokugamage et al., 2020). However, further supportive pieces of evidence are required to support this therapeutic regime. Monoclonal antibody therapies are also in the line of investigation and clinical trial phase for the treatment of COVID-19. However, few of them are also in clinical practice based on identified benefits from investigations with small number of patients (Xu et al., 2020; Yao et al., 2020). Tocilizumab, an IL-6 receptor antagonist, is FDA approved to treat rheumatoid arthritis and cytokine release syndrome following chimeric antigen receptor T-cell therapy. Due to these past therapeutic history, tocilizumab has been used in patients with severe COVID-19 with early reports of success (Xu et al., 2020). In COVID-19, psychological distress along with neurological disorders accompany the pathophysiological manifestations and correlates with the severity of the disease. Although symptomatic treatment of physical health deterioration lessens the associated mental health consequences, therapeutic interventions may directly affect the neuropsychological magnitudes in patients (García et al., 2020). Steroidal anti-inflammatory agents, through steroid receptors with their abundant presence in the hippocampus, affect the psychological well-being of patients even in COVID-19. Psychological effects of corticosteroids in COVID-19 range from mild to moderate including hypomania, depression, and mood disorders (García et al., 2020). Neurotoxicity of antiviral drugs is also reported (Abers et al., 2014). Moreover, lopinavir/ ritonavir induced the loss of taste (Abers et al., 2014) may lead to low appetite and consequently poor nutrition. Delirium-like symptoms with usages of antibiotics prescribed in therapeutic regimen (Sirois, 2002) can be expected to negatively affect the nutrition and immune response. Such consequences will have a compounding effect and hinder the objectives of treatment. Further, IFN-$\beta$ therapy has been linked with severe depression disorders (Fragoso et al., 2010). Interestingly, tocilizumab have the protective effect against psychotic disorders and can be speculated to improve the mental health along with the physical heath of COVID-19. Although, direct-acting action on mental health is not well established for most of the therapeutic agents used for COVID-19, their ability to modulate PNEI response can largely affect the recuperation phase. Therefore, its neuropsychiatric consequences and patients' mental health must be taken into account during designing therapeutic regimens at a personalized level.

Medical nutritional therapy is also taken into consideration for clinical management of COVID-19 (Bedock et al., 2020; Calder, 2020; Rodriguez-Leyva and Pierce, 2021; Silverio et al., 2021; Thibault et al., 2021). The food ingredients including those rich in calories are being considered to improve the nutritional status of the patients affected with COVID-19 (Barazzoni et al., 2020; Bedock et al., 2020; Calder, 2020; Fedele et al., 2021; Nicolau et al., 2021; Thibault et al., 2021). Protein-rich food items such as mushrooms and legumes can provide benefits to various human disorders (Rodriguez-Leyva and Pierce, 2021; Silverio et al., 2021; Singh et al., 2021). Moreover, the medicinal properties of food ingredients like mushrooms, herbs, and spices also aid in clinical measures to combat COVID-19. Conditional amino acid therapy replenishes the

essential amino acids in affected patients (Soni et al., 2020d; Mehta et al., 2021; Rozga et al., 2021). Food items enriched with essential amino acids such as mushrooms, legumes, seafood can also fulfill the requirement, at least partially, and prevent the requirement of conditional amino acid therapy. The integration of the "dietetics approach" in the management of COVID-19 will have adjuvant benefits to the clinical measures against this pandemic.

## Herbal Remedies

Historically, the traditional medicinal plants have been known as universal healers. Historical uses for their medicinal properties, easy availability, minimal side effects, and low cost make them potential candidates against diverse forms of human pathologies. Natural herbs are an extensive source of antiviral recipes and immune boosters. Currently, compounds of herbal origin are playing a potential role in the disease prevention and cure against several clinical illnesses including the ongoing COVID-19 (Goothy et al., 2020; Khanna et al., 2020; Soni et al., 2020a). There is a wide range of herbal drugs used in traditional Chinese medicine or Ayurvedic medicinal practices, which were extensively explored against previous CoV outbreaks including *Astragali Radix* (*Huangqi*), *Saposhnikoviae Radix* (*Fangfeng*), *Glycyrrhizae Radix Et Rhizoma* (*Gancio*), *Atractylodis Macrocephalae Rhizoma* (*Baizhu*), and *Lonicerae Japonicae Flo* (Luo et al., 2020; Soni et al., 2021); and are expected to aid in the clinical management of on-going pandemic. However, the lack of adequate data and inconsistent results on herbal remedies against COVID-19 necessitate further studies to understand antiviral mechanisms at the molecular level (Wang et al., 2020).

Metabolites of some traditional herbal medicine are known to possess modulatory activity on ACE2 (Khanna et al., 2020; Soni et al., 2020a; Warner et al., 2020). This includes curcumin, tanshinones, magnolol, baicalin, withanone, tinocordiside, and rosmarinic acid (Khanna et al., 2020; Shree et al., 2020; Saggam et al., 2021). Further explorations of these natural herbs and their components against COVID-19 are required. Notably, curcumin is highly suggestive as a gold standard remedial option for the cure of COVID-19 infection in many literature reviews. Curcumin is a broadly explored agent hijacking the several steps of viral biochemistry by acting as a protease inhibitor, cellular signaling pathways modulator (Soni et al., 2020c; Zahedipour et al., 2020). Moreover, traditional plant-derived metabolites are recently characterized as modulators of immune responses including cytokines and eicosanoids levels (Khanna et al., 2020). In some preclinical experiments, crude extract of *Sambucus nigra* L., *Echinacea angustifolia* DC. and *Echinacea purpurea* L. (Moench.), Larch (*Larix* sp.) and plant extracts or food supplements rich in Vitamin D increases the production of IL-1β and IL-18 by immune-deficient cells (Alschuler et al., 2020). Authority on practices of alternative and complementary medicine systems, AYUSH (Government of India) advised the use of herbal medicines for the management of COVID-19. Among these herbs, tulsi (holy basil) is highly suggested for SARC-CoV-2 (Goothy et al., 2020). Additionally, AYUSH experts recommended some remedial plans to cope

up with this current outbreak including the use of *Tinospora cardiofolia* (Giloy) for chronic fever, *Andrographis paniculata* (Kalmegh) for fever and cold, *Cydonia oblonga* (Quince), *Zizyphus jujube* (red date), *Withania somnifera* (Ashwagandha) for cold and flu, and *Cordia myxa* (Assyrian plum) are recommended as antioxidant, immune-modulator, anti-allergic, smooth muscle relaxant, anti-influenza activity (Goothy et al., 2020; Khanna et al., 2020; Shree et al., 2020; Saggam et al., 2021). Homeopathic medicine *Arsenicum album* 30 also acts as an immune-modulator and found effective against SARS-CoV-2 infection (Maurya et al., 2020). For the management of respiratory manifestation associated with COVID-19, Ayurvedic preparation including Agastya Haritaki and Anu taila (oil) are recommended (Vellingiri et al., 2020).

The direct antiviral effects of herbal preparations along with immunomodulatory potential have been sought as exigent benefits in COVID-19 (Shree et al., 2020; Saggam et al., 2021). Apart from these, neuropsychological benefits are also suggested (Aubry et al., 2019; Khanna et al., 2020; Soni et al., 2020b). Many of these bioactive phytochemicals alleviate psychosomatic stress (Fedotova et al., 2017; Aubry et al., 2019; Soni et al., 2020b). COVID-19 pandemic effects have distress consequences (Clemente-Suárez et al., 2020; Popkova et al., 2021; Rababah et al., 2021); and herbal medicinal preparation or bioactive phytochemical-rich diet can moderate these social distress disorders (Aubry et al., 2019). Due to uncertainty on COVID-19 pandemic, anxiety and similar disorders become frequent. The phytochemical has been shown to annul a wide range of these disorders (Fedotova et al., 2017). Herbal drugs can be expected to deliver benefits either directly or through indirect action on components of the PNEI system. Alleviating neuropsychiatric distress will improve the immune response and recuperative ability of patients. Although traditional medicinal preparations are being used based on their established benefits against symptomatic manifestations, many of them are also under early-stage validation for their efficacy in the clinical management of COVID-19 (Maurya et al., 2020).

## Psychological Counseling

In addition to the deterioration of physical health, the psychological burden during the ongoing pandemic dramatically influences the treatment outcome and recovery of COVID-19 patients affecting millions of lives worldwide (Clemente-Suárez et al., 2020). The psychological reaction may vary from aggressive or panic behavior to pervasive feelings of hopelessness and desperation (Thakur and Jain, 2020). These reactions connect with negative psychological extremes including suicidal behavior (Thakur and Jain, 2020). From the onset of the viral outbreak in 2019 to current counter measures including lockdowns, quarantines, and other restrictions are enforced infrequently compelling people to stay home and work-from-home (Brooks et al., 2020). Therefore, individuals are experiencing deviations from their normal behavioral patterns and report anxiety, depression, lack of concentration, and mood disorders (Rao et al., 2008). In these vents, psychology/psychiatry associations and authorities recommend counseling to mitigate the burden of lockdown and quarantine in the COVID-19 situation on mental health (Kontoangelos et al., 2020). The need for

psychological counseling is to enhance mental well-being through bringing modulation in decision making and behavioral changes during a time of crisis (Hammami et al., 2020; Lai et al., 2020). Globally this has been accompanied by the implementation of various public health policies and guidelines designed to fix routine life style through alleviation of psychological distress and establishment of mental and physical well-being (Brooks et al., 2020). Emerging pieces of evidence depict the psychological impact of COVID-19 on individuals directly as well as indirectly in both infected and healthy individuals including the near ones of infected patients and those who are facing social distancing measures (Alschuler et al., 2020; Brooks et al., 2020; Guang et al., 2021). Indeed, it should be emphasized that the majority of the population is not expected to suffer from mental illness forced from the pandemic and its impact (Taylor, 2019). Recently, a study conducted in India identified the key stressors acting as potent drivers for bad psychological illness including fear of one's health, the well-being of the family, economic difficulties, sense of isolation due to quarantine, job security, disturbed social systems and overabundance of misinformation (infodemics) by media and other sources (Banerjee, 2020). These facts indicate that abnormal psychological nature is damaging the people's lives during COVID-19 pandemic. Therefore, demonstration of the benefits of psychological science for mental well-being through scientific strategies is warranted. This will also influence the socio-economic status of the society (Clemente-Suárez et al., 2020) and will provide adjunct benefits in COVID-19 pandemic.

## Mental Health Welfare and Scientific Awareness

COVID-19 is one of the major global health crises at present which hurt millions of people by influencing their lives in several ways including physically, socially, psychologically, and spiritually. It is now well documented that the COVID-19 pandemic poses a major burden to mental health (Loades et al., 2020; Vindegaard and Benros, 2020; da Silva et al., 2021). Psychologically, COVID-19 pandemic effects act as major drivers of stress impacting mental fitness worldwide. The pre-existing mental disorder can negatively affect the immune response and prompt the severity of COVID-19. A large number of reports indicate dramatic disruption of mental health and behavior with SARS-CoV-2 infection (Cunningham and Firozi, 2020). Notably, the mental health hotline in the United States experienced 10 times increase during pandemic-associated lockdown (Raw et al., 2021). Notably, the parts of the world with a low economy have compelling priorities to improve their physical healthcare system over mental healthcare. The inadequacy of mental healthcare cannot be negated in compounding the detrimental consequences amid COVID-19 (Antonova et al., 2021). Some medical data reported elevated abnormal mental nature and more suicides probably because of poor mental fitness (Hollyfield, 2020). Therefore, to address mental health welfare and scientific awareness a broad range of government policies and assignments are highly recommended to win the battle in eradicating the COVID-19 pandemic. First of all, there should be a priority to identify the common psychological threats and myths associated

with COVID-19. In addition, various mental awareness programs should be run by the healthcare system to reduce the pandemic induced fear, stress, and depression. Scientific awareness among the population about COVID-19 is expected to aid in efficient combating strategies. Government authorities and public initiatives are also contributing to spreading awareness about COVID-19. The existence of scientific awareness is high in a few investigations (Singh et al., 2020). However, the existence of a huge amount of information on various sources creates an Infodemic"; and causes a state of confusion among common people in the decision to follow which advice. The data mining, processing, and artificial intelligence methods can be expected to assist in designing combat strategies and forecasting their success (Carvalho et al., 2021). Nevertheless, among many other factors, practices of convenience sampling due to pandemic measures may also deviate the finding from the true prevailing scenario. Therefore, continuous efforts to spread awareness about the disease, preventive measures, and related information must be ongoing.

## DISCUSSION

The interplay of nutrition and the PNEI system is very crucial for manifestations of disease and its course. The COVID-19 pandemic has a large impact not only on human health conditions but also impacted human lives through disturbing the social and economic conditions and interactions at local as well as at global levels (Godman et al., 2020; Carvalho et al., 2021; Chattu et al., 2021; Soni et al., 2021). The impact of COVID-19 is also relayed to human lives through distorting of daily routines and leisure activities (Alschuler et al., 2020; Godman et al., 2020; Soni et al., 2021). The differences in countries belonging to different economic groups like BRICS, G7, EM7, OECD, etc. at demographic and socioeconomic levels served as a factor in combat against COVID-19. Although the COVID-19 affected each part of the world, the countries' priority toward the healthcare sector, their preparedness, the difference in policymaking, and strategies for their executions served as a decisive factor in recuperation from this pandemic. The differences at the demographic and socioeconomic level in the population residing in BRICS nations and country members of other economic groups like OECD, G7, and EM7 also determined the pace of COVID-19 spread, the effectiveness of containment strategies, and clinical measures. The preexisting differences in healthcare systems in different country members of various groups including BRICS cannot be neglected to have a major role in the effective management of COVID-19. The guidelines recommended by various regulatory organizations including WHO have been implemented by most of the countries; however, the local restraints also exist. The religion and lifestyle practiced in countries, even in some parts, have a large impact on the success of pandemic measures both at the social level and at the clinical level. The differences in food habits among populations belonging to different countries, regions, religions, and believes is also a precursor of the nutritional status of individuals and the population at large. The food preferences and restrictions are also derived from religious beliefs and have an impact on nutritional balance.

**FIGURE 7 |** Set-up of COVID-19 cases, case fatality rate (CFR), undernourishment, and mental disorders in BRICS nations.
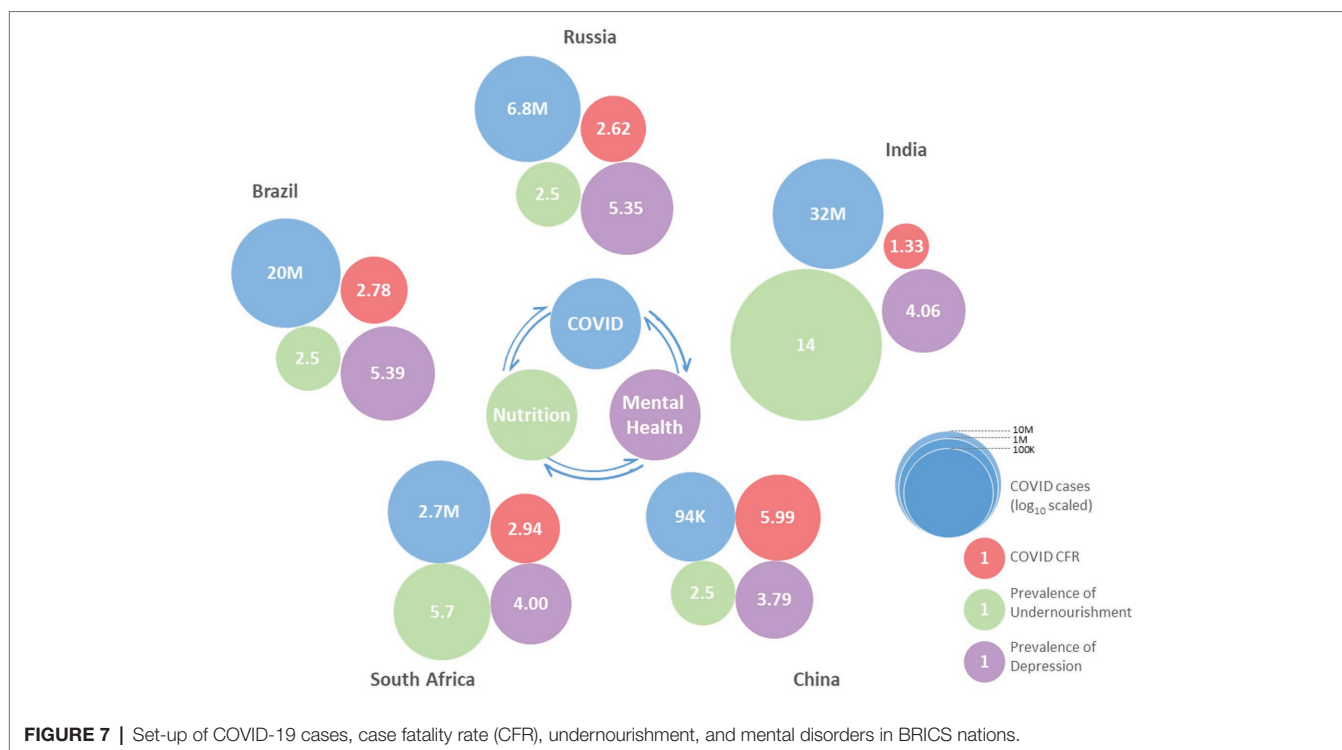
Restrictions in food items and intake can be permanent observance or can be observed during special religious days at weeks, months, or annual cycles. The diurnal restrictions in food habits can also affect the susceptibility of individuals toward many infectious disorders including COVID-19. Apart from socioeconomic differences, the nourishment status of different countries' populations also exists. Most of the BRICS nations, except India, have a smaller population fraction suffering from undernourishment as compared to the world level (**Figure 3**). However, the large population size of India affects the collective nourishment status of BRICS nations. Psychopsychiatric wellness has also been shown to affect the susceptibility toward disease conditions including SARS-CoV-2 infection as well as therapeutic measures. The prevalence of mental illness is higher in most of the BRICS nations compared to its world average (**Figure 4**). As per the recent statistics, only China has the lowest prevalence of depression in the BRICS countries which is also smaller than the world average. However, in many regions of the world including those in BRICS nations, mental illness is not given priority and medical consultation is not a common measure leading to underreporting. Interdependence of nutrition and mental well-being suggests the coexistence of nutritional deficiency and neuropsychiatric illness.

The COVID-19 drives the nutritional deficiency through raising energy and nutrient demand as well as through physiological and anatomical damages caused in the GI tract. While the preexisting nutritional deficiencies can worsen the outcome, owing to PNEI modulation, the neuroendocrine disturbances compound the manifestation of the disease in COVID-19 and lead to severe symptoms, systemic spread and associated morbidities. The large proportion of the population affected with either nutritional deficits, mental illness, or both in BRICS nations have the high

risk of undesired outcome of SARS-COV-2 infection and measures for its clinical management. Moreover, the steps to prevent the spread of SARS-CoV-2 infection including lockdown, and social distancing led to financial uncertainty and hindrance in the availability of essential supplies including food items and medicine (Godman et al., 2020; Chattu et al., 2021). Although guidelines are being released at the national and global level by the regulatory organization, the absolute implementation is mostly far from achieved due to demographic, socioeconomic, population size, religious beliefs, educational status, and healthcare availability reasons. The country members of other economic groups are also impacted with COVID-19 and have undergone a sharp surge in confirmed COVID-19 cases. However, strategies against COVID-19 and their probability of implementation with success differ due to differences exist among members of BRICS nations as well G7, EM7, and OECD members. Among many factors influencing COVID-19 manifestations, availability of healthcare (UHC effective coverage index) and preexisting physical and mental health conditions among the population can be expected as the major determinant for the initial surge of confirmed cases of COVID-19 and deaths. As the evidence from investigations start pouring, the medical councils/authorities of individual nations as well WHO provided the standard operating procedure for SARS-CoV-2-infected patients. Initial investigations were primarily focused on the molecular pathology of SARS-CoV-2 infection; however, later investigations demonstrated the involvement of nutritional deficiencies and neuropsychiatric illnesses in worsening the COVID-19 pathological manifestations. Moreover, the impact of social measures to prevent spread of SARS-CoV-2 infection drive the psychological derailment; and is also suggested to be considered for effective management of the COVID-19 pandemic

(Girdhar et al., 2020; Soni et al., 2020b,d; Kumar and Nayar, 2021; Mehta et al., 2021; Nadalin et al., 2021).

The measures have been taken by member countries from different economic groups against COVID-19; however, the collective measures by BRICS nations will have a huge impact on global outcome owing to large contribution in worldwide population, economy, and terrestrial area. BRICS nations have developed or are manufacturers of a major proportion of vaccines against COVID-19 (**Table 1**). Along with the modern medicine system, traditional medicinal practices are common in BRICS nations including Ayurveda, Traditional Chinese Medicine, Russian Traditional medicine, African traditional medicine, and Brazilian Traditional Medicine. Most of these traditional medicinal practices use herbs as their preferential ingredients to prevent and cure various human diseases. Ayurveda and other traditional medicine practices also recommend specific diet preferences during different human illnesses. It reflects that nutritional management during disease conditions is already an integrative part of traditional medicine practiced in countries including members of BRICS. Along with modern medicine, integration of traditional medicinal practices has also been recommended by WHO to boost the immunity and prevent he contract with infectious agents including SARS-CoV-2.

As the experiment-based evidence reflects the involvement of nutritional management and PNEI as one of the major determinants of COVID-19 manifestation, most of the national and global authorities recommend the incorporation of these courses of actions in standard operating procedures. However, the existing prevalence of mental illness and undernourishment in BRICS nations and other similar countries must be included in consideration in designing the policies to combat the current pandemic. Although, the distortion in daily routine including decreased physical activity and financial uncertainty brings anxiety and depression along with nutritional imbalance impacting every country, the unique status of each member country of the BRICS group must be considered critically in the investigation of the consequences of COVID-19. This will also help in designing successful strategies at the global level to combat the COVID-19 pandemic not only at the clinical level but also socioeconomic front.

## CONCLUSION

Nutrition and neuropsychological disorders play a critical role in the causes and consequences of COVID-19 severity. The interplay between the PNEI axis and nutrition largely affects the outcome of therapeutic interventions in COVID-19. The high confirmed cases and COVID-19 death number in BRICS nations reflect the perilous condition. The nutritional deficiencies may aggravate the COVID-19 severity, and high undernourishment (PoU index) among BRICS countries poses a threat of severe SORS-CoV-2 infections in their populations. The nutritional state has an accumulative effect on physical as well as mental health through PNEI modulation. The qualitative and quantitative immune responses are at least partially governed by the psychological state of the individuals. The bilateral regulatory events between neuroendocrine and immune response are superintended by nutrition-derived level and type of nutrition-derived factors. The high prevalence of mental health disorders in BRICS nations is here suggested as a factor having compounded effect on protection and immunity against COVID-19. The country members of other economic groups have a distinctive state as compared to BRICS nations. Many factors affect the COVID-19-associated manifestations including clinical symptoms and socioeconomic consequences. Amid the COVID-19 pandemic, the perceived fear attracted the neuropsychiatric presentations; and financial and economic losses lead the increased food insecurity causing an escalation in undernourishment globally as well as in BRICS nations. Collectively this sets a favorable stage for COVID-19 spread and comorbidities (**Figure 7**). Various strategies have been suggested to prevent this interdependent "tsunami" of psychological consequences and COVID-19. Conditional supplementations (amino acids and vitamins) can be suggested to improve both immunity and mental well-being. Considering the prevalence of undernourishment and mental health conditions in BRICS and a large number of COVID-19 cases, the nutritional monitoring and psychological interventions especially for COVID-19 affected patients can be suggested to have adjunctive influence in the clinical management of SARS-CoV-2 infection.

## AUTHOR CONTRIBUTIONS

NV, DS, and SP conceptualized the study. AM, YR, VS, KS, and AT contributed to literature search and analysis. Critical evaluations and revisions were made by NV, DS, SK, and KS. All authors contributed to the article and approved the submitted version.

## ACKNOWLEDGMENTS

## REFERENCES

Abers, M. S., Shandera, W. X., and Kass, J. S. (2014). Neurological and psychiatric adverse effects of antiretroviral drugs. *CNS Drugs* 28, 131–145. doi: 10.1007/s40263-013-0132-4

Alpert, O., Begun, L., Garren, P., and Solhkhah, R. (2020). Cytokine storm induced new onset depression in patients with COVID-19. A new look into the association between depression and cytokines -two case reports. *Brain Behav. Immun. Health* 9:100173. doi: 10.1016/j.bbih.2020.100173

Alschuler, L., Weil, A., Horwitz, R., Stamets, P., Chiasson, A. M., Crocker, R., et al. (2020). Integrative considerations during the COVID-19 pandemic. *Exp. Dermatol.* 16, 354–356. doi: 10.1016/j.explore.2020.03.007

Al-Tawfiq, J. A., Al-Homoud, A. H., and Memish, Z. A. (2020). Remdesivir as a possible therapeutic option for the COVID-19. *Travel Med. Infect. Dis.* 34:101615. doi: 10.1016/j.tmaid.2020.101615

Ambrus, J. L., and Ambrus, J. L. (2004). Nutrition and infectious diseases in developing countries and problems of acquired immunodeficiency syndrome. *Exp. Biol. Med.* 229, 464–472. doi: 10.1177/153537020422900603

Amore, S., Puppo, E., Melara, J., Terracciano, E., Gentili, S., and Liotta, G. (2021). Impact of COVID-19 on older adults and role of long-term care facilities during early stages of epidemic in Italy. *Sci. Rep.* 11:12530. doi: 10.1038/s41598-021-91992-9

Amruta, N., Chastain, W. H., Paz, M., Solch, R. J., Murray-Brown, I. C., Befeler, J. B., et al. (2021). SARS-CoV-2 mediated neuroinflammation and the impact of COVID-19 in neurological disorders. *Cytokine Growth Factor Rev.* 58, 1–15. doi: 10.1016/j.cytogfr.2021.02.002

Antonova, E., Schlosser, K., Pandey, R., and Kumari, V. (2021). Coping with COVID-19: mindfulness-based approaches for mitigating mental health crisis. *Front. Psych.* 12:563417. doi: 10.3389/fpsyt.2021.563417

Aoyagi, Y., Inamoto, Y., Shibata, S., Kagaya, H., Otaka, Y., and Saitoh, E. (2021). Clinical manifestation, evaluation, and rehabilitative strategy of dysphagia associated with COVID-19. *Am. J. Phys. Med. Rehabil.* 100, 424–431. doi: 10.1097/PHM.0000000000001735

Aubry, A. V., Khandaker, H., Ravenelle, R., Grunfeld, I. S., Bonnefil, V., Chan, K. L., et al. (2019). A diet enriched with curcumin promotes resilience to chronic social defeat stress. *Neuropsychopharmacology* 44, 733–742. doi: 10.1038/s41386-018-0295-2

Awe, O. O., Dogbey, D. M., Sewpaul, R., Sekgala, D., and Dukhi, N. (2021). Anaemia in children and adolescents: a bibliometric analysis of BRICS countries (1990–2020). *Int. J. Environ. Res. Public Health* 18:5756. doi: 10.3390/ijerph18115756

Banerjee, D. (2020). How COVID-19 is overwhelming our mental health. Nature India. 26: 2020.

Barazzoni, R., Bischoff, S. C., Breda, J., Wickramasinghe, K., Krznaric, Z., Nitzan, D., et al. (2020). ESPEN expert statements and practical guidance for nutritional management of individuals with SARS-CoV-2 infection. *Clin. Nutr.* 39, 1631–1638. doi: 10.1016/j.clnu.2020.03.022

Basheer, S., Natarajan, A., Amelsvoort, T. V., Venkataswamy, M. M., Ravi, V., Srinath, S., et al. (2017). Vitamin D status of children with autism spectrum disorder: case-control study from India. *Asian J. Psychiatr.* 30, 200–201. doi: 10.1016/j.ajp.2017.10.031

Bedock, D., Lassen, P. B., Mathian, A., Moreau, P., Couffignal, J., Ciangura, C., et al. (2020). Prevalence and severity of malnutrition in hospitalized COVID-19 patients. *Clin. Nutr. ESPEN* 40, 214–219. doi: 10.1016/j.clnesp.2020.09.018

Bennett, G., Young, E., Butler, I., and Coe, S. (2020). The impact of lockdown during the COVID-19 outbreak on dietary habits in various population groups: a scoping review. *Front. Nutr.* 8:626432. doi: 10.3389/fnut.2021.626432

Bjork, J. M., Dougherty, D. M., Moeller, F. G., and Swann, A. C. (2000). Differential behavioral effects of plasma tryptophan depletion and loading in aggressive and nonaggressive men. *Neuropsychopharmacology* 22, 357–369. doi: 10.1016/S0893-133X(99)00136-0

Briguglio, M., Pregliasco, F. E., Lombardi, G., Perazzo, P., and Banfi, G. (2020). The malnutritional status of the host as a virulence factor for new coronavirus SARS-CoV-2. *Front. Med.* 7:146. doi: 10.3389/fmed.2020.00146

Brooks, S. K., Webster, R. K., Smith, L. E., Woodland, L., Wessely, S., Greenberg, N., et al. (2020). The psychological impact of quarantine and how to reduce it: rapid review of the evidence. *Lancet* 395, 912–920. doi: 10.1016/S0140-6736(20)30460-8

Calder, P. C. (2020). Nutrition, immunity and COVID-19. *BMJ Nutr. Prev. Health* 3, 74–92. doi: 10.1136/bmjnph-2020-000085

Cao, B., Wang, Y., Wen, D., Liu, W., Wang, J., Fan, G., et al. (2020). A trial of lopinavir–ritonavir in adults hospitalized with severe Covid-19. *N. Engl. J. Med.* 382, 1787–1799. doi: 10.1056/NEJMoa2001282

Carnegie, R., Zheng, J., Sallis, H. M., Jones, H. J., Wade, K. H., Evans, J., et al. (2020). Mendelian randomisation for nutritional psychiatry. *Lancet Psychiatry* 7, 208–216. doi: 10.1016/S2215-0366(19)30293-7

Carvalho, K., Vicente, J. P., Jakovljevic, M., and Teixeira, J. P. R. (2021). Analysis and forecasting incidence, intensive care unit admissions, and projected mortality attributable to COVID-19 in Portugal, the UK, Germany, Italy, and France: predictions for 4 weeks ahead. *Bioengineering* 8:84. doi: 10.3390/bioengineering8060084

Cava, E., and Carbone, S. (2021). Coronavirus disease 2019 pandemic and alterations of body composition. *Curr. Opin. Clin. Nutr. Metab. Care* 24, 229–235. doi: 10.1097/MCO.0000000000000740

CDC (2021). About COVID-19. Available at https://www.cdc.gov/coronavirus/2019-ncov/your-health/about-covid-19.html (Accessed September 01, 2021).

Ceolin, G., Mano, G. P. R., Hames, N. S., Antunes, L. D. C., Brietzke, E., Rieger, D. K., et al. (2021). Vitamin D, depressive symptoms, and Covid-19 pandemic. *Front. Neurosci.* 15:670879. doi: 10.3389/fnins.2021.670879

Charlson, F. J., Baxter, A. J., Cheng, H. G., Shidhaye, R., and Whiteford, H. A. (2016). The burden of mental, neurological, and substance use disorders in China and India: a systematic analysis of community representative epidemiological studies. *Lancet* 388, 376–389. doi: 10.1016/S0140-6736(16)30590-6

Chattu, V. K., Singh, B., Kaur, J., and Jakovljevic, M. (2021). COVID-19 vaccine, TRIPS, and global health diplomacy: India's role at the WTO platform. *Biomed. Res. Int.* 2021:6658070. doi: 10.1155/2021/6658070

Chen, P., Mao, L., Nassis, G. P., Harmer, P., Ainsworth, B. E., and Li, F. (2020a). Coronavirus disease (COVID-19): the need to maintain regular physical activity while taking precautions. *J. Sport Health Sci.* 9, 103–104. doi: 10.1016/j.jshs.2020.02.001

Chen, G., Wu, D., Guo, W., Cao, Y., Huang, D., Wang, H., et al. (2020b). Clinical and immunological features of severe and moderate coronavirus disease 2019. *J. Clin. Invest.* 130, 2620–2629. doi: 10.1172/JCI137244

Chen, X., Xu, J., Tang, J., Dai, X., Huang, H., Cao, R., et al. (2020c). Dysregulation of amino acids and lipids metabolism in schizophrenia with violence. *BMC Psychiatry* 20:97. doi: 10.1186/s12888-020-02499-y

Chen, C., Zhang, Y., Huang, J., Yin, P., Cheng, Z., Wu, J., et al. (2020d). Favipiravir versus arbidol for COVID-19: a randomized clinical trial. MedRxiv. doi: 10.1101/2020.11.27.20239616, PMID: 34013296 [Preprint].

Childs, C. E., Calder, P. C., and Miles, E. A. (2019). Diet and Immune Function. *Nutrients.* 11:1933. doi: 10.3390/nu11081933

Choi, G. J., Kim, H. M., and Kang, H. (2020). The potential role of dyslipidemia in COVID-19 severity: an umbrella review of systematic reviews. *J. Lipid Atheroscler.* 9, 435–448. doi: 10.12997/jla.2020.9.3.435

Chu, C. M., Cheng, V. C. C., Hung, I. F. N., Wong, M. M. L., Chan, K. H., Chan, K. S., et al. (2004). Role of lopinavir/ritonavir in the treatment of SARS: initial virological and clinical findings. *Thorax* 59, 252–256. doi: 10.1136/thorax.2003.012658

Clemente-Suárez, V. J., Dalamitros, A. A., Beltran-Velasco, A. I., Mielgo-Ayuso, J., and Tornero-Aguilera, J. F. (2020). Social and psychophysiological consequences of the COVID-19 pandemic: an extensive literature review. *Front. Psychol.* 11:580225. doi: 10.3389/fpsyg.2020.580225

Cornish, S., and Mehl-Madrona, L. (2008). The role of vitamins and minerals in psychiatry. *Integr. Med. Insights* 3, 33–42. doi: 10.4137/117863370800300003

Cunningham, P.W., and Firozi, P. (2020). The health 202: texts to federal government mental health hotline up roughly 1,000 percent. Available at: https://www.washingtonpost.com/ (Accessed September 01, 2021).

Cutrera, A. P., Zenuto, R. R., Luna, F., and Antenucci, C. D. (2010). Mounting a specific immune response increases energy expenditure of the subterranean rodent *Ctenomys talarum* (tuco-tuco): implications for intraspecific and interspecific variation in immunological traits. *J. Exp. Biol.* 213, 715–724. doi: 10.1242/jeb.037887

Czeisler, M. É., Lane, R. I., Petrosky, E., Wiley, J. F., Christensen, A., Njai, R., et al. (2020). Mental health, substance use, and suicidal ideation during the COVID-19 pandemic—United States, June 24-30, 2020. *MMWR Morb. Mortal. Wkly Rep.* 69, 1049–1057. doi: 10.15585/mmwr.mm6932a1

da Silva, M. L., Rocha, R. S. B., Buheji, M., Jahrami, H., and da Costa Cunha, K. (2021). A systematic review of the prevalence of anxiety symptoms during coronavirus epidemics. *J. Health Psychol.* 26, 115–125. doi: 10.1177/1359105320951620

Dash, D. P., Sethi, N., and Dash, A. K. (2021). Infectious disease, human capital, and the BRICS economy in the time of COVID-19. *MethodsX* 8:101202. doi: 10.1016/j.mex.2020.101202

de Almondes, K. M., Bizarro, L., Miyazaki, M. C. O. S., Soares, M. R. Z., Peuker, A. C., Teodoro, M., et al. (2021). Comparative analysis of psychology responding to COVID-19 pandemic in brics nations. *Front. Psychol.* 12:567585. doi: 10.3389/fpsyg.2021.567585

Deng, L., Li, C., Zeng, Q., Liu, X., Li, X., Zhang, H., et al. (2020). Arbidol combined with LPV/r versus LPV/r alone against corona virus disease 2019: a retrospective cohort study. *J. Inf. Secur.* 81, e1–e5. doi: 10.1016/j.jinf.2020.03.002

Di Nicola, M., Dattoli, L., Moccia, L., Pepe, M., Janiri, D., Fiorillo, A., et al. (2020). Serum 25-hydroxyvitamin D levels and psychological distress symptoms

in patients with affective disorders during the COVID-19 pandemic. *Psychoneuroendocrinology* 122:104869. doi: 10.1016/j.psyneuen.2020.104869

Elmadfa, I., and Meyer, A. L. (2019). The role of the status of selected micronutrients in shaping the immune function. *Endocr Metab Immune Disord Drug Targets* 19, 1100–1115. doi: 10.2174/1871530319666190529101816

FAO, IFAD, UNICEF, WFP, and WHO (2021). Transforming food systems for food security, improved nutrition and affordable healthy diets for all. In The State of Food Security and Nutrition in the World 2021.

Fedele, D., De Francesco, A., Riso, S., and Collo, A. (2021). Obesity, malnutrition, and trace element deficiency in the coronavirus disease (COVID-19) pandemic: an overview. *Nutrition* 81:111016. doi: 10.1016/j.nut.2020.111016

Fedotova, J., Kubatka, P., Büsselberg, D., Shleikin, A. G., Caprnda, M., Dragasek, J., et al. (2017). Therapeutical strategies for anxiety and anxiety-like disorders using plant-derived natural compounds and plant extracts. *Biomed. Pharmacother.* 95, 437–446. doi: 10.1016/j.biopha.2017.08.107

Ferguson, M., Capra, S., Bauer, J., and Banks, M. (1999). Development of a valid and reliable malnutrition screening tool for adult acute hospital patients. *Nutrition* 15, 458–464. doi: 10.1016/S0899-9007(99)00084-2

Fragoso, Y. D., Frota, E. R. C., Lopes, J. S., Noal, J. S., Giacomo, M. C., Gomes, S., et al. (2010). Severe depression, suicide attempts, and ideation during the use of interferon beta by patients with multiple sclerosis. *Clin. Neuropharmacol.* 33, 312–316. doi: 10.1097/WNF.0b013e3181f8d513

França, K., and Lotti, T. M. (2017). "Psycho-neuro-endocrine-immunology: A psychobiological concept" in *Ultraviolet Light in Human Health, Diseases and Environment*. ed. S. I. Ahmad (Cham: Springer International Publishing), 123–134.

Fullman, N., Yearwood, J., Abay, S. M., Abbafati, C., Abd-Allah, F., Abdela, J., et al. (2018). Measuring performance on the healthcare access and quality index for 195 countries and territories and selected subnational locations: a systematic analysis from the global burden of disease study 2016. *Lancet* 391, 2236–2271. doi: 10.1016/S0140-6736(18)30994-2

Gao, J., Tian, Z., and Yang, X. (2020). Breakthrough: chloroquine phosphate has shown apparent efficacy in treatment of COVID-19 associated pneumonia in clinical studies. *Biosci. Trends* 14, 72–73. doi: 10.5582/bst.2020.01047

García, C. A. C., Sánchez, E. B. A., Huerta, D. H., and Gómez-Arnau, J. (2020). Covid-19 treatment-induced neuropsychiatric adverse effects. *Gen. Hosp. Psychiatry* 67, 163–164. doi: 10.1016/j.genhosppsych.2020.06.001

Gauttam, P., Patel, N., Singh, B., Kaur, V. J., Chattu, V. K., and Jakovljevic, M. (2021). Public health policy of India and COVID-19: diagnosis and prognosis of the combating response. *Sustainability* 13:3415. doi: 10.3390/su13063415

Girdhar, R., Srivastava, V., and Sethi, S. (2020). Managing mental health issues among elderly during COVID-19 pandemic. *J. Geriatr. Care Res.* 7, 32–35.

Godman, B., Haque, M., Islam, S., Iqbal, S., Urmi, U. L., Kamal, Z. M., et al. (2020). Rapid assessment of price instability and paucity of medicines and protection for COVID-19 across Asia: findings and public health implications for the future. *Front. Public Health* 8:585832. doi: 10.3389/fpubh.2020.585832

Goothy, S. S. K., Goothy, S., Choudhary, A., Chakraborty, H., Poety, C. G., Kumar, A. H. S., et al. (2020). Ayurveda's holistic lifestyle approach for the management of coronavirus disease (COVID-19): possible role of tulsi. *Int. J. Res. Pharm. Sci.* 11, 16–18. doi: 10.26452/ijrps.v11iSPL1.1976

Guang, C., DunnGalvin, A., and Campbell, D. E. (2021). Impact of COVID-19 pandemic on quality of life for children and adolescents with food allergy. Clin. Exp. Allergy doi: 10.1111/cea.13973, PMID: 34157164 [Epub ahead of print].

Guo, T., Fan, Y., Chen, M., Wu, X., Zhang, L., He, T., et al. (2020). Cardiovascular implications of fatal outcomes of patients with coronavirus disease 2019 (COVID-19). *JAMA Cardiol.* 5, 811–818. doi: 10.1001/jamacardio.2020.1017

Gupta, A., Madhavan, M. V., Sehgal, K., Nair, N., Mahajan, S., Sehrawat, T. S., et al. (2020). Extrapulmonary manifestations of COVID-19. *Nat. Med.* 26, 1017–1032. doi: 10.1038/s41591-020-0968-3

Hadjadj, J., Yatim, N., Barnabei, L., Corneau, A., Boussier, J., Smith, N., et al. (2020). Impaired type I interferon activity and inflammatory responses in severe COVID-19 patients. *Science* 369, 718–724. doi: 10.1126/science.abc6027

Hammami, A., Harrabi, B., Mohr, M., and Krustrup, P. (2020). Physical activity and coronavirus disease 2019 (COVID-19): specific recommendations for home-based physical training. *Manag. Sport Leisure*. doi: 10.1080/23750472.2020.1757494. [Epub ahead of print]

Hensley, L. E., Fritz, L. E., Jahrling, P. B., Karp, C. L., Huggins, J. W., and Geisbert, T. W. (2004). Interferon-β 1a and SARS coronavirus replication. *Emerg. Infect. Dis.* 10, 317–319. doi: 10.3201/eid1002.030482

Hernández, J. L., Nan, D., Fernandez-Ayala, M., García-Unzueta, M., Hernández-Hernández, M. A., López-Hoyos, M., et al. (2021). Vitamin D status in hospitalized patients with SARS-CoV-2 infection. *J. Clin. Endocrinol. Metab.* 106, e1343–e1353. doi: 10.1210/clinem/dgaa733

HLPE (2020). Impacts of COVID-19 on food security and nutrition: Developing effective policy responses to address the hunger and malnutrition pandemic. Committee on World Food Security High Level Panel of Experts on Food Security and Nutrition, Rome.

Holick, M. F. (2017). The vitamin D deficiency pandemic: approaches for diagnosis, treatment and prevention. *Rev. Endocr. Metab. Disord.* 18, 153–165. doi: 10.1007/s11154-017-9424-1

Hollyfield, A. (2020). Coronavirus impact: Suicides on the rise amid shelter-in-place order, Bay Area medical professionals. Available at: https://abcnews.go.com/ (Accessed September 01, 2021)

Holmes, E. A., O'Connor, R. C., Perry, V. H., Tracey, I., Wessely, S., Arseneault, L., et al. (2020). Multidisciplinary research priorities for the COVID-19 pandemic: a call for action for mental health science. *Lancet Psychiatry* 7, 547–560. doi: 10.1016/S2215-0366(20)30168-1

Huang, C., Wang, Y., Li, X., Ren, L., Zhao, J., Hu, Y., et al. (2020). Clinical features of patients infected with 2019 novel coronavirus in Wuhan, China. *Lancet* 395, 497–506. doi: 10.1016/S0140-6736(20)30183-5

Jakovljevic, M. (2014). The key role of leading emerging BRIC markets for the future of global health care. *Ser. J. Exp. Clin. Res.* 15, 139–143. doi: 10.2478/sjecr-2014-0018

Jakovljevic, M. B. (2015). BRIC's growing share of global health spending and their diverging pathways. *Front. Public Health* 3:135. doi: 10.3389/fpubh.2015.00135

Jakovljevic, M. M. (2016). Comparison of historical medical spending patterns among the BRICS and G7. *J. Med. Econ.* 19, 70–76. doi: 10.3111/13696998.2015.1093493

Jakovljevic, M., Potapchik, E., Popovich, L., Barik, D., and Getzen, T. E. (2017). Evolving health expenditure landscape of the BRICS nations and projections to 2025. *Health Econ.* 26, 844–852. doi: 10.1002/hec.3406

Jakovljevic, M., Sugahara, T., Timofeyev, Y., and Rancic, N. (2020). Predictors of (in) efficiencies of healthcare expenditure among the leading asian economies–comparison of OECD and non-OECD nations. *Risk Manag. Healthc. Policy* 13, 2261–2280. doi: 10.2147/RMHP.S266386

Jakovljevic, M., Timofeyev, Y., Ekkert, N. V., Fedorova, J. V., Skvirskaya, G., Bolevich, S., et al. (2019). The impact of health expenditures on public health in BRICS nations. *J. Sport Health Sci.* 8, 516–519. doi: 10.1016/j.jshs.2019.09.002

Jamshidi, E., Asgary, A., Tavakoli, N., Zali, A., Dastan, F., Daaee, A., et al. (2021). Symptom prediction and mortality risk calculation for COVID-19 using machine learning. *Front. Artif. Intell.* 4:673527. doi: 10.3389/frai.2021.673527

Jones, K. S., Redmond, J., Fulford, A. J., Jarjou, L., Zhou, B., Prentice, A., et al. (2017). Diurnal rhythms of vitamin D binding protein and total and free vitamin D metabolites. *J. Steroid Biochem. Mol. Biol.* 172, 130–135. doi: 10.1016/j.jsbmb.2017.07.015

Jordan, R. E., Adab, P., and Cheng, K. K. (2020). Covid-19: risk factors for severe disease and death. *BMJ* 368:m1198. doi: 10.1136/bmj.m1198

Kalil, A. C., Patterson, T. F., Mehta, A. K., Tomashek, K. M., Wolfe, C. R., Ghazaryan, V., et al. (2021). Baricitinib plus remdesivir for hospitalized adults with Covid-19. *N. Engl. J. Med.* 384, 795–807. doi: 10.1056/NEJMoa2031994

Khanna, K., Kohli, S. K., Kaur, R., Bhardwaj, A., Bhardwaj, V., Ohri, P., et al. (2020). Herbal immune-boosters: substantial warriors of pandemic Covid-19 battle. *Phytomedicine* 85:153361. doi: 10.1016/j.phymed.2020.153361

Kontoangelos, K., Economou, M., and Papageorgiou, C. (2020). Mental health effects of COVID-19 pandemia: a review of clinical and psychological traits. *Psychiatry Investig.* 17, 491–505. doi: 10.30773/pi.2020.0161

Kumar, A., and Nayar, K. R. (2021). COVID 19 and its Mental Health Consequences *Journal of Mental Health* 30, 1–2. doi: 10.1080/09638237.2020.1757052

Lai, J., Ma, S., Wang, Y., Cai, Z., Hu, J., Wei, N., et al. (2020). Factors associated with mental health outcomes among health care workers exposed to coronavirus disease 2019. *JAMA Netw. Open* 3:e203976. doi: 10.1001/jamanetworkopen.2020.3976

Lanham-New, S. A., Webb, A. R., Cashman, K. D., Buttriss, J. L., Fallowfield, J. L., Masud, T., et al. (2020). Vitamin D and SARS-CoV-2 virus/COVID-19 disease. *BMJ Nutr. Prev. Health* 3, 106–110. doi: 10.1136/bmjnph-2020-000089

Lee, M.-D., Lin, C. H., Lei, W. T., Chang, H. Y., Lee, H. C., Yeung, C. Y., et al. (2018). Does vitamin D deficiency affect the immunogenic responses to influenza vaccination? A systematic review and meta-analysis. *Nutrients* 10:409. doi: 10.3390/nu10040409

Lipszyc, P. S., Cremaschi, G. A., Zorrilla-Zubilete, M., Bertolino, M. L. A., Capani, F., Genaro, A. M., et al. (2013). Niacin modulates pro-inflammatory cytokine secretion. A potential mechanism involved in its anti-atherosclerotic effect. *Open Cardiovasc. Med. J.* 7, 90–98. doi: 10.2174/1874192401307010090

Loades, M. E., Chatburn, E., Higson-Sweeney, N., Reynolds, S., Shafran, R., Brigden, A., et al. (2020). Rapid systematic review: the impact of social isolation and loneliness on the mental health of children and adolescents in the context of COVID-19. *J. Am. Acad. Child Adolesc. Psychiatry* 59, 1218–1239. doi: 10.1016/j.jaac.2020.05.009

Lokugamage, K.G., Hage, A., Schindewolf, C., Rajsbaum, R., and Menachery, V. D. (2020). SARS-CoV-2 is sensitive to type I interferon pretreatment. BioRxiv doi: 10.1101/2020.03.07.982264, PMID: 32511335 [Preprint].

Lordan, R. (2021). Notable developments for vitamin D amid the COVID-19 pandemic, but caution warranted overall: a narrative review. *Nutrients* 13:740. doi: 10.3390/nu13030740

Luo, H., Tang, Q. L., Shang, Y. X., Liang, S. B., Yang, M., Robinson, N., et al. (2020). Can Chinese medicine be used for prevention of corona virus disease 2019 (COVID-19)? A review of historical classics, research evidence and current prevention programs. *Chin. J. Integr. Med.* 26, 243–250. doi: 10.1007/s11655-020-3192-6

Mack, D. P., Chan, E. S., Shaker, M., Abrams, E. M., Wang, J. W., Fleischer, D. W., et al. (2020). Novel approaches to food allergy management during COVID-19 inspire long-term change. *J. Allergy Clin. Immunol. Pract.* 8, 2851–2857. doi: 10.1016/j.jaip.2020.07.020

Mak, J. W. Y., Chan, F. K. L., and Ng, S. C. (2020). Probiotics and COVID-19: one size does not fit all. *Lancet Gastroenterol. Hepatol.* 5, 644–645. doi: 10.1016/S2468-1253(20)30122-9

Mao, L., Jin, H., Wang, M., Hu, Y., Chen, S., He, Q., et al. (2020). Neurologic manifestations of hospitalized patients with coronavirus disease 2019 in Wuhan, China. *JAMA Neurol.* 77, 683–690. doi: 10.1001/jamaneurol.2020.1127

Maurya, V. K., Kumar, S., Bhatt, M. L. B., and Saxena, S. K. (2020). "Therapeutic development and drugs for the treatment of COVID-19" in *Medical Virology: From Pathogenesis to Disease Control*. ed. S. Saxena (Springer, Singapore), 109–126.

Mehta, A., Soni, V. K., Sharma, K., Ratre, Y. K., Shukla, D., Singh, A. K., et al. (2021). Finding Horcrux of psychiatric symptoms in COVID-19: deficiencies of amino acids and vitamin D. *Asian J. Psychiatr.* 55:102523. doi: 10.1016/j.ajp.2020.102523

Mengheri, E., Nobili, F., Crocchioni, G., and Lewis, J. A. (1992). Protein starvation impairs the ability of activated lymphocytes to produce interferon-γ. *J. Interf. Res.* 12, 17–21. doi: 10.1089/jir.1992.12.17

Mitchell, F. (2020). Vitamin-D and COVID-19: do deficient risk a poorer outcome? *Lancet Diabetes Endocrinol.* 8:570. doi: 10.1016/S2213-8587(20)30183-2

Mobarhan, S., and DeMeo, M. (1995). Diarrhea induced by enteral feeding. *Nutr. Rev.* 53, 67–70. doi: 10.1111/j.1753-4887.1995.tb01504.x

Mohan, M., Cherian, J. J., and Sharma, A. (2020). Exploring links between vitamin D deficiency and COVID-19. *PLoS Pathog.* 16:e1008874. doi: 10.1371/journal.ppat.1008874

Muralikumar, S., Vetrivel, U., Narayanasamy, A., and Das, U. N. (2017). Probing the intermolecular interactions of PPARγ-LBD with polyunsaturated fatty acids and their anti-inflammatory metabolites to infer most potential binding moieties. *Lipids Health Dis.* 16, 1–11. doi: 10.1186/s12944-016-0404-3

Nadalin, S., Jakovac, H., Peitl, V., Karlović, D., and Buretić-Tomljanović, A. (2021). Dysregulated inflammation may predispose patients with serious mental illnesses to severe COVID-19 (review). *Mol. Med. Rep.* 24:611. doi: 10.3892/mmr.2021.12250

Nicolau, J., Ayala, L., Sanchís, P., Olivares, J., Dotres, K., Soler, A. G., et al. (2021). Influence of nutritional status on clinical outcomes among hospitalized patients with COVID-19. *Clin. Nutr. ESPEN* 43, 223–229. doi: 10.1016/j.clnesp.2021.04.013

Pan, L., Mu, M., Yang, P., Sun, Y., Wang, R., Yan, R., et al. (2020). Clinical characteristics of COVID-19 patients with digestive symptoms in Hubei, China: a descriptive, cross-sectional, multicenter study. *Am. J. Gastroenterol.* 115, 766–773. doi: 10.14309/ajg.0000000000000620

Penkert, R. R., Rowe, H. M., Surman, S. L., Sealy, R. E., Rosch, J., and Hurwitz, J. L. (2019). Influences of vitamin A on vaccine immunogenicity and efficacy. *Front. Immunol.* 10:1576. doi: 10.3389/fimmu.2019.01576

Persynaki, A., Karras, S., and Pichard, C. (2017). Unraveling the metabolic health benefits of fasting related to religious beliefs: a narrative review. *Nutrition* 35, 14–20. doi: 10.1016/j.nut.2016.10.005

Popkova, E., DeLo, P., and Sergi, B. S. (2021). Corporate social responsibility amid social distancing during the COVID-19 crisis: BRICS vs. OECD countries. *Res. Int. Bus. Financ.* 55:101315. doi: 10.1016/j.ribaf.2020.101315

Pourabbasi, A., Ahangar, A. A., and Nouriyengejeh, S. (2021). Value-based eating habits; exploring religio-cultural nutritional behavior norms. *J. Diabetes Metab. Dis.* 20, 187–192. doi: 10.1007/s40200-021-00728-z

Prosekov, A. Y., and Ivanova, S. A. (2018). Food security: the challenge of the present. *Geoforum* 91, 73–77. doi: 10.1016/j.geoforum.2018.02.030

Rababah, A., Nikitina, N. I., Grebennikova, V. M., Gardanova, Z. R., Zekiy, A. O., Ponkratov, V. V., et al. (2021). University social responsibility during the COVID-19 pandemic: universities' case in the BRICS countries. *Sustain. For.* 13:7035. doi: 10.3390/su13137035

Ranabhat, C. L., Jakovljevic, M. M., and Kim, C.-B. (2021). COVID-19 pandemic: an opportunity for universal health coverage. *Front. Public Health* 9:673542. doi: 10.3389/fpubh.2021.673542

Rao, T. S. S., Asha, M. R., Ramesh, B. N., and Rao, K. S. J. (2008). Understanding nutrition, depression and mental illnesses. *Indian J. Psychiatry* 50, 77–82. doi: 10.4103/0019-5545.42391

Ratre, Y. K., Vishvakarma, N. K., Bhaskar, L. V. K. S., and Verma, H. K. (2020). Dynamic propagation and impact of pandemic influenza A (2009 H1N1) in children: a detailed review. *Curr. Microbiol.* 77, 3809–3820. doi: 10.1007/s00284-020-02213-x

Raw, J., Waite, P., Pearcey, S., Shum, A., Patalay, P., and Creswell, C. (2021). Examining changes in parent-reported child and adolescent mental health throughout the UK's first COVID-19 national lockdown. J. Child Psychol. Psychiatry doi: 10.1111/jcpp.13490. [Epub ahead of print].

Reshetnikov, V., Mitrokhin, O., Shepetovskaya, N., Belova, E., and Jakovljevic, M. (2020). Organizational measures aiming to combat COVID-19 in the Russian federation: the first experience. *Exp. Rev. Pharmacoecon. Outcomes Res.* 20, 571–576. doi: 10.1080/14737167.2020.1823221

Ribeiro, D. E., Oliveira-Giacomelli, A., Glaser, T., Arnaud-Sampaio, V. F., Andrejew, R., Dieckmann, L., et al. (2021). Hyperactivation of P2X7 receptors as a culprit of COVID-19 neuropathology. *Mol. Psychiatry* 26, 1044–1059. doi: 10.1038/s41380-020-00965-3

Ribeiro-Silva, R. D. C., Pereira, M., Campello, T., Aragão, E., de Medeiros Guimarães, J. M., Ferreira, A., et al. (2020). Implicações da pandemia COVID-19 para a segurança alimentar e nutricional no Brasil. *Ciên. Saúde Colet.* 25, 3421–3430. doi: 10.1590/1413-81232020259.22152020

Ritchie, H., and Roser, M. (2018). Mental Health. Available at: https://ourworldindata.org/ (Accessed July 30, 2021).

Rodriguez-Leyva, D., and Pierce, G. N. (2021). The impact of nutrition on the COVID-19 pandemic and the impact of the COVID-19 pandemic on nutrition. *Nutrients* 13:1752. doi: 10.3390/nu13061752

Roser, M., and Ritchie, H. (2019). Hunger and Undernourishment. Available at: https://ourworldindata.org/ (Accessed September 01, 2021).

Rozga, M., Cheng, F. W., Moloney, L., and Handu, D. (2021). Effects of micronutrients or conditional amino acids on COVID-19-related outcomes: an evidence analysis center scoping review. *J. Acad. Nutr. Diet.* 121, 1354–1363. doi: 10.1016/j.jand.2020.05.015

Saggam, A., Limgaokar, K., Borse, S., Chavan-Gautam, P., Dixit, S., Tillu, G., et al. (2021). Opportunity for clinical repurposing in COVID-19 management. *Front. Pharmacol.* 12:623795. doi: 10.3389/fphar.2021.623795

Sahu, T., Mehta, A., Ratre, Y. K., Jaiswal, A., Vishvakarma, N. K., Bhaskar, L. V. K. S., et al. (2021). Current understanding of the impact of COVID-19 on gastrointestinal disease: challenges and openings. *World J. Gastroenterol.* 27, 449–469. doi: 10.3748/wjg.v27.i6.449

Sanders, J. M., Monogue, M. L., Jodlowski, T. Z., and Cutrell, J. B. (2020). Pharmacologic treatments for coronavirus disease 2019 (COVID-19): a review. *JAMA* 323, 1824–1836. doi: 10.1001/jama.2020.6019

Sarris, J., Logan, A. C., Akbaraly, T. N., Amminger, G. P., Balanzá-Martínez, V., Freeman, M. P., et al. (2015). Nutritional medicine as mainstream in psychiatry. *Lancet Psychiatry* 2, 271–274. doi: 10.1016/S2215-0366(14)00051-0

Savarino, A., Boelaert, J. R., Cassone, A., Majori, G., and Cauda, R. (2003). Effects of chloroquine on viral infections: an old drug against today's diseases. *Lancet Infect. Dis.* 3, 722–727. doi: 10.1016/S1473-3099(03)00806-5

Shakoor, H., Feehan, J., Al Dhaheri, A. S., Ali, H. I., Platat, C., Ismail, L. C., et al. (2020). Immune-boosting role of vitamins D, C, E, zinc, selenium and omega-3 fatty acids: could they help against COVID-19? *Maturitas* 43, 1–9. doi: 10.1016/j.maturitas.2020.08.003

Shi, Q., Zhang, X., Jiang, F., Zhang, X., Hu, N., Bimu, C., et al. (2020). Clinical characteristics and risk factors for mortality of COVID-19 patients with diabetes in Wuhan, China: a two-center, retrospective study. *Diabetes Care* 43, 1382–1391. doi: 10.2337/dc20-0598

Shree, P., Mishra, P., Selvaraj, C., Singh, S. K., Chaube, R., Garg, N., et al. (2020). Targeting COVID-19 (SARS-CoV-2) main protease through active phytochemicals of ayurvedic medicinal plants–Withania somnifera (Ashwagandha), Tinospora cordifolia (Giloy) and Ocimum sanctum (Tulsi)–a molecular docking study. *J. Biomol. Struct. Dyn.* doi: 10.1080/07391 102.2020.1810778. [Epub ahead of print]

Silverio, R., Gonçalves, D. C., Andrade, M. F., and Seelaender, M. (2021). Coronavirus disease 2019 (COVID-19) and nutritional status: the missing link? *Adv. Nutr.* 12, 682–692. doi: 10.1093/advances/nmaa125

Singh, A. K., Agrawal, B., Sharma, A., and Sharma, P. (2020). COVID-19: assessment of knowledge and awareness in Indian society. *J. Public Aff.* 20:e2354. doi: 10.1002/pa.2354

Singh, M. P., Rai, S. N., Dubey, S. K., Pandey, A. T., Tabassum, N., Chaturvedi, V. K., et al. (2021). Biomolecules of mushroom: a recipe of human wellness. *Crit. Rev. Biotechnol.* doi: 10.1080/07388551. 2021.1951649. [Epub ahead of print]

Sirois, F. (2002). Délirium associé à l'azithromycine. *Can. J. Psychiatr.* 47, 585–586. doi: 10.1177/070674370204700622

Slominski, A., Semak, I., Pisarchik, A., Sweatman, T., Szczesniewski, A., and Wortsman, J. (2002). Conversion of L-tryptophan to serotonin and melatonin in human melanoma cells. *FEBS Lett.* 511, 102–106. doi: 10.1016/ S0014-5793(01)03319-1

Soni, V. K., Mehta, A., Ratre, Y. K., Tiwari, A. K., Amit, A., Singh, R. P., et al. (2020a). Curcumin, a traditional spice component, can hold the promise against COVID-19? *Eur. J. Pharmacol.* 886:173551. doi: 10.1016/j.ejphar.2020.173551

Soni, V.K., Mehta, A., Sharma, K., Ratre, Y. K., Dwivedi, M., Chaturvedi, N., et al. (2021). Immunity boosters in COVID-19: Reality or myth? Medicine India.

Soni, V. K., Mehta, A., Shukla, D., Kumar, S., and Vishvakarma, N. K. (2020b). Fight COVID-19 depression with immunity booster: curcumin for psychoneuroimmunomodulation. *Asian J. Psychiatr.* 53:102378. doi: 10.1016/j.ajp.2020.102378

Soni, V. K., Sharma, K., Mehta, A., Ratre, Y. K., Kumar, S., Shukla, D., et al. (2020d). A physiological link for psychiatric symptoms in COVID-19: role of amino acid deficiency. *Asian J. Psychiatr.* 53:102426. doi: 10.1016/j.ajp.2020.102426

Soni, V. K., Shukla, D., Kumar, A., and Vishvakarma, N. K. (2020c). Curcumin circumvent lactate-induced chemoresistance in hepatic cancer cells through modulation of hydroxycarboxylic acid receptor-1. *Int. J. Biochem. Cell Biol.* 123:105752. doi: 10.1016/j.biocel.2020.105752

Steardo, L., and Verkhratsky, A. (2020). Psychiatric face of COVID-19. *Transl. Psychiatry* 10, 1–12. doi: 10.1038/s41398-020-00949-5

Tan, M.-M., Chan, C. K. Y., and Reidpath, D. D. (2013). Religiosity and spirituality and the intake of fruit, vegetable, and fat: a systematic review. *Evid. Based Complement. Alternat. Med.* 2013:146214. doi: 10.1155/2013/146214

Tandon, R. (2020). COVID-19 and mental health: preserving humanity, maintaining sanity, and promoting health. *Asian J. Psychiatr.* 51:102256. doi: 10.1016/j.ajp.2020.102256

Taylor, S. (2019). *The Psychology of Pandemics: Preparing for the Next Global Outbreak of Infectious Disease.* United Kingdom: Cambridge Scholars Publishing.

Teasdale, S. B., Ward, P. B., Samaras, K., Firth, J., Stubbs, B., Tripodi, E., et al. (2019). Dietary intake of people with severe mental illness: systematic review and meta-analysis. *Br. J. Psychiatry* 214, 251–259. doi: 10.1192/bjp.2019.20

Thakur, V., and Jain, A. (2020). COVID 2019-suicides: a global psychological pandemic. *Brain Behav. Immun.* 88, 952–953. doi: 10.1016/j.bbi.2020.04.062

Thibault, R., Coëffier, M., Joly, F., Bohé, J., Schneider, S. M., and Déchelotte, P. (2021). How the Covid-19 epidemic is challenging our practice in clinical nutrition—feedback from the field. *Eur. J. Clin. Nutr.* 75, 407–416. doi: 10.1038/s41430-020-00757-6

Tong, S., Su, Y., Yu, Y., Wu, C., Chen, J., Wang, S., et al. (2020). Ribavirin therapy for severe COVID-19: a retrospective cohort study. *Int. J. Antimicrob. Agents* 56:106114. doi: 10.1016/j.ijantimicag.2020.106114

Ulrich, E. S., and Kaufmann, S. H. E. (2007). Malnutrition and infection: complex mechanisms and global impacts. *PLoS Med.* 4:e115. doi: 10.1371/journal.pmed.0040115

UNICEF (2020). Levels and trends in child malnutrition: Key findings of the 2020 edition. Available at: https://www.unicef.org/reports/joint-child-malnutrition-estimates-levels-and-trends-child-malnutrition-2020 (Accessed September 01, 2021).

Vellingiri, B., Jayaramayya, K., Iyer, M., Narayanasamy, A., Govindasamy, V., Giridharan, B., et al. (2020). COVID-19: a promising cure for the global panic. *Sci. Total Environ.* 725:138277. doi: 10.1016/j.scitotenv.2020.138277

Vindegaard, N., and Benros, M. E. (2020). COVID-19 pandemic and mental health consequences: systematic review of the current evidence. *Brain Behav. Immun.* 89, 531–542. doi: 10.1016/j.bbi.2020.05.048

Von Polier, G. G., Biskup, C. S., Kötting, W. F., Bubenzer, S., Helmbold, K., Eisert, A., et al. (2014). Change in electrodermal activity after acute tryptophan depletion associated with aggression in young people with attention deficit hyperactivity disorder (ADHD). *J. Neural Transm.* 121, 451–455. doi: 10.1007/s00702-013-1119-5

Wang, M., Cao, R., Zhang, L., Yang, X., Liu, J., Xu, M., et al. (2020). Remdesivir and chloroquine effectively inhibit the recently emerged novel coronavirus (2019-nCoV) in vitro. *Cell Res.* 30, 269–271. doi: 10.1038/s41422-020-0282-0

Wang, Q., Xu, R., and Volkow, N. D. (2021). Increased risk of COVID-19 infection and mortality in people with mental disorders: analysis from electronic health records in the United States. *World Psychiatry* 20, 124–130. doi: 10.1002/wps.20806

Warner, F. J., Rajapaksha, H., Shackel, N., and Herath, C. B. (2020). ACE2: from protection of liver disease to propagation of COVID-19. *Clin. Sci.* 134, 3137–3158. doi: 10.1042/CS20201268

WHO (2021). WHO Coronavirus (COVID-19) Dashboard. 2021. Available at https://covid19.who.int/ (Accessed September 01, 2021).

Xu, X., Han, M., Li, T., Sun, W., Wang, D., Fu, B., et al. (2020). Effective treatment of severe COVID-19 patients with tocilizumab. *Proc. Natl. Acad. Sci. U. S. A.* 117, 10970–10975. doi: 10.1073/pnas.2005615117

Yamamoto, V., Bolanos, J. F., Fiallos, J., Strand, S. E., Morris, K., Shahrokhinia, S., et al. (2020). COVID-19: review of a 21st century pandemic from etiology to neuro-psychiatric implications. *J. Alzheimers Dis.* 77, 459–504. doi: 10.3233/JAD-200831

Yang, J., Zheng, Y., Gou, X., Pu, K., Chen, Z., Guo, Q., et al. (2020). Prevalence of comorbidities and its effects in patients infected with SARS-CoV-2: a systematic review and meta-analysis. *Int. J. Infect. Dis.* 94, 91–95. doi: 10.1016/j.ijid.2020.03.017

Yao, T. T., Qian, J. D., Zhu, W. Y., Wang, Y., and Wang, G. Q. (2020). A systematic review of lopinavir therapy for SARS coronavirus and MERS coronavirus—a possible reference for coronavirus disease-19 treatment option. *J. Med. Virol.* 92, 556–563. doi: 10.1002/jmv.25729

Yoshii, K., Hosomi, K., Sawane, K., and Kunisawa, J. (2019). Metabolism of dietary and microbial vitamin B family in the regulation of host immunity. *Front. Nutr.* 6:48. doi: 10.3389/fnut.2019.00048

Zahedipour, F., Hosseini, S. A., Sathyapalan, T., Majeed, M., Jamialahmadi, T., Al-Rasadi, K., et al. (2020). Potential effects of curcumin in the treatment of COVID-19 infection. *Phytother. Res.* 34, 2911–2920. doi: 10.1002/ptr.6738

Zhang, M., and Jativa, D. F. (2018). Vitamin C supplementation in the critically ill: A systematic review and meta-analysis. *SAGE Open Med.* 6:2050312118807615. doi: 10.1177/2050312118807615

Zhao, A., Li, Z., Ke, Y., Huo, S., Ma, Y., Zhang, Y., et al. (2020). Dietary diversity among Chinese residents during the COVID-19 outbreak and its associated factors. *Nutrients* 12:1699. doi: 10.3390/nu12061699

Zhou, F., Yu, T., Du, R., Fan, G., Liu, Y., Liu, Z., et al. (2020). Clinical course and risk factors for mortality of adult inpatients with COVID-19 in Wuhan, China: a retrospective cohort study. *Lancet* 395, 1054–1062. doi: 10.1016/S0140-6736(20)30566-3

Zhu, J., Yan, W., and Liu, J. (2021). COVID-19 pandemic in BRICS countries and its association with socio-economic and demographic characteristics, health vulnerability, resources, and policy response. *Infect. Dis. Poverty* 10, 1–8. doi: 10.1186/s40249-021-00881-w

Zubair, A. S., McAlpine, L. S., Gardin, T., Farhadian, S., Kuruvilla, D. E., and Spudich, S. (2020). Neuropathogenesis and neurologic manifestations of the coronaviruses in the age of coronavirus disease 2019: a review. *JAMA Neurol.* 77, 1018–1027. doi: 10.1001/jamaneurol.2020.2065

Zvolensky, M. J., Garey, L., Rogers, A. H., Schmidt, N. B., Vujanovic, A. A., Storch, E. A., et al. (2020). Psychological, addictive, and health behavior implications of the COVID-19 pandemic. *Behav. Res. Ther.* 134:103715. doi: 10.1016/j.brat.2020.103715

**Conflict of Interest:** The authors declare that the research was conducted in the absence of any commercial or financial relationships that could be construed as a potential conflict of interest.

Check for
updates

# Kaposi's Sarcoma-Associated Herpesvirus, but Not Epstein-Barr Virus, Co-infection Associates With Coronavirus Disease 2019 Severity and Outcome in South African Patients

Melissa J. Blumenthal[1,2,3]*, Humaira Lambarey[1,2,3], Abeen Chetram[1], Catherine Riou[2,4,5], Robert J. Wilkinson[2,4,6,7] and Georgia Schäfer[1,2,3,4]* on behalf of the HIATUS Consortium[†]

[1] International Centre for Genetic Engineering and Biotechnology (ICGEB), Cape Town, South Africa, [2] Institute of Infectious Disease and Molecular Medicine (IDM), Faculty of Health Sciences, University of Cape Town, Cape Town, South Africa, [3] Department of Integrative Biomedical Sciences, Faculty of Health Sciences, University of Cape Town, Cape Town, South Africa, [4] Wellcome Centre for Infectious Disease Research in Africa, University of Cape Town, Cape Town, South Africa, [5] Division of Medical Virology, Department of Pathology, University of Cape Town, Cape Town, South Africa, [6] Department of Infectious Diseases, Imperial College London, London, United Kingdom, [7] The Francis Crick Institute, London, United Kingdom

In South Africa, the Coronavirus Disease 2019 (COVID-19) pandemic is occurring against the backdrop of high Human Immunodeficiency Virus (HIV), tuberculosis and non-communicable disease burdens as well as prevalent herpesviruses infections such as Epstein-Barr virus (EBV) and Kaposi's sarcoma-associated herpesvirus (KSHV). As part of an observational study of adults admitted to Groote Schuur Hospital, Cape Town, South Africa during the period June–August 2020 and assessed for Severe Acute Respiratory Syndrome Coronavirus 2 (SARS-CoV-2) infection, we measured KSHV serology and KSHV and EBV viral load (VL) in peripheral blood in relation to COVID-19 severity and outcome. A total of 104 patients with PCR-confirmed SARS-CoV-2 infection were included in this study. 61% were men and 39% women with a median age of 53 years (range 21–86). 29.8% (95% CI: 21.7–39.1%) of the cohort was HIV positive and 41.1% (95% CI: 31.6–51.1%) were KSHV seropositive. EBV VL was detectable in 84.4% (95% CI: 76.1–84.4%) of the cohort while KSHV DNA was detected in 20.6% (95% CI: 13.6–29.2%), with dual EBV/KSHV infection in 17.7% (95% CI: 11.1–26.2%). On enrollment, 48 [46.2% (95% CI: 36.8–55.7%)] COVID-19 patients were classified as severe on the WHO ordinal scale reflecting oxygen therapy and supportive care requirements and 30 of these patients [28.8% (95% CI: 20.8–38.0%)] later died. In COVID-19 patients, detectable KSHV VL was associated with death after adjusting for age, sex, HIV status and detectable EBV VL [$p = 0.036$, adjusted $OR = 3.17$ (95% CI: 1.08–9.32)]. Furthermore, in HIV negative COVID-19 patients, there was a trend indicating that KSHV VL may be related to COVID-19 disease severity [$p = 0.054$, unstandardized co-efficient 0.86 (95% CI: –0.015–1.74)] in addition

to death [$p$ = 0.008, adjusted $OR$ = 7.34 (95% CI: 1.69–31.49)]. While the design of our study cannot distinguish if disease synergy exists between COVID-19 and KSHV nor if either viral infection is indeed fueling the other, these data point to a potential contribution of KSHV infection to COVID-19 outcome, or SARS-CoV-2 infection to KSHV reactivation, particularly in the South African context of high disease burden, that warrants further investigation.

# INTRODUCTION

Coronavirus disease 2019 (COVID-19), the disease resulting from infection with the Severe Acute Respiratory Syndrome Coronavirus 2 (SARS-CoV-2), emerged in December 2019 and rapidly reached global proportions, officially declared a "pandemic" in March 2020 (Hui et al., 2020; World Health Organization, 2020). Since, the devastating COVID-19 pandemic has caused more than 212 million infections and 4.43 million deaths worldwide (Ritchie et al., 2020). Importantly, in countries such as South Africa with high numbers of people living with Human Immunodeficiency Virus (HIV-1), significant burdens of *Mycobacterium tuberculosis* (Mtb) and non-communicable diseases, the intersecting COVID-19 pandemic poses a significant public health crisis. Furthermore, latent oncogenic herpesvirus infections such as Epstein-Barr virus (EBV) and Kaposi's sarcoma-associated herpesvirus (KSHV) are highly prevalent in South Africa (Sitas et al., 1999; Wilkinson et al., 1999; Schaftenaar et al., 2014; Blumenthal et al., 2018, 2019).

Mounting evidence points to potential interplay between SARS-CoV-2 infection and reactivation of opportunistic herpesvirus infections. This has been demonstrated for EBV, suggesting that reactivation of underlying EBV infection may contribute to COVID-19 symptoms, severity and time to recovery (Chen T. et al., 2021; Gold et al., 2021; Paolucci et al., 2021; Saade et al., 2021). In addition, secondary reactivation of herpes simplex virus (HSV) and Cytomegalovirus (CMV) has been reported in patients admitted to ICU with severe COVID-19 (Saade et al., 2021). Furthermore, SARS-CoV-2 encoded proteins have been shown to induce KSHV lytic reactivation *in vitro* (Chen J. et al., 2021).

While EBV infection is considered ubiquitous (Rochford, 2009), the prevalence of KSHV varies geographically and is particularly high in sub-Saharan Africa (seroprevalence 30–50%) and the Mediterranean region (20–30%) (de Sanjose et al., 2009; Mesri et al., 2010; Blumenthal et al., 2019). EBV and KSHV, both gamma-herpesviruses, have oncogenic potential, particularly in immunosuppressed patients (Schäfer et al., 2015). EBV is causally associated with Burkitt's lymphoma, Hodgkin's lymphoma, T and NK cell lymphomas, immunosuppression-related lymphoma, nasopharyngeal carcinoma and stomach carcinoma (Thompson and Kurzrock, 2004; Schäfer et al., 2015). KSHV is the causative agent of Kaposi's Sarcoma, multicentric Castleman disease and primary effusion lymphoma (Mesri et al., 2010). Additionally, a lytic KSHV syndrome referred to as

KSHV-related inflammatory cytokine syndrome (KICS) has been recently described (Uldrick et al., 2010; Polizzotto et al., 2012) which presents with generalized inflammatory symptoms and cytokine storm clinically akin to that of severe COVID-19 (Hu et al., 2021).

As an airborne virus, curbing SARS-CoV-2 transmission has posed a major challenge globally despite stringent travel restrictions and national and regional lock downs. This has been further exacerbated by the emergence of new highly transmissible variants of concern (van Oosterhout et al., 2021). Despite widespread vaccination programs being implemented globally, COVID-19 is likely to persist for years to come, be it due to emerging variants, transmission among unvaccinated subpopulations or waning vaccine efficacy (Phillips, 2021). The long-term effects of SARS-CoV-2 infection on virus-associated cancers, particularly in regions with high underlying EBV, KSHV, and HIV prevalence, are currently unknown and may present a public health challenge that outlasts the pandemic.

We herein present observational data on the association of KSHV and EBV co-infection on COVID-19 severity and outcome in a cross-sectional study of hospitalized COVID-19 patients recruited during the first COVID-19 wave in South Africa.

# MATERIALS AND METHODS

## Study Cohort

A cohort of 104 hospitalized adult patients with confirmed acute COVID-19 (by RT-PCR) were recruited to the HIATUS (SARS-CoV-2, HIV-1, and *M. tuberculosis*) study (Riou et al., 2021) from Groote Schuur Hospital in Cape Town, South Africa between June and August 2020, during South Africa's first wave of COVID-19 disease. The clinical characteristics of patients included in this study are presented in **Table 1**.

The study was conducted according to the declaration of Helsinki, conformed to South African Good Clinical Practice guidelines, and was approved by the University of Cape Town's Health Sciences Research Ethical Committee (HREC 207/2020).

## Clinical Data

Clinical and demographic details including patient co-morbidities were collected at enrollment. Absolute CD4 count (for HIV-1-infected patients) and white cell counts (WCC) were obtained from patients' medical files. Full blood count and differential cell count, C-reactive protein (CRP), Ferritin,

**TABLE 1** | Baseline characteristics of COVID-19 patients (n = 104).

| Demographic information | N (%) or Median (range) | |
|---|---|---|
| Male sex | 63 (60.6%) | |
| Age (years) | 53.0 (21.2–85.7) | |
| **Virological information** | **N (%) or Median (range)** | |
| SARS-CoV-2 PCR positive | 104 (100%) | |
| SARS-CoV-2 antibody positive | 72 (69.2%) | |
| COI[a] | 7.07 (0.06–83.03) | |
| HIV positive | 31 (29.8%) | |
| Receiving ART | 23 (74.2%) | |
| HIV VL (copies/ml) | 20 (20–523,463) | |
| CD4 (cells/$\mu$l) | 135 (3–1,367) | |
| KSHV seropositive | 39 (41.1%) | |
| KSHV VL detectable in blood sample | 21 (20.6%) | |
| KSHV VL (copies/$10^6$ cells) | 1.0 (1.0–38784.0) | |
| EBV VL detectable in blood sample | 81 (84.4%) | |
| EBV VL (copies/$10^6$ cells) | 1152.0 (1.0–1.44 × $10^6$) | |
| KSHV and EBV infection | 17 (17.7%) | |
| **Comorbidities** | **(N,%)** | |
| Tuberculosis | 15 (14.4%) | |
| Diabetes | 41 (39.4%) | |
| Hypertension | 50 (48.1%) | |
| Obesity | 32 (30.8%) | |
| **Laboratory abnormalities** | **Abnormal[b] [N (%)]** | **Median (range)** |
| C-reactive protein (mg/l) | 97 (94.2%) | 170 (6–467) |
| D-dimer ($\mu$g/ml) | 89 (89.9%) | 0.6750 (0.2–5.26) |
| LDH (U/l) | 97 (97%) | 396.5 (148.0–894.0) |
| Ferritin (ng/ml) | 93 (91.2%) | 1571.0 (65.0–4217.0) |
| Sodium (mmol/l) | 42 (46.2%) | 136.0 (119.0–148.0) |
| Potassium (mmol/l) | 12 (13.3%) | 4.35 (3.2–6.6) |
| Hemoglobin (g/dl) | 46 (45.1%) | 12.5 (5.8–17.2) |
| White cell count (×$10^9$/l) | 51 (49.0%) | 10.9 (2.64–33.7) |
| Neutrophils (×$10^9$/l) | 46 (57.5%) | 7.4 (2.1–26.9) |
| Lymphocytes (×$10^9$/l) | 43 (53.8%) | 1.2 (0.40–3.1) |
| Eosinophils (×$10^9$/l) | 0 (0%) | 0.0 (0.0–0.45) |
| Monocytes (×$10^9$/l) | Low: 21 (26.3%) High: 10 (12.5%) | 0.5 (0.0–1.5) |
| Creatinine ($\mu$mol/l) | Low: 35 (34.3%) High: 22 (21.4%) | 78.5 (35.0–374.0) |
| Platelets (×$10^9$/l) | Low: 18 (17.6%) High: 19 (18.6%) | 272.0 (32.0–679.0) |
| **Severity and outcome** | **N (%) or Median (range)** | |
| WHO score on enrollment: severe (≥ 5) | 48 (46.2%) | |
| PC1 severity[c] | 0.09 (–3.01 to 4.07) | |
| Outcome: died | 30 (28.8%) | |

Data are presented as number and percentage of total or median and range, as appropriate. Missing data are excluded per characteristic.

[a]SARS-CoV-2 serology was performed using the Roche Elecsys® assay, measuring SARS-CoV-2 nucleocapsid-specific antibodies.

[b]Abnormal refers to elevated C-reactive protein (> 10 mg/l); elevated D-dimer (> 0.5 $\mu$g/ml); elevated LDH (> 250U/l); elevated ferritin (males > 300 ng/ml; females > 200 ng/ml); low sodium (< 135 mmol/l); elevated potassium (> 5 mmol/l); low hemoglobin (females < 12 g/dl; males < 13 g/dl); low white cell count (< 3.9 × $10^9$/l); elevated neutrophils (males > 6.98 × $10^9$/l; females > 8.3 × $10^9$/l); low lymphocytes (< 1.4 × $10^9$/l); elevated eosinophils (females > 0.4 × $10^9$/l; males > 0.95 × $10^9$/l); low (females < 0.2 × $10^9$/l; males < 0.3 × $10^9$/l) or elevated (> 0.8 × $10^9$/l) monocytes; low (females < 49$\mu$mol/l; males < 64$\mu$mol/l) or elevated (females > 90$\mu$mol/l; males > 104$\mu$mol/l) creatinine; and low (< 186 × $10^9$/l) or elevated (females > 454 × $10^9$/l; males > 388 × $10^9$/l) platelet count.

[c]PC1 severity score refers to the calculated grading of COVID-19 disease (see **Figure 1**).

ART, antiretroviral treatment; COI, Cut-off index of Roche Elecsys® assay; CRP, C-Reactive protein; LDH, lactate dehydrogenase; VL, viral load.

D-dimer, Lactate dehydrogenase (LDH), blood electrolytes, tuberculosis Gene Xpert nucleic amplification testing, and HIV-1 ELISA and viral load (VL) tests were performed by the National Health Laboratory Services, as well as SARS-CoV-2 diagnostic RT-PCR and nucleocapsid-specific IgG (see "SARS-CoV-2 detection"). Posteroanterior chest radiographs were assessed for the total percentage of the lung fields unaffected by any visible pathology.

Clinical, demographic and experimental data were recorded and stored on an electronic REDCap database (Harris et al., 2009), hosted by the University of Cape Town.

## Severe Acute Respiratory Syndrome Coronavirus 2 Detection

Diagnostic RT-PCR (Seegene, Roche or Gene Xpert) for SARS-CoV-2 was performed using nasopharyngeal or oropharyngeal aspirates sampled at the time of enrollment. SARS-CoV-2 specific antibodies were assayed by the Elecsys® Anti-SARS-CoV-2 immunoassay (Roche Diagnostics). The assay was interpreted according to the manufacturer's instructions (Roche: V 1.0 2020-05).

## Quantifying Coronavirus Disease 2019 Severity

On enrollment, patients' COVID-19 severity based on clinical status was assessed according to the WHO ordinal scale (WHO, 2020). Briefly, patients were classified as: WHO 2: Ambulatory with limitation of activities; WHO 3: Hospitalized without requiring oxygen therapy; WHO 4: Hospitalized with oxygen required by mask or nasal prongs; WHO 5: Hospitalized and requiring non-invasive ventilation or high-flow oxygen; WHO 6: Hospitalized and receiving invasive mechanical ventilation; or WHO 7: Hospitalized and receiving invasive mechanical ventilation and additional organ support.

Additionally, a COVID-19 severity score ("PC1 severity") was calculated using clinical indicators associated with COVID-19 severity, as previously described (Riou et al., 2021). Briefly, eight clinical parameters, namely WHO ordinal scale scoring, Roche Elecsys® anti-SARS-CoV-2 antibody cut-off index (COI), WCC, CRP, D-dimer, Ferritin, LDH and radiographic evidence of disease, were graded in a non-supervised two-way hierarchical clustering analysis (HCA, ward method) segregated by outcome (died or survived). Principal component analysis was performed using the eight clinical parameters described to produce the "PC1 severity score."

## Kaposi's Sarcoma-Associated Herpesvirus and Epstein-Barr Virus Virological Assays

KSHV serology and KSHV and EBV VL assays were performed for all patients. Cryopreserved plasma was tested by enzyme-linked immunosorbent assay (ELISA) for antibodies against a lytic structural glycoprotein (K8.1) and latency-associated nuclear antigen (open reading frame [ORF] 73), following established specifications (Mbisa et al., 2010), and patients were considered KSHV seropositive if antibodies to either antigen were detected.

To perform VL assays, DNA was extracted from whole blood with plasma removed using the QIAamp DNA Blood Midi kit (Qiagen). KSHV and EBV DNA were quantified by real-time qPCR targeting the KSHV K6 gene (De Sanjosé et al., 2002) and EBV polymerase gene (Labo et al., 2019), respectively. Each reaction was performed in triplicate with 250 ng input DNA, 100 pmole forward and reverse primers,

5 pmole FAM/TAMRA labeled probe and 2X Universal Master Mix (Applied Biosystems). DNA was quantified against standard curves constructed by serial dilution of a K6 or EBV-pol plasmid. Cycling conditions on a LightCycler 480II System (Roche) were as follows: 2 min at 50°C; 8 min at 95°C; and 45 cycles of 15 s at 95°C and 1 min at 60°C for the KSHV assay and 2 min at 50°C; 10 min at 95°C; and 45 cycles of 15 s at 95°C and 1 min at 57°C for the EBV assay. Cellular equivalents per sample were determined using a quantitative assay for human endogenous retrovirus 3 (Yuan et al., 2001) and reported as viral DNA copies per million cells. Samples that failed to amplify in one or two replicates, or with detectable viral DNA in each replicate lower than the limit of detection for each assay (3 copies/reaction for KSHV and < 10 copies for EBV) were classified as qualitatively positive and arbitrarily assigned the value of 1 and 3 copies, respectively, as previously reported (Labo et al., 2019).

## Statistical Analysis

Statistical analysis was performed in SPSS version 25 (IBM Corp., 2017). Graphical representations were performed in Prism (v5; GraphPad Software Inc., San Diego, CA, United States) and JMP (v15.0.0; SAS Institute, Cary, NC, United States). Univariate analyses consisted of non-parametric Wilcoxon rank-sum tests and Fisher exact tests, as appropriate. Multivariate analyses were performed using binomial logistic regression for the categorical dependent variable, "outcome," in relation to the specified covariates. Linearity of the continuous variables with respect to the logit of the dependent variable was confirmed via the Box–Tidwell procedure (Box and Tidwell, 1962), and studentized residuals with values < 2.5 standard deviations were accepted. Multiple linear regression was performed to assess the association of categorical and continuous independent variables with the continuous dependent variable, "PC1 severity." Continuous variables were transformed, where appropriate, to approximate normal distributions. $P$-values are 2-tailed and were considered significant if < 0.05. Participants with missing data were excluded pairwise in each analysis.

# RESULTS

## Clinical Characteristics of the Study Participants

The clinical characteristics of the patients with RT-PCR proven SARS-CoV-2 infection included in this study ($n = 104$) are listed in **Table 1**.

Briefly, 61% of patients were men and 39% women with a median age of 53 years (range: 21–86). Serology assays indicated that 69.2% (95% CI: 59.9–77.5) were positive for SARS-CoV-2 antibodies and 41.1% (95% CI: 31.6–51.1%) were KSHV seropositive. About a third of the patients [29.8% (95% CI: 21.7–39.1%)] were HIV-1 positive, the majority of whom were on antiretroviral therapy [74.2% (95% CI: 57.1–87.0)]. The median HIV-1 VL among the HIV positive patients was 20 copies/ml with a range of 20–523,463 copies/ml and median CD4 count was 134 cells/µl (range: 3–1,367).

EBV VL was detectable in 84.4% (95% CI: 76.1–84.4%) of the cohort with a median VL of 1,152 copies/$10^6$ cells (range: 1.0–1.44 × $10^6$ copies/$10^6$ cells); similarly, in a pre-pandemic South African cohort of HIV-positive controls, EBV was detectable in 78.3% (95% CI: 58.7–91.2) with a median VL of 6,885 copies/$10^6$ cells (range: 1.0–1.65 × $10^6$ copies/$10^6$ cells; n = 23; data not shown). KSHV DNA was detected in 20.6% (95% CI: 13.6–29.2%) with a median VL of 1.0 copies/$10^6$ cells (range 1.0–38,784 copies/$10^6$ cells). This percentage positive is significantly higher than that reported in our previous study (Blumenthal et al., 2019) [6.4% (95% CI: 4.7–8.4%); p < 0.0001]. Both EBV and KSHV DNA was detectable in 17.7% (95% CI: 11.1–26.2%) of the cohort. There was no correlation between HIV VL and EBV VL or KSHV VL (data not shown). EBV VL detection did not differ between HIV positive and HIV negative patients (80.8% in HIV positive vs. 85.7% in HIV negative, p = 0.541) but EBV VL was significantly higher among HIV positive patients (**Supplementary Table 1**). KSHV VL detection was greater, although not statistically significant, among HIV positive patients compared to HIV negative patients (27.5% in HIV positive vs. 17.8% in HIV negative, p = 0.287) and KSHV seroprevalence was significantly greater among HIV positive patients (63.3% in HIV positive vs. 30.7% in HIV negative, p = 0.004) with higher ORF73 OD values (**Supplementary Table 1**).

Most patients had an elevated CRP (94.2%), D-Dimer (89.9%), LDH (97%) and ferritin (91.2%) levels. Also of note, large proportions of COVID-19 patients exhibited abnormal hemoglobin (45.1%), WCC (49.0%), neutrophils (57.5%) and lymphocytes (53.8%).

On enrollment 48 [46.2% (95% CI: 36.8–55.7%)] COVID-19 patients were classified as severe on the WHO ordinal scale reflecting oxygen therapy and supportive care requirements. Hierarchical clustering analysis and subsequent principal component analysis based on eight clinical variables included in this study (WHO ordinal scale, Roche Elecsys® anti-SARS-CoV-2 antibody COI, WCC, CRP, D-dimer, ferritin, LDH and radiographic evidence of disease extent (expressed as% of unaffected lung) showed distinct separation by COVID-19 disease outcome (**Figures 1A,B**). PC1 accounted for 26.3% and PC2 18.8% of the variance in the distribution. The range of PC1 severity scores in the cohort was –3.01 to 4.07 (**Figure 1D**, reproduced from Riou et al., 2021; **Table 1**). Thirty [28.8% (95% CI: 20.8–38.0%)] COVID-19 patients died and this group had a significantly higher PC1 score compared to patients who survived (p < 0.0001, **Figure 1D**, reproduced from Riou et al., 2021).

## Association of Kaposi's Sarcoma-Associated Herpesvirus and Epstein-Barr Virus With Coronavirus Disease 2019 Severity and Outcome in the Entire Coronavirus Disease 2019 Cohort

The association of KSHV, EBV, and the detection of both viruses with COVID-19 severity (as measured by PC1 severity score and

WHO ordinal scale score) as well as outcome was first assessed in univariate analyses (**Table 2** and **Figure 2**).

PC1 severity score and KSHV VL did not correlate (Spearman's rho correlation coefficient = 0.083, p = 0.456) but the median PC1 severity score was slightly higher in patients with detectable KSHV, although this did not reach statistical significance (p = 0.394, **Figure 2A**). EBV VL similarly did not correlate with PC1 severity (Spearman's rho correlation coefficient = 0.065, p = 0.569). The distribution of WHO ordinal scale scores amongst patients with and without detectable KSHV VL and EBV VL was not significantly different (**Figure 2B**). While EBV was detectable in most COVID-19 patients (84.4%) with no discernable difference in detection nor VL between patients who died and those who survived (**Table 2**), KSHV was detected more frequently (although this trend was not significant) among the patients who died (died: 33.3% vs. survived: 15.3%, p = 0.059, **Table 2** and **Figure 2C**). This, however, is not reflected in KSHV seropositivity as a greater proportion of patients who survived were indeed KSHV seropositive (p = 0.036). Similarly, there was an overrepresentation of detection of both KSHV and EBV among patients who died (died: 31.0% vs. survived: 11.9%, p = 0.039), however, this is likely due to the almost ubiquitous detection of EBV reflecting a difference in KSHV detection between groups rather than any contribution of dual detection.

Further assessment of parameters that differed between the patients who died and survived indicated that male sex, severe WHO score on enrollment, higher PC1 severity score, elevated CRP, D-dimer, LDH, Ferritin, creatinine, WCC and neutrophil count were similarly associated with death on a univariate level (**Supplementary Table 2**); these parameters were therefore considered in multivariate analysis. In COVID-19 patients, detectable KSHV VL was associated with death after adjusting for age, sex, HIV status, detectable EBV VL, creatinine, neutrophils and PC1 severity [**Table 3A**, p = 0.036, adjusted OR = 7.35 (95% CI: 1.14–47.58)]. To avoid overfitting the model, variables that were not significant in model A were removed and a stripped-down logistic regression was run confirming that detectable KSHV VL was associated with death after adjusting for sex, age and PC1 severity [**Table 3B**, p = 0.045, adjusted OR = 4.59 (95% CI: 1.04–20.31)].

## Association of Kaposi's Sarcoma-Associated Herpesvirus and Epstein-Barr Virus With Coronavirus Disease 2019 Severity and Outcome in the Human Immunodeficiency Virus-1 Negative Sub-Cohort

In a further analysis, we excluded HIV-1 positive patients as PC1 severity among HIV-1 positive patients was significantly lower than in HIV negative patients (data not shown, p = 0.032) indicating a recruitment bias due to the presentation and hospitalization of HIV positive patients for HIV-related health issues other than COVID-19. In HIV negative COVID-19 patients, there was a trend of greater detection of KSHV VL with COVID-19 disease severity when controlling for sex and age [**Table 4**, p = 0.054, unstandardized co-efficient 0.86 (95% CI: –0.015 to 1.74)]. Additionally, detectable KSHV VL was
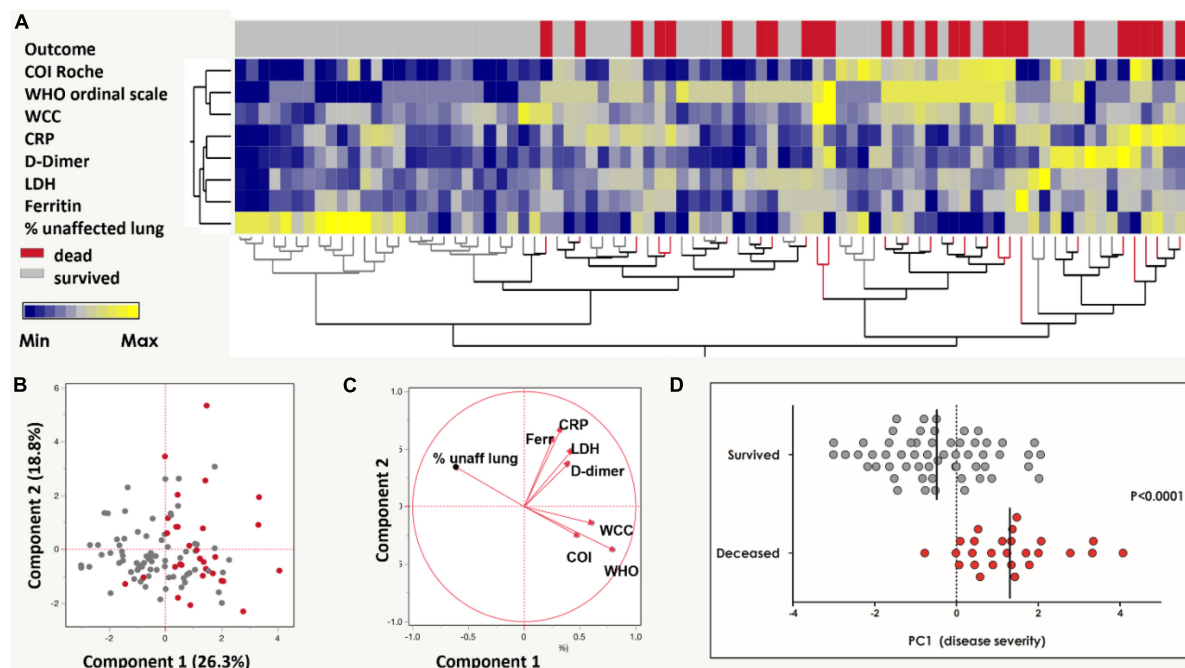
**FIGURE 1 |** Grading of COVID-19 disease severity among the SARS-CoV-2 infected cohort ($n$ = 104). **(A)** A two-way hierarchical cluster analysis using the WHO ordinal scale, anti-SARS-CoV-2 antibody cut-off index (COI, Roche Elecsys®), white cell count (WCC), C-reactive protein (CRP), D-dimer, Ferritin, lactate dehydrogenase (LDH) and radiographic evidence of disease extent (expressed as% of unaffected lung) was used to grade COVID-19 disease by outcome (patients survived in gray and deceased in red). Data are depicted as a heatmap colored from minimum to maximum values detected for each parameter. **(B)** Principal component analysis (PCA) based on the eight clinical parameters (as in **A**) was used to explain the variance of the data distribution in the cohort. Each dot represents a participant; 20 participants with missing data were excluded. The two axes represent principal components 1 (PC1) and 2 (PC2). Their contribution to the total data variance is shown as a percentage. **(C)** Loading plot showing each parameter's influence on PC1 and PC2. **(D)** Comparison of PC1 scores between patients with COVID-19 who survived and died (reproduced from Riou et al., 2021). Bars represent medians and *P*-value is by the non-parametric Mann-Whitney test.

**TABLE 2 |** Univariate analysis comparing virological parameters between COVID-19 patients ($n$ = 104) who died and survived.

| Parameter | Died (30) N (%) or Median (range) | Discharged (74) N (%) or Median (range) | *P*-value |
|---|---|---|---|
| KSHV VL detectable | 10 (33.3%) | 11 (15.3%) | 0.059 |
| KSHV VL (copies/$10^6$ cells) | 1.0 (1.0–1.0) | 1.0 (1.0–38783.96) | 0.314 |
| EBV VL detectable | 23 (79.3%) | 58 (86.6%) | 0.374 |
| EBV VL (copies/$10^6$ cells) | 1018.56 (1.0–201276.1) | 3.0 (1.0–1.44E6) | 0.168 |
| KSHV seropositive | 6 (23.1%) | 33 (47.8%) | 0.036 |
| K8.1 positive | 4 (15.4%) | 18 (26.1%) | 0.414 |
| ORF73 positive | 5 (19.2%) | 27 (39.1%) | 0.089 |
| K8.1 OD | 1.51 (0.76–2.96) | 1.18 (0.21–3.43) | 0.391 |
| ORF73 OD | 1.31 (0.83–5.19) | 2.66 (0.15–8.28) | 0.227 |
| KSHV-EBV coinfection | 9 (31.0%) | 8 (11.9%) | 0.039 |

*Participants with missing data were excluded pairwise. P-values are by Fisher's Exact test for categorical variables and Mann-Whitney U-test for categorical variables. ART, antiretroviral therapy; HIV, human immunodeficiency virus; KSHV, Kaposi sarcoma-associated herpesvirus; VL, viral load; EBV, Epstein-Barr virus.*

associated with death when controlling for PC1 severity, sex and age [**Table 5**, $p$ = 0.008, adjusted $OR$ = 7.34 (95% CI: 1.69–31.49)].

# DISCUSSION

Systemic reactivation of herpesviruses has been reported in critically ill COVID-19 patients (Simonnet et al., 2021). The herein presented data support these observations and

suggest an association between KSHV and COVID-19 outcome; however, it is not clear if the underlying KSHV infection is contributing to severity of COVID-19 or if SARS-CoV-2 infection is causing reactivation of KSHV. On the contrary, detection of EBV in our cohort was similar to what we have seen in a previous pre-pandemic cohort and what has been previously reported (Schaftenaar et al., 2014) and our results do not show EBV to be related to COVID-19 severity or outcome.
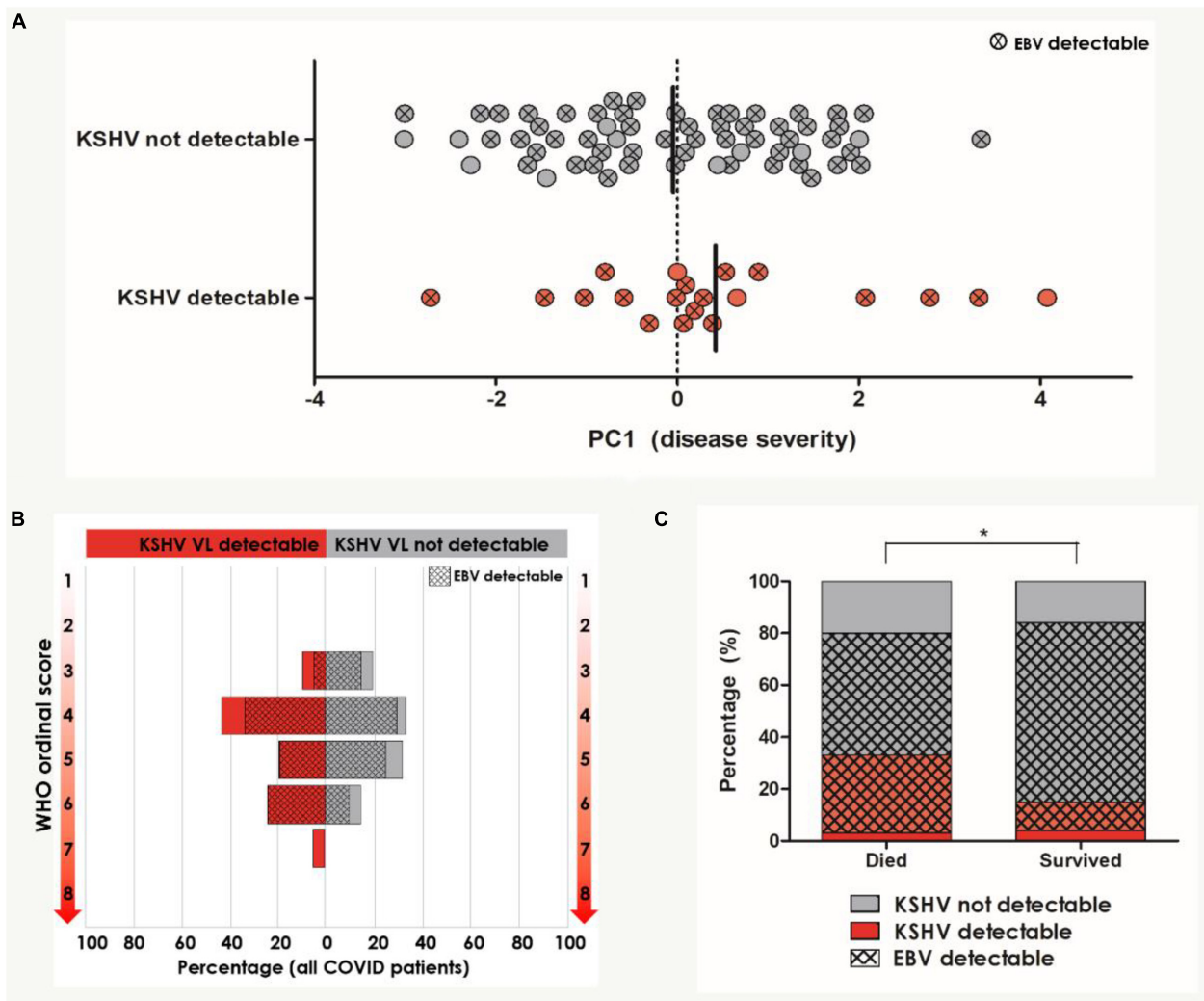
**FIGURE 2 |** Univariate analysis of KSHV and EBV VL detection in relation to COVID-19 severity and outcome ($n = 104$). **(A)** PC1 severity score amongst patients with and without detectable KSHV VL in the blood. Circles indicated with an X represent patients who also have detectable EBV VL in the blood. Bars indicate median. **(B)** The distribution of WHO ordinal scale scores between patients with and without detectable KSHV VL. Hash pattern indicates percentages of patients with detectable EBV VL. **(C)** The distribution of patients with and without detectable KSHV VL between patients who died and survived. Hash pattern indicates patients with detectable EBV VL. *Indicates the statistically significant proportion of patients with detectable KSHV and EBV VL who died compared to those who survived ($p = 0.039$). Participants with missing data were excluded pairwise.

Previous research has demonstrated EBV lytic reactivation following SARS-CoV-2 infection (Paolucci et al., 2021). Moreover, EBV lytic reactivation was found to enhance SARS-CoV2 infection (Chen T. et al., 2021; Verma et al., 2021). While this was not evident in our cohort, possibly due to almost ubiquitous EBV detection in the South African population even before the COVID-19 pandemic, it is tempting to speculate that similar mechanisms play a role for the related herpesvirus, KSHV, in our cohort, causing some disease synergy. Indeed, we found a higher than usual detection of lytic KSHV compared to previous pre-pandemic HIV-1-infected patient cohorts from the same geographic area (Blumenthal et al., 2019), and *in vitro* studies have also suggested that SARS-CoV-2 and drugs used in COVID-19 treatment, namely

Azithromycin and Nafamostat mesylate, can induce KSHV lytic reactivation (Chen J. et al., 2021). This suggests that SARS-CoV-2 infection may cause reactivation of KSHV in latently infected individuals.

We unexpectedly noted several patients with detectable KSHV VL who were KSHV seronegative. KSHV infection is generally considered to be obtained in childhood in sub-Saharan Africa, with KSHV seroprevalence peaking before adulthood (Bourboulia et al., 1998) therefore it is unlikely these cases represent new infections. Indeed, while KSHV detection is greater in this cohort than what we have seen in pre-pandemic cohorts (Blumenthal et al., 2019), viral loads are significantly lower and it is plausible that the antibody levels in these cases fall below the detection limit of our assay.

**TABLE 3** | Logistic regression for death outcome in COVID-19 positive patients ($n$ = 104).

| Characteristic | Unadjusted OR | 95% CI for unadjusted OR | | Adjusted OR | 95% CI for adjusted OR | | P-value |
|---|---|---|---|---|---|---|---|
| | | Lower | Upper | | Lower | Upper | |
| **Model A** | | | | | | | |
| Detectable KSHV VL[a] | 2.773 | 1.026 | 7.493 | 7.347 | 1.135 | 47.574 | 0.036 |
| Detectable EBV VL[b] | 0.595 | 0.190 | 1.860 | 0.222 | 0.007 | 6.787 | 0.388 |
| Sex[c] | 2.793 | 1.068 | 7.306 | 3.244 | 0.528 | 19.922 | 0.204 |
| Age | 0.969 | 0.934 | 1.006 | 0.996 | 0.920 | 1.079 | 0.930 |
| HIV status[d] | 0.490 | 0.177 | 1.354 | 6.507 | 0.595 | 71.129 | 0.125 |
| Creatinine | 0.990 | 0.983 | 0.998 | 0.998 | 0.986 | 1.009 | 0.709 |
| Neutrophils | 0.914 | 0.824 | 1.013 | 1.111 | 0.890 | 1.387 | 0.352 |
| PC1 severity | 3.546 | 1.961 | 6.410 | 6.757 | 2.024 | 22.727 | 0.002 |
| **Model B** | | | | | | | |
| Detectable KSHV VL[a] | 2.773 | 1.026 | 7.493 | 4.585 | 1.035 | 20.314 | 0.045 |
| PC1 severity | 3.546 | 1.961 | 6.410 | 4.219 | 2.033 | 8.772 | <0.001 |
| Sex[c] | 2.793 | 1.068 | 7.306 | 2.711 | 0.717 | 10.256 | 0.142 |
| Age | 0.969 | 0.934 | 1.006 | 1.004 | 0.948 | 1.063 | 0.892 |

[a]Detectable KSHV VL is for detectable VL compared to not detectable VL.
[b]Detectable EBV VL is for detectable VL compared to not detectable VL.
[c]Sex is for male compared to female.
[d]HIV status is for HIV positive compared to HIV negative.

**TABLE 4** | Multiple regression for PC1 severity in HIV negative COVID-19 positive patients ($n$ = 73).

| Characteristic | Unstandardized coefficient | Standard error | Standardized coefficient | P-value |
|---|---|---|---|---|
| Detectable KSHV VL[a] | 0.864 | 0.439 | 0.253 | 0.054 |
| Sex[b] | −0.041 | 0.395 | −0.013 | 0.919 |
| Age | 0.035 | 0.017 | 0.269 | 0.042 |

[a]Detectable KSHV VL is for detectable VL compared to not detectable VL.
[b]Sex is for male compared to female.

**TABLE 5** | Logistic regression for death outcome in HIV negative COVID positive patients ($n$ = 73).

| Characteristic | Unadjusted OR | 95% CI for unadjusted OR | | Adjusted OR | 95% CI for adjusted OR | | P-value |
|---|---|---|---|---|---|---|---|
| | | Lower | Upper | | Lower | Upper | |
| Detectable KSHV VL[a] | 4.400 | 1.254 | 15.440 | 23.000 | 2.019 | 261.964 | 0.012 |
| PC1 severity | 3.968 | 1.876 | 8.403 | 6.536 | 2.045 | 20.833 | 0.002 |
| Sex[b] | 3.167 | 0.937 | 10.701 | 8.385 | 1.170 | 60.083 | 0.034 |
| Age | 0.959 | 0.918 | 1.003 | 0.954 | 0.885 | 1.028 | 0.213 |

[a]Detectable KSHV VL is for detectable VL compared to not detectable VL.
[b]Sex is for male compared to female.

In severely ill patients, lytic KSHV infection can culminate in generalized inflammation and an IL-6 induced cytokine storm (described as KICS) (Uldrick et al., 2010; Polizzotto et al., 2012; Blumenthal et al., 2019). Similarly, a cytokine storm has been described in severely ill COVID-19 patients as a crucial cause of death (Hu et al., 2021). Further, lytically associated multicentric Castleman disease as well as primary effusion lymphoma and KS pose major diagnostic challenges globally and particularly in low resource settings due to non-specific presentation, especially in the context of high COVID-19, TB and HIV prevalence, and technically difficult diagnostic requirements. While the low global prevalence of latent KSHV infection and potentially associated disease synergy with lytic reactivation and COVID-19 severity are unlikely to represent a major public health concern, geographic regions where KSHV is highly prevalent may be faced with a rising incidence of lytic KSHV-related syndromes.

The observation that HIV-1 positive patients in our cohort presented with a lower PC1 severity score was interesting although likely reflects a recruitment bias rather than any protective effect of HIV-1. HIV negative patients were hospitalized on clinical suspicion of COVID-19 disease whereas HIV positive patents may have been hospitalized due to HIV-1-related diseases, such as TB, and found to have a concurrent SARS-COV-2 infection. Examination of COVID-19 disease in the HIV positive population in South Africa has shown HIV-1 to be independently associated with increased

risk of severe COVID-19 disease and death (Boulle et al., 2020; Davies, 2020) while HIV positive patients who were virally suppressed due to ART do not have altered SARS-CoV-2 CD4 T cell function (Riou et al., 2021). Our relatively small subset of HIV positive patients with COVID-19 disease disallows us from commenting specifically on the interplay of HIV-1, KSHV/EBV and SARS-CoV-2.

Although longitudinal studies are required to support our data, our results have potential implications for future KSHV- and EBV-related disease development following the COVID-19 pandemic, particularly in regions where prevalence of these herpesviruses and HIV-1 co-infection is high. In this context, prioritization of COVID-19 vaccination in these populations should be considered and history of COVID-19 disease, even after full recovery, should be taken into account as a potential risk factor for virus-associated cancer in the future management and screening of these patients. These data support the clinical monitoring of KSHV VL both in COVID-19 disease and future management of patients with KSHV infection.

## DATA AVAILABILITY STATEMENT

The original contributions presented in the study are included in the article/**Supplementary Material**, further inquiries can be directed to the corresponding author/s.

## ETHICS STATEMENT

The studies involving human participants were reviewed and approved by the University of Cape Town's Faculty of Health Sciences Research Ethical Committee (HREC 207/2020). The patients/participants provided their written informed consent to participate in this study.

## AUTHOR CONTRIBUTIONS

MB, CR, RW, and GS designed the study. CR and RW facilitated clinical recruitment. MB, HL, and AC performed the diagnostic experiments. MB, CR, and GS performed the data analysis and interpretation. MB and GS wrote the manuscript with all authors.

## SUPPLEMENTARY MATERIAL

The Supplementary Material for this article can be found online at: https://www.frontiersin.org/articles/10.3389/fmicb.2021.795555/full#supplementary-material

## REFERENCES

Blumenthal, M. J., Schutz, C., Barr, D., Locketz, M., Marshall, V., Whitby, D., et al. (2019). The contribution of kaposi's sarcoma-associated herpesvirus to mortality in hospitalized human immunodeficiency virus-infected patients being investigated for tuberculosis in South Africa. *J. Infect. Dis.* 220, 841–851. doi: 10.1093/infdis/jiz180

Blumenthal, M. J., Schutz, C., Meintjes, G., Mohamed, Z., Mendelson, M., Ambler, J. M., et al. (2018). EPHA2 sequence variants are associated with susceptibility to Kaposi's sarcoma-associated herpesvirus infection and Kaposi's sarcoma prevalence in HIV-infected patients. *Cancer Epidemiol.* 56, 133–139. doi: 10.1016/j.canep.2018.08.005

Boulle, A., Davies, M.-A., Hussey, H., Ismail, M., Morden, E., Vundle, Z., et al. (2020). Risk factors for coronavirus disease 2019 (COVID-19) death in a population cohort study from the Western Cape Province,

South Africa. *Clin. Infect. Dis.* 73, e2005–e2015. doi: 10.1093/cid/ciaa1198

Bourboulia, D., Whitby, D., Boshoff, C., Newton, R., Beral, V., Carrara, H., et al. (1998). Serologic evidence for mother-to-child transmission of kaposi sarcoma-associated herpesvirus infection. *J. Am. Med. Assoc.* 280, 31–32. doi: 10.1001/jama.280.1.31-a

Box, A. G. E. P., and Tidwell, P. W. (1962). Transformation of the independent variables. *Technometrics* 4, 531–550. doi: 10.1080/00401706.1962.10490038

Chen, J., Dai, L., Barrett, L., James, J., Plaisance-Bonstaff, K., Post, S. R., et al. (2021). SARS-CoV-2 proteins and anti-COVID-19 drugs induce lytic reactivation of an oncogenic virus. *Commun. Biol.* 4, 2–7. doi: 10.1038/s42003-021-02220-z

Chen, T., Song, J., Liu, H., Zheng, H., and Chen, C. (2021). Positive epstein–barr virus detection in coronavirus disease 2019 (COVID-19) patients. *Sci. Rep.* 11:10902. doi: 10.1038/s41598-021-90351-y

Davies, M.-A. (2020). HIV and risk of COVID-19 death?: a population cohort study from the Western Cape Province, South Africa. *medRxiv* [Preprint] doi: 10.1101/2020.07.02.20145185v2

De Sanjosé, S., Marshall, V., Solà, J., Palacio, V., Almirall, R., Goedert, J. J., et al. (2002). Prevalence of Kaposi's sarcoma-associated herpesvirus infection in sex workers and women from the general population in Spain. *Int. J. Cancer.* 98, 155–158. doi: 10.1002/ijc.10190

de Sanjose, S., Mbisa, G., Perez-Alvarez, S., Benavente, Y., Sukvirach, S., Hieu, N. T., et al. (2009). Geographic variation in the prevalence of kaposi sarcoma–associated herpesvirus and risk factors for transmission. *J. Infect. Dis.* 199, 1449–1456. doi: 10.1086/598523

Gold, J. E., Okyay, R. A., Licht, W. E., and Hurley, D. J. (2021). Investigation of long COVID prevalence and its relationship to epstein-barr virus reactivation. *Pathogens* 10:763. doi: 10.3390/pathogens10060763

Harris, P. A., Taylor, R., Thielke, R., Payne, J., Gonzalez, N., and Conde, J. G. (2009). Research electronic data capture (REDCap)-A metadata-driven methodology and workflow process for providing translational research informatics support. *J. Biomed. Inform.* 42, 377–381. doi: 10.1016/j.jbi.2008.08.010

Hu, B., Huang, S., and Yin, L. (2021). The cytokine storm and COVID-19. *J. Med. Virol.* 93, 250–256.

Hui, D. S., Azhar, E. I., Madani, T. A., Ntoumi, F., Kock, R., Dar, O., et al. (2020). The continuing 2019-nCoV epidemic threat of novel coronaviruses to global health — the latest 2019 novel coronavirus outbreak in Wuhan, China. *Int. J. Infect. Dis.* 91, 264–266. doi: 10.1016/j.ijid.2020.01.009

Labo, N., Marshall, V., Miley, W., Davis, E., McCann, B., Stolka, K. B., et al. (2019). Mutual detection of Kaposi's sarcoma-associated herpesvirus and Epstein–Barr virus in blood and saliva of Cameroonians with and without Kaposi's sarcoma. *Int. J. Cancer* 145, 2468–2477. doi: 10.1002/ijc.32546

Mbisa, G. L., Miley, W., Gamache, C. J., Gillette, W. K., Esposito, D., Hopkins, R., et al. (2010). Detection of antibodies to Kaposi's sarcoma-associated herpesvirus: a new approach using K8.1 ELISA and a newly developed recombinant LANA ELISA. *J. Immunol. Methods* 356, 39–46. doi: 10.1016/j.jim.2010.02.015

Mesri, E. A., Cesarman, E., and Boshoff, C. (2010). Kaposi's sarcoma and its associated herpesvirus. *Nat. Rev. Cancer* 10, 707–719. doi: 10.1038/nrc2888

Paolucci, S., Cassaniti, I., Novazzi, F., Fiorina, L., Piralla, A., Comolli, G., et al. (2021). EBV DNA increase in COVID-19 patients with impaired lymphocyte subpopulation count. *Int. J. Infect. Dis.* 104, 315–319. doi: 10.1016/j.ijid.2020.12.051

Phillips, N. (2021). The coronavirus is here to stay - here's what that means. *Nature* 590, 382–384. doi: 10.1038/d41586-021-00396-2

Polizzotto, M. N., Uldrick, T. S., Hu, D., and Yarchoan, R. (2012). Clinical manifestations of Kaposi sarcoma herpesvirus lytic activation: multicentric castleman disease (KSHV-MCD) and the KSHV inflammatory cytokine syndrome. *Front. Microbiol.* 3:73. doi: 10.3389/fmicb.2012.00073

Riou, C., du Bruyn, E., Stek, C., Daroowala, R., Goliath, R. T., Abrahams, F., et al. (2021). Relationship of SARS-CoV-2–specific CD4 response to COVID-19 severity and impact of HIV-1 and tuberculosis coinfection. *J. Clin. Invest.* 131, e149125. doi: 10.1172/JCI149125

Ritchie, H., Ortiz-Ospina, E., Beltekian, D., Mathieu, E., Hasell, J., Macdonald, B., et al. (2020). *Coronavirus Pandemic (COVID-19). OurWorldInData.org.* Geneva: World Health Organization.

Rochford, R. (2009). "Epidemiology of EBV," in *DNA Tumor Viruses*, eds B. Damania and J. Pipas (Berlin: Springer), 794.

Saade, A., Moratelli, G., Azoulay, E., and Darmon, M. (2021). Herpesvirus reactivation during severe COVID-19 and high rate of immune defect. *Infect. Dis. Now.* 51, 676–679. doi: 10.1016/j.idnow.2021.07.005

Schäfer, G., Blumenthal, M. J., and Katz, A. A. (2015). Interaction of human tumor viruses with host cell surface receptors and cell entry. *Viruses* 7, 2592–2617. doi: 10.3390/v7052592

Schaftenaar, E., Verjans, G. M. G. M., Getu, S., McIntyre, J. A., Struthers, H. E., Osterhaus, A. D. M. E., et al. (2014). High seroprevalence of human herpesviruses in HIV-infected individuals attending primary healthcare facilities in rural South Africa. *PLoS One* 9:e99243. doi: 10.1371/journal.pone.0099243

Simonnet, A., Engelmann, I., Moreau, A. S., Garcia, B., Six, S., El Kalioubie, A., et al. (2021). High incidence of epstein–barr virus, cytomegalovirus, and human-herpes virus-6 reactivations in critically ill patients with COVID-19. *Infect. Dis. Now.* 51, 296–299. doi: 10.1016/j.idnow.2021.01.005

Sitas, F., Carrara, H., Beral, V., Newton, R., Reeves, G., Bull, D., et al. (1999). Antibodies against human herpesvirus 8 in black South African patients with cancer. *N. Engl. J. Med.* 340, 1863–1871. doi: 10.1056/NEJM199906173402403

Thompson, M. P., and Kurzrock, R. (2004). Epstein-barr virus and cancer. *Clin. Cancer Res.* 10, 803–821.

Uldrick, T. S., Wang, V., O'Mahony, D., Aleman, K., Wyvill, K. M., Marshall, V., et al. (2010). An Interleukin-6-related systemic inflammatory syndrome in patients co-infected with Kaposi sarcoma-associated herpesvirus and HIV but without multicentric castleman disease. *Clin. Infect. Dis.* 51, 350–358. doi: 10.1086/654798

van Oosterhout, C., Hall, N., Ly, H., and Tyler, K. M. (2021). COVID-19 evolution during the pandemic–implications of new SARS-CoV-2 variants on disease control and public health policies. *Virulence* 12, 507–508. doi: 10.1080/21505594.2021.1877066

Verma, D., Church, T. M., and Swaminathan, S. (2021). Epstein-barr virus lytic replication induces ACE2 expression. *J. Virol.* 95, e192–e121. doi: 10.1128/JVI.00192-21

WHO (2020). *Novel Coronavirus: COVID-10 Therapeutic Trial Synopsis. R&D Blueprint.* Geneva: World Health Organization.

Wilkinson, D., Sheldon, J., Gilks, C. F., and Schulz, T. F. (1999). Prevalence of infection with human herpesvirus 8/Kaposi's sarcoma herpesvirus in rural South Africa. *South Afr. Med. J.* 89, 3–6.

World Health Organization (2020). *WHO Director-General's opening remarks at the media briefing on COVID-19 - 11 March 2020. WHO Director General's speeches.* Geneva: World Health Organization.

Yuan, C. C., Miley, W., and Waters, D. (2001). A quantification of human cells using an ERV-3 real time.pdf. *J. Virol. Methods* 91, 109–117. doi: 10.1016/s0166-0934(00)00244-5

# Fatal Pneumonia Associated With a Novel Genotype of Human Coronavirus OC43

Susanna Kar Pui Lau*[†], Kenneth Sze Ming Li[†], Xin Li[†], Ka-Yan Tsang, Siddharth Sridhar and Patrick Chiu Yat Woo*

Department of Microbiology, Li Ka Shing Faculty of Medicine, The University of Hong Kong, Hong Kong, Hong Kong SAR, China

Since its first discovery in 1967, human coronavirus OC43 (HCoV-OC43) has been associated with mild self-limiting upper respiratory infections worldwide. Fatal primary pneumonia due to HCoV-OC43 is not frequently described. This study describes a case of fatal primary pneumonia associated with HCoV-OC43 in a 75-year-old patient with good past health. The viral loads of the respiratory tract specimens (bronchoalveolar lavage and endotracheal aspirate) from diagnosis to death were persistently high ($3.49 \times 10^6$–$1.10 \times 10^{10}$ copies/ml). HCoV-OC43 at a $6.46 \times 10^3$ copies/ml level was also detected from his pleural fluid 2 days before his death. Complete genome sequencing and phylogenetic analysis showed that the present HCoV-OC43 forms a distinct cluster with three other HCoV-OC43 from United States, with a bootstrap value of 100% and sharing 99.9% nucleotide identities. Pairwise genetic distance between this cluster and other HCoV-OC43 genotypes ranged from $0.27 \pm 0.02\%$ to $1.25 \pm 0.01\%$. In contrast, the lowest pairwise genetic distance between existing HCoV-OC43 genotypes was $0.26 \pm 0.02\%$, suggesting that this cluster constitutes a novel HCoV-OC43 genotype, which we named genotype I. Unlike genotypes D, E, F, G, and H, no recombination event was observed for this novel genotype. Structural modeling revealed that the loop with the S1/S2 cleavage site was four amino acids longer than other HCoV-OC43, making it more exposed and accessible to protease, which may have resulted in its possible hypervirulence.

Keywords: human coronavirus OC43, fatal, pneumonia, novel genotype, hypervirulence

## INTRODUCTION

Coronaviruses (CoVs) are classified into four genera, *Alphacoronavirus*, *Betacoronavirus*, *Gammacoronavirus*, and *Deltacoronavirus*. AlphaCoVs and betaCoVs are found exclusively in mammals, whereas gammaCoVs and deltaCoVs mainly infect birds (Woo et al., 2012; Lau et al., 2021). Among all the CoVs, seven are known to infect humans. Three of them (all betaCoVs), including Severe Acute Respiratory Syndrome CoV (SARS-CoV) and SARS-CoV-2 that emerged from China in 2002/2003 and 2019, respectively, and Middle East Respiratory Syndrome CoV (MERS-CoV) that emerged from the Middle East in 2012, probably originated from recent animal-to-human transmission and resulted in highly fatal pneumonia (Lau et al., 2005; Zaki et al., 2012; Lau et al., 2020). The other four, namely human CoV (HCoV)-OC43 (a betaCoV), HCoV-229E

(an alphaCoV), HCoV-NL63 (an alphaCoV), and HCoV-HKU1 (a betaCoV), are HCoVs that are primarily associated with upper respiratory infections (Hamre and Procknow, 1966; McIntosh et al., 1967; van der Hoek et al., 2004; Woo et al., 2005a).

Since its first discovery in 1967, HCoV-OC43 has been reported to be associated with mild self-limiting upper respiratory infections worldwide (McIntosh et al., 1967). Fatal primary pneumonia due to HCoV-OC43 is not frequently described. In 2011, based on phylogenetic analysis of the complete RNA-dependent RNA polymerase (RdRp), spike (S), and nucleocapsid (N) genes, we subclassified HCoV-OC43 into genotypes A, B, C and D, and showed that genotype D was generated through natural recombination (Lau et al., 2011). Four additional genotypes, namely E, F, G, and H, were described (Zhang et al., 2015; Oong et al., 2017; Zhu et al., 2018) in the last 10 years. This article describes a patient with fatal pneumonia associated with HCoV-OC43. Complete genome sequencing and phylogenetic analysis revealed that it is distinct from all these eight genotypes of HCoV-OC43. Based on these results, we propose a novel genotype of HCoV-OC43, named genotype I. The possible pathogenic mechanism for this virus leading to fatal infection is also discussed.

## MATERIALS AND METHODS

### Patient and Clinical Specimens

Various clinical samples, including bronchoalveolar lavage, tracheal aspirate, sputum, endotracheal aspirate, and pleural fluid, were collected at different time points from the patient. The respiratory samples were then detected for respiratory pathogens, including 17 viruses and 4 bacteria, by BioFire® FilmArray® Respiratory Panel 2 (RP2) and as well as bacterial/fungal culture and PCR. Due to the recent emergence of COVID-19, the samples were also tested for SARS-CoV-2 retrospectively. The collection and use of clinical samples and data were approved by the Institutional Review Board of the University of Hong Kong/Hospital Authority Hong Kong West Cluster (UW 16-365 20-07-2016).

### RNA Extraction

Viral RNA was extracted from the clinical specimens of the patient using QIAamp Viral RNA Mini Kit (QIAgen, Hilden, Germany). The RNA was eluted in 60 µl of Buffer AVE and was used as the template for RT-PCR.

### Complete Genome Sequencing

Complete genome sequencing of the HCoV-OC43 from the patient (HK19-01) was performed using primers and strategies as we described previously (Lau et al., 2011). The viral RNA was reverse transcribed to cDNA by a combined random priming and oligo(dT) priming strategy. The cDNA was amplified by degenerate primers designed by multiple alignments of available HCoV-OC43 complete genome sequences. Additional primers were designed from the results of the first and subsequent rounds of sequencing. These primer sequences are available on request. The 5′ ends of the viral genomes were confirmed by rapid

amplification of cDNA ends using the 5′/3′ RACE kit (Roche, Germany). Sequences were assembled and manually edited to produce the final sequence of the viral genome.

### Quantitative Real-Time RT-PCR

Viral loads of HCoV-OC43 in different clinical specimens collected from the patient were performed by quantitative real-time RT-PCR targeting the N gene. RNA was amplified in a LightCycler instrument with SuperScript III Platinum One-Step Quantitative RT-PCR System (Invitrogen, San Diego, CA, United States) using forward primer 5′-CGAT GAGGCTATTCCGACTAGGT-3′, reverse primer 5′-CCTTCC TGAGCCTTCAATATAGTAACC-3′ and probe 5′-(FAM)-TCC GCCTGGCACGGTACTCCCT-(BHQ-1)-3′, with the following cycling protocol: 30 min at 50°C for reverse transcription, followed by 2 min at 95°C and 50 cycles of 15 s at 95°C and 30 s at 55°C. For quantitative analysis, a reference standard was prepared using the pCRII-TOPO vector (Invitrogen, San Diego, CA, United States) containing the target sequence. A calibration curve was generated by serial 10-fold dilutions equivalent to $2.21 \times 10^2$–$2.21 \times 10^9$ copies per reaction mixture parallel with test samples.

### Phylogenetic, Recombination, and Genome Analysis

Opening reading frames (ORFs) of the HCoV-OC43 genome encoding proteins were predicted using ORFfinder (NIH, United States) and compared to available complete HCoV-OC43 genomes. Phylogenetic analysis of the complete HCoV-OC43 genomes was performed using the maximum likelihood method using MEGA X (Kumar et al., 2018), with the best-fit model (TN93 + G) selected and bootstrap values calculated from 1,000 trees. Pairwise genetic distances between HCoV-OC43 genotypes based on the complete genome sequences were calculated using MEGA X.

Recombination analysis was performed using Simplot version 3.5.1 as described previously (Lole et al., 1999). Bootscan analysis for a recombination event was performed on a gapless nucleotide alignment of the HCoV-OC43 genome sequences of different genotypes generated by MEGA X with the proposed novel genotype I as the query sequence. A sliding window of 1,000 nucleotides and a step size of 200 nucleotides were used as the scanning settings.

### Estimation of Synonymous and Non-synonymous Substitution Rates

The number of synonymous substitutions per synonymous site, Ks, and the number of non-synonymous substitutions per non-synonymous site, Ka, for each coding region was calculated using the Nei-Gojobori method (Jukes-Cantor) in MEGA X.

### Protein Structural Modeling

The structure of HCoV-OC43 S glycoprotein trimer was predicted using a web-based homology-modeling server, SWISS-MODEL (Waterhouse et al., 2018). BLASTp search was performed against Protein Data Bank (PDB) with the default
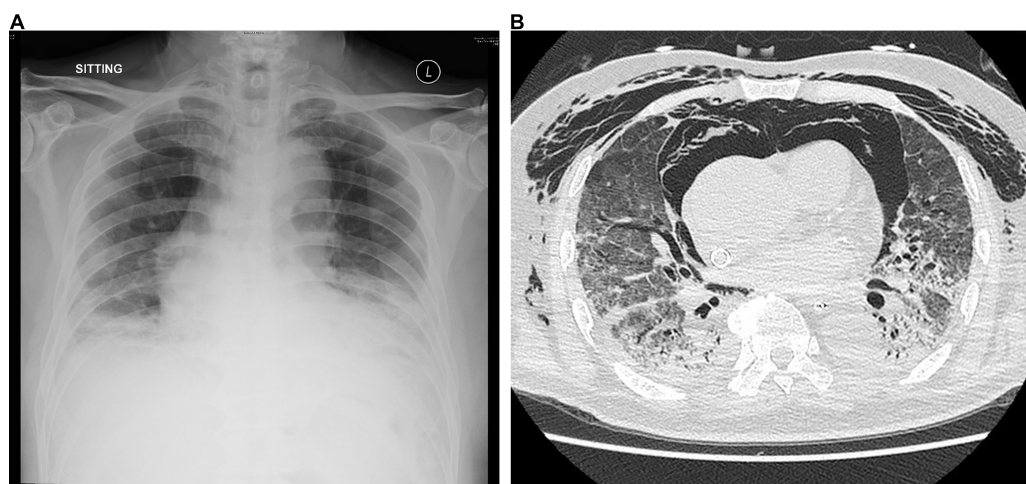
**FIGURE 1 | (A)** Chest radiograph on admission showing bilateral lower zone reticulonodular shadows and **(B)** CT scan of the thorax on day 15 showing mixed consolidative and atelectatic changes in the dependent regions of both lungs.

parameters to find suitable templates for homology modeling. Based on the higher sequence identity, QMEAN Z-score, coverage, and lower e-value, the crystal structure of the HCoV-OC43 S (PDB code: 6NZK) was selected as the template.

## Nucleotide Sequence Accession Number

The genome sequence of the HCoV-OC43 from the patient was deposited in GenBank sequence database under accession no. MW938760.

## RESULTS

### Patient

A 75-year-old Chinese man with good past health was admitted to the hospital in August 2019 because of 1-week breath shortness. He also complained of dry cough, decreased appetite, and subjective low-grade fever. On admission, the temperature was 37.2°C. The blood pressure was 128/70 mmHg and pulse rate 91/min. Chest examination showed bilateral lower zone fine crepitation. The chest radiograph revealed bilateral lower zone reticulonodular shadows (**Figure 1A**). The total white cell count was $8.9 \times 10^9$/L (reference range $3.7$–$9.3 \times 10^9$/L), with mild neutrophilia of $7.7 \times 10^9$/L (reference range $1.8$–$6.2 \times 10^9$/L) and lymphopenia of $0.6 \times 10^9$/L (reference range $1.0$–$3.2 \times 10^9$/L). There was mild hyponatremia with a serum sodium level of 135 mmol/L (range 136–145 mmol/L). The renal function test was normal. The serum bilirubin was normal, but both alkaline phosphatase and alanine transaminase were high at 212 U/L (reference range 30–120 U/L) and 87 U/L (reference range < 50 U/L), respectively. A clinical and radiological diagnosis of community acquired pneumonia was made. A nasopharyngeal swab was obtained for multiplex RT-PCR detection of influenza virus A, B and C, adenovirus, parainfluenza virus 1–4, respiratory syncytial virus, human metapneumovirus and enterovirus/rhinovirus. Sputum was collected for bacterial

culture and urine for *Streptococcus pneumoniae* and *Legionella* antigen detection. Empirical intravenous ceftriaxone was commenced. All the preliminary microbiological investigations showed negative results.

Despite the treatment, his conditions gradually deteriorated, with increased oxygen requirement and serial chest radiographs showed increased bilateral reticular shadows. On day 7, ceftriaxone was stopped, and intravenous piperacillin-tazobactam and oral doxycycline were started. Intravenous hydrocortisone was also started. However, his condition continued to deteriorate. He required high-flow oxygen on day 11 and was intubated on day 12. He also developed hypotension requiring inotrope support. Due to persistently low oxygenation despite maximum ventilatory support, he was put on venous-venous extracorporeal membrane oxygenation (VV-ECMO) and transferred to our teaching hospital on day 13 of admission.

Bronchoalveolar lavage was performed on day 14. Rapid respiratory pathogen detection using the BioFire® FilmArray® Respiratory Panel 2 (RP2) was positive for HCoV-OC43 only and was negative for other viruses. RT-PCR for SARS-CoV-2 was also negative. The HCoV-OC43 from the patient in this study was designated as HK19-01. Bacterial culture showed scanty growth of *Pseudomonas aeruginosa*. Fungal culture, mycobacterial culture, and PCR detection of *Mycobacterium*

**TABLE 1 |** Viral loads of different respiratory samples collected from the patient infected with the novel HCoV-OC43 genotype at different time points.

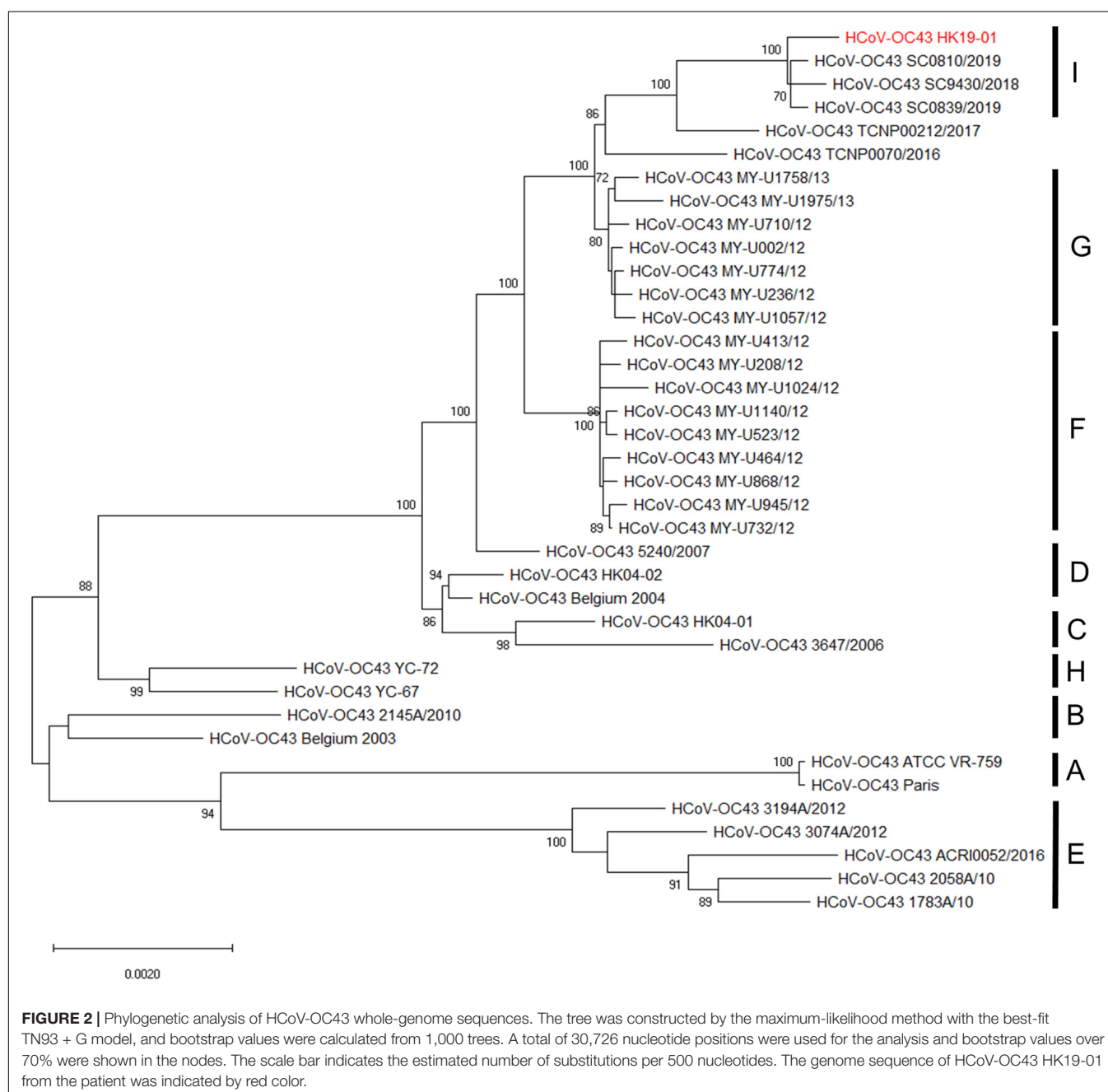| Collection date | Specimen | Viral load (copy no./ml) |
| --- | --- | --- |
| Day 14 | Bronchoalveolar lavage | $3.13 \times 10^9$ |
| Day 18 | Endotracheal aspirate | $1.10 \times 10^{10}$ |
| Day 19 | Endotracheal aspirate | $8.21 \times 10^8$ |
| Day 22 | Endotracheal aspirate | $8.38 \times 10^8$ |
| Day 28 | Pleural fluid | $6.46 \times 10^3$ |
| Day 29 | Bronchoalveolar lavage | $3.49 \times 10^6$ |

*tuberculosis*, *Legionella pneumophila*, *Pneumocystis jirovecii*, cytomegalovirus, herpes simplex virus and varicella zoster virus were all negative. A computed tomography scan of the thorax showed mixed consolidative/atelectatic changes in the dependent regions of both lungs (**Figure 1B**). The antibiotics were switched to intravenous meropenem, levofloxacin and vancomycin. However, the patient remained VV-ECMO-dependent and developed oliguric renal failure requiring continuous veno-venous hemofiltration. He developed *Candida albicans* fungemia on day 22, and intravenous anidulafungin was added. Despite all the treatment, his clinical condition continued to deteriorate with multiorgan failure. He finally succumbed on day 30.

## Viral Load

The viral load of the respiratory tract samples (bronchoalveolar lavage and endotracheal aspirate) from diagnosis to his death were persistently high ($3.49 \times 10^6$–$1.10 \times 10^{10}$ copies/ml) (**Table 1**). HCoV-OC43 at a level of $6.46 \times 10^3$ copies/ml was also detected from his pleural fluid 2 days before his death.

## Phylogenetic Analysis

Phylogenetic analysis using the complete genome sequences showed that HCoV-OC43 HK19-01 forms a distinct cluster with three other HCoV-OC43 from United States (GenBank



**FIGURE 2 |** Phylogenetic analysis of HCoV-OC43 whole-genome sequences. The tree was constructed by the maximum-likelihood method with the best-fit TN93 + G model, and bootstrap values were calculated from 1,000 trees. A total of 30,726 nucleotide positions were used for the analysis and bootstrap values over 70% were shown in the nodes. The scale bar indicates the estimated number of substitutions per 500 nucleotides. The genome sequence of HCoV-OC43 HK19-01 from the patient was indicated by red color.

TABLE 2 | Signature amino acid substitutions of the novel HCoV-OC43 genotype.

| Genotype | Strain | ORF1a nsp2 (150) | ORF1a nsp2 (543) | ORF1a nsp3 (143) | ORF1a nsp3 (424) | ORF1a nsp3 (1797) | ORF1b nsp12 (71) | ORF1b nsp14 (44) | ORF1b nsp14 (5) | HE Insertion between 166 and 167 | HE | HE | HE | S (262) | S (504) | S Insertion between 762 and 763 | S | S | S | ns5a (887) | ns5a (99) |
|---|---|---|---|---|---|---|---|---|---|---|---|---|---|---|---|---|---|---|---|---|---|
| A | ATCC VR-759 | S | A | Q | P | A | V | G | P | – | – | – | – | L | P | – | – | – | – | S | T |
| B | Belgium 2003 | . | . | . | . | . | . | . | . | – | – | – | – | . | . | – | – | – | – | . | . |
| C | HK04-01 | . | . | . | . | . | . | . | . | – | – | – | – | . | . | – | – | – | – | . | . |
| D | HK04-02 | . | . | . | . | . | . | . | . | – | – | – | – | . | . | – | – | – | – | . | . |
| E | 3194A/2012 | . | . | . | . | . | . | . | . | – | – | – | – | . | . | – | – | – | – | . | . |
| F | MY-U1024/12 | . | . | . | . | . | . | . | . | – | – | – | – | . | . | – | – | – | – | . | . |
| G | MY-U1057/12 | . | . | . | . | . | . | . | . | – | – | – | – | . | . | – | – | – | – | . | . |
|  | MY-U774/12 | . | . | . | . | . | . | . | . | – | – | – | – | . | . | – | – | – | – | . | . |
|  | TCNP0070/2016 | . | . | . | . | . | . | . | . | K | L | K | N | . | . | – | – | – | – | . | . |
|  | TCNP00212/2017 | . | . | . | . | . | . | . | . | K | L | K | N | . | . | – | – | – | – | . | . |
| H | YC-72 | . | . | . | . | . | . | . | . | – | – | – | – | . | . | – | – | – | – | . | . |
| I | SC9430/2018 | L | . | R | . | S | . | S | S | K | L | K | N | P | S | – | – | – | – | A | . |
|  | SC0839/2019 | L | . | R | . | S | . | S | S | K | L | K | N | P | S | – | – | – | – | A | . |
|  | SC0810/2019 | L | . | R | . | S | . | S | S | K | L | K | N | P | S | – | – | – | – | A | . |
|  | HK19-01 | L | V | R | H | S | I | S | S | K | L | K | N | P | S | A | S | D | I | A | N |

*Amino acid position of respective viral proteins of different HCoV-OC43 genotypes.
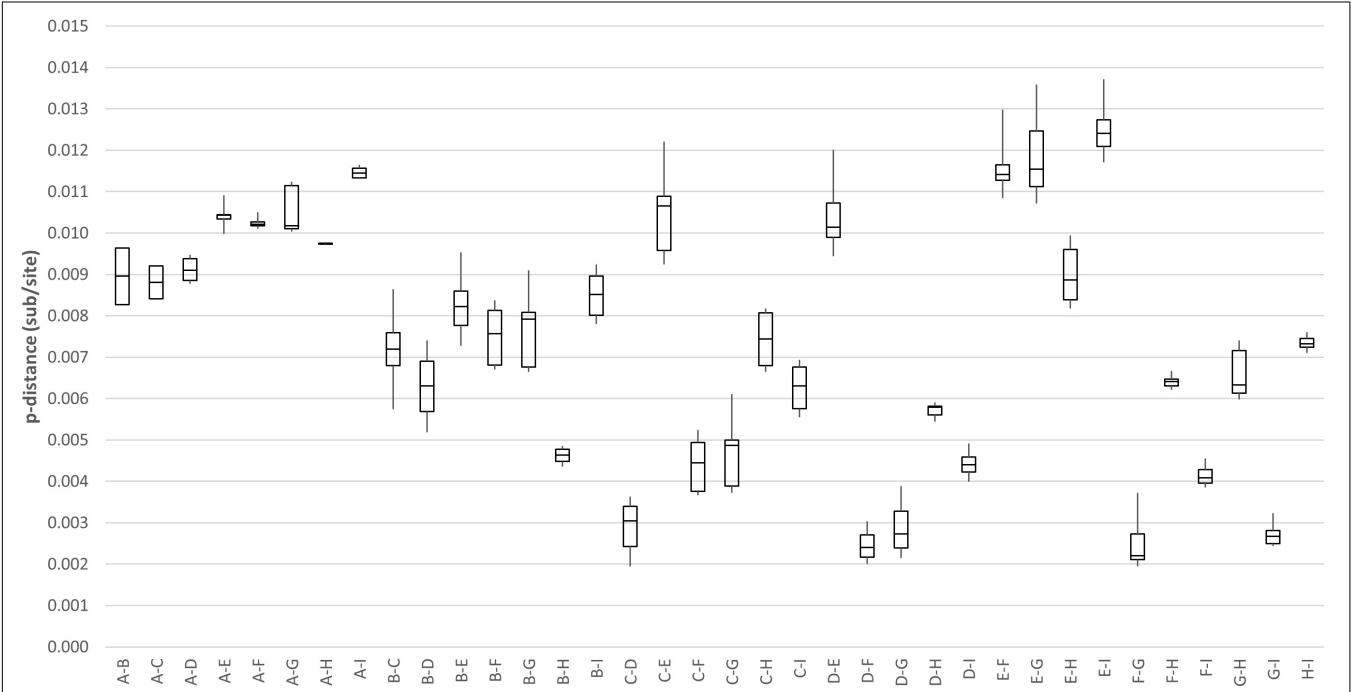
FIGURE 3 | Estimation of pairwise genetic distances between genotype I and other existing genotypes of HCoV-OC43 based on the whole-genome sequences.

accession numbers MN306041, MN306042, and MN306053), with a bootstrap value of 100% and sharing 99.9% nucleotide identities (Figure 2).

## Genome Analysis

Genome analysis revealed a distinct four-amino-acid (768ASDI771) insertion in the S2 region just downstream to the S1/S2 cleavage site of HCoV-OC43 HK19-01 (Table 2). Another four-amino-acid (167KLKN170) insertion in the hemagglutinin-esterase protein present in some HCoV-OC43 of genotype G is also present (Table 2). The three other HCoV-OC43 from United States in this cluster shared nearly the same genome sequence as that of HCoV-OC43 HK19-01 except without certain amino acid substitution/insertion in nsp2,

**TABLE 3 |** Estimation of non-synonymous and synonymous substitution rates of the novel HCoV-OC43 genotype.

| Gene | $K_a$ | $K_s$ | $K_a/K_s$ |
|---|---|---|---|
| nsp1 | 0 | 0.0060 | 0 |
| nsp2 | 0.0011 | 0 | |
| nsp3 | 0.0003 | 0.0028 | 0.1071 |
| nsp4 | 0 | 0.0028 | 0 |
| nsp5 | 0 | 0.0024 | 0 |
| nsp6 | 0 | 0 | |
| nsp7 | 0 | 0 | |
| nsp8 | 0 | 0 | |
| nsp9 | 0 | 0 | |
| nsp10 | 0 | 0 | |
| nsp11 | 0 | 0 | |
| nsp12 | 0.0002 | 0.0008 | 0.2500 |
| nsp13 | 0 | 0.0012 | 0 |
| nsp14 | 0 | 0.0029 | 0 |
| nsp15 | 0.0006 | 0 | |
| nsp16 | 0 | 0.0050 | 0 |
| ns2a | 0 | 0.0029 | 0 |
| HE | 0.0010 | 0.0034 | 0.2941 |
| S | 0.0011 | 0.0011 | 1.0000 |
| ns5a | 0.0020 | 0 | |
| E | 0.0026 | 0 | |
| M | 0 | 0 | |
| N | 0 | 0.0016 | 0 |

nsp3, nsp12, S, and ns5a proteins as in HCoV-OC43 HK19-01 (**Table 2**). Previously, a new genotype was proposed when the pairwise genetic distance of the whole genome sequence between a certain strain and the other genotypes was higher than that among the existing genotypes (Oong et al., 2017; Zhu et al., 2018). In this study, pairwise genetic distance between this cluster and other HCoV-OC43 genotypes ranged from

$0.27 \pm 0.02\%$ to $1.25 \pm 0.01\%$. In contrast, the lowest pairwise genetic distance between existing HCoV-OC43 genotypes was $0.26 \pm 0.02\%$ (**Figure 3**), suggesting that this cluster constitutes a novel HCoV-OC43 genotype, which we named genotype I. Bootscan analysis did not reveal any recombination leading to this new genotype I (**Supplementary Figure 1**).

## Estimation of Synonymous and Non-synonymous Substitution Rates

Using all four available proposed genotype I HCoV-OC43 genome sequences for analysis, the Ka/Ks ratios for the various coding regions were calculated (**Table 3**). The highest Ka/Ks ratios in this genotype were observed at S (1.0000), suggesting that the S gene in genotype I is under higher selection pressure. The Ka/Ks ratio for the S gene in genotype I is much higher than that in other genotypes (0.0426–0.4731), in which the Ka/Ks ratio for the S gene dropped to 0.2827 when using 54 strains of different genotypes for analysis.

## DISCUSSION

We describe a patient with fatal pneumonia caused by a novel genotype of HCoV-OC43. Although HCoV-OC43 is much more commonly associated with upper respiratory tract infections, its role as the causative agent of pneumonia in the present case is evident by the persistent detection of high viral loads in multiple lower respiratory tract samples throughout the course of the patient's illness, even before the death of the patient. This is in contrast to cases of respiratory viral infections complicated by fatal secondary pneumonia, in which the viral loads often decrease gradually. Still, pneumonia caused by pyogenic bacteria,



**FIGURE 4 |** Structure of the HCoV-OC43 spike glycoprotein trimer predicted by SWISS-MODEL homology modeling. Models were generated using the structure of HCoV-OC43 (Protein Data Bank code 6NZK). The black square zone is magnified, and the red rectangle shows loop containing the S1/S2 furin protease cleavage site (aa residues 756–772). The left and right panel represents HCoV-OC43 HK04-01 and HK19-01, respectively.

such as *Streptococcus pneumoniae* and *Staphylococcus aureus*, is the cause of severe sepsis, respiratory failure, and death of the patients. Moreover, no significant bacterial pathogen causing secondary bacterial pneumonia was isolated from the present patient, and he failed to respond to broad-spectrum antibiotic therapy. The HCoV-OC43 HK19-01 from the patient represents a novel genotype because the pairwise genetic distance between this novel genotype and other genotypes of HCoV-OC43 is higher than the lowest pairwise genetic distance between all the known HCoV-OC43 genotypes. However, unlike genotypes D, E, F, G and H, no recombination event was observed for this novel genotype. It is of note that although occasional fatalities as a result of primary viral pneumonia have been described in human betaCoVs such as HCoV-OC43 or HCoV-HKU1 (Vabret et al., 2003; Woo et al., 2005b), hypervirulence has not been reported in other genotypes of HCoV-OC43 or the three genotypes of HCoV-HKU1 (Woo et al., 2006; Lau et al., 2011; Zhang et al., 2015; Oong et al., 2017; Zhu et al., 2018). Nevertheless, this could be a result of our lack of knowledge on the molecular epidemiology of HCoVs, as genotyping of HCoVs is generally not performed in routine clinical microbiology laboratories.

The possible hypervirulence of this strain or novel genotype of HCoV-OC43 may be related to the four-amino-acid insertion in the S2 region just downstream to the S1/S2 cleavage site. It has been well-recognized that modifying the amino acid residues at the S1/S2 junction or improving the conditions that facilitate cleavage of the S proteins in SARS-CoV-2 and MERS-like-CoV, respectively, enhances their infectivities (Andersen et al., 2020; Menachery et al., 2020; Johnson et al., 2021). This in turn generates a higher viral load and may make the viruses more pathogenic. As for HCoV-OC43 HK19-01, although it has already possessed the optimal amino acid residues at the cleavage site, an 768ASDI771 insertion was present just downstream to the S1/S2 junction. Three-dimensional structural modeling showed that the loop that contained the S1/S2 cleavage site is 17 amino acids long in HCoV-OC43 HK19-01, as compared to 13 amino acids in other HCoV-OC43 (**Figure 4**). We speculate that this could have made the S1/S2 cleavage site more exposed and accessible to the protease. Notably, the corresponding loop with the S1/S2 cleavage site in SARS-CoV-2 (15 amino acids) is also four aa longer than other SARSr-CoVs (11 amino acids) (Lemmin et al., 2020). Further experiments will reveal the relative importance of the length of the loop in comparison to the amino acid composition of the cleavage site itself and other factors. On the contrary, the disease information and patient condition of the other three viruses from United States of this novel genotype are lacking. Hence, it cannot be excluded that the current fatal case may be exceptional.

## DATA AVAILABILITY STATEMENT

The datasets presented in the study are deposited in the GenBank sequence database, accession number MW938760.

## ETHICS STATEMENT

The studies involving human participants were reviewed and approved by the Institutional Review Board of the University of Hong Kong/Hospital Authority Hong Kong West Cluster (UW 16-365 20-07-2016). The patients/participants provided their written informed consent to participate in this study. Written informed consent was obtained from the individual(s) for the publication of any potentially identifiable images or data included in this article.

## AUTHOR CONTRIBUTIONS

SL, KL, XL, and PW conceived and designed the experiments and drafted the manuscript. KL, XL, and K-YT performed the experiments. SL, KL, XL, K-YT, SS, and PW contributed to the analysis. All authors provided critical feedback and revised the manuscript.

## FUNDING

## SUPPLEMENTARY MATERIAL

The Supplementary Material for this article can be found online at: https://www.frontiersin.org/articles/10.3389/fmicb.2021.795449/full#supplementary-material

## REFERENCES

Andersen, K. G., Rambaut, A., Lipkin, W. I., Holmes, E. C., and Garry, R. F. (2020). The proximal origin of SARS-CoV-2. *Nat. Med.* 26, 450–452. doi: 10.1038/s41591-020-0820-9

Hamre, D., and Procknow, J. J. (1966). A new virus isolated from the human respiratory tract. *Proc. Soc. Exp. Biol. Med.* 121, 190–193. doi: 10.3181/00379727-121-30734

Johnson, B. A., Xie, X., Bailey, A. L., Kalveram, B., Lokugamage, K. G., Muruato, A., et al. (2021). Loss of furin cleavage site attenuates SARS-CoV-2 pathogenesis. *Nature* 591, 293–299. doi: 10.1038/s41586-021-03237-4

Kumar, S., Stecher, G., Li, M., Knyaz, C., and Tamura, K. (2018). MEGA X: molecular evolutionary genetics analysis across computing platforms. *Mol. Biol. Evol.* 35, 1547–1549. doi: 10.1093/molbev/msy096

Lau, S. K. P., Fan, R. Y. Y., Zhu, L., Li, K. S. M., Wong, A. C. P., Luk, H. K. H., et al. (2021). Isolation of MERS-related coronavirus from lesser bamboo bats that uses DPP4 and infects human-DPP4-transgenic mice. *Nat. Commun.* 12:216. doi: 10.1038/s41467-020-20458-9

Lau, S. K. P., Lee, P., Tsang, A. K. L., Yip, C. C. Y., Tse, H., Lee, R. A., et al. (2011). Molecular epidemiology of human coronavirus OC43 reveals evolution of different genotypes over time and recent emergence of a novel genotype due to natural recombination. *J. Virol.* 85, 11325–11337.s doi: 10.1128/JVI.05512-11

Lau, S. K. P., Luk, H. K. H., Wong, A. C. P., Li, K. S. M., Zhu, L., He, Z., et al. (2020). Possible bat origin of severe acute respiratory syndrome coronavirus 2. *Emerg. Infect. Dis.* 26, 1542–1547. doi: 10.3201/eid2607.200092

Lau, S. K. P., Woo, P. C. Y., Li, K. S. M., Huang, Y., Tsoi, H. W., Wong, B. H. L., et al. (2005). Severe acute respiratory syndrome coronavirus-like virus in Chinese horseshoe bats. *Proc. Natl. Acad. Sci. U.S.A.* 102, 14040–14045. doi: 10.1073/pnas.0506735102

Lemmin, T., Kalbermatter, D., Harder, D., Plattet, P., and Fotiadis, D. (2020). Structures and dynamics of the novel S1/S2 protease cleavage site loop of the SARS-CoV-2 spike glycoprotein. *J. Struct. Biol. X* 4:100038. doi: 10.1016/j.yjsbx.2020.100038

Lole, K. S., Bollinger, R. C., Paranjape, R. S., Gadkari, D., Kulkarni, S. S., Novak, N. G., et al. (1999). Full-length human immunodeficiency virus type 1 genomes from subtype C-infected seroconverters in India, with evidence of intersubtype recombination. *J. Virol.* 73, 152–160. doi: 10.1128/JVI.73.1.152-160.1999

McIntosh, K., Dees, J. H., Becker, W. B., Kapikian, A. Z., and Chanock, R. M. (1967). Recovery in tracheal organ cultures of novel viruses from patients with respiratory disease. *Proc. Natl. Acad. Sci. U.S.A.* 57, 933–940. doi: 10.1073/pnas.57.4.933

Menachery, V. D., Dinnon, K. H. I. I. I., Yount, B.L.Jr, McAnarney, E. T., Gralinski, L. E., Hale, A., et al. (2020). Trypsin treatment unlocks barrier for Zoonotic Bat coronavirus infection. *J. Virol.* 94, e1774–e1819. doi: 10.1128/JVI.01774-19

Oong, X. Y., Ng, K. T., Takebe, Y., Ng, L. J., Chan, K. G., Chook, J. B., et al. (2017). Identification and evolutionary dynamics of two novel human coronavirus OC43 genotypes associated with acute respiratory infections: phylogenetic, spatiotemporal and transmission network analyses. *EMI* 6:e3. doi: 10.1038/emi.2016.132

Vabret, A., Mourez, T., Gouarin, S., Petitjean, J., and Freymuth, F. (2003). An outbreak of coronavirus OC43 respiratory infection in Normandy, France. *Clin. Infect. Dis.* 36, 985–989. doi: 10.1086/374222

van der Hoek, L., Pyrc, K., Jebbink, M. F., Vermeulen-Oost, W., Berkhout, R. J. M., Wolthers, K. C., et al. (2004). Identification of a new human coronavirus. *Nat. Med.* 10, 368–373.

Waterhouse, A., Bertoni, M., Bienert, S., Studer, G., Tauriello, G., Gumienny, R., et al. (2018). SWISS-MODEL: homology modelling of protein structures and complexes. *Nucleic Acids Res.* 46, W296–W303. doi: 10.1093/nar/gky427

Woo, P. C. Y., Lau, S. K. P., Chu, C. M., Chan, K. H., Tsoi, H. W., Huang, Y., et al. (2005a). Characterization and complete genome sequence of a novel coronavirus, coronavirus HKU1, from patients with pneumonia. *J. Virol.* 79, 884–895. doi: 10.1128/JVI.79.2.884-895.2005

Woo, P. C. Y., Lau, S. K. P., Tsoi, H. W., Huang, Y., Poon, R. W. S., Chu, C. M., et al. (2005b). Clinical and molecular epidemiological features of coronavirus HKU1-associated community-acquired pneumonia. *J. Infect. Dis.* 192, 1898–1907. doi: 10.1086/497151

Woo, P. C. Y., Lau, S. K. P., Lam, C. S. F., Lau, C. C. Y., Tsang, A. K. L., Lau, J. H. N., et al. (2012). Discovery of seven novel *Mammalian* and avian coronaviruses in the genus *Deltacoronavirus* supports bat coronaviruses as the gene source of *Alphacoronavirus* and *Betacoronavirus* and *Avian coronaviruses* as the gene source of *Gammacoronavirus* and *Deltacoronavirus*. *J. Virol.* 86, 3995–4008. doi: 10.1128/JVI.06540-11

Woo, P. C. Y., Lau, S. K. P., Yip, C. C. Y., Huang, Y., Tsoi, H. W., Chan, K. H., et al. (2006). Comparative analysis of 22 coronavirus HKU1 genomes reveals a novel genotype and evidence of natural recombination in coronavirus HKU1. *J. Virol.* 80, 7136–7145. doi: 10.1128/JVI.00509-06

Zaki, A. M., van Boheemen, S., Bestebroer, T. M., Osterhaus, A. D., and Fouchier, R. A. (2012). Isolation of a novel coronavirus from a man with pneumonia in Saudi Arabia. *N. Engl. J. Med.* 367, 1814–1820. doi: 10.1056/NEJMoa1211721

Zhang, Y., Li, J., Xiao, Y., Zhang, J., Wang, Y., Chen, L., et al. (2015). Genotype shift in human coronavirus OC43 and emergence of a novel genotype by natural recombination. *J. Infect.* 70, 641–650. doi: 10.1016/j.jinf.2014.12.005

Zhu, Y., Li, C., Chen, L., Xu, B., Zhou, Y., Cao, L., et al. (2018). A novel human coronavirus OC43 genotype detected in mainland China. *EMI* 7:173. doi: 10.1038/s41426-018-0171-5

# Identification of Hypericin as a Candidate Repurposed Therapeutic Agent for COVID-19 and Its Potential Anti-SARS-CoV-2 Activity

Aline da Rocha Matos[1†], Braulia Costa Caetano[1†], João Luiz de Almeida Filho[2],
Jéssica Santa Cruz de Carvalho Martins[1], Michele Gabrielle Pacheco de Oliveira[1],
Thiago das Chagas Sousa[1], Marco Aurélio Pereira Horta[3], Marilda Mendonça Siqueira[1]
and Jorge Hernandez Fernandez[2]*

[1] Laboratório de Vírus Respiratórios e do Sarampo, Insituto Oswaldo Cruz, Fundação Oswaldo Cruz (LVRS-IOC-Fiocruz), Rio de Janeiro, Brazil, [2] Laboratório de Química e Função de Proteínas e Peptídeos, Centro de Biociências e Biotecnologia, Universidade Estadual do Norte Fluminense (LQFPP-CBB-UENF), Campos dos Goytacazes, Brazil, [3] Plataforma de Laboratórios de Biossegurança Nível 3, Instituto Oswaldo Cruz, Fundação Oswaldo Cruz (NB3-IOC-Fiocruz), Rio de Janeiro, Brazil

The COVID-19 pandemic has had an unprecedented impact on the global economy and public health. Its etiologic agent, the severe acute respiratory syndrome coronavirus 2 (SARS-CoV-2) is highly transmissible, pathogenic and has a rapid global spread. Currently, the increase in the number of new confirmed cases has been slowed down due to the increase of vaccination in some regions of the world. Still, the rise of new variants has influenced the detection of additional waves of rising cases that some countries have experienced. Since the virus replication cycle is composed of many distinct stages, some viral proteins related to them, as the main-protease (Mpro) and RNA dependent RNA polymerase (RdRp), constitute individual potential antiviral targets. In this study, we challenged the mentioned enzymes against compounds pre-approved by health regulatory agencies in a virtual screening and later in Molecular Mechanics/Poisson–Bolzmann Surface Area (MM/PBSA) analysis. Our results showed that, among the identified potential drugs with anti-SARS-CoV-2 properties, Hypericin, an important component of the *Hypericum perforatum* that presents antiviral and antitumoral properties, binds with high affinity to viral Mpro and RdRp. Furthermore, we evaluated the activity of Hypericin anti-SARS-CoV-2 replication in an *in vitro* model of Vero-E6 infected cells. Therefore, we show that Hypericin inhibited viral replication in a dose dependent manner. Moreover, the cytotoxicity of the compound, in cultured cells, was evaluated, but no significant activity was found. Thus, the results observed in this study indicate that Hypericin is an excellent candidate for repurposing for the treatment of COVID-19, with possible inhibition of two important phases of virus maturation.

**Keywords: SARS-CoV-2, COVID-19, Hypericin, RdRp, Mpro, drug repurposing**

# INTRODUCTION

Since the coronavirus disease 2019 (COVID-19) pandemic was declared by WHO in March 2020, severe acute respiratory syndrome coronavirus 2 (SARS-CoV-2) has caused more than 260 million infections worldwide, with more than 5.1 million deaths (WHO, 2021). In Brazil, positive cases for COVID-19 have already reached more than 22 million and surpassed 600 thousand deaths (Ministério, 2021). Of note, the number of cases has experienced a decrease as the COVID-19 vaccines are being delivered worldwide. Despite that, the emergence of the virus variants,[1] such as the alfa, gamma, delta, and the recently described omicron, in addition to the relaxation of pandemic restrictions has been associated with new waves of increasing number of cases regionally (Lemey et al., 2021; Naveca et al., 2021).

The clinical presentation of COVID-19 is characterized by the exhibition of distinct signs and symptoms, which influence the disease severity, ranging from asymptomatic and mild cases to acute respiratory distress syndrome (ARDS), respiratory and multiple organ failure, and ultimately death. Risk groups for the development of the severe COVID-19 comprise individuals of advanced age and who present some comorbidities, as pre-existing chronic medical conditions, such as diabetes (Zhou et al., 2020). A cytokine storm, associated with exacerbation of proinflammatory cytokine release due to the viral infection, is related to the emergence of ARDS and the evolution to the severe disease (Lucas et al., 2020; Ye et al., 2020).

Presently, the process of vaccination against SARS-CoV-2 is ongoing worldwide with distinct types of immunogens, including inactivated virus, adenoviral vectors, and viral RNA, among others (Abdulla et al., 2021; Kumar et al., 2021). Vaccines constitute one of the most important public health strategies to reduce disease burden. However, it is important to emphasize that there are important issues regarding access to vaccines globally, such as their uneven distribution and the need for differentiated infrastructure for their inter and intra-country dissemination, which compromises the coverage necessary for homogeneous immunological protection of populations (Günl et al., 2021). In addition, depending on the vaccine platform used, there are differences in their efficacy and safety in individuals from some risk groups and against the SARS-CoV-2 variants of concern (VOCs) (Harvey et al., 2021).

The therapeutic management of the infection with SARS-CoV-2 has changed significantly since the beginning of the pandemic. In Europe (European Medicines Agency[2]) and in the US (Food and Drug Administration[3]), so far, only the antiviral Remdesivir, a nucleoside analog that targets the viral RNA-dependent RNA polymerase (RdRp), and neutralizing antibodies have been approved as treatment options for COVID-19, in the modality of emergency use. However, their therapeutic benefits are still being fully determined. Additionally, several antiviral drugs have been investigated for the treatment of COVID-19

in clinical trials, such as Favipiravir, Lopinavir/Ritonavir, Umifenovir (arbidol), and the new drug Paxvolid (Jomah et al., 2020; Kumar et al., 2021; Mahase, 2021). Furthermore, host directed therapies, aiming to impair virus-host specific interface mechanisms, and immunomodulators that would counteract the exacerbated immune response associated with the disease severity are other relevant therapeutic options under investigation (Kumar et al., 2021).

Since the beginning of the COVID-19 pandemic, drug repurposing has been deployed as one agile mechanism for the identification of new SARS-CoV-2 targets for drugs already approved, however, outside the scope of its original nomination. Through this strategy, time and investment needed for drug development could be reduced as the greater part of the pre-clinical phase is already completed, especially the safety assessment phase and formulation development (Hernandez et al., 2017; Montes-Grajales et al., 2020; Egieyeh et al., 2021). In addition, repurposing decreases the chance that the compound will be unsuccessful in the clinical phases, as this step has usually been completed with the original indication (Ismail et al., 2021). Among one of the strategies used to identify active molecules is Structure-Based Virtual Screening (SBVS), a computational technique that uses the structural information of a protein from the pathogen to find possible inhibitors in a library of compounds that bind the protein with the highest affinity (Li and Shah, 2017). Usually, the classification of these compounds is done through molecular docking experiments, that is, the calculation of binding mode between the ligand and the receptor protein (Fradera and Babaoglu, 2018). Thus, docking added to the current computational power, and the use of virtual libraries of free compounds like ZINC15 (Sterling and Irwin, 2015) turn a personal computer into a powerful tool for drug search and design, which is highly advantageous for drug repurposing and also provides support for next steps of the drug development process (Montes-Grajales et al., 2020).

The virus replication cycle is composed of many distinct stages. Viral proteins acting in each of these stages each constitute individual potential antiviral targets. One of them is the SARS-CoV-2 main-protease (Mpro), also called 3-chymotrypsin-like protease (3CLpro), which is mainly responsible for processing the viral polyproteins (pp) 1a and 1ab into the non-structural proteins (NSPs), including the RNA-dependent RNA Polymerase (RdRp), the helicase, and the Mpro itself (Hegyi and Ziebuhr, 2002). Data from other studies have demonstrated that the activity of this enzyme is critical for replication of coronaviruses (Kim et al., 1995; Stobart et al., 2012). In addition, there are no described human analogs of this protein. Moreover, protease inhibitors are successfully implemented in the treatment against other viral diseases (Hoetelmans et al., 1997; Chary and Holodniy, 2010; Bacon et al., 2011). Altogether, these characteristics make the Mpro a promising antiviral drug target.

An additional relevant target is the RdRp, an enzyme that is responsible for the replication of viral RNA (**Figure 1A**), possessing an essential role in SARS-CoV-2 life cycle. This protein functions as a tripartite polymerase complex with NSP-7 and NSP-8 that further associates with NSP-14, which confers a proofreading exonuclease function (Subissi et al., 2014). Due

---

[1] who.int/en/activities/tracking-SARS-CoV-2-variants

[2] ema.europa.eu

[3] fda.gov
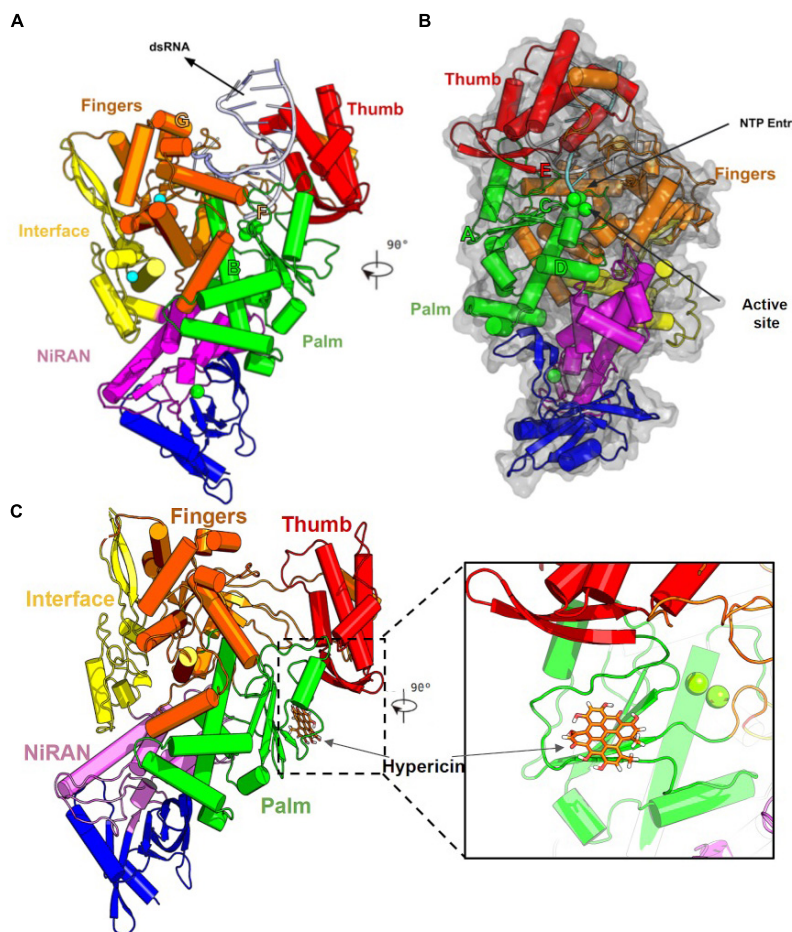
**FIGURE 1 |** Structure of the SARS-CoV-2 RdRp polymerase in complex with Hypericin. **(A)** General structure of SARS-CoV2 RdRp and important parts of the active site. The Structure of SARS-CoV2 RdRp (NSP12) core contains an interface (Yellow), Nidovirus RdRp-associated nucleotidyltransferase (NiRAN in Magenta), and RdRp domains. The RdRp domain looks like a right hand containing the Thumb (in red), Palm (in green), and Finger (in orange) subdomains. **(B)** SARS-CoV2 presents a catalytic triad (GDD) at the center of the Palm subdomain that catalyzes the synthesis of an RNA strand complementary to the RNA template through the binding of NTP's. Furthermore, the RdRp have six motifs named A to F that are well conserved. These motifs are responsible for template binding (Motif B), polymerization and recognition of NTPs (Motif D), coordination of ions and active site (motif A and C), conformational changes and support of the primer strand (Motif E). **(C)** Our docking calculations show that Hypericin interacts in the palm domain of RdRp near the catalytic center, represented by Mg ions. In this position, Hypericin blocks the natural pathway of ribonucleotides in the active site of the RdRp enzyme. Secondary structure of RpRd enzyme represented in cartoon style and colored according to protein domains, Mg ions represented in VDW and Hypericin is represented in orange licorice.

to the particularities of this protein, several inhibitors for RdRp from Flaviviruses and SARS-CoV have been reported and some are being evaluated in pre-clinical and clinical phases (Niyomrattanakit et al., 2010; Montes-Grajales et al., 2020; Tian et al., 2021).

In this sense, the central goal of this work was to find compounds approved by international agencies as candidate therapeutic agents for repurposing against the SARS-CoV-2 through the SBVS experiment, specifically focusing on compounds that bind Mpro and RdRp. Secondly, we aimed to confirm the inhibitory action of promising compounds *in vitro*. As a result, one of the candidates identified was Hypericin, an antraquinone with antiviral and antifungal functions (Miskovsky, 2002). Additionally, we show that Hypericin acts as anti-SARS-CoV-2 replication inhibitor in μM

concentrations in an *in vitro* model of Vero-E6 infected cells. These results qualify this drug as a promising antiviral candidate against SARS-Cov-2 and further experiments, including *in vivo* studies, are the next step of our experimentation.

## METHODOLOGY

## Structure Based Virtual Screening Experiment

In the SBVS experiment, essential proteins for the replication and maturation of SARS-CoV-2 were selected. The structures of the Mpro domain (pdb 6LU7) (Hatada et al., 2020) and the RdRp domain (7bv2) (Yin et al., 2021) from the Research Collaboratory for Structural Bioinformatics Protein Data Bank (RSCB PDB)

(Berman et al., 2000) were used as receptor proteins. In both structures, all water and hetero-atoms were removed for docking experiments. In some experiments, Mg ions were maintained in the active site of the SARS-CoV-2 RdRp. Docking space was defined as a $\pm 2$ nm (in X, Y, Z) at the center of the active site. For the SBVS campaign, the enzymes Mpro and RdRp were challenged against ligand database (ZINC15/Enzyme/Trial and ZINC15/Enzyme/World) that have a total of 3,400 molecules already approved by several international regulatory agencies. HTP SurflexDock pipeline uses GROMACS 5.2 (Abraham et al., 2015) for molecular simulations and receptor ensemble sampling and Autodock 4.2 (Morris et al., 2009) for docking experiments (de Almeida Filho and Fernandez, 2020). In the initial HTP SurflexDock scoring results, a functional cut-off of Ki less than 10E-9 kcal/mol were considered as good candidates for re-scoring experiment. From this ranking, the 10 best inhibitors were evaluated for favorable binding on the protein active site and were re-evaluated through a post-processing step implemented in the HTP SurflexDock. Furthermore, the accurate binding energy inference ($\Delta \Delta G$) of the most promising compounds was estimated using Molecular Mechanics/Poisson–Bolzmann Surface Area (MM/PBSA) methodology (Genheden and Ryde, 2015; Wang et al., 2018).

## The HTP SurflexDock Pipeline for Structure Based Virtual Screening

The HTP SurflexDock 1.0 pipeline[4] is based on MDR SurflexDock pipeline (de Almeida Filho and Fernandez, 2020), modified to perform 'docking and scoring' experiments to classify promising compounds in SBVS experiments. Thus, we incorporated two types of post-processing analysis into the HTP SurflexDock pipeline: (1) Manual refinement and re-scoring of compounds and (2) Inference of binding free energy ($\Delta \Delta G$) for most promising complexes using MM/PBSA. In the post-processing module for the inference of the $\Delta \Delta G$ calculated from molecular simulations based on the MM/PBSA protocol was used (Mobley and Dill, 2009; Genheden and Ryde, 2015). MM/PBSA is widely used in affinity inference analyses, as well as compound re-scoring (Wang et al., 2019). In this context, in HTP SurflexDock we used the g_mmbpsa software (Ren et al., 2020) for complex affinity inference. The g_mmpbsa is configured to calculate the free energy of the last 3 ns simulation and the initial 7 ns are used for the equilibrium of the system. At the end of the calculation, the python mmpbsa.py script is used to generate the graph of the $\Delta G$ variation as a function of time and a summary containing the averages of the energy contributions.

## Cell Culture

We used Vero E6 cells (African green monkey kidney cells) for SARS-CoV-2 isolation and propagation, as well as for assays of evaluation of the antiviral potential of the candidate compound. All cell culture reagents were from Gibco (Thermo Fisher Scientifc, Waltham, MA, United States). Sterile, pyrogen free, culture-treated plastic ware was purchased from Corning and Sarstedt. The basic culture medium used for Vero E6 cells consisted of Dulbecco's Modified Eagle

Medium (DMEM) formulated with D-glucose (4.5 g/l) and L-Glutamine (3.9 mM). Basic medium was supplemented with $100\times$ penicillin-streptomycin solution (to final 100 U/ml and 100 µg/ml, respectively) and with inactivated fetal bovine serum (USDA-qualified region FBS) at 10%. Both cell and viral cultures were incubated at 37°C and 5% $CO_2$.

## Severe Acute Respiratory Syndrome Coronavirus 2 Isolate

The SARS-CoV-2 isolate used in the assays was obtained from a respiratory sample collected from a COVID-19 patient diagnosed in March 2020, in Rio de Janeiro, Brazil. The original sample was a combination of two mid-turbinate nasal swabs and one pharyngeal swab, all collected in 3 ml of viral transport medium (DMEM supplemented with 1% bovine serum albumin and $1\times$ penicillin-streptomycin). For virus isolation, 200 µl of the sample were inoculated in a confluent monolayer of Vero E6 cells in a T25 culture flask. Culture was incubated for 96 hs, with inspections for development of cytopathic effect and collection of supernatants every 24 h to evaluate viral replication. The viral isolate was further characterized by whole genome sequencing (published on gisaid.org, accession number EPI ISL 414045) and transmission electron microscopy (Barreto-Vieira et al., 2021). Viral titer of the isolate was increased by an additional passage in Vero E6 cells, to obtain a working stock. The 50% Tissue Culture Infectious Dose ($TCID_{50}$) titer of the viral working stock was determined by limiting dilution and infection of Vero E6 cells. All the procedures related with the viral isolate culture and further treatment were performed in biosafety level 3 laboratory, in accordance with the WHO guidelines.[5] Regarding ethical aspects, the patient sample used for viral isolation was collected at a sentinel health unit of the respiratory disease surveillance network of the Brazilian Ministry of Health, as part of routine procedures of the COVID-19 surveillance program. As the National Influenza Center and National SARS-CoV-2 Reference Laboratory for the surveillance network, our laboratory systematically receives respiratory samples for viral detection, sequencing, and isolation. All procedures involving patient samples were approved by the Committee of Ethics in Human Research of the Oswaldo Cruz Institute (registration number CAAE 68118417.6.0000.5248).

## Virus Inhibition Assay

All incubation steps of the assays were performed at 37°C and 5% $CO_2$. First, cells were plated and cultured overnight to obtain confluent monolayers. Next day, cells were washed once with plain PBS, then, SARS-CoV-2 inoculums were incubated for one hour. The viral dose of the inoculums corresponded to a multiplicity of infection (MOI) of 0.01 $TCID_{50}$. After infection, inoculums were removed from wells and replaced by the appropriate supplemented medium with distinct concentrations of the candidate compound. The candidate compound was diluted in NaOH (1 M), which was used as a control and was diluted similarly to the compound, reaching a concentration of 2 mM in the following experiments. Supernatants for viral quantification were collected 48 h post-infection (hpi).

---

## Viral Quantification

We evaluated SARS-CoV-2 replication in the candidate compound-treated versus non-treated cultures by measuring the number of viral RNA copies in the supernatants. For this purpose, we used the real time reverse transcription-polymerase chain reaction method (real time qRT-PCR) (Corman et al., 2020). This protocol employs TaqMan primers and probes specific to the gene encoding the envelope (E) protein. As quantification standard, we used a synthetic RNA molecule comprising the reference sequence of the E target, with a known number of copies ($10^7$ copies/mL, kindly provided by Charité Virology through Pan American Health Organization). A concentration curve was prepared by serial dilution of the positive control from $10^6$ to 10 copies/mL. Viral RNA was extracted from 140 μL of cell-free culture supernatants using QIAamp Viral RNA mini kit (Qiagen, Hilden, Germany), according to manufacturer's instructions. Reverse transcription and gene amplification were performed in one-step reactions with a qRT-PCR kit developed by the Biomanguinhos Institute (Fiocruz, Rio de Janeiro, Brazil), in ABI 7500 thermocycler (Applied Biosystems, Waltham, MA, United States). The candidate compound concentration required to decrease the viral RNA by 50% ($IC_{50}$) was calculated using GraphPad Prism (GraphPad Software Inc., San Diego, CA, United States).

## Cellular Cytotoxicity

Vero E6 cells were plated at $10^4$ cells per well in 96-well plates and incubated overnight to obtain confluent monolayers. The following day, distinct concentrations of the candidate compound was added to the cultures, in triplicate. This was followed by incubation for 48 h at 37°C and 5% $CO_2$. Cell supernatants were used to measure LDH released by cell death with the commercial kit CyQUANT$^{TM}$ LDH Cytotoxicity Assay (Thermofisher, Waltham, MA, United States). Briefly, 50 μl of the supernatants from the treated cells and of the controls were transferred to a microtiter plate. Then, 50 μl of LDH colorimetric substrate was added to each sample and incubated for 30 min at room temperature, protected from light. LDH activity was determined by absorbance (OD) at 490/680 nm. Cytotoxicity was determined according to the manufacturer's guidelines.

## Statistical Analysis

Statistical analysis was performed with GraphPad Prism (GraphPad Software Inc., San Diego, CA, United States) by using One-way ANOVA with Dunnett's multiple comparison tests. Results were considered significant when $p < 0.05$.

## RESULTS

## *In silico* Analysis of Main-Protease and RNA Dependent RNA Polymerase Inhibitor Candidates

To identify good candidates for repurposing for SARS-Cov-2 Mpro and RdRp, we made a SBVS experiment with these proteins and a set of 3,400 molecules using the HTP SurflexDock.

For SARS-Cov-2 Mpro, our analysis ranked nine promising compounds as nM and pM inhibitors: Nelfinavir, Hypericin, Mitoxantrone, Saquinavir, Remikiren, Aclarubicin, ZINC24447427, Indinavir, and Dihydroergotamine, which comprise a group of anti-HIV, antitumor, and antifungal drugs (**Table 1**).

In addition, for SARS-Cov-2 RdRp our results indicated the 6 best candidates for RdRp inhibition as: Trypan blue, Hypericin, Mitoxantrone, Glycyrrhizinate Dipotassium, Lifitegrast, and Tudca, which obtained high affinity with the SARS-CoV-2 RdRp active site (**Table 2**) and represent molecules in clinical testing phases for treatment of neoplasms, lymphomas, antifungals, anti-HIV among other applications, which may indicate that these compounds are good candidates for broad-spectrum therapeutic antivirals.
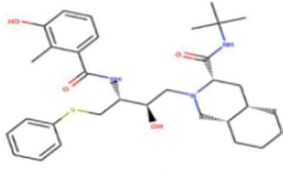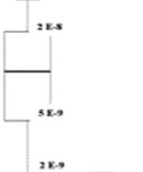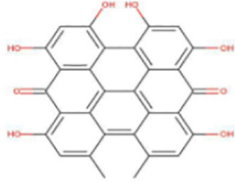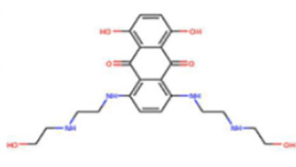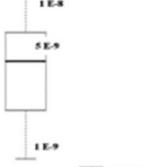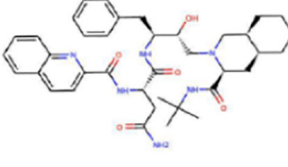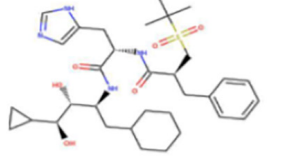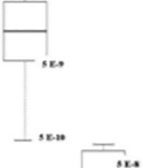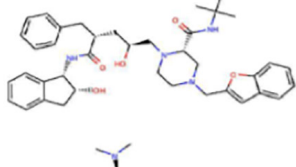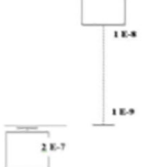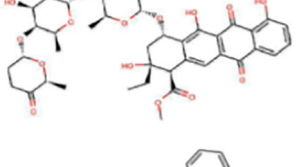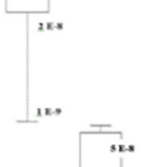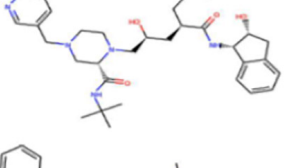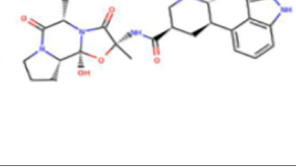
Obtained results suggest Hypericin and Mitoxantrone as best candidates for *in vitro* further experiments, as pointed as nM inhibitor for both enzymes in docking experiments. Moreover, for RdRp-Hypericin complex, a consecutive MM/PBSA experiment pointed a stable interaction of Hypericin near motif C in the active site (**Figures 1B,C**) with calculated $\Delta G = -22.704 \pm 4.008$ Kcal/mol (**Supplementary Figure 1**). Most of the other well-ranked molecules for the RdRp enzyme in our *in silico* experiments also are potential candidates for repurposing for the therapeutic treatment of SARS-CoV2.

## Hypericin Reduces Replication of Severe Acute Respiratory Syndrome Coronavirus 2 *in vitro* at Non-cytotoxic Concentrations

As the *in silico* analysis demonstrated that Hypericin was a potential candidate for the binding and inhibition of SARS-CoV-2 Mpro and RdRp proteins, we were interested in analyzing if this potential interaction would have an impact on the replication of the SARS-CoV-2 in our model of *in vitro* infection with the virus. Our results show that Hypericin significantly reduced viral replication in a concentration dependent fashion (**Figure 2A**). The highest Hypericin concentrations tested (10 and 100 μM) resulted in the highest degree of reduction in supernatant viral RNA ($p < 0.05$) and reached 84 and 96% of inhibition, respectively.
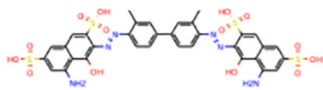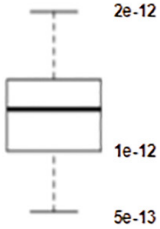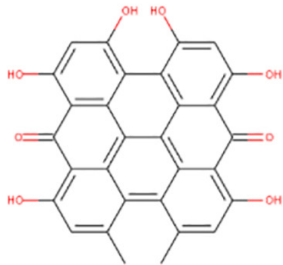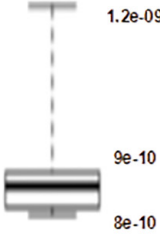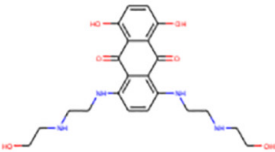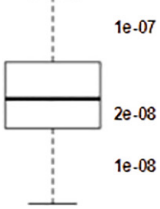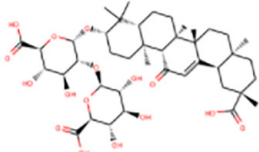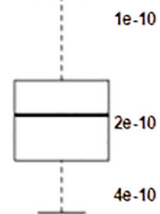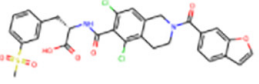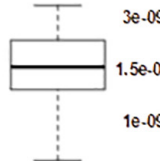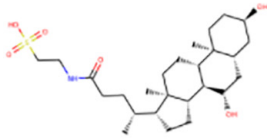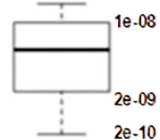
Moreover, to confirm that the reduction in viral replication was related to the inhibition of the viral replication cycle and not to an indirect effect on the host cell, we next evaluated the potential cytotoxic effects of the compound by measuring the release of LDH in non-infected cells for 48 h. As a result, there was no significant increase in extracellular LDH in cells treated with increasing concentration of the drug (0.01–100 μM), as compared to the cells treated with the drug vehicle NaOH (**Figure 2B**). Of note, total cell lysate was used as a positive control and presented a significant increase in LDH detection. These findings strengthen our computational screening experiments as Hypericin has come out to be one of the most interesting hits against the two viral proteins.

**TABLE 1 |** Docking hits for SARS-Cov-2 Mpro (pdb 6lu7 structure).

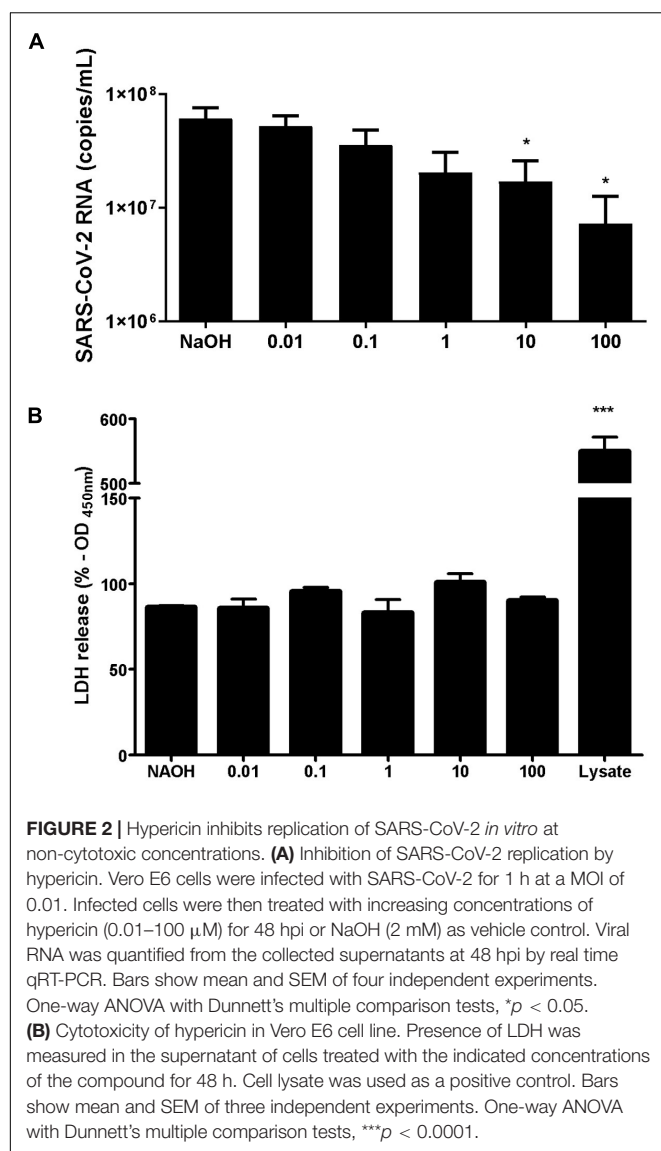| Molecule | Ligands | Activities described on Databases | Clinical trials | Molecular structure | Ki * (Mol) |
|---|---|---|---|---|---|
| ZINC3833846 CHEMBL584 Nelfinavir | Trialxx575 Trialxx576 Trialxx577 Trialxx578 Worldxx219 Worldxx222 | - Pol polyprotein (Virus)* - Multidrug resistance protein 1 - Cytochrome P450 3A4 - Sodium-dependent noradrenaline transporter | - NCT00000859; - NCT00000885 ;(1) - NCT00000887 ;(2) - NCT00000892  HIV Infections. |  | 2 E-8 5 E-9 2 E-9 |
| ZINC3780340 * CHEMBL286494 Hypericin | Trialxx276 | - Corticotropin-releasing factor receptor 1 - D(3) dopamine receptor - Pol polyprotein (Virus)* - Cytochrome P450 3A4 - Glutathione reductase | - NCT00000645 ; (1) - NCT00000792 ; (1)  HIV infections  - NCT02448381 ; (1) Cutaneous Mycosis, Fungoides, Lymphoma |  | 5 E-9 5 E-10 5 E-11 |
| ZINC3794794 * CHEMBL58 Mitoxantrone | Worldxx1214 Trialxx1848 | -Multidrug and toxin extrusion protein 1 - 5-hydroxytryptamine receptor 2C - Pol polyprotein (Virus)* - Potassium voltage-gated channel subfamily H member 2 - Solute carrier organic anion transporter family member 1B3 | - NCT00002003 (2) - NCT00002259 (2)  HIV Infections  - NCT00003858 (2) Prostatic Neoplasms  - NCT03250338 (3) Myeloid Leukemia |  | 1 E-8 5 E-9 1 E-9 |
| ZINC3914596 CHEMBL114 Saquinavir | Trialxx908 Worldxx510 | - Pol polyprotein (Virus)* - Cytochrome P450 3A4 - Multidrug resistance protein 1 - Kappa-type opioid receptor | -NCT00000848 (2) -NCT00000891 (2) -NCT00000892 -NCT00000898 -NCT00000906  HIV Infections. |  | 8 E-11 7 E-11 4 E-11 |
| ZINC4217406 CHEMBL31601 Remikiren | Trialxx355 Trialxx356 | - Renin | No |  | 5 E-8 5 E-9 5 E-10 |
| ZINC24447427 CHEMBL1233940 | Trialxx372 Trialxx373 Trialxx374 | - Pol polyprotein (Virus)* | No |  | 5 E-8 1 E-8 1 E-9 |
| ZINC85537142 CHEMBL502620 Aclarubicin | Worldxx51 Worldxx52 | - 5-hydroxytryptamine receptor 2B - 72 kDa type IV collagenase | - NCT03026842 (4) - NCT03045627 (2) - NCT03181815 (2) - NCT02723448 (1) Leukemia, Myeloid, Acute |  | 2 E-7 2 E-8 1 E-9 |
| ZINC22448696 CHEMBL115 Indinavir | Trialxx1799 World1162 | - Pol polyprotein (Virus)* - Cytochrome P450 3A4 - Protease - Multidrug and toxin extrusion protein 1 - Substance-K receptor | - NCT00000804 - NCT00000841 (3) - NCT00000848 (2) - NCT00000850 (2) - NCT00000859  HIV Infections. |  | 5 E-8 5 E-9 5 E-10 |
| ZINC3978005 CHEMBL1732 Dihydroergotamine | Trialxx1534 worldxx901 worldxx902 | - 5-hydroxytryptamine receptor 1A - Alpha-2A adrenergic receptor - D(2) dopamine receptor - D(1A) dopamine receptor -Alpha-1D adrenergic receptor | - NCT02582996, (3) - NCT02706015, (3) Migraine Disorders - NCT01191723, (1) |  | 1 E-7 2 E-8 2 E-9 |

**TABLE 2 |** Docking hits for SARS-Cov-2 RdRp (pdb 7aap structure).

| Molecule | Original Activity | Clinical Trial (Phase) | Molecular Structure | Ki (Kcal/mol) |
|---|---|---|---|---|
| ZINC169289767 CHEMBL1089641 *Trypan blue* | - Serine/threonine-protein kinase AKT3 - Renin | - Oftalmologic surgery (4) | | 2e-12 1e-12 5e-13 |
| ZINC3780340 CHEMBL286494 *Hypericin* | - Corticotropin-releasing factor receptor 1 - D(3) dopamine receptor - Pol polyprotein (v) - Cytochrome P450 3A4 - Glutathione reductase | - NCT00000645 (1) - NCT00000792 (1) HIV Infections - NCT02448381 (3) Cutaneous Mycosis, Fungoides, Lymphoma | | 1.2e-09 9e-10 8e-10 |
| CHEMBL58 ZINC3794794 *MITOXANTRONE* | - Multidrug and toxin extrusion protein 1 - 5-hydroxytryptamine receptor 2C - Pol polyprotein (virus) - Potassium voltage-gated channel subfamily H member 2 - Solute carrier organic anion transporter family member 1B3 | - NCT00002003 (2 - NCT00002259 (2 HIV infections - NCT00003858 (2 Prostatic Neoplas - NCT00859001 (2 Lymphoma - NCT03250338 (3 Leukemia, Myelo | | 1e-07 2e-08 1e-08 |
| ZINC96015174 CHEMBL1923952 *Glycyrrhizinate Dipotassium* | - Corticosteroid 11-beta-dehydrogenase isozyme 1 - Corticosteroid 11-beta-dehydrogenase isozyme 2 - Canalicular multispecific organic anion transporter 1 - Solute carrier organic anion transporter family member 1B2 | No | | 1e-10 2e-10 4e-10 |
| ZINC84668739 CHEMBL2048028 *Lifitegrast* | - Intercellular adhesion molecule 1 - Cytochrome P450 2C9 | No | | 3e-09 1.5e-09 1e-09 |
| ZINC3914813 CHEMBL272427 *Tudca* | No | No | | 1e-08 2e-09 2e-10 |

**FIGURE 2 |** Hypericin inhibits replication of SARS-CoV-2 *in vitro* at non-cytotoxic concentrations. **(A)** Inhibition of SARS-CoV-2 replication by hypericin. Vero E6 cells were infected with SARS-CoV-2 for 1 h at a MOI of 0.01. Infected cells were then treated with increasing concentrations of hypericin (0.01–100 μM) for 48 hpi or NaOH (2 mM) as vehicle control. Viral RNA was quantified from the collected supernatants at 48 hpi by real time qRT-PCR. Bars show mean and SEM of four independent experiments. One-way ANOVA with Dunnett's multiple comparison tests, $*p < 0.05$. **(B)** Cytotoxicity of hypericin in Vero E6 cell line. Presence of LDH was measured in the supernatant of cells treated with the indicated concentrations of the compound for 48 h. Cell lysate was used as a positive control. Bars show mean and SEM of three independent experiments. One-way ANOVA with Dunnett's multiple comparison tests, $***p < 0.0001$.

## DISCUSSION

Almost 2 years after the identification of SARS-CoV-2 and the declaration of the COVID-19 pandemic, many treatment options have been investigated, but just a few have displayed enough effect against the disease to be considered for emergency use, such as remdesivir and monoclonal antibodies, or to be regarded as a promising therapy by the health authorities, such as Paxlovid.[6]

Furthermore, they are targeted to specific clinical stages of the disease or patient groups. In search for more therapeutic options to contain the morbidity and mortality caused by SARS-CoV-2, drugs that target the viral proteins and the host molecules that drive the response against infection are being studied, as combination therapies are a good approach to successfully fight this disease (Kumar et al., 2021). Also,

[6]www.pfizer.com/news/press-release/press-release-detail/pfizers-novel-covid-19-oral-antiviral-treatment-candidate

drug repurposing has been highlighted as a relevant strategy to speed up the identification of compounds with anti-SARS-CoV-2 activity and, more importantly, reduce time and cost for clinical implementation of any potential drugs identified in experimental conditions.

Here, we screened a database of 3,400 known chemical compounds by computational analysis, to identify molecules able to interact with the viral proteins Mpro and RdRp, both essential for replication of SARS-CoV-2. The ligands were further classified according to their affinity of interaction with the viral targets, by molecular docking. This analysis indicated several compounds with high affinity to the viral proteins that could, in theory, display anti-SARS-CoV-2 properties. In general, viral protease inhibitors are widely studied drugs by the academic community. Many of ranked compounds identified in this study include inhibitors developed for HIV treatment (Bardsley-Elliot and Plosker, 2000), most of them (Indinavir, Saquinavir, Indinavir and Hypericin) already tested *in silico* or *in vitro* as candidates for repurposing for the SARS-CoV-2 (Bello et al., 2020). Obtained here results for SARS-Cov-2 Mpro (**Table 1**) were in concordance with the general picture found in other *in silico* SBVS academic works and were interpreted as excellent positive control for our SBVS experimental pipeline. Interestingly, Hypericin appeared as one of the top hits in the panel of possible ligands for both Mpro and RdRp viral proteins (**Tables 1**, **2**). Moreover, we showed that Hypericin reduced SARS-CoV-2 replication at μM concentrations in an *in vitro* experimental model and had no significant cytotoxic effect in the same model (**Figures 1**, **2**).

Hypericin is an anthraquinone member of the naftodianthrone class of chemical components obtained primarily from plants of the genus *Hypericum*, particularly *Hypericum perforatum* (commonly known as St. John's wort). Previous reports have shown that Hypericin presents antiviral activity against some viruses, such as hepatitis C, HIV, and influenza A (Lenard et al., 1993; Jacobson et al., 2001; Pu et al., 2009; Shih et al., 2018), as well as for the avian coronavirus IBV (Chen et al., 2019). Additionally, Hypericin possess antitumor properties (Rook et al., 2010; Dong et al., 2021). Recent studies have reported relevant interaction between Hypericin and Mpro by molecular docking analysis with $IC_{50}$ of 65 μM (Pitsillou et al., 2020a,b; Shivanika et al., 2020; Yalçın et al., 2021) and by inhibition of the protease activity *in vitro* (Pitsillou et al., 2020a), although in a different report employing fluorescence resonance energy transfer (FRET) experiments, Hypericin was considered a weak SARS-Cov2 Mpro inhibitor (Loschwitz et al., 2021). In addition, some studies evaluated *in silico* the interaction of Hypericin with the SARS-CoV-2 Spike, papain-like protease (PLpro) and NSP14 proteins (Pitsillou et al., 2020b, 2021; Romeo et al., 2020; Liu et al., 2021). However, none of these previous reports have demonstrated Hypericin antiviral activity against SARS-CoV-2 isolates.

Noteworthy, among additional antivirals identified, ranked compounds include inhibitors developed during the 1990s for HIV treatment (Noble and Faulds, 1996; Plosker and Noble, 1999; Bardsley-Elliot and Plosker, 2000). These are widely studied

drugs by the academic community and has already been explored as possible candidates for repurposing for the SARS-CoV2 by other authors (Bello et al., 2020). In this sense, Ohashi and co-workers point out that Nefilnavir can block the replication of SARS-CoV-2 in synergy with the anti-inflammatory Cefarantin *in vitro* (Ohashi et al., 2021). In addition, *in silico* simulations performed by Yamamoto et al. (2020) indicate that Nelfinavir inhibits virus replication by binding to the Mpro protein, while Cefarantin interferes with the interaction of Spike protein with the ACE2 enzyme, preventing intrusion into the cell. Other studies indicate that Nelfinavir also has a systemic effect by avoiding the oxytocin storm in patients infected with HIV-1 and, in this context, Xu et al. (2020) suggest that Nelfinavir can prevent complications caused in severe cases of COVID-19. Another well-rated antiretroviral in our tests was Saquinavir, widely used in the treatment of SARS together with Ribavirin in the 2003 epidemic (Tan et al., 2004). A study by Yamamoto et al. (2020) pointed out that Saquinavir can inhibit SARS-CoV2 replication at low concentrations ($EC_{50}$ = 8.83 μM) and suggests that the drug prevents the entry of the virus into the cell in addition to inhibiting the viral replication. Finally, Indinavir is also an antiretroviral that has also been well ranked in other SBVS but without *in vitro* validation (Shah et al., 2020). In the antitumor drug group, Mitoxantrone is an agent of the anthraquinone family used in the treatment of leukemia (Lokhande et al., 2021). *In silico* simulations with the Mpro of SARS-CoV2 indicate that Mitoxantrone binds strongly to the active site of enzyme through a network of hydrogen bonds and hydrophobic interactions inhibiting the replication of the virus (Farag et al., 2021). On the other hand, Aclarubicin is a drug of the anthracycline family in clinical trials for the treatment of acute myeloid leukemia. This drug has been evaluated *in silico* as a possible inhibitor of the interaction RBD-ACE2, hampering virus entrance into the host cell (Senathilake et al., 2020).

In conclusion, most of the well-ranked molecules for the Mpro and RdRp enzymes in our *in silico* experiments are good candidates for repurposing for the therapeutic treatment of SARS-CoV-2 and, among them, Hypericin presented promising results as a drug not previously evaluated for antiviral activity against SARS-CoV-2. Further experiments are under way, such as definition of Hypericin anti-SARS-CoV-2 $IC_{50}$ in human cellular *in vitro* model by determination of specific virus viability after hypericin treatments and confirmation of Hypericin specific antiviral mechanisms of action and to compare its activity to other approved drugs like Remdesivir. Also in the scope of our interest is a phase I dose escalation study to determine antiviral activity of hypericin against SARS-Cov-2 and the safety in animal models.

## DATA AVAILABILITY STATEMENT

The original contributions presented in the study are included in the article/**Supplementary Material**, further inquiries can be directed to the corresponding author/s.

## AUTHOR CONTRIBUTIONS

ARM, BCC, JLAF, MMS, and JHF designed the experiments and wrote the manuscript. ARM, BCC, JLAF, JSCCM, MGPO, and TCS conducted the experiments. MAPH provided the access and the training for working in BSL-3 facilities that are necessary to perform all experiments involving live SARS-CoV-2 virus manipulation. All authors contributed to manuscript formulation and review and approved the submitted version.

## FUNDING

## ACKNOWLEDGMENTS

## SUPPLEMENTARY MATERIAL

The Supplementary Material for this article can be found online at: https://www.frontiersin.org/articles/10.3389/fmicb.2022.828984/full#supplementary-material

**Supplementary Figure 1 |** Molecular Mechanics/Poisson–Bolzmann Surface Area experimentation pointed to a stable interaction in Hypericin-SARS-Cov-2 RdRp complex. **(A)** Best docking results suggest that Hypericin interacts with RdRp active site near motif C and the Mg ion coordination residues, thus acting as competitive inhibitor of the ribonucleotide in RdRp polymerase activity. Residues interacting with Hypericin were numbered according to the nomenclature of 7bv2 pdb (Yin et al., 2021). **(B)** Calculated $\Delta G$ = −22.704 ± 4.008 Kcal/mol over the 60 ns of complex simulation. After small fluctuation, complex interaction was stable over the last 20 ns of simulation. **(C)** Energetic contribution of residues contacting the RdRp catalytic site in Hypericin binding, according to color code mapped on the secondary structure os the SARS-Cov-2 RdRp. On average, residues in blue contributed negatively to the interaction with Hypericin while residues in green, yellow and red favored the binding (in Kcal/Mol) over the 60 ns of simulations. Energetic contributions were calculated according to the methodology in (g_mmpbsa/single_protein_ligand_energy_contributions.html), thus modified for using Pymol 1.8.6 (www.pymol.org) for the visualization of the structures.

# REFERENCES

Abdulla, Z. A., Al-Bashir, S. M., Al-Salih, N. S., Aldamen, A. A., and Abdulazeez, M. Z. (2021). A summary of the sars-cov-2 vaccines and technologies available or under development. *Pathogens* 10:788. doi: 10.3390/pathogens10070788

Abraham, M. J., Murtola, T., Schulz, R., Páll, S., Smith, J. C., Hess, B., et al. (2015). GROMACS: High performance molecular simulations through multi-level parallelism from laptops to supercomputers. *SoftwareX* 1, 19–25.

Bacon, B. R., Gordon, S. C., Lawitz, E., Marcellin, P., Vierling, J. M., Zeuzem, S., et al. (2011). Boceprevir for Previously Treated Chronic HCV Genotype 1 Infection. *N. Engl. J. Med.* 364, 1207–1217. doi: 10.1056/NEJMoa1009482

Bardsley-Elliot, A., and Plosker, G. L. (2000). Nelfinavir: an update on its use in HIV infection. *Drugs* 59, 581–620. doi: 10.2165/00003495-200059030-00014

Barreto-Vieira, D. F., da Silva, M. A. N., Garcia, C. C., Miranda, M. D., Matos, A., da, R., et al. (2021). Morphology and morphogenesis of sars-cov-2 in vero-e6 cells. *Mem. Inst. Oswaldo Cruz* 116:e200443. doi: 10.1590/0074-02760200443

Bello, M., Mart-Muñoz, A., and Balbuena-Rebolledo, I. (2020). Identification of saquinavir as a potent inhibitor of dimeric SARS-CoV2 main protease through MM/GBSA. *J. Mol. Model.* 26:340

Berman, H. M., Westbrook, J., Feng, Z., Gilliland, G., Bhat, T. N., Weissig, H., et al. (2000). The Protein Data Bank. *Nucleic Acids Res.* 28, 235–242. doi: 10.1093/nar/28.1.235

Chary, A., and Holodniy, M. (2010). Recent Advances in Hepatitis C Virus Treatment: review of HCV Protease Inhibitor Clinical Trials. *Rev. Recent Clin. Trials* 5, 158–173. doi: 10.2174/157488710792007293

Chen, H., Muhammad, I., Zhang, Y., Ren, Y., Zhang, R., Huang, X., et al. (2019). Antiviral Activity Against Infectious Bronchitis Virus and Bioactive Components of Hypericum perforatum L. *Front. Pharmacol.* 10:1272. doi: 10.3389/fphar.2019.01272

Corman, V., Bleicker, T., Brunink, S., Drosten, C., Landt, O., Koopmans, M., et al. (2020). *Diagnostic Detection of Wuhan Coronavirus 2019 by Real-Time RT-PCR. A Protoc. New Coronavirus 2019 Detect. Dev.* Berlin: Charite Vrology.

de Almeida Filho, J. L., and Fernandez, J. H. (2020). MDR surflexdock:a semi-automatic webserver for discrete receptor-ensemble docking. *J. Global* 11347, 41–47.

Dong, X., Zeng, Y., Zhang, Z., Fu, J., You, L., He, Y., et al. (2021). Hypericin-mediated photodynamic therapy for the treatment of cancer: a review. *J. Pharm. Pharmacol.* 73, 425–436. doi: 10.1093/jpp/rgaa018

Egieyeh, S., Egieyeh, E., Malan, S., Christofells, A., and Fielding, B. (2021). Computational drug repurposing strategy predicted peptide-based drugs that can potentially inhibit the interaction of SARS-CoV-2 spike protein with its target (humanACE2). *PLoS One* 16:e0245258. doi: 10.1371/journal.pone.0245258

Farag, A., Wang, P., Ahmed, M., and Sadek, H. (2021). *Identification of FDA Approved Drugs Targeting COVID-19 Virus by Structure-Based Drug Repositioning.* Geneva: WHO.

Fradera, X., and Babaoglu, K. (2018). Overview of methods and strategies for conducting virtual small molecule screening. *Curr. Protoc. Chem. Biol.* 9, 196–212.

Genheden, S., and Ryde, U. (2015). The MM/PBSA and MM/GBSA methods to estimate ligand-binding affinities. *Expert Opin. Drug Discov.* 10, 449–461.

Günl, F., Mecate-Zambrano, A., Rehländer, S., Hinse, S., Ludwig, S., and Brunotte, L. (2021). Shooting at a moving target—effectiveness and emerging challenges for sars-cov-2 vaccine development. *Vaccines* 9, 1–30. doi: 10.3390/vaccines9101052

Harvey, W. T., Carabelli, A. M., Jackson, B., Gupta, R. K., Thomson, E. C., Harrison, E. M., et al. (2021). SARS-CoV-2 variants, spike mutations and immune escape. *Nat. Rev. Microbiol.* 19, 409–424. doi: 10.1038/s41579-021-00573-0

Hatada, R., Okuwaki, K., Mochizuki, Y., Handa, Y., Fukuzawa, K., Komeiji, Y., et al. (2020). Fragment Molecular Orbital Based Interaction Analyses on COVID-19 Main Protease- Inhibitor N3 Complex (PDB ID: 6LU7). *J. Chem. Inf. Model.* 60, 3593–3602.

Hegyi, A., and Ziebuhr, J. (2002). Conservation of substrate specificities among coronavirus main proteases. *J. Gen. Virol.* 83, 595–599. doi: 10.1099/0022-1317-83-3-595

Hernandez, J. J., Pryszlak, M., Smith, L., Yanchus, C., Kurji, N., Shahani, V. M., et al. (2017). Giving drugs a second chance: overcoming regulatory and financial hurdles in repurposing approved drugs as cancer therapeutics. *Front. Oncol.* 7:273. doi: 10.3389/fonc.2017.00273

Hoetelmans, R. M., Meenhorst, P. L., Mulder, J. W., Burger, D. M., Koks, C. H., and Beijnen, J. H. (1997). Clinical pharmacology of HIV protease inhibitors: focus on saquinavir, indinavir, and ritonavir. *Pharm. World Sci.* 19, 159–175. doi: 10.1023/a:1008629608556

Ismail, M. I., Ragab, H. M., Bekhit, A. A., and Ibrahim, T. M. (2021). Targeting multiple conformations of SARS-CoV2 Papain-Like Protease for drug repositioning: an in-silico study. *Comput. Biol. Med.* 131, 104295.

Jacobson, J. M., Feinman, L., Liebes, L., Ostrow, N., Koslowski, V., Tobia, A., et al. (2001). Pharmacokinetics. *Antimicrob. Agents Chemother.* 45, 517–524. doi: 10.1128/AAC.45.2.517-524.2001

Jomah, S., Asdaq, S. M. B., and Al-Yamani, M. J. (2020). Clinical efficacy of antivirals against novel coronavirus (COVID-19):a review. *J. Infect. Public Health* 13, 1187–1195. doi: 10.1016/j.jiph.2020.07.013

Kim, J. C., Spence, R. A., Currier, P. F., Lu, X., and Denison, M. R. (1995). Coronavirus Protein Processing and RNA Synthesis Is Inhibited by the Cysteine Proteinase Inhibitor E64d. *Virology* 208, 1–8. doi: 10.1006/viro.1995.1123

Kumar, S., Çalışkan, D. M., Janowski, J., Faist, A., Conrad, B. C. G., Lange, J., et al. (2021). Beyond Vaccines:clinical Status of Prospective COVID-19 Therapeutics. *Front. Immunol.* 12:752227. doi: 10.3389/fimmu.2021.752227

Lemey, P., Ruktanonchai, N., Hong, S. L., Colizza, V., Poletto, C., Van den Broeck, F., et al. (2021). Untangling introductions and persistence in COVID-19 resurgence in Europe. *Nature* 595, 713–717. doi: 10.1038/s41586-021-03754-2

Lenard, J., Rabson, A., and Vanderoef, R. (1993). Photodynamic inactivation of infectivity of human immunodeficiency virus and other enveloped viruses using hypericin and rose bengal: inhibition of fusion and syncytia formation. *Proc. Natl. Acad. Sci. U.S.A.* 90, 158–162. doi: 10.1073/pnas.90.1.158

Li, Q., and Shah, S. (2017). "Structure-based virtual screening," in *Protein Bioinformatics* (Berlin: Springer), 111–124.*

Liu, C., Zhu, X., Lu, Y., Zhang, X., Jia, X., and Yang, T. (2021). Potential treatment with Chinese and Western medicine targeting NSP14 of SARS-CoV-2. *J. Pharm. Anal.* 11, 272–277. doi: 10.1016/j.jpha.2020.08.002

Lokhande, K. B., Doiphode, S., Vyas, R., and Swamy, K. V. (2021). Molecular docking and simulation studies on SARS-CoV-2 Mpro reveals Mitoxantrone. *J. Biomol. Struct. Dyn.* 39, 7294–7305. doi: 10.1080/07391102.2020.1805019

Loschwitz, J., Jäckering, A., Keutmann, M., Olagunju, M., Eberle, R. J., Coronado, M. A., et al. (2021). Novel inhibitors of the main protease enzyme of SARS-CoV-2 identified via molecular dynamics simulation-guided in vitro assay. *Bioorg. Chemistry* 111:104862. doi: 10.1016/j.bioorg.2021.104862

Lucas, C., Wong, P., Klein, J., Castro, T. B. R., Silva, J., Sundaram, M., et al. (2020). Longitudinal analyses reveal immunological misfiring in severe COVID-19. *Nature* 584, 463–469. doi: 10.1038/s41586-020-2588-y

Mahase, E. (2021). Covid-19: Pfizer's paxlovid is 89% effective in patients at risk of serious illness, company reports. doi: 10.1136/bmj.n2713

Ministério, D. M. (2021). *Boletim epidemiológico especial - Doença Pelo Novo Coronavírus - COVID-19.* Berlin: Springer.

Miskovsky, P. (2002). Hypericin-a new antiviral and antitumor photosensitizer: mechanism of action and interaction with biological macromolecules. *Curr. Drug Targets* 3, 55–84.

Mobley, D. L., and Dill, K. A. (2009). Binding of Small-Molecule Ligands to Proteins: "What You See" Is Not Always "What You Get. *Structure* 17, 489–498. doi: 10.1016/j.str.2009.02.010

Montes-Grajales, D., Puerta-Guardo, H., Espinosa, D. A., Harris, E., Caicedo-Torres, W., Olivero-Verbel, J., et al. (2020). In silico drug repurposing for the identification of potential candidate molecules against arboviruses infection. *Antiviral Res.* 173:104668.

Morris, G. M., Huey, R., Lindstrom, W., Sanner, M. F., Belew, R. K., Goodsell, D. S., et al. (2009). AutoDock4 and AutoDockTools4: automated docking with selective receptor flexibility. *J. Comput. Chem.* 30, 2785–2791.

Naveca, F. G., Nascimento, V., de Souza, V. C., Corado, A., de, L., Nascimento, F., et al. (2021). COVID-19 in Amazonas. *Nat. Med.* 27, 1230–1238. doi: 10.1038/s41591-021-01378-7

Niyomrattanakit, P., Chen, Y.-L., Dong, H., Yin, Z., Qing, M., Glickman, J. F., et al. (2010). Inhibition of dengue virus polymerase by blocking the RNA tunnel. *J. Virol.* 84, 5678–5686.

Noble, S., and Faulds, D. (1996). Saquinavir. A review of its pharmacology and clinical potential in the management of HIV infection. *Drugs* 52, 93–112. doi: 10.2165/00003495-199652010-00007

Ohashi, H., Watashi, K., Saso, W., Shionoya, K., Iwanami, S., Hirokawa, T., et al. (2021). Potential anti-COVID-19 agents, cepharanthine and nelfinavir, and their usage for combination treatment. *iScience* 24:102367. doi: 10.1016/j.isci.2021.102367

Pitsillou, E., Liang, J., Karagiannis, C., Ververis, K., Darmawan, K. K., Ng, K., et al. (2020a). Interaction of small molecules with the SARS-CoV-2 main protease in silico and in vitro validation of potential lead compounds using an enzyme-linked immunosorbent assay. *Comput. Biol. Chem.* 89:107408. doi: 10.1016/j.compbiolchem.2020.107408

Pitsillou, E., Liang, J., Ververis, K., Lim, K. W., Hung, A., and Karagiannis, T. C. (2020b). Identification of Small Molecule Inhibitors of the Deubiquitinating Activity of the SARS-CoV-2 Papain-Like Protease: in silico Molecular Docking Studies and in vitro Enzymatic Activity Assay. *Front. Chem.* 8:623971. doi: 10.3389/fchem.2020.623971

Pitsillou, E., Liang, J., Ververis, K., Hung, A., and Karagiannis, T. C. (2021). Interaction of small molecules with the SARS-CoV-2 papain-like protease: in silico studies and in vitro validation of protease activity inhibition using an enzymatic inhibition assay. *J. Mol. Graph. Model.* 104:107408. doi: 10.1016/j.jmgm.2021.107851

Plosker, G. L., and Noble, S. (1999). Indinavir: a review of its use in the management of HIV infection. *Drugs* 58, 1165–1203. doi: 10.2165/00003495-199958060-00011

Pu, X., Liang, J., Wang, X., Xu, T., Hua, L., Shang, R., et al. (2009). Anti-influenza A virus effect of Hypericum perforatum L. extract. *Virol. Sin.* 24, 19–27. doi: 10.1007/s12250-009-2983-x

Ren, J., Yuan, X., Li, J., Lin, S., Yang, B., Chen, C., et al. (2020). Assessing the performance of the g_mmpbsa tools to simulate the inhibition of oseltamivir to influenza virus neuraminidase by molecular mechanics Poisson–Boltzmann surface area methods. *J. Chinese Chem. Soc.* 67, 46–53.

Romeo, A., Iacovelli, F., and Falconi, M. (2020). Targeting the SARS-CoV-2 spike glycoprotein prefusion conformation: virtual screening and molecular dynamics simulations applied to the identification of potential fusion inhibitors. *Virus Res.* 286:198068. doi: 10.1016/j.virusres.2020.198068

Rook, A. H., Wood, G. S., Duvic, M., Vonderheid, E. C., Tobia, A., and Cabana, B. (2010). A phase II placebo-controlled study of photodynamic therapy with topical hypericin and visible light irradiation in the treatment of cutaneous T-cell lymphoma and psoriasis. *J. Am. Acad. Dermatol.* 63, 984–990. doi: 10.1016/j.jaad.2010.02.039

Senathilake, K., Samarakoon, S., and Tennekoon, K. (2020). Virtual screening of inhibitors against spike glycoprotein of SARS-CoV-2: a drug repurposing approach. *Hypothesis* [Preprints] 2020030042. [Epub ahead of print]. doi: 10.20944/preprints202003.0042.v2

Shah, B., Modi, P., and Sagar, S. R. (2020). Since January 2020 Elsevier has created a COVID-19 resource centre with free information in English and Mandarin on the novel coronavirus COVID- 19. *Life Sci. J.* 252:13.

Shih, C.-M., Wu, C.-H., Wu, W.-J., Hsiao, Y.-M., and Ko, J.-L. (2018). Hypericin inhibits hepatitis C virus replication via deacetylation and down-regulation of heme oxygenase-1. *Phytomedicine* 46, 193–198. doi: 10.1016/j.phymed.2017.08.009

Shivanika, C., Kumar, D. S., Ragunathan, V., Tiwari, P., A, S., and P, B. D. (2020). Molecular docking, validation, dynamics simulations, and pharmacokinetic prediction of natural compounds against the SARS-CoV-2 main-protease. *J. Biomol. Struct. Dyn.* 8, 1–27. doi: 10.1080/07391102.2020.1815584

Sterling, T., and Irwin, J. J. (2015). ZINC 15 – Ligand Discovery for Everyone. *J. Chem. Inf. Model.* 55, 2324–2337. doi: 10.1021/acs.jcim.5b00559

Stobart, C. C., Lee, A. S., Lu, X., and Denison, M. R. (2012). Temperature-Sensitive Mutants and Revertants in the Coronavirus Nonstructural Protein 5 Protease (3CLpro) Define Residues Involved in Long-Distance Communication and Regulation of Protease Activity. *J. Virol.* 86, 4801–4810. doi: 10.1128/jvi.06754-11

Subissi, L., Posthuma, C. C., Collet, A., Zevenhoven-Dobbe, J. C., Gorbalenya, A. E., Decroly, E., et al. (2014). One severe acute respiratory syndrome coronavirus protein complex integrates processive RNA polymerase and exonuclease activities. *Proc. Natl. Acad. Sci. U.S.A.* 111, E3900–E3909. doi: 10.1073/pnas.1323705111

Tan, E. L. C., Ooi, E. E., Lin, C.-Y., Tan, H. C., Ling, A. E., Lim, B., et al. (2004). Inhibition of SARS coronavirus infection in vitro with clinically approved antiviral drugs. *Emerg. Infect. Dis.* 10:581.

Tian, L., Qiang, T., Liang, C., Ren, X., Jia, M., Zhang, J., et al. (2021). RNA-dependent RNA polymerase (RdRp) inhibitors: the current landscape and repurposing for the COVID-19 pandemic. *Eur. J. Med. Chem.* 213:113201.

Wang, C., Greene, D., Xiao, L., Qi, R., and Luo, R. (2018). Recent Developments and Applications of the MMPBSA Method. *Front. Mol. Biosci.* 4:87. doi: 10.3389/fmolb.2017.00087

Wang, E., Sun, H., Wang, J., Wang, Z., Liu, H., Zhang, J. Z. H., et al. (2019). End-Point Binding Free Energy Calculation with MM/PBSA and MM/GBSA:strategies and Applications in Drug Design. *Chem. Rev.* 119, 9478–9508. doi: 10.1021/acs.chemrev.9b00055

WHO (2021). *COVID-19 Weekly Epidemiological Update 68*. Geneva: WHO.

Xu, Z., Yao, H., Shen, J., Wu, N., Xu, Y., Lu, X., et al. (2020). Nelfinavir is active against SARS-CoV-2 in Vero E6 cells. *ChemRxiv* [Epub online ahead of print] doi: 10.26434/chemrxiv.12039888

Yalçın, S., Yalçınkaya, S., and Ercan, F. (2021). Determination of Potential Drug Candidate Molecules of the Hypericum perforatum for COVID-19 Treatment. *Curr. Pharmacol. Rep.* 7, 42–48. doi: 10.1007/s40495-021-00254-9

Yamamoto, N., Matsuyama, S., Hoshino, T., and Yamamoto, N. (2020). Nelfinavir inhibits replication of severe acute respiratory syndrome coronavirus 2 in vitro. *BioRxiv* [Preprint] doi: 10.1101/2020.04.06.026476

Ye, Q., Wang, B., and Mao, J. (2020). The pathogenesis and treatment of the 'Cytokine Storm' in COVID-19.'. *J. Infect.* 80, 607–613. doi: 10.1016/j.jinf.2020.03.037

Yin, W., Luan, X., Li, Z., Zhou, Z., Wang, Q., Gao, M., et al. (2021). Structural basis for inhibition of the SARS-CoV-2 RNA polymerase by suramin. *Nat. Struct. Mol. Biol.* 28, 319–325. doi: 10.1038/s41594-021-00570-0

Zhou, F., Yu, T., Du, R., Fan, G., Liu, Y., Liu, Z., et al. (2020). Clinical course and risk factors for mortality of adult inpatients with COVID-19 in Wuhan. *China* 395, 1054–1062. doi: 10.1016/S0140-6736(20)30566-3

# Respiratory Mucosal Immunity: Kinetics of Secretory Immunoglobulin A in Sputum and Throat Swabs From COVID-19 Patients and Vaccine Recipients

Cuiping Ren[1,2,3,4,5†], Yong Gao[6†], Cong Zhang[1,2,3,4,5†], Chang Zhou[1,2,3,4,5], Ying Hong[7], Mingsheng Qu[1,2,3,4,5], Zhirong Zhao[7], Yinan Du[1,2,3,4,5], Li Yang[1,2,3,4,5], Boyu Liu[1,2,3,4,5], Siying Wang[1,2,3,4,5], Mingfeng Han[6*], Yuxian Shen[1,2,3,4,5*] and Yan Liu[1,2,3,4,5*]

[1] Department of Microbiology and Parasitology, Anhui Medical University, Hefei, China, [2] Anhui Provincial Laboratory of Pathogen Biology, Anhui Medical University, Hefei, China, [3] Anhui Key Laboratory of Zoonosis of High Institution, Anhui Medical University, Hefei, China, [4] Laboratory of Tropical and Parasitic Diseases Control, Anhui Medical University, Hefei, China, [5] School of Basic Medical Sciences, Anhui Medical University, Hefei, China, [6] Department of Clinical Laboratory, The Second People's Hospital of Fuyang, Fuyang, China, [7] Maanshan Center for Disease Control and Prevention, Maanshan, China

While IgM and IgG response to SARS-CoV-2 has been extensively studied, relatively little is known about secretory IgA (sIgA) response in respiratory mucosa. Here we report IgA response to the SARS-CoV-2 in sputum, throat swabs, and serum with nucleocapsid protein (NP) enzyme-linked immunosorbent assays (ELISA) in a cohort of 28 COVID-19 patients and 55 vaccine recipients. The assays showed sIgA in respiratory mucosa could be detected on the first day after illness onset (AIO), and the median conversion time for sIgA in sputum, throat swabs, and serum was 3, 4, and 10 days, respectively. The positive rates of sIgA first week AIO were 100% (24/28) and 85.7% (24/28) in sputum and throat swabs, respectively, and were both 100% during the mid-onset (2–3 weeks AIO). During the recovery period, sIgA positive rates in sputum and throat swabs gradually decreased from 60.7% (17/28) and 57.1% (16/28) 1 month AIO and the sIgA antibodies were all undetectable 6 months AIO. However, serum IgA positive rate was still 100% at 4 months and 53.6% (15/28) at 6 months. Throat swabs obtained from volunteers who received inactivated SARS-CoV-2 vaccines by intramuscular delivery all showed negative results in IgA ELISA. These findings will likely improve our understanding of respiratory mucosal immunity of this emerging disease and help in containing the pandemic and developing vaccines.

Keywords: COVID-19, mucosal immunity, IgA, sputum, throat swab, nucleocapsid protein, vaccine

## INTRODUCTION

Severe acute respiratory syndrome coronavirus 2 (SARS-CoV-2) virus is very infectious, primarily infecting the respiratory tract mucosal surfaces (Gorbalenya et al., 2020; Zhu et al., 2020; Hu et al., 2021). Mucosal immunity in the upper airways and nasal passages is particularly important as the first defensive barrier, affecting the initial viral spread (Mazanec et al., 1995; See et al., 2006).

Among antibody isotypes, secretory immunoglobulin A (sIgA) at mucosal surfaces plays a crucial role in protecting against respiratory virus infection (Mazanec et al., 1995; Terauchi et al., 2018). A previous study by Sterlin et al. (2021) reported that both serum IgA and mucosal IgA could effectively neutralize SARS-CoV-2 and dominated the neutralizing antibody response to SARS-CoV-2 in the early phase of infection. Recent studies have reported that dimeric IgA, the secretory form of IgA in the mucosa, was a more potent neutralizer than IgG and serum IgA monomers against authentic SARS-CoV-2 (Ejemel et al., 2020; Wang et al., 2021). These results suggest that SARS-CoV-2 induces specific sIgA and strong mucosal immunity within the respiratory system effectively against virus infection.

It was already known that vaccines delivered by inhalation can elicit IgA response in both mucosal surfaces and serum, whereas vaccines delivered intramuscularly primarily elicit serum IgG (Torrieri-Dramard et al., 2011; Ku et al., 2021; Lund and Randall, 2021). van Doremalen et al. (2021) recently reported that intranasal ChAdOx1 nCoV-19/AZD1222 vaccination, an approved adenovirus-vectored vaccine, reduced shedding of SARS-CoV-2 from the upper respiratory tract in vaccinated macaques and hamsters, whereas intramuscular vaccination protected against lung inflammation and pathology but did not reduce shedding. A similar result was also reported by Hassan et al. (2020) adenovirus-vectored vaccine ChAd-SARS-CoV-2-S delivered by inhalation could provide more effective sterilizing protection than intramuscular delivery, and promote systemic and mucosal IgA response when intramuscular delivery failed to induce IgA.

Although IgA response to SARS-CoV-2 in respiratory tract is particularly important in neutralizing the virus and affecting the initial viral spread, long time longitudinal studies of mucosal IgA kinetics were relatively rarely reported. In this study, we established an indirect ELISA method for IgA detection using nucleocapsid protein (NP) and detected COVID-19 samples of patients collected at different time points within 6 months and throat swabs of 55 volunteers who have received at least one dose of inactivated SARS-CoV-2 vaccines. Our results showed the kinetics of sIgA to SARS-CoV-2 in sputum and throat swabs and non-secretory IgA in the blood sample, which could improve our understanding of the mucosal immune response of the virus and provide new ideas for immunological evaluation of pandemic prevention and control.

## MATERIALS AND METHODS

### Clinical Specimens

Throat swabs, sputum, and serum were collected from 28 laboratory-confirmed COVID-19 patients who were hospitalized at the Second People's Hospital of Fuyang in Anhui, China between February 8 and September 25, 2020. Sequential specimens at various time points after illness onset of these patients were collected for SARS-CoV-2 NP IgA ELISA. Thirty healthy subjects without any known history of SARS-CoV-2 infection were recruited, and throat swabs, sputum, and serum specimens were collected as healthy control. Serum specimens collected contemporaneously in 2020 from 30 human immunodeficiency virus (HIV)-positive patients, 30 hepatitis B (HB) patients, and 30 hepatitis C (HC) patients and throat swabs from 30 unknown fever (UF) and 30 patients with H1 influenza were provided by Maanshan Municipal Center for Disease Control and prevention. In this study, we also obtained throat swabs from 55 vaccinated volunteers who received at least one dose of inactivated SARS-CoV-2 vaccine (Sinovac Life Sciences) by intramuscular delivery for NP IgA detection. Throat swabs were collected with synthetic fiber swabs by physicians and inserted into 3-ml viral transport medium. Sputum samples were collected in a 50-ml screw-top plastic tube containing 3 ml of viral transport medium. All samples were stored at −80°C since collection. Detailed information of the COVID-19 patients and vaccinated volunteers are shown in **Supplementary Table 1**.

Informed consent was obtained from all individual participants included in the study. The study was approved by the Ethics Committee of Anhui Medical University, with adherence to the Declaration of Helsinki. The approval ID of Ethics Committee is 2020H015.

## Severe Acute Respiratory Syndrome Coronavirus 2 Nucleocapsid Protein Immunoglobulin A Enzyme-Linked Immunosorbent Assays

SARS-CoV-2 NP IgA ELISA was performed according to the conventional method (Ren et al., 2017). The NP antigen used is a recombinant eukaryotic expression protein. It was purchased from T&J Biomedical, Beijing, China. The HRP-labeled rabbit anti-human IgA was purchased from Abcam, Cambridge, United Kingdom (ab97215). The operational concentrations of clinical samples, antigen, antibodies, and reaction time were determined in preliminary experiments using the chessboard method. Mixed serum samples of 30 individuals with SARS-CoV-2 infection and mixed serum samples from 30 healthy subjects were used in preliminary experiments.

Based on the results of the preliminary experiments, the SARS-CoV-2 NP IgA ELISA was established. The microtiter plates were coated with 100 μl/well of NP antigen (5 μg/ml), overnight at 4°C. After washing three times with 0.05% Tween20-PBS (w/v) and blocking with 2% BSA-PBS (w/v) for 1 h, the plates were incubated with specimens for 1 h. Serum was diluted at 1:200 and added 100 μl/well. For each sputum or throat swab specimen, 100 μl/well was added. Samples had been heated at 56°C for 30 min to inactivate the virus before the SARS-CoV-2 NP IgA ELISA experiments. The HRP-labeled rabbit anti-human IgA (Abcam, United States) was diluted 1:100,000. All steps were carried out at room temperature. Absorbance values were read using a plate spectrophotometer (Molecular Devices, United States) at a wavelength of 450 nm. Positive and negative controls were used throughout the study. A blank was also included on each plate. Each sample was tested in duplicate. The cutoff value for a positive reaction was the mean plus two standard deviations of the absorbance reading in the controls, and it was 0.235 in our SARS-CoV-2 NP IgA ELISA.
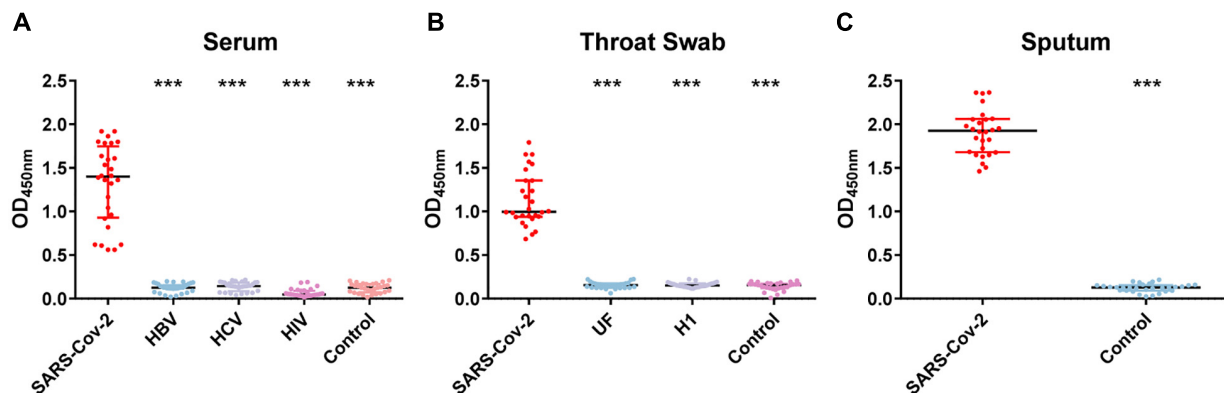
**FIGURE 1** | $OD_{450}$ value of nucleocapsid protein (NP)–immunoglobulin A (IgA) enzyme-linked immunosorbent assay (ELISA) for the detection of the NP-IgA antibody from non-SARS-CoV-2 infected patients and severe acute respiratory syndrome coronavirus 2 (SARS-CoV-2)-infected patients. **(A)** Serum samples from different populations; HBV represents patients with hepatitis B virus infection, HCV represents patients with hepatitis C virus infection, HIV represents HIV-positive patients. **(B)** Throat swab samples from different populations; UF represents patients with unknown fever, H1 represents patients with H1 influenza. **(C)** Sputum samples from SARS-CoV-2-infected patients and healthy controls. Data are presented as the median with interquartile range. ***$p < 0.001$ (two-tailed multiple comparison test with Kruskal–Wallis method).

## Statistical Analysis

The $OD_{450}$ values of sputum, throat swab, and serum detected by IgA ELISA at different time points were statistically analyzed by repeated measures ANOVA or multiple independent sample non-parametric test. The positive rates of IgA ELISA in serum, throat swab, and sputum were statistically compared with the Chi-square test or Fisher's exact test. Power calculation has been done. The sample size of the current study may not be optimal, but should be sufficient to draw a conclusion that may guide clinical practice. A $p$-value $< 0.05$ was considered statistically significant. All statistical analyses were conducted by SPSS software.

## RESULTS

### Severe Acute Respiratory Syndrome Coronavirus 2 Nucleocapsid Protein Immunoglobulin A Enzyme-Linked Immunosorbent Assays

To evaluate the sensitivity of COVID-19 NP-IgA ELISA, the levels of SARS-CoV-2-specific NP-IgA antibodies were measured in sputum ($n = 28$), throat swabs ($n = 28$), and serum specimens ($n = 28$) of COVID-19 patients 15–21 days after infection. The results showed that the positive rates of antibody in sputum, throat swabs, and serum were all 100% (**Figure 1**). No cross-reactivity was found in the serum collected from patients uninfected with SARS-CoV-2 but diagnosed with hepatitis B (HB, $n = 30$), hepatitis C (HC, $n = 30$), or HIV infection ($n = 30$) detected by SARS-CoV-2 NP IgA ELISA. In addition, there was no positive reaction in the throat swabs of flu patients ($n = 30$) and unknown fever (UF, $n = 30$). None of the healthy volunteers, including serum specimens ($n = 30$), sputum samples ($n = 30$), and throat swabs ($n = 30$), tested positive for IgA (**Figure 1**). The assay showed an overall specificity of 100%.

## Nucleocapsid Protein Immunoglobulin A Detection in COVID-19 Patients and Vaccinated Volunteers

Using the method of NP IgA ELISA we established, we detected NP IgA levels of serum, throat swabs, and sputum sequential samples of 28 COVID-19 patients and throat swabs of 55 vaccinated volunteers.

In the early stages of infection, within 1 week after symptom onset, the NP IgA antibody positive rates of the sputum, throat swab, and serum specimens were 100% (28/28), 85.7% (24/28), and 42.9% (13/28), respectively (**Figure 2**). The positive rates of
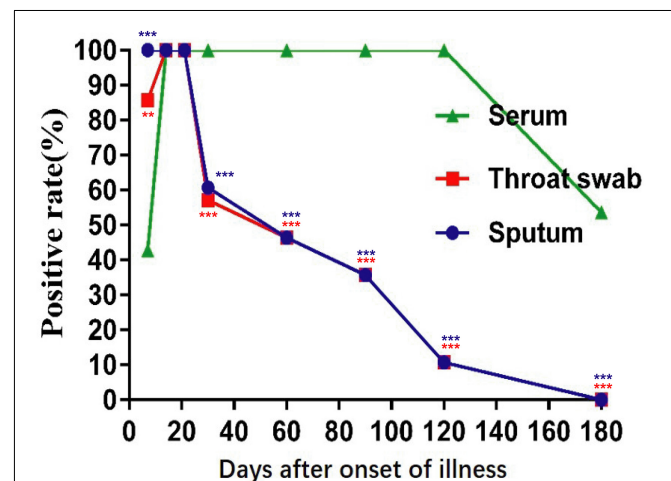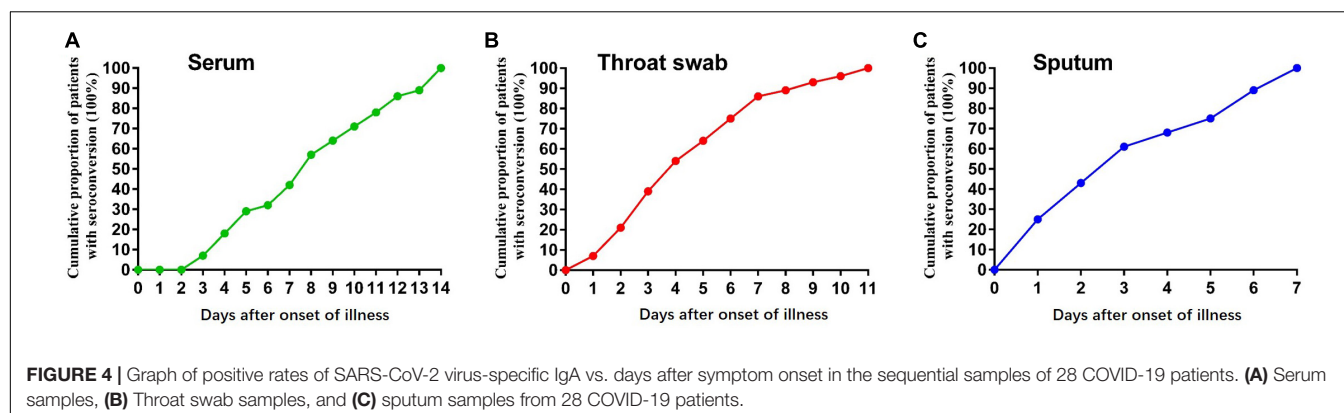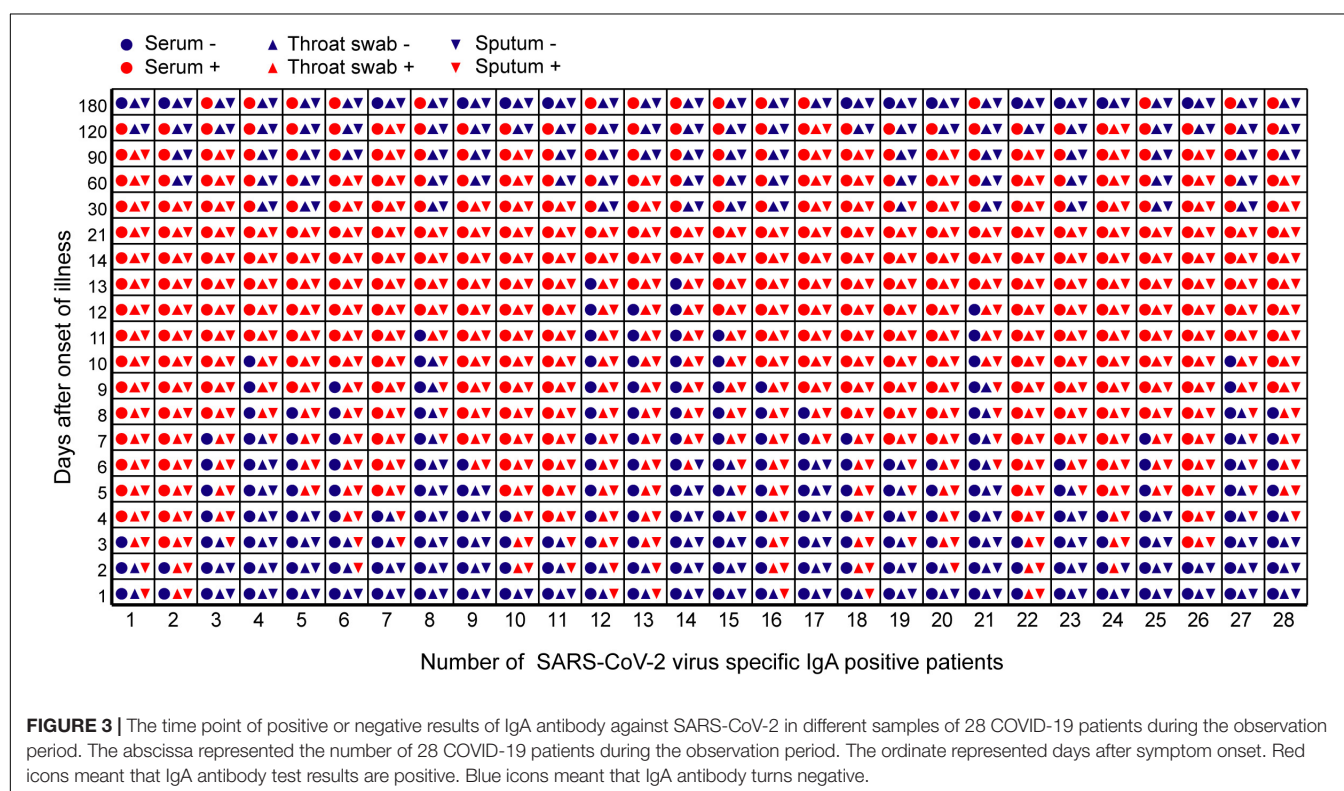


**FIGURE 2** | Positive rates of NP-IgA ELISA for detection of the sequential samples of 28 COVID-19 patients with different disease courses from the symptom onset. Sequential samples include serum, throat swabs, and sputum from all phases of the disease. **$p < 0.01$, ***$p < 0.001$ (compared with positive rates of serum, two-tailed Fisher's exact test).
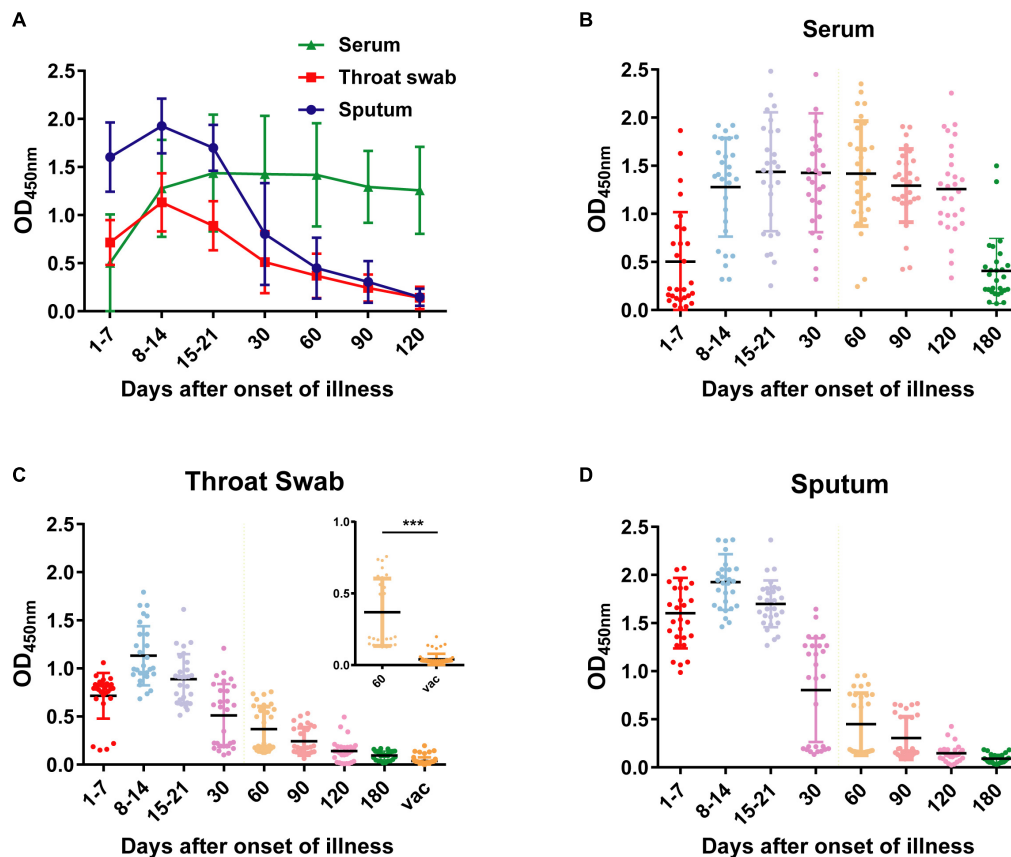
NP IgA antibody in sputum and in throat swabs were significantly higher than that in serum (Fisher's exact test, throat swab vs. serum, $p < 0.01$, sputum vs. serum, $p < 0.001$). The NP IgA antibody of seven sputum specimens and two throat swab specimens among 28 patients could be detected on the first day of illness onset (**Figure 3**), while IgA in the serum was first detected on the third day after illness onset (**Figure 3**). According to the cumulative seroconversion curve, the median conversion time for IgA in sputum, throat swabs, and serum was 3, 4, and 10 days, respectively (**Figure 4**). The IgA positivity rates in three specimens were all 100% (28/28) from 2 to 3 weeks after symptoms (**Figure 2**). The $OD_{450}$ value showed the highest IgA antibody titer in sputum and throat swabs for this time period (**Figure 5A**). These results indicate that there is an early IgA response in mucosal surfaces, which may particularly be important in neutralizing the virus at the upper respiratory tract and lungs.

During the recovery phase, the positive rates and $OD_{450}$ value of NP IgA antibody in sputum and in throat swabs decreased significantly from 1 month after the onset of the disease (**Figures 2**, **5**). The positive rates of IgA in sputum, and throat swabs were 60.7% (17/28) and 57.1% (16/28) at 1 month after illness onset, respectively, and both were significantly lower than that of the rate in serum 100% (28/28) (**Figure 2**) (Fisher's exact test, throat swab/sputum vs. serum, $p < 0.001$). At 4 months after the onset of the disease, the rates dropped to 10.7% (3/28) in either sputum or throat swabs. The serum IgA positivity rate in COVID-19 patients remained 100% at 4 months after onset, and there is also no tendency for $OD_{450}$ values to decrease (**Figures 2**, **5**). After 6 months of the onset, the IgA antibody



**FIGURE 3 |** The time point of positive or negative results of IgA antibody against SARS-CoV-2 in different samples of 28 COVID-19 patients during the observation period. The abscissa represented the number of 28 COVID-19 patients during the observation period. The ordinate represented days after symptom onset. Red icons meant that IgA antibody test results are positive. Blue icons meant that IgA antibody turns negative.



**FIGURE 4 |** Graph of positive rates of SARS-CoV-2 virus-specific IgA vs. days after symptom onset in the sequential samples of 28 COVID-19 patients. **(A)** Serum samples, **(B)** Throat swab samples, and **(C)** sputum samples from 28 COVID-19 patients.

**FIGURE 5 |** OD$_{450}$ values of NP-IgA ELISA for detection of the sequential samples of 28 COVID-19 patients and 55 vaccine recipients. **(A)** OD$_{450}$ values of the sequential serum, throat swab and sputum samples of 28 COVID-19 patients. Scatter plots of OD$_{450}$ values of **(B)** serum samples, **(C)** throat swab samples, and **(D)** sputum samples at different phases of the disease or 50 d after vaccine. Vac, represents vaccine recipients. Data are presented as the mean ± SD. ***$p < 0.001$ (two-tailed unpaired $t$-test).

level in sputum and throat swabs of all COVID-19 patients were undetectable (**Figure 2**). The IgA positivity rate in the serum of patients dropped to 53.6% (15/28) (**Figure 2**). Our results suggested that the production of sIgA in the lung epithelium is time limited.

To evaluate the mucosal IgA level of vaccinated volunteers, we also obtained 60 throat swabs from 55 vaccinated volunteers at 50 days after vaccination. All the volunteers received at least one dose of inactivated SARS-CoV-2 vaccine by intramuscular delivery. Compared with the throat swab specimens of COVID-19 patients 60 days after illness onset, specimens from vaccinated volunteers had significantly lower OD$_{450}$ value of detected IgA (**Figure 5C**) (two-tailed unpaired $t$-test, $p < 0.001$). All the throat swab specimens from vaccinated volunteers showed negative results, indicating insufficient mucosal immunity and IgA response in respiratory tract after the vaccination.

## DISCUSSION

As a mucosal targeted virus, SARS-CoV-2 can generate sIgA and induce strong mucosal immunity (Arakawa et al., 2019;

Yu et al., 2020). Our study reports the kinetics of sIgA response to SARS-CoV-2 in the mucosa of the respiratory system and non-secretory IgA in the blood. We found that IgA could be detected at the early stage of virus infection in sputum and throat swabs, and some patients even on the first day after the onset. The median conversion time for IgA in sputum and throat swabs was less than 4 days, 6–7 days earlier than in serum. Moreover, IgA in sputum could be all detected among patients within 1 week after the onset of the disease. Other studies have shown that the first seroconversion day of IgM and IgG in serum was 5 days after onset. The median conversion time for IgM and IgG was 14 and 14–15 days, respectively (Wang et al., 2020; Yu et al., 2020). The proportion of patients with positive virus-specific IgG reached 100%, approximately 17–19 days after symptom onset, while the proportion of patients with positive virus-specific IgM reached a peak of 94.1%, approximately 20–22 days after symptom onset (Long et al., 2020; Zhou et al., 2021). Our study demonstrated that IgA response to SARS-CoV-2 in the respiratory mucosa was much earlier than IgG and IgM. Other studies have reported that mucosal IgA had more efficient neutralization potential than IgG and was dominant in early SARS-CoV-2 neutralizing antibody (Sterlin et al., 2021; Wang et al., 2021). These results indicated

particularly the important role of mucosal sIgA against the initial SARS-CoV-2 viral spread.

Meantime, our results suggested that there is a particular value of mucosal sIgA detection in COVID-19 diagnosis. Our SARS-CoV-2 NP IgA ELISA method showed excellent specificity in the detection of SARS-CoV-2-infected patients. There was no cross-reaction when it was used to detect other non-SARS-CoV-2-infected patients, such as HB, HC, HIV, UF, or H1 influenza. Our IgA ELISA assay could be useful when the suspected cases are repeatedly negative by RT-qPCR in the diagnosis of acute phase. Detection of sIgA can aid diagnosis as soon as possible, which is important for effective intervention and isolation of patients to prevent further spread of infection.

Moreover, according to our results, sIgA, compared with non-secretory IgA, would rapidly turn negative during the recovery period. NP IgA in the sputum and throat swab of the patient had turned negative partially at 1 month after onset and more than half by 2 months after onset. A previous study of Isho et al. (2020) detected anti-spike and anti-RBD IgA levels in the saliva of the patient, and the results also showed significant decreases from 1 month and barely detectable IgA level on day 100. These results indicated that production of sIgA in the lung epithelium is time limited. Although reinfection cases of SARS-CoV-2 was very uncommon, it occurred in 1.39% health-care workers at a median of 7 months after the onset of the first episode in a large, multicenter, prospective cohort study (Hall et al., 2021). Another report reviewed 60 cases of reinfection with viral sequencing, and episodes of infection were separated by a median of 116 days (Qureshi et al., 2021). As one crucial part of mucosal immunity barrier against virus invasion, the short duration of sIgA and insufficient level at an indicated time may contribute to the occurrence of reinfection.

Given that intramuscular vaccine primarily elicits serum IgG and IgM, the role of IgM and IgG neutralizing antibodies attract most attention of scientists. However, SARS-CoV-2 viremia is associated with COVID-19 severity, and viremia in patients generally occurred in severe illness (Jacobs et al., 2021; Li et al., 2021). Elicited IgM and IgG antibodies seem to mainly protect vaccinated people from severe pathology. Their antiviral effect on respiratory mucosal epithelial cells is not as important as secreted IgA, or it even has not much effect (Mazanec et al., 1995). Our study suggested that there is insufficient mucosal immunity and IgA response in respiratory tract in vaccinated people with intramuscular delivery. Despite various intramuscular delivery vaccines have shown high efficacy against SARS-CoV-2 infection, rare breakthrough infections have been reported, and most of them were mild or asymptomatic (Bergwerk et al., 2021). This may also be a problem that current vaccinators have to consider because even asymptomatic infected people could spread the virus and bring great challenge to the society. Interestingly, recent studies of two adenovirus-vectored vaccines showed that intranasal vaccination could reduce shedding of virus and induce higher levels of neutralizing antibodies, particularly systemic and mucosal IgA than intramuscular delivery (Hassan et al., 2020; van Doremalen et al., 2021). Therefore, to further improve the immune effect of the vaccine, multiple dosage forms of vaccine immunization strategies (injection and spray) should be considered by scientists and government decision-making departments.

A limitation of our study is that our results do not directly imply the protection of mucosal immunity against SARS-CoV-2, given that the NP antibody is not a neutralizing antibody. NP protein is a suitable candidate for diagnosis due to its high immunogenicity. Previous studies have shown closely similar patterns between anti-NP antibodies and anti-spike and anti-RBD IgA/IgG responses (Isho et al., 2020; Sterlin et al., 2021). Our study of kinetics of sIgA suggested that anti-NP IgA detection of sputum and throat swabs may have some diagnostic value for pandemic prevention and control.

## DATA AVAILABILITY STATEMENT

The original contributions presented in the study are included in the article/**Supplementary Material**, further inquiries can be directed to the corresponding author/s.

## ETHICS STATEMENT

The studies involving human participants were reviewed and approved by the Ethics Committee of Anhui Medical University. The patients/participants provided their written informed consent to participate in this study.

## AUTHOR CONTRIBUTIONS

CR, YG, and CZha carried out the experiment and drafted the manuscript. CZho, YH, MQ, ZZ, YD, LY, BL, and SW participated in the design and coordination of the study. YL, YS, and MH were the project coordinators, responsible for the project design, implementation, and oversaw all aspects of case definition, fieldwork, laboratory activities, and data analysis. All authors read and approved the final manuscript.

## FUNDING

## SUPPLEMENTARY MATERIAL

The Supplementary Material for this article can be found online at: https://www.frontiersin.org/articles/10.3389/fmicb.2022.782421/full#supplementary-material

# REFERENCES

Arakawa, S., Suzukawa, M., Watanabe, K., Kobayashi, K., Matsui, H., Nagai, H., et al. (2019). Secretory immunoglobulin A induces human lung fibroblasts to produce inflammatory cytokines and undergo activation. *Clin. Exp. Immunol.* 195, 287–301. doi: 10.1111/cei.13253

Bergwerk, M., Gonen, T., Lusti, Y., Amit, S., Lipsitch, M., Cohen, C., et al. (2021). Covid-19 breakthrough infections in vaccinated health care workers. *N. Engl. J. Med.* 385, 1629–1630. doi: 10.1056/NEJMoa2109072

Ejemel, M., Li, Q., Hou, S., Schiller, Z. A., Tree, J. A., Wallace, A., et al. (2020). cross-reactive human IgA monoclonal antibody blocks SARS-CoV-2 spike-ACE2 interaction. *Nat. Commun.* 11:4198. doi: 10.1038/s41467-020-18058-8

Gorbalenya, A. E., Baker, S., Baric, R., and de Groot, R. J. (2020). The species severe acute respiratory syndrome-related coronavirus: classifying 2019-nCoV and naming it SARS-CoV-2. *Nat. Microbiol.* 5, 536–544. doi: 10.1038/s41564-020-0695-z

Hall, V. J., Foulkes, S., Charlett, A., Atti, A., Monk, E., Simmons, R., et al. (2021). CoV-2 infection rates of antibody-positive compared with antibody-negative health-care workers in England: a large, multicentre, prospective cohort study (SIREN). *Lancet* 397, 1459–1469. doi: 10.1016/S0140-6736(21)00675-9

Hassan, A. O., Kafai, N. M., Dmitriev, I. P., Fox, J. M., Smith, B. K., Harvey, I. B., et al. (2020). A single-dose intranasal ChAd vaccine protects upper and lower respiratory tracts against SARS-CoV-2. *Cell* 183, 169–184.e13. doi: 10.1016/j.cell.2020.08.026

Hu, B., Guo, H., Zhou, P., and Shi, Z. L. (2021). Characteristics of SARS-CoV-2 and COVID-19. *Nat. Rev. Microbiol.* 19, 141–154. doi: 10.1038/s41579-020-00459-7

Isho, B., Abe, K. T., Zuo, M., Jamal, A. J., Rathod, B., Wang, J. H., et al. (2020). Persistence of serum and saliva antibody responses to SARS-CoV-2 spike antigens in COVID-19 patients. *Sci. Immunol.* 5:eabe5511. doi: 10.1126/sciimmunol.abe5511

Jacobs, J. L., Bain, W., Naqvi, A., Staines, B., Castanha, P., Yang, H., et al. (2021). SARS-CoV-2 viremia is associated with COVID-19 severity and predicts clinical outcomes. *Clin. Infect. Dis.* [Online ahead of print]. doi: 10.1093/cid/ciab686

Ku, M. W., Bourgine, M., Authie, P., Lopez, J., Nemirov, K., Moncoq, F., et al. (2021). Intranasal vaccination with a lentiviral vector protects against SARS-CoV-2 in preclinical animal models. *Cell. Host Microbe.* 29, 236–249.e6. doi: 10.1016/j.chom.2020.12.010

Li, Y., Schneider, A. M., Mehta, A., Sade-Feldman, M., Kays, K. R., Gentili, M., et al. (2021). SARS-CoV-2 viremia is associated with distinct proteomic pathways and predicts COVID-19 outcomes. *J. Clin. Invest.* 131:ciab686. doi: 10.1172/JCI148635

Long, Q. X., Liu, B. Z., Deng, H. J., Wu, G. C., Deng, K., Chen, Y. K., et al. (2020). Antibody responses to SARS-CoV-2 in patients with COVID-19. *Nat. Med.* 26, 845–848. doi: 10.1038/s41591-020-0897-1

Lund, F. E., and Randall, T. D. (2021). Scent of a vaccine. *Science* 373, 397–399. doi: 10.1126/science.abg9857

Mazanec, M. B., Coudret, C. L., and Fletcher, D. R. (1995). Intracellular neutralization of influenza virus by immunoglobulin A anti-hemagglutinin monoclonal antibodies. *J. Virol.* 69, 1339–1343. doi: 10.1128/JVI.69.2.1339-1343.1995

Qureshi, A. I., Baskett, W. I., Huang, W., Lobanova, I., Naqvi, S. H., and Shyu, C. R. (2021). Re-infection with SARS-CoV-2 in patients undergoing serial laboratory testing. *Clin. Infect. Dis.* 69, 651–655. doi: 10.1093/cid/ciab345

Ren, C. P., Liu, Q., Liu, F. C., Zhu, F. Y., Cui, S. X., Liu, Z., et al. (2017). Development of monoclonal antibodies against Sj29 and its possible application for schistosomiasis diagnosis. *Int. J. Infect. Dis.* 61, 74–78. doi: 10.1016/j.ijid.2017.04.009

See, R. H., Zakhartchouk, A. N., Petric, M., Lawrence, D. J., Mok, C., Hogan, R. J., et al. (2006). Comparative evaluation of two severe acute respiratory syndrome (SARS) vaccine candidates in mice challenged with SARS coronavirus. *J. Gen. Virol.* 87, 641–650. doi: 10.1099/vir.0.81579-0

Sterlin, D., Mathian, A., Miyara, M., Mohr, A., Anna, F., Claer, L., et al. (2021). IgA dominates the early neutralizing antibody response to SARS-CoV-2. *Sci. Transl. Med.* 13:eabd2223. doi: 10.1126/scitranslmed.abd2223

Terauchi, Y., Sano, K., Ainai, A., Saito, S., Taga, Y., Ogawa-Goto, K., et al. (2018). IgA polymerization contributes to efficient virus neutralization on human upper respiratory mucosa after intranasal inactivated influenza vaccine administration. *Hum. Vaccin. Immunother.* 14, 1351–1361. doi: 10.1080/21645515.2018.1438791

Torrieri-Dramard, L., Lambrecht, B., Ferreira, H. L., Van den Berg, T., Klatzmann, D., and Bellier, B. (2011). Intranasal DNA vaccination induces potent mucosal and systemic immune responses and cross-protective immunity against influenza viruses. *Mol. Ther.* 19, 602–611. doi: 10.1038/mt.2010.222

van Doremalen, N., Purushotham, J. N., Schulz, J. E., Holbrook, M. G., Bushmaker, T., Carmody, A., et al. (2021). Intranasal ChAdOx1 nCoV-19/AZD1222 vaccination reduces viral shedding after SARS-CoV-2 D614G challenge in preclinical models. *Sci. Transl. Med.* 13:eabh0755. doi: 10.1126/scitranslmed.abh0755

Wang, B., Wang, L., Kong, X., Geng, J., Xiao, D., Ma, C., et al. (2020). Long-term coexistence of SARS-CoV-2 with antibody response in COVID-19 patients. *J. Med. Virol.* 92, 1684–1689. doi: 10.1002/jmv.25946

Wang, Z., Lorenzi, J., Muecksch, F., Finkin, S., Viant, C., Gaebler, C., et al. (2021). Enhanced SARS-CoV-2 neutralization by dimeric IgA. *Sci. Transl. Med.* 13:eabf1555. doi: 10.1126/scitranslmed.abf1555

Yu, H. Q., Sun, B. Q., Fang, Z. F., Zhao, J. C., Liu, X. Y., Li, Y. M., et al. (2020). Distinct features of SARS-CoV-2-specific IgA response in COVID-19 patients. *Eur. Respir. J.* 56:2001526. doi: 10.1183/13993003.01526-2020

Zhou, C., Bu, G., Sun, Y., Ren, C., Qu, M., Gao, Y., et al. (2021). Evaluation of serum IgM and IgG antibodies in COVID-19 patients by enzyme linked immunosorbent assay. *J. Med. Virol.* 93, 2857–2866. doi: 10.1002/jmv.26741

Zhu, N., Zhang, D., Wang, W., Li, X., Yang, B., Song, J., et al. (2020). Novel coronavirus from patients with pneumonia in China, 2019. *N. Engl. J. Med.* 382, 727–733. doi: 10.1056/NEJMoa2001017

Check for
updates

# Evaluation of Performance of Detection of Immunoglobulin G and Immunoglobulin M Antibody Against Spike Protein of SARS-CoV-2 by a Rapid Kit in a Real-Life Hospital Setting

**Monica Irungbam[1†], Anubhuti Chitkara[1†], Vijay Kumar Singh[2],**
**Subash Chandra Sonkar[2*], Abhisek Dubey[1], Aastha Bansal[1], Ritika Shrivastava[1],**
**Binita Goswami[1,2], Vikas Manchanda[3], Sonal Saxena[3], Ritu Saxena[4], Sandeep Garg[5],**
**Farah Husain[6], Tanmay Talukdar[7], Dinesh Kumar[8] and Bidhan Chandra Koner[1,2*]**

[1] Department of Biochemistry, Maulana Azad Medical College and Associated Hospitals, New Delhi, India, [2] Multidisciplinary Research Unit (MRU), Maulana Azad Medical College and Associated Hospitals, New Delhi, India, [3] Department of Microbiology, Maulana Azad Medical College and Associated Hospitals, New Delhi, India, [4] Emergency Department, Lok Nayak Jai Prakash Narayan (LNJP) Hospital, New Delhi, India, [5] Department of Medicine, Lok Nayak Jai Prakash Narayan (LNJP) Hospital, New Delhi, India, [6] Department of Anesthesiology, Lok Nayak Jai Prakash Narayan (LNJP) Hospital, New Delhi, India, [7] Department of TB & Chest Diseases/Pulmonary Medicine, Lady Hardinge Medical College (LHMC), New Delhi, India, [8] Food Safety and Standards Authority of India, Ministry of Health and Family Welfare (MoHFW), New Delhi, India

**Background:** Antibody testing is often used for serosurveillance of coronavirus disease 2019 (COVID-19). Enzyme-linked immunosorbent assay and chemiluminescence-based antibody tests are quite sensitive and specific for such serological testing. Rapid antibody tests against different antigens are developed and effectively used for this purpose. However, their diagnostic efficiency, especially in real-life hospital setting, needs to be evaluated. Thus, the present study was conducted in a dedicated COVID-19 hospital in New Delhi, India, to evaluate the diagnostic efficacy of a rapid antibody kit against the receptor-binding domain (RBD) of the spike protein of severe acute respiratory syndrome coronavirus 2 (SARS-CoV-2).

**Methods:** Sixty COVID-19 confirmed cases by reverse transcriptase–polymerase chain reaction (RT-PCR) were recruited and categorized as early, intermediate, and late cases based on the days passed after their first RT-PCR–positive test report, with 20 subjects in each category. Twenty samples from pre-COVID era and 20 RT-PCR–negative collected during the study period were taken as controls. immunoglobulin M (IgM) and immunoglobulin G (IgG) antibodies against the RBD of the spike (S) protein of SARS-CoV-2 virus were detected by rapid antibody test and compared with the total antibody against the nucleocapsid (N) antigen of SARS-CoV-2 by electrochemiluminescence-based immunoassay (ECLIA).

**Results:** The detection of IgM against the RBD of the spike protein by rapid kit was less sensitive and less specific for the diagnosis of SARS-CoV-2 infection. However,

diagnostic efficacy of IgG by rapid kit was highly sensitive and specific when compared with the total antibody against N antigen measured by ECLIA.

**Conclusion:** It can be concluded that detection of IgM against the RBD of S protein by rapid kit is less effective, but IgG detection can be used as an effective diagnostic tool for SARS-CoV-2 infection in real-life hospital setting.

Keywords: SARS-CoV-2, COVID-19, receptor-binding domain (RBD), spike surface glycoprotein, chemiluminescence analysis, rapid antibody tests for COVID-19

## INTRODUCTION

The world is facing the outbreak of coronavirus disease 2019 (COVID-19), which has become a public health event of international concern (Afzal, 2020; Dubey et al., 2020, 2021; Feng et al., 2020; He et al., 2020; Nilsson et al., 2021). Accurate and rapid diagnosis of severe acute respiratory syndrome coronavirus 2 (SARS-CoV-2) infection is needed for prompt and effective patient care. Quantitative reverse transcriptase–polymerase chain reaction (RT-PCR) is the clinically accepted standard method for molecular diagnosis of SARS-CoV-2 detection. Alternatively, rapid antigen test (RAT) kit is also used for COVID-19 diagnosis. However, RT-PCR test has 70% sensitivity and 95% specificity and poses risks related to specimen collection and sample handling (Long et al., 2020a; Pray et al., 2021). A recent meta-analysis revealed that the average sensitivity and specificity of RAT for SARS-CoV-2 were 56.2 and 99.5%, respectively (Long et al., 2020b). These tests may also be falsely negative due to quality of sample or timing of carrying the test as the viral load in upper respiratory tract secretions peaks in the first week of symptoms, but may decline below the limit of detection in those presenting later. In individuals who have recovered, RT-PCR provides no information about prior exposure or immunity. Addressing this concern, various researchers developed a solution to minimize these risks by assaying immunoglobulin G (IgG) and immunoglobulin M (IgM) against the virus. Serological testing with good detection performance can be used as supplementary diagnosis of COVID-19 suspect cases with negative nucleic acid test result (Young et al., 2020). Also, to diagnose patients after the acute phase of the infection or with atypical clinical presentation with no nasopharyngeal shedding of the virus, serology testing is very useful (Noh et al., 2020; Young et al., 2020; Alsaud et al., 2021). In addition, serological testing provides a useful surveillance tool to track seroprevalence and assess the immune status in a community and may also be useful for decisions on lockdown entry–exit strategies (Parai et al., 2021).

The human body produces specific antibodies after the virus invades. The specific IgM antibody appears first, and then the titer of IgG antibody rises. Thus, the detection of IgM and IgG is believed to be another important diagnostic tool along with RT-PCR and RAT. The tests available detects anti–SARS-CoV-2 immunoglobulins, which are usually formed in the patient's body at the earliest by 1 week and on average within 2–3 weeks from the onset of infection (Jacofsky et al., 2020; Long et al., 2020a).

Various SARS-CoV-2 serological tests using different targeted antigenic proteins have been available now. Some of them use whole virus lysate, recombinant full S (spike) or N (nucleocapsid) proteins, peptides of the N, or specific domains S1, S2, or RBD (receptor-binding domain) of the S protein. Studies have shown that S and N proteins of the virus are the most immunogenic, and these serological tests can be performed with various techniques (Saif, 1993; Duan et al., 2020). Enzyme-linked immunosorbent assay (ELISA) and chemiluminescence are considered standard methods for the same. Rapid antibody kits are also available as a point-of-care testing tool. This rapid serological test is a simple procedure, needs no special equipment, is relatively cheap, and gives fast results. However, utility of this type of rapid antibody detection kit in the diagnosis of COVID-19 in real-life hospital settings is warranted. This study is conducted to evaluate the sensitivity and specificity of a rapid antibody kit in real-life hospital setting that detects IgM and IgG separately by comparing with the total antibody detection by chemiluminescence method.

## MATERIALS AND METHODS

The observational study was conducted in the Department of Biochemistry in collaboration with the Multidisciplinary Research Unit, Maulana Azad Medical College and Department of Medicine Lok Nayak Hospital, New Delhi, India, after ethical approval. Ethical approval number of the study is F.1/IEC/MAMC/(81/09/2020/No: 278) dated 24 November 2020. The study was carried out between December 2020 and June 2021.

### Cases and Controls

All the cases included in this study were COVID-19 cases confirmed by RT-PCR. Blood samples sent in red-capped blood collection vials for other biochemical tests were used, and no separate sample from them was collected for the study. Patients were categorized as "early cases" (group I) if they were recruited within the first week of positive RT-PCR test, as "intermediate cases" (group II) if taken between 8 and 14 days, and "late cases" (group III) if recruited after 14 days of their first RT-PCR–positive test. Recruitment continued until 20 samples were collected in each group. Blood sample was collected from 20 RT-PCR–negative subjects who were treated as controls. Twenty serum samples collected during January 2019 to June 2019 and preserved at −80°C were used as pre–COVID-19 era controls. Pre–COVID-19 samples (archived serum sample of pre–COVID-19) was used as negative controls for additional confirmation of test results.

**TABLE 1 |** Distribution of various comorbidities among different study groups.

| Comorbidity | 0–7 days (group I) (*n* = 20) | 8–14 days (group II) (*n* = 20) | >14 days (group III) (*n* = 20) | PCR-negative and pre-COVID era group (*n* = 40) |
|---|---|---|---|---|
| Diabetes mellitus (DM) | 4 | 2 | 2 | 0 |
| Hypertension (HTN) | 2 | 1 | 3 | 0 |
| DM + HTN | 6 | 5 | 0 | 0 |
| Chronic pulmonary obstructive disease (COPD) | 1 | 1 | 0 | 0 |
| DM + COPD + renal failure | 1 | 1 | 0 | 0 |
| Coronary artery disease (CAD) | – | 1 | – | – |
| DM + CAD | 1 | 1 | – | – |
| Bronchial asthma + HTN | – | – | 2 | – |
| Spondylitis | – | – | 1 | – |
| No comorbidity | 5 | 8 | 12 | 40 |
| Smokers | 5 | 4 | 5 | 2 |
| Smoker and alcoholic as well | 3 | 4 | 2 | 1 |

## Reference Method of Anti–COVID-19 Antibody Assay

Total antibody against the nucleocapsid (N) antigen of SARS-CoV-2 was assayed from the serum of these samples using electrochemiluminescence (ECL)–based Elecsys® Anti–SARS-CoV-2 immunoassay kit manufactured by Roche Diagnostics adapted to fully automated Cobas e411 immunoassay system. The cut-off indices for positive immunoassay was greater than 1.0 (arbitrary unit) by this method.

## Test Procedure for Antibody Detection Method by Rapid Kit

The ImmunoQuick COVID-19 kit evaluated in this study was produced by ImmunoScience India Private Limited, Pune, Maharashtra, India. ImmunoQuick COVID-19 was developed using the principle of immunochromatography for the rapid and qualitative detection of IgM and IgG antibodies against the RBD of spike (S) protein of COVID-19 virus in human serum, plasma, or whole blood. In an internal evaluation of

the performance characteristics of the rapid kit carried out by the manufacturer, serum, plasma, and whole blood samples of total 125 RT-PCR–negative and 160 RT-PCR COVID-19–positive were used. Sensitivity and specificity were found to be 97.5% (156/160) and 98.4% (123/125), respectively. Cross-reactivity studied with dengue-, HIV-, hepatitis C virus-, and HBsAg-positive serum samples showed no cross-reactivity. Endpoint titer was found satisfactory. External evaluation of the ImmunoQuick COVID-19 IgM/IgG test kit was performed by the National Institute of Virology–Indian Council of Medical Research, Department of Health Research, Government of India at Pune and was found satisfactory as per the Centers for Disease Control and Prevention and World Health Organization guidelines. The manufacturer obtained the regulatory approval for manufacturing the kit from the Central Drugs Standard Control Organization under Directorate General of Health Services, Ministry of Health & Family Welfare, Government of India. The manufacturing of the kit followed the ISO 13485:2016 QMS guidelines. The tests were performed at the Immunoassay Laboratory of Department of Biochemistry, Maulana Azad Medical College, New Delhi, by laboratory technicians/resident doctors immediately after receiving the blood samples by the method described below:

Test cassette, specimens, buffer, and/or controls were allowed to equilibrate to the temperature of an air-conditioned room (20–22°C) prior to testing. The test cassette was removed from the sealed foil pouch and was used as earliest possible. At the time of executing the test, it was made sure that the test device was placed on a clean and level surface. Sample was taken with mini plastic dropper provided in the kit, and one drop of it was transferred to the specimen well (marked as S on the cassette) of the test device. Then two drops of sample buffer were added to the buffer well (B) immediately, and air bubbles were avoided while dispensing it. As the fluid migrates through the membrane on which antigens are impregnated, the color line(s) develop. The results were read within 10 min. The results were visible as soon as 2 min. The result was read as negative when the colored line in the control line region (C) changed from blue to red and no line appeared in the test line regions M or G. The test result indicated the presence of IgM anti–SARS-CoV-2 antibodies when the colored line in the control line region (C) changed from blue to red and a colored line appeared in the test line region M. The test result indicated the presence of IgG anti–SARS-CoV-2 antibodies when the colored line in the control line region (C) changed from blue to red and a colored line appeared in the test line region G. The test results indicated the presence of IgM

**TABLE 2 |** Distribution of total antibody against nucleocapsid protein of SARS-CoV-2 test results at 0–7, 8–14, and >14 days of RT-PCR–positive confirmed COVID-19 cases, PCR-negative subjects, and pre–COVID-19 controls.

| Antibody titer against nucleocapsid protein by ECLIA | COVID cases confirmed by RT-PCR | | | PCR–negative subjects | Pre-COVID samples | Fisher exact test (*p*) |
|---|---|---|---|---|---|---|
| | 0–7 days (group I) | 8–14 days (group II) | >14 days (group III) | | | |
| >1.0 | 16 | 19 | 20 | 2 | 0 | <0.00001 |
| <1.0 | 4 | 1 | 0 | 18 | 20 | |

*p-value by Fischer exact test for this 5 × 2 table was <0.00001, which is statistically significant.*

**TABLE 3 |** Accuracy indices of total antibody assay against nucleocapsid protein by ECLIA at 0–7, 8–14, and >14 days of COVID diagnosis by RT-PCR with reference to pre-COVID era samples and RT-PCR–negative samples collected during the study period.

| | Within 0–7 days of RT-PCR report | Within 8–14 days of RT-PCR report | >14 days of RT-PCR report |
|---|---|---|---|
| **With reference to pre-COVID era samples** | | | |
| Sensitivity (%) | 80 | 95 | 100 |
| Specificity (%) | 100 | 100 | 100 |
| PPV (%) | 100 | 95 | 100 |
| NPV (%) | 83.3 | 95.2 | 100 |
| **With reference to RT-PCR–negative samples collected during study period** | | | |
| Sensitivity (%) | 80 | 95 | 100 |
| Specificity (%) | 80 | 80 | 80 |
| PPV (%) | 88 | 90.4 | 90.9 |
| NPV (%) | 66.6 | 88.8 | 100 |

and IgG anti–SARS-CoV-2 antibodies when the colored line in the control line region (C) changed from blue to red and two colored lines appear in the test line regions M and G. The result was considered as invalid when the control line was partially red and failed to completely change from blue to red. Insufficient specimen volume or incorrect procedural techniques were the most likely reasons for control line failure. During the study, we never encountered any invalid test result.

## Statistical Analysis

Data of the test results were arranged in the table as follows:

| | ECL anti–SARS-CoV-2–positive | ECL anti–SARS-CoV-2–negative |
|---|---|---|
| Rapid kit antibody–positive | a | b |
| Rapid kit antibody–negative | c | d |

Specificity, sensitivity, negative predictive value (NPV), and positive predictive value (PPV) of anti-RBD IgM and IgG were calculated from a $2 \times 2$ table using formulas as follows:

$$\text{Sensitivity} = [a/(a + c)] \times 100$$

$$\text{Specificity} = [d/(b + d)] \times 100$$

$$\text{PPV} = [a/(a + b)] \times 100$$

$$\text{NPV} = [d/(c + d)] \times 100$$

The strength of the agreement of the two methods was calculated by using the Cohen κ index. Results were interpreted according to the following κ values: (i) 0.01–0.20, slight agreement; (ii) 0.21–0.40, fair agreement; (iii) 0.41–0.60, moderate agreement; (iv) 0.61–0.80, substantial agreement; and (v) 0.81–1.00, perfect agreement. $p < 0.05$ was considered statistically significant for all statistical tests.

**TABLE 4 |** Table showing distribution of positive and negative antibody test results by rapid test kit and ECLIA method on samples collected from COVID patients at 0–7, 8–14, and after 14 days of RT-PCR–positive and RT-PCR–negative subjects and pre-COVID samples.

| Rapid test | | Total antibody assayed by ECL method | | | | | | | | | |
|---|---|---|---|---|---|---|---|---|---|---|---|
| | | Within 0–7 days of RT-PCR | | Within 8–14 days of RT-PCR | | After 14 days of RT-PCR | | RT-PCR–negative | | Pre-COVID era samples | |
| | | Positive | Negative | Positive | Negative | Positive | Negative | Positive | Negative | Positive | Negative |
| IgM | Positive | 06 | 00 | 06 | 00 | 00 | 00 | 01 | 00 | 00 | 00 |
| | Negative | 10 | 04 | 13 | 01 | 20 | 00 | 00 | 19 | 00 | 20 |
| IgG | Positive | 14 | 01 | 18 | 00 | 17 | 00 | 02 | 00 | 00 | 00 |
| | Negative | 02 | 03 | 01 | 01 | 02 | 01 | 00 | 18 | 00 | 20 |

**TABLE 5 |** Accuracy indices of IgM and IgG antibody (against the RBD of the spike protein of SARS-CoV-2 virus) by rapid test for the diagnosis of COVID-19 (calculated by taking total antibody levels by ECL as standard methods.

| | Diagnostic accuracy of IgM by rapid kit | | | | | Diagnostic accuracy of IgG by rapid kit | | | | |
|---|---|---|---|---|---|---|---|---|---|---|
| | Sample collected within 0–7 days of positive RT-PCR | Sample collected within 8–14 days of positive RT-PCR | Sample collected after 14 days of positive RT-PCR | Pre-COVID samples | RT-PCR–negative | Sample collected within 0–7 days of positive RT-PCR | Sample collected within 8–14 days of positive RT-PCR | Sample collected with after 14 days of positive RT-PCR | Pre-COVID samples | RT-PCR – negative |
| Sensitivity (%) | 37.5 | 31.6 | 0 | 100 | 100 | 87.5 | 94.73 | 89.47 | 100 | 100 |
| Specificity (%) | 100 | 100 | 0 | 100 | 100 | 75 | 100 | 100 | 100 | 100 |
| PPV (%) | 100 | 100 | 0 | 100 | 100 | 93 | 100 | 100 | 100 | 100 |
| NPV (%) | 28 | 7.14 | 0 | 100 | 100 | 60 | 50 | 33.3 | 100 | 100 |
| Cohen κ | 0.1935 | 0.044 | 0 | | | 0.5714 | 0.6428 | 0.459 | | |

# RESULTS

Of the 60 patients enrolled in the study, patients were having mild, moderate, or severe COVID-19 and were divided into three groups as early, intermediate, and late cases as previously mentioned. Male-to-female ratio was 14:6 in group I, 16:4 in group II, and 15:5 in group III. Gender difference in these groups was statistically insignificant. The ages of the participants in the study groups ranged from 21 to 68 years, with no statistically significant difference among the groups. Of 100 participants, 16% were smokers, and 10% were smokers and alcoholic as well. The distribution of comorbid conditions in different groups is shown in **Table 1**.

The results of total antibody positive (level $>1.0$) and negative (level $<1.0$) against N protein of SARS-CoV-2 virus and achieved pre-COVID era non-COVID samples by ECL-based immunoassay (ECLIA) are presented in **Table 2**.

# DISCUSSION

The present study was designed to evaluate the diagnostic efficacy of a rapid antibody kit against the RBD of the S protein of COVID-19 in a real-life hospital setting. Among the diagnostic immunoassay methods, chemiluminescence-based immunoassay (CLIA) is considered to be very sensitive and effective. In the present study, diagnostic efficacy of total antibody assay against nucleocapsid protein by ECL method in the early, intermediate, and late cases was performed. **Tables 2**, **3** show that during first 7 days after PCR positivity, the sensitivity, specificity, PPV, and NPV of ECLIA-based antibody assay were 80, 100, 100, and 83.3%, respectively; between 8 and 14 days after PCR positivity, those were 95, 100, 95, and 95.2%, respectively, and for late cases, those were 100% for all indices. This indicates that ECLIA is a very effective diagnostic tool for COVID-19, and its efficacy after 7 days is very close to that of RT-PCR. Even within 7 days, it was found to be very effective. Thus, for comparison of any other antibody testing method for COVID-19, ECLIA-based immunoassay of total antibody against nucleocapsid protein can be considered as a standard method.

For the assessment of seroprevalence, most of the authorities recommend antibody assay either by ELISA or CLIA-based methods. The manufacturers of rapid antibody assays claim that rapid test is also effective in serosurveillance particularly in remote areas where there are no laboratory facilities. However, the diagnostic efficacy of these rapid antibody kit has also been evaluated in standard laboratory conditions (Li et al., 2020; Zhang et al., 2020), but not in real-life hospital settings treating COVID-19 patients. Performance evaluation in real-life situation is an important component of postmarket surveillance. There are limited data to prove their efficacy in the hospital setting. Thus, in this study, we tried that in a dedicated COVID hospital.

**Tables 4**, **5** show that the assay of IgM by rapid kit has sensitivity of 37.5% for early cases and 31.6% for intermediate cases, although specificity and PPV were 100%. NPV was found to be 28 and 7.14%, and Cohen κ was 0.1935 and 0.044, respectively. After 14 days, as expected, IgM antibody by rapid kit was undetectable because of class switching of the antibody. Hence, we conclude that IgM detection by rapid kit has very limited effectiveness as a diagnostic tool for COVID-19 in real-life hospital setting.

As shown in **Tables 4**, **5**, detection of IgG by rapid kit for early intermediate and late cases was 87.5, 94.7, and 89.5%, respectively, and specificity was 75, 100, and 100%, respectively. Similarly, PPV was 93, 100, and 100%, respectively; NPV was 60, 50, and 33.3%, respectively; and Cohen κ was 0.5714, 0.6428, and 0.459, respectively. This indicates that IgG detection is effective enough in the diagnosis of COVID-19 in the hospital setting. Even within 0–7 days, its sensitivity and specificity were high, indicating a possible early class switching of antibody against the RBD of the spike protein. These observations go against the contention that antibody detection or assay best suits the serosurveillance and not the diagnosis. From this, we conclude that the efficacy of IgG against the RBD of the spike protein is as effective as that by CLIA and can be utilized in the hospital setting. However, combining IgM detection with IgG does not improve the diagnostic efficacy and hence is a mere wastage of resources. Thus, we recommend IgG (against the RBD of S protein) assay by rapid kit in the diagnosis of COVID-19 for the screening of suspected patients where RT-PCR or CLIA-based antibody assay facility is not available. Even a variation in performances of assays is likely to exist when diagnosing different populations such as individuals with different diet habits, mental well-being, and so on (Soni et al., 2020a,b,c; Mehta et al., 2021).

However, the limitation of the present study is that while evaluating rapid test, we evaluated the detection of antibody against the RBD of the spike protein of SARS-CoV-2 virus but took assay of total antibody against a different one, that is, nucleocapsid (N) protein, as our standard reference method. Another limitation is that the study was conducted in only one hospital of New Delhi involving a limited number of samples from the local population. Immune response being variable in different populations, its applicability in other populations is worth evaluating.

# DATA AVAILABILITY STATEMENT

The original contributions presented in the study are included in the article. Further inquiries can be directed to the corresponding author/s.

# AUTHOR CONTRIBUTIONS

## FUNDING

## REFERENCES

Afzal, A. (2020). Molecular diagnostic technologies for COVID-19: limitations and challenges. *J. Adv. Res.* 26, 149–159. doi: 10.1016/j.jare.2020.08.002

Alsaud, A. E., Nair, A. P., Matarneh, A. S., Sasi, S., El Hassan, R., Khan, F., et al. (2021). Case report: prolonged viral shedding in six COVID-19 patients. *Am. J. Trop. Med. Hyg.* 104, 1472–1475. doi: 10.4269/ajtmh.20-0933

Duan, L., Zheng, Q., Zhang, H., Niu, Y., Lou, Y., and Wang, H. (2020). The SARS-CoV-2 spike glycoprotein biosynthesis, structure, function, and antigenicity: implications for the design of spike–based vaccine immunogens. *Front. Immunol.* 11:576622. doi: 10.3389/fimmu.2020.576622

Dubey, A., Bansal, A., Sonkar, S. C., Goswami, B., Makwane, N., Manchanda, V., et al. (2020). In–house assembled protective devices in laboratory safety against SARS-nCoV-2 in clinical biochemistry laboratory of a COVID dedicated hospital. *medRxiv* [Preprint] medRxiv 2020 08.24.20155713, doi: 10.1101/2020.08.24.20155713

Dubey, A., Kotnala, G., Mandal, T. K., Sonkar, S. C., Singh, V. K., Guru, S. A., et al. (2021). Evidence of the presence of SARS-CoV-2 virus in atmospheric air and surfaces of a dedicated COVID hospital. *J. Med. Virol.* 93, 5339–5349. doi: 10.1002/jmv.27029

Feng, W., Newbigging, A. M., Le, C., Pang, B., Peng, H., Cao, Y., et al. (2020). Molecular diagnosis of COVID-19: challenges and research needs. *Anal. Chem.* 92, 10196–10209.

He, J., Hu, P., Gao, Y., Zheng, S., Xu, C., Liu, R., et al. (2020). Comparison and application of different immunoassay methods for the detection of SARS-CoV-2. *J. Med. Virol.* 92, 2777–2784. doi: 10.1002/jmv.26187

Jacofsky, D., Jacofsky, E. M., and Jacofsky, M. (2020). Understanding antibody testing for COVID-19. *J Arthroplasty.* 35, S74–S81.

Li, Z., Yi, Y., Luo, X., Xiong, N., Liu, Y., Li, S., et al. (2020). Development and clinical application of a rapid IgM–IgG combined antibody test for SARS-CoV-2 infection diagnosis. *J. Med. Virol.* 92, 1518–1524. doi: 10.1002/jmv.25727

Long, Q.-X., Liu, B.-Z., Deng, H.-J., Wu, G.-C., Deng, K., Chen, Y.-K., et al. (2020a). Antibody responses to SARS-CoV-2 in patients with COVID-19. *Nat. Med.* 26, 845–848.

Long, Q.-X., Tang, X.-J., Shi, Q.-L., Li, Q., Deng, H.-J., Yuan, J., et al. (2020b). Clinical and immunological assessment of asymptomatic SARS-CoV-2 infections. *Nat. Med.* 26, 1200–1204. doi: 10.1038/s41591-020-0965-6

Mehta, A., Soni, V. K., Sharma, K., Ratre, Y. K., Shukla, D., Singh, A. K., et al. (2021). Finding horcrux of psychiatric symptoms in COVID-19: deficiencies of amino acids and vitamin D. *Asian J. Psychiatr.* 55:102523. doi: 10.1016/j.ajp.2020.102523

Nilsson, A. C., Holm, D. K., Justesen, U. S., Gorm-Jensen, T., Andersen, N. S., Øvrehus, A., et al. (2021). Comparison of six commercially available SARS-CoV-2 antibody assays–choice of assay depends on intended use. *Int. J. Infect. Dis.* 103, 381–388. doi: 10.1016/j.ijid.2020.12.017

Noh, J. Y., Yoon, J. G., Seong, H., Choi, W. S., Sohn, J. W., Cheong, H. J., et al. (2020). Asymptomatic infection and atypical manifestations of COVID-19: comparison of viral shedding duration. *J. Infect.* 81, 816–846. doi: 10.1016/j.jinf.2020.05.035

Parai, D., Dash, G. C., Choudhary, H. R., Peter, A., Rout, U. K., Nanda, R. R., et al. (2021). Diagnostic accuracy comparison of three fully automated chemiluminescent immunoassay platforms for the detection of SARS-CoV-2 antibodies. *J. Virol Methods* 292:114121. doi: 10.1016/j.jviromet.2021.114121

Pray, I. W., Ford, L., Cole, D., Lee, C., Bigouette, J. P., Abedi, G. R., et al. (2021). Performance of an antigen–based test for asymptomatic and symptomatic SARS-CoV-2 testing at two university campuses – wisconsin, September–October 2020. *MMWR Morb. Mortal. Wkly. Rep.* 69, 1642–1647. doi: 10.15585/mmwr.mm695152a3

Saif, L. J. (1993). Coronavirus immunogens. *Vet. Microbiol.* 37, 285–297.

Soni, V. K., Mehta, A., Ratre, Y. K., Tiwari, A. K., Amit, A., Singh, R. P., et al. (2020a). Curcumin, a traditional spice component, can hold the promise against COVID-19? *Eur. J. Pharmacol.* 886:173551. doi: 10.1016/j.ejphar.2020.173551

Soni, V. K., Mehta, A., Shukla, D., Kumar, S., and Vishvakarma, N. K. (2020b). Fight COVID-19 depression with immunity booster: curcumin for psychoneuroimmunomodulation. *Asian J. Psychiatr.* 53:102378. doi: 10.1016/j.ajp.2020.102378

Soni, V. K., Shukla, D., Kumar, A., and Vishvakarma, N. K. (2020c). Curcumin circumvent lactate–induced chemoresistance in hepatic cancer cells through modulation of hydroxycarboxylic acid receptor-1. *Int. J. Biochem. Cell Biol.* 123:105752. doi: 10.1016/j.biocel.2020.105752

Young, B. E., Ong, S. W. X., Kalimuddin, S., Low, J. G., Tan, S. Y., Loh, J., et al. (2020). Epidemiologic features and clinical course of patients infected with SARS-CoV-2 in Singapore. *JAMA* 323, 1488–1494. doi: 10.1001/jama.2020.3204

Zhang, C., Zhou, L., Liu, H., Zhang, S., Tian, Y., Huo, J., et al. (2020). Establishing a high sensitivity detection method for SARS-CoV-2 IgM/IgG and developing a clinical application of this method. *Emerg. Microbes Infect.* 9, 2020–2029. doi: 10.1080/22221751.2020.1811161

Check for updates

# Atypical Antibody Dynamics During Human Coronavirus HKU1 Infections

Ferdyansyah Sechan[1,2], Marloes Grobben[1,2], Arthur W. D. Edridge[1,2], Maarten F. Jebbink[1,2], Katherine Loens[3,4], Margareta Ieven[4], Herman Goossens[3,4], Susan van Hemert-Glaubitz[5], Marit J. van Gils[1,2] and Lia van der Hoek[1,2]*

[1] Laboratory of Experimental Virology, Department of Medical Microbiology and Infection Prevention, Amsterdam UMC, University of Amsterdam, Amsterdam, Netherlands, [2] Amsterdam Institute for Infection and Immunity, Amsterdam, Netherlands, [3] Department of Medical Microbiology, Vaccine & Infectious Disease Institute (VAXINFECTIO), University of Antwerp, Antwerpen, Belgium, [4] Department of Microbiology, University Hospital Antwerp, Edegem, Belgium, [5] Julius Centre for Health Sciences and Primary Care, University Medical Centre Utrecht, Utrecht University, Utrecht, Netherlands

Human coronavirus HKU1 (HCoV-HKU1) is one of the four endemic coronaviruses. It has been suggested that there is a difference in incidence, with PCR-confirmed HCoV-NL63 and HCoV-OC43 infections occurring more commonly, whereas HCoV-HKU1 is the least seen. Lower incidence of HCoV-HKU1 infection has also been observed in serological studies. The current study aimed to investigate antibody dynamics during PCR-confirmed HCoV-HKU1 infections using serum collected during infection and 1 month later. We expressed a new HCoV-HKU1 antigen consisting of both the linker and carboxy-terminal domain of the viral nucleocapsid protein and implemented it in ELISA. We also applied a spike-based Luminex assay on serum samples from PCR-confirmed infections by the four endemic HCoVs. At least half of HCoV-HKU1-infected subjects consistently showed no antibody rise *via* either assay, and some subjects even exhibited substantial antibody decline. Investigation of self-reported symptoms revealed that HCoV-HKU1-infected subjects rated their illness milder than subjects infected by other HCoVs. In conclusion, HCoV-HKU1 infections reported in this study displayed atypical antibody dynamics and milder symptoms when compared to the other endemic HCoVs.

Keywords: endemic seasonal coronavirus, HCoV-HKU1, HCoV-OC43, HCoV-229E, HCoV-NL63, nucleocapsid protein, spike protein, IgG response

## INTRODUCTION

Human coronavirus (HCoV) HKU1 is a positive-strand RNA virus that belongs to the genus *Betacoronavirus*. In the year 2005, this virus was reported for the first time in a 71-year-old male patient for the first time with unexplainable pneumonia (Woo et al., 2005). Together with the other endemic HCoVs (HCoV-229E, HCoV-OC43, and HCoV-NL63), it is known as a common cold coronavirus infecting humans. The virus has a worldwide distribution (Vabret et al., 2008; Mackay et al., 2012; Liu et al., 2014; Al-Khannaq et al., 2016; Yip et al., 2016; Killerby et al., 2018; Masse et al., 2020). There are at least three co-circulating genotypes of HCoV-HKU1: A, B, and C, with recombination occurring frequently among them (Woo et al., 2006). Studying the HCoV-HKU1 infections in population remains challenging, because this virus is the least frequently detected HCoV. For example, the

RT-PCR test to diagnose HCoV-HKU1 was discontinued in Scotland, in 2012, due to low detection rate (Nickbakhsh et al., 2020).

The four endemic HCoVs are suspected of having animal origins (Cui et al., 2019), similar to SARS-CoV-2. However, unlike SARS-CoV-2, they have circulated in humans for centuries, and infection mostly results in non-life-threatening common-cold-like symptoms. Considering that SARS-CoV-2 may soon become an endemic human coronavirus, possibly sharing epidemic and/or pathogenic characteristics with other endemic HCoVs, we were interested in the features that these four viruses share, and also those that separate them. The HCoVs share the characteristic that first infections occur in early childhood (Dijkman et al., 2012; Zhou et al., 2013), protective immunity is short-lived, and reinfection in humans occurs frequently (Edridge et al., 2020; Galanti and Shaman, 2020; Petrie et al., 2021). Serological studies show that HCoV-HKU1 (re-)infection occurs the least comparatively (Dijkman et al., 2012; Edridge et al., 2020). Edridge et al also showed that some HCoV-HKU1 infections are not accompanied by increased antibody titer (Edridge et al., 2020). In that particular study, a partial nucleocapsid protein (N) of HCoV-HKU1 was used as the respective ELISA antigen.

The N protein of coronaviruses is structural, and the tertiary structure is conserved across different coronavirus species. There are two structural domains: the C-terminal (Ct) and N-terminal (Nt) domains, connected by a flexible linker domain (McBride et al., 2014; Zhou et al., 2020). Due to the high amino acid sequence identity, the use of full N antigen in serology can result in cross-reactivity between HCoV species belonging to the same genus (Lehmann et al., 2008). The Ct domain of N (NCt) is used in many serology studies since *Alphacoronavirus* serology was identified to be most specific (Mourez et al., 2007; Dijkman et al., 2008; Severance et al., 2008; Sastre et al., 2011). However, it could be that the NCt antigen of HCoV-HKU1 contains too few epitopes, thus, explaining the lack of HKU1-antibody increase (Edridge et al., 2020). The HKU1-antibody ELISA could potentially be improved by expressing and using an HCoV-HKU1 antigen that includes the linker (L) domain as well as the NCt domain (NLCt protein). The flexible linker domain of HCoV-HKU1 N-protein is most probably immunogenic since the linker domain of HCoV-OC43 N-protein also displays immunogenicity (Liang et al., 2013). Furthermore, since recent studies of SARS-CoV-2 infection revealed that spike (S) and N antibodies might have different dynamics, we anticipated that a serological assay using S protein may also improve the HKU1-serology (Brochot et al., 2020; Röltgen et al., 2020). Thus, we included S-antibody Luminex tests for all four HCoVs in the current study. The study aimed to determine whether HCoV-HKU1 antibody dynamics truly differ from those of other endemic human coronaviruses.

## MATERIALS AND METHODS

### Serum Samples

A total of 108 serum samples were obtained from 54 subjects with a PCR-confirmed endemic HCoV infection. The number of subjects with HCoV-HKU1, HCoV-OC43, HCoV-NL63, and HCoV-229E was 13, 14, 11, and 16, respectively. The causative agent of disease for each subject was confirmed using multiplex RT-PCR assay on the nasopharyngeal sample (Loens et al., 2012). A cycle threshold (Ct) value of 30 and lower was used as a cutoff to select subjects with confirmed HCoV infection, except for HCoV-HKU1. For HCoV-HKU1, the RespiFinder test was used (PathoFinder, Maastricht, The Netherlands). The Respifinder assay, version RespiFinder plus - RespiFinder Smart 21, allows testing specifically for HCoV-HKU1, yet no cycle threshold value could be derived.

The 54 subjects were part of the Genomics to combat Resistance against Antibiotics in Community-acquired LRTI in Europe (GRACE) study. Participants were recruited between November 2007 and April 2010 by primary care practitioners in 16 networks from 12 European countries. The details of the GRACE cohort study are described in detail elsewhere (Ieven et al., 2018). Subjects aged 18 years or above with acute or worsened cough, or other symptoms indicating lower respiratory tract infection (LRTI), as reported by their general practitioner (GP), were invited to participate, and written consent was obtained before asking for participation. All recruiting GPs received standardized sampling material and a protocol with detailed instructions on the sampling of the patients. Within 24 h of first presentation and inclusion, blood, sputum if available, and two nasopharyngeal flocked swabs (NPS) (Copan Italia, Brescia, Italy) were taken [visit 1 (V1)]. At days 28–35, serum sampling and the two NPS were repeated [visit 2(V2)]. Serum, and NPS were stored frozen in the local laboratories until regular shipment to the central laboratory (University Hospital Antwerp), where specimens were stored at -80°C until analysis.

Demographic data and clinical manifestation of LRTI for each subject were recorded using a standardized case report form (CRF) that was completed by the GP during V1. Demographic data included age, gender, presence of comorbidities, and the estimated duration of illness or cough before the first visit. Within the CRF, subjects were also asked whether any of the 14 symptoms/conditions were present, and to rate the severity in case any symptom was present. These 14 symptoms are cough, phlegm, shortness of breath, wheezing, runny nose, fever, chest pain, muscle ache, headache, disturbed sleep, generally feeling unwell, interference with normal daily activities, confusion/disorientation, and diarrhea. The severity of each symptom was scored as follows: 0 = symptom absent/not a problem, 1 = mild problem, 2 = moderate problem, 3 = severe problem, and mean symptom severity score (SSS) for each subject was calculated as average score value from all 14 symptoms (Vos et al., 2021). Clinical data of one subject infected with HCoV-NL63 and three subjects infected with HCoV-229E were missing, therefore, 50 subjects were included in the demographic and symptom analyses.

The GRACE study was approved by the local ethics committees in all participating centers and by the competent authorities in each country: Cardiff and Southampton (United Kingdom): Southampton and South West Hampshire Research Ethics Committee A; Utrecht (Netherlands): Medisch Etische Toetsingcommissie Universitair Medisch Centrum Utrecht; Barcelona (Spain): Comité étic d'Investigació clínica

Hospital Clínic de Barcelona; Mataro (Spain): Comitè d'Ètica d'Investigació Clínica (CEIC) del Consirci Sanitari del Maresme; Rotenburg (Germany): Ethik-Kommission der Medizinischen Fakultät der Georg-August-Universitat Göttingen; Antwerp (Belgium): UZ Antwerpen Comité voor Medische Ethiek; Lodz, Szeczecin and Bialystok (Poland): Komisja Bioetyki Uniwersytetu Medycznego W Lodzi; Milano (Italy):IRCCS Fondazione Cà Granda Policlinico; Jonkoping (Sweden): Regionala etikprövningsnämden I Linköping; Bratislava (Slovakia): Etika Komisia Bratislavskeho; Gent (Belgium): Ethisch Comité Universitair Ziekenhuis Gent; Nice (France): Comité de Protection des Personnes Sud-Méditerranée II, Hôpital Salvator; and Jesenice (Slovenia): Komisija Republike Slovenije za Medicinsko Etiko.

## Design of Recombinant Coronavirus HKU1 Nucleocapsid Protein

The location of HCoV-OC43 linker domain (Liang et al., 2013) was aligned with the amino acid sequence of HCoV-HKU1 N using global pairwise alignment (Madeira et al., 2019). GenBank accession number AAR01019.1 (HCoV-OC43 isolate VR-759) and ADN03343.1 (HCoV-HKU1 isolate Caen1) were used for the alignment. It was estimated that the linker domain of HCoV-HKU1 N was located between amino acids 172 and 299. Therefore, the new antigen "NLCt" was designed to start at amino acid 172 and run to the end (amino acid 441) (**Figure 1A**). Multiple sequence alignment was done between HCoV-HKU1 NLCt amino acid sequence with corresponding sequences on other endemic coronaviruses to estimate the possibility of cross-reaction between species. HKU1-NLCt shared 64.33% percent identity with HCoV-OC43 while the values are lower for HCoV-NL63 and HCoV-229E (percent identity of 24.56 and 24.85%, respectively). The presumed L domain of HCoV-NL63 and HCoV-229E (**Figure 1B**) was also found by amino acid alignment using HCoV-OC43 N protein as the reference (Liang et al., 2013). Furthermore, to account for the possibility that antibodies against one genotype could not recognize epitopes from other genotypes, the amino acid sequence of the NLCt protein from one representative of each genotype as mentioned by Woo et al. (2006) were aligned with the NLCt sequence based on HCoV-HKU1 strain Caen1. The sequence shared is used to construct a phylogenetic tree alongside the Caen1 nucleocapsid sequence. The Caen1 strain clustered with HCoV-HKU1 genotype A. The HKU1-NLCt antigen we produced shared > 94% identity with the corresponding sequence from HCoV-HKU1 genotypes B and C.

## Expression of Recombinant Coronavirus HKU1 Nucleocapsid Protein

The production of the HKU1-NLCt antigen, starting with the generation of the plasmid construct to the expression of the protein, was done similarly to previously described methods (Dijkman et al., 2012). In short, the HKU1-NLCt gene fragment was amplified using PCR with Q5 High Fidelity DNA Polymerase (New England Biolabs, Ipswitch, MA, United States). The template used in the PCR was the full nucleocapsid protein gene from HCoV-HKU1 strain Caen1 (GenBank accession number HM0384837.1), and the sequences for the forward and reverse primer were 5′ – CACCACTAGGTTTCCGCCTG – 3′ (5′-HKU1-NLCt) and 5′–TTAAGCAACAGAGTCTTCTACATAAG–3′ (3′-HKU1-end), respectively. The PCR product was cloned into pET/100/D-TOPO expression plasmids (Thermo Fisher Scientific, Waltham, MA, United States), which were transformed into *Escherichia coli* DH5α competent cells (Thermo Fisher Scientific). Sequencing on the generated pET-HKU1-NLCt plasmid confirmed that the cloned gene was identical to Caen1. The HKU1-NLCt antigen was then expressed and purified using steps described previously (Dijkman et al., 2008). Since the first purified product still contained impurities (assumed to be bacterial proteins, **Supplementary Figure 1A**), the purification step was done two times (**Supplementary Figure 1B**).

## HKU1 Nucleocapsid ELISA

The NLCt ELISA protocol used in this study was similar to the one previously described (Edridge et al., 2020), with some modifications. The antigen was coated overnight on 96-well half-area microplates (Greiner Bio-One, Alphen aan de Rijn, The Netherlands), with 3 µg/ml antigen in 0.1 M carbonate buffer, at pH 9.6. The plates were incubated for 1 h at 20°C with 5% skimmed milk (Honeywell Fluka, Landsmeer, The Netherlands) solution in PBS with 0.1% Tween (PBST) to block non-specific binding sites, followed by three washing steps with PBST. The serum samples were diluted at 1:200 in PBST supplemented with 1% skimmed milk. The diluted serum samples were added to the washed plates in duplicate and incubated for 1 h at 20°C, followed by a washing step. After that, alkaline phosphatase-conjugated AffiniPure Goat Anti-Human IgG, Fc Fragment Specific (Jackson ImmunoResearch, West Grove, PA, United States), diluted 1:1,500 in 1% skimmed milk and PBST solution was added. Plates were incubated for 1 h at 20°C, followed by washing. Finally, the luminescence signal was developed using LumiPhos (Lumigen, Southfield, MI, United States) and the plates were incubated in the dark for 20 min at 20°C. The luminescence (ELISA signal value) was measured using GloMax 96 Microplate Luminometer (Promega, Madison, WI, United States). The final ELISA signal value for each serum sample was calculated as the average of the two measurements. ELISA signal fold-change was calculated by dividing the value of ELISA signal from V2 with the value from V1.

A cutoff value of 1.40 was used for significant antibody rise in response to an infection. This cutoff was established previously by Edridge et al. (2020), by measuring the natural fluctuation in measles virus antibodies in consecutive samples from 10 individuals, assuming that measles infection did not occur during follow-up. Fold changes in ELISA signal for measles antibodies ranged between 0.85 and 1.28. Edridge et al. subsequently showed that for the coronaviruses, outliers were found for signal fold changes ≥1.40 by evaluating the distribution of the signal fold change for each of the seasonal

coronaviruses. In addition, Edridge et al confirmed that self-reported influenza-like illnesses directly preceded the ≥1.40-fold rise in antibodies. Finally, the ELISA ≥1.40 rise of HCoV-NL63 were compared with neutralization titers for HCoV-NL63 and an increase in neutralization titer indeed accompanied a ≥1.40-fold rise in antibodies.

## Recombinant Prefusion Spike Coronavirus Luminex Assay

The Luminex assay using prefusion S antigen of endemic HCoVs was done as previously described (Grobben et al., 2021). For HCoV-HKU1, the S antigens were stabilized in the prefusion conformation by mutating two amino acid residues at position 1067 and 1068 into two prolines and by substitution

of the furin cleavage site with amino acid sequence GGSGS to prevent cleavage and subunit dissociation during the production process (Kirchdoerfer et al., 2016; Brouwer et al., 2021). The S antigen of HCoV-HKU1 was derived from isolate N5 (NCBI accession code: Q0ZME7), which belongs to genotype C (Woo et al., 2006). The protein was expressed in HEK293F cells (Invitrogen, Waltham, MA, United States) in a Freestyle medium and purified with affinity chromatography using NiNTA agarose beads (Qiagen, Venlo, The Netherlands). Each antigen was then coupled to Luminex Magplex beads using a two-step carbodiimide reaction as previously described (Grobben et al., 2021; Keuning et al., 2021). The coupled beads (20 beads per μl of each S of endemic HCoVs), together with serum samples diluted to 1:10,000, were used in the Luminex assay, with Goat-anti-human IgG-PE (SouthernBiotech, Birmingham,
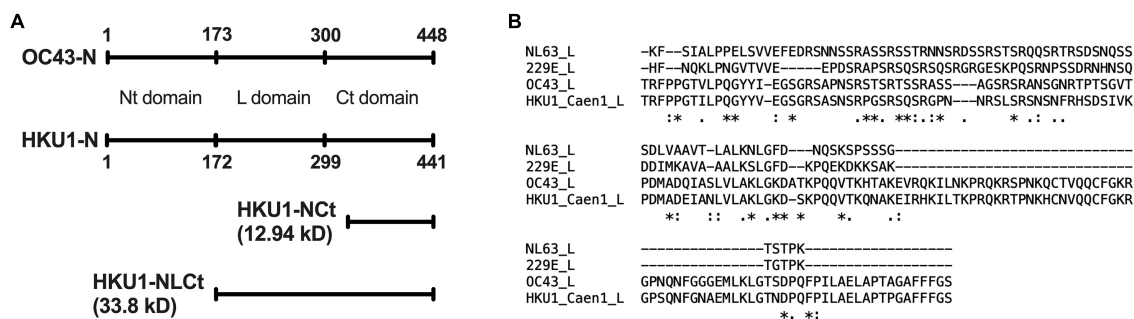


FIGURE 1 | (A) Location of Nt-, Ct-, and linker (L)-domain of HCoV-HKU1 N as determined by pairwise alignment with HCoV-OC43, as well as the comparison of size between HKU1-NLCt and the HKU1-NCt antigen. (B) Multiple alignment of the nucleocapsid L domain of HCoV-NL63, HCoV-229E, HCoV-OC43, and HCoV-HKU1. The symbols below the aligned amino acid sequence represent the consensus symbol of amino acid residue at each position: asterisks (*) denotes fully conserved residue, colons (:) denotes amino acid residues with strongly similar property, periods (.) denotes amino acid residues with weakly similar property, and the absence of symbol denotes completely different property.
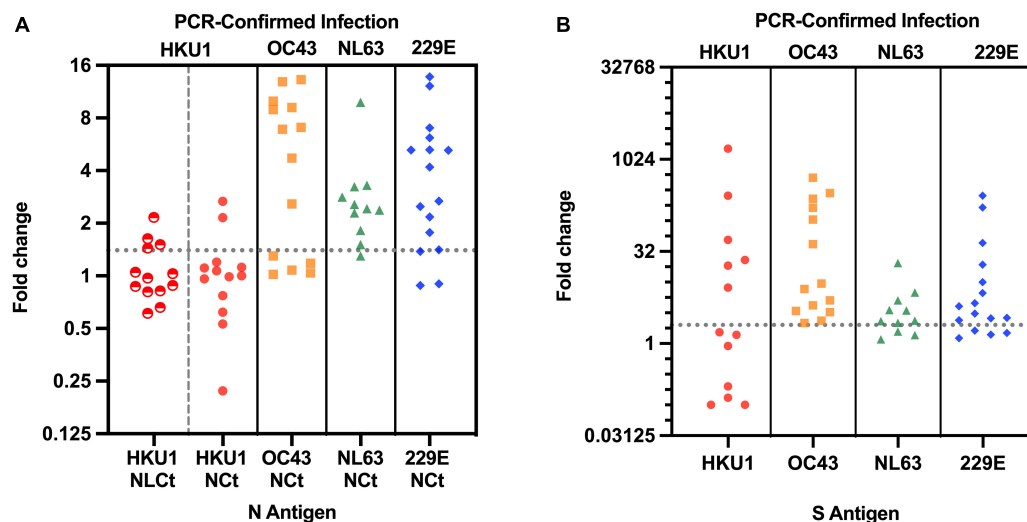


FIGURE 2 | (A) V1-V2 Fold change in antibody values of 54 subjects with PCR-confirmed endemic HCoV infection, as assayed with ELISA with matched N antigen. For HCoV-HKU1-infections, both HKU1-NLCt (half-filled red circles) and HKU1-NCt (full red circles) were used for the N assay. Dotted line represents cutoff of significant antibody rise (fold change of 1.40 or higher). The NCt ELISA fold change values for all four endemic coronaviruses have been published previously Edridge et al. (2020). (B) V1-V2 Fold change in antibody values using matched S antigens for each HCoV infection in the S-Luminex assay. Dotted line represents the cutoff of significant S-antibody rise (fold change of 2.01 or higher).

AL, United States) as the secondary antibody. Positive and negative controls (tetanus toxoid-coupled beads and uncoupled beads, respectively) were included in each run. The readout was expressed as Median Fluorescence Intensity of at least 50 beads per antigen. Fold change values were calculated as the ratio of V2:V1. The cutoff for significant antibody rise or antibody decrease was defined as the upper fence (Q3 + 1.5*IQR) or lower fence (Q1 – 1.5*IQR) of fold change values derived from tetanus toxoid-coupled beads (positive control) (**Supplementary Figure 2**). The cutoff values were defined as 2.01 and 0.23 for antibody rise and antibody decrease, respectively.

## Statistical Analysis

Statistical analyses were done using SPSS version 27 (IBM, Armonk, NY, United States) and R version 4.0.3, while the figures were made with Prism version 9.3.0 (GraphPad, San Diego, CA, United States). Correlations between two (non-parametric) numerical variables were determined using Spearman's Rank Order Correlation. The distribution of categorical variables between groups was compared using Fisher's exact test. Numerical variables between HCoV-HKU1 subjects and other HCoV subjects (pooled into one group) were compared for the difference using the Mann–Whitney $U$ test. The effect of HCoV-HKU1 infection on the possible influence of age as a confounding factor for selecting "illness interfering with daily activities" (binomial categorical variable, yes-no) as "no" was investigated using logistic regression.

# RESULTS

A total of 13 subjects with lower respiratory tract infection that visited their GP with a PCR-confirmed HCoV-HKU1 infection were included in the study. We tested for antibodies in serum collected at two time points. The first time point (V1) was the moment of the GP visit, which is also the date of PCR-positive testing for HCoV-HKU1. The second serum sampling moment (V2) was 1 month later, at that time the patient had

**TABLE 1** | The V1-V2 antibody fold change values of individual HCoV-HKU1-infected-subjects assayed by HKU1 S, NLCt, and NLCt antigen.

| HKU1 subject | HKU1 antigen fold change | | |
|---|---|---|---|
| | **S** | **NLCt** | **NCt** |
| HK-01[c] | **0,13** | **0,66** | **0,53** |
| HK-02 | 0,91 | 1,03 | 1,07 |
| HK-03[a] | **49,57** | **2,16** | **2,67** |
| HK-04[b] | 261,57 | 1,05 | 0,99 |
| HK-05 | 1,53 | 0,97 | 0,96 |
| HK-06[d] | 0,10 | 0,82 | 0,77 |
| HK-07[d] | 0,10 | 0,88 | 1,00 |
| HK-08[b] | 18,82 | 0,87 | 1,12 |
| HK-09 | 1,39 | 0,81 | 0,22 |
| HK-10[a] | **1534,43** | **1,51** | 1,20 |
| HK-11[c] | **0,20** | **0,61** | **0,62** |
| HK-12[a] | **8,22** | **1,44** | 1,11 |
| HK-13[a] | **23,18** | **1,63** | **2,15** |

[a] Subject with fold change by S assay and either of the N assays above the cutoff value (fold change value in black and bold).
[b] Subject with only fold change by S assay above the cutoff value (fold change value in black and underlined).
[c] Subject with fold change by S assay and either of the N assays below the cutoff value (fold change value in red and bold).
[d] Subject with only fold change by S assay below the cutoff value (fold change value in red and underlined).

**TABLE 2** | Demographic data comparison between subjects with infection by endemic HCoVs.

| Demographic[a] | HKU1 $n = 13$ | OC43 $n = 14$ | NL63 $n = 10$ | 229E $n = 13$ |
|---|---|---|---|---|
| Age | **38 (26–56)[e]** | 55 (29–74) | 46.5 (22–64) | 53 (21–75) |
| Male gender | 4 (30.8) | 5 (35.7) | 4 (40) | 6 (46.2) |
| White racial background | 12 (92.3) | 14 (100) | 10 (100) | 13 (100) |
| Smoking past/present | 8 (61.5) | 7 (50) | 2 (20) | 4 (30.8) |
| **Comorbidity** | | | | |
| COPD | 0 | 1 (7.1) | 0 | 2 (15.4) |
| Asthma | 0 | 1 (7.1) | 0 | 2 (15.4) |
| Other lung disease | 0 | 0 | **2 (20)[c]** | 0 |
| Heart failure | 0 | 0 | 0 | 0 |
| Ischemic heart disease | 0 | 0 | 0 | 1 (7.7) |
| Other heart disease | 1 (7.7) | 1 (7.1) | 0 | 1 (7.7) |
| Diabetes | 0 | 0 | 1 (10) | 0 |
| Prev. hospitalization | 1 (7.7) | 0 | 0 | 0 |
| **Symptoms** | | | | |
| Cough | 13 (100) | 14 (100) | 10 (100) | 13 (100) |
| Phlegm | 12 (92.3) | 12 (85.7) | 7 (70) | 9 (69.2) |
| Shortness of breath | 6 (46.2) | 9 (64.3) | 5 (50) | 7 (53.8) |
| Wheezing | 4 (30.8) | 7 (50) | 3 (30) | 2 (15.4) |
| Runny nose | 10 (76.9) | 13 (92.9) | 7 (70) | 11 (84.6) |
| Fever | 3 (23.1) | 7 (50) | 6 (60) | 2 (15.4) |
| Chest pain | 3 (23.1) | 6 (42.9) | 5 (50) | 7 (53.8) |
| Muscle ache | 5 (38.5) | 8 (57.1) | 4 (40) | 5 (38.5) |
| Headache | 9 (69.2) | 9 (64.3) | 7 (70) | 10 (76.9) |
| Disturbed sleep | 5 (38.5) | 8 (57.1) | 8 (80) | 8 (61.5) |
| Feeling generally unwell | 11 (84.6) | 13 (92.9) | 8 (80) | 11 (84.6) |
| Interference of daily activity | **6 (46.2)[c]** | 13 (92.9) | 9 (90) | 11 (84.6) |
| Confusion/disorientation | 0 | 3 (21.4) | 0 | 1 (7.7) |
| Diarrhea | 0 | **4 (28.6)[d]** | 0 | 0 |
| Mean SSS[b] | **0.6 (0.4–1.7)[e]** | 1.1 (0.5–2.1) | 1.3 (0.4–2.4) | 0.9 (0.3–1.4) |
| Duration of prior illness | 7 (1–21) | 5 (2–14) | 3 (1–20) | 4 (2–20) |
| Duration of prior cough | **8 (1–28)[e]** | 5 (2–20) | 3 (1–20) | 4 (1–20) |

[a] Data is presented as either median (age, mean symptom severity score, duration of prior illness, and duration or prior cough, with range between brackets), or frequency (gender, Caucasian ethnicity, presence of comorbidity, and symptom presentation, with percentage between brackets).
[b] Mean symptom score is the average of symptom score for each of the 14 symptoms (0 = no problem, 1 = mild problem, 2 = moderate problem, 3 = severe problem) (Vos et al., 2021). No cutoff of severity was established for this score.
[c] In bold: significance by Fisher's exact test, $p < 0.05$.
[d] In bold: Significance by Fisher's exact test, $p < 0.001$.
[e] In bold: Significance by Mann-Whitney U test, $p < 0.05$.

**TABLE 3 |** Association between demographic categories and S-antibody dynamics in HCoV-HKU1-infected symptoms.

| Demographic categories (13) | S antibody stable (3) | S antibody rise (6) | | S antibody fall (4) | |
|---|---|---|---|---|---|
| | N | N (%) [a] | p-value | N (%) [a] | p-value |
| Age 41 or over (6) | 1 | 2 (33) | 0.592 | 3 (75) | 1 |
| Male (4) | 2 | 1 (17) | 0.559 | 1 (25) | 1 |
| Presence of comorbidity (2) | 1 | 0 | 0.462 | 1 (25) | 1 |
| Smoking past/present (8) | 1 | 5 (83) | 0.266 | 2 (50) | 1 |
| Prior illness ≥ 1 week (8) | 2 | 2 (33) | 0.103 | 4 (100) | 0.105 |
| Prior cough ≥ 1 week (9) | 2 | 4 (67) | 1 | 3 (75) | 1 |
| Phlegm (12) | 3 | 5 (83) | 0.462 | 4 (100) | 1 |
| Shortness of breath (6) | 2 | 2 (33) | 0.592 | 2 (50) | 1 |
| Wheezing (4) | 1 | 0 | 0.070 | 3 (75) | 0.217 |
| Runny nose (10) | 2 | 6 (100) | 0.192 | 2 (50) | 0.203 |
| Fever (3) | 1 | 1 (17) | 1 | 1 (25) | 1 |
| Chest pain (3) | 1 | 0 | 0.192 | 2 (50) | 0.203 |
| Muscle ache (5) | 1 | 2 (33) | 1 | 2 (50) | 1 |
| Headache (9) | 3 | 4 (67) | 1 | 2 (50) | 0.537 |
| Disturbed sleep (5) | 2 | 1 (17) | 0.266 | 3 (75) | 1 |
| Feeling generally unwell (11) | 2 | 6 (100) | 0.462 | 3 (75) | 1 |
| Interference of daily activities (6) | 2 | 3 (50) | 1 | 1 (25) | 0.266 |
| Mean SSS is average[b] or higher (6) | 0 | 3 (50) | 1 | 3 (75) | 0.267 |

[a] To compare the proportion between antibody rise and non-rise, subjects with antibody fall and antibody stable were grouped as non-rise. Similarly, to compare the proportion between fall and non-fall, subjects with antibody rise and antibody stability were coded as non-fall. Fisher's exact test was used to calculate p-value between antibody rise vs. no-rise, as well as between antibody fall vs. no-fall.
[b] The average of a mean symptom score for people with HCoV-HKU1 infection is 0.7 (**Table 2**).

recovered and the PCR test for HCoV-HKU1 was negative. We expressed a protein containing the Ct part and the linker domain of the HCoV-HKU1 N-protein in *E. coli*, to be used as antigen in HKU1-ELISA antibody tests (**Figure 1A** and **Supplementary Figure 1**). V1 and V2 serums were tested using ELISA and the rise or decrease was measured *via* fold change. A V1-V2 fold change of >1.40 represents a significant rise (Edridge et al., 2020). Four of 13 (31%) subjects were presented with a significant V1-V2 NLCt-antibody ELISA signal increase (**Figure 2A**). To investigate whether this low frequency of HKU1-antibody response only occurs for antibodies recognizing the N-protein, we also tested for antibodies recognizing the S protein using the HKU1-S Luminex assay. Six of the 13 (46%) subjects showed a significant S-antibody rise (**Figure 2B**). Curiously, of the other seven samples, more than half (57%, 4 of 7) exhibited a significant decrease in antibodies (fold change values of 0.20 or lower, **Figure 2B** and **Table 1**, values in red). In two of these subjects, HK-01 and HK-11, the fold change values by both HKU1-NLCt and HKU1-NCt antigens were significantly decreased (<0.7) while the other two subjects (HK-06 and HK-07) showed fold change values close to 1 for HKU1-NLCt and HKU1-NCt. One subject (HK-09) showed a decrease with a fold change of 0.22 by HKU1-NLCt antigen ELISA, but the S or NLCt fold change values showed no significant difference (fold change of 1,39 and 0,81, respectively).

We investigated 41 subjects infected by HCoVs other than HCoV-HKU1 (HCoV-NL63 n = 11; HCoV-OC43 n = 14; HCoV-229E n = 16). In 80% (33 of 41) of these subjects, ELISAs using respective NCt antigen showed antibody rises above the cutoff

(**Figure 2A**), and the same was observed in the fold change by the respective S Luminex assay, with significant antibody increase in 35 out of the 41 subjects (**Figure 2B**). In total, the difference of antibody rise/no rise between HCoV-HKU1 and the other HCoVs was significantly distinct for both assays (S-Luminex Fisher's exact test p = 0.025; N-ELISA Fisher's exact test, p = 0.002). Furthermore, none of the NL63, OC43, or 229E-infected subjects presented with significant antibody decreases between V1 and V2.

We subsequently examined whether patient characteristics for the HCoV-HKU1-infected subjects were different compared to the subjects infected by other coronaviruses. The demographic data, including age, gender, ethnicity, smoking history, possible comorbidities (8 items), symptom manifestation at the beginning of the disease (14 items), and estimated duration of prior illness and prior cough, were compared and summarized in **Table 2** for each endemic HCoV. The HKU1-infected subjects tended to be younger than other subjects (median age 38 years for HKU1-infected subjects *versus* 53 years for other subjects; Mann–Whitney *U* test, p = 0.029), but no difference was observed for other demographic characteristics. The vast majority of our study subjects were white, and the possible influence of racial background could thus not be measured in the study.

The HCoV-HKU1 infection was associated with a lower risk of interference with normal daily activities (including work/study, housework, family, and leisure activities, odds ratio (OR) 0.10, 95% confidence interval (CI) 0.02–0.45, p = 0.003). When we corrected for age—given HKU1-infected individuals were slightly younger—a similar association was found (OR

0.04, 95% CI 0.00–0.26, $p$ = 0.002). The subjectively milder symptoms of HCoV-HKU1 infection were also reflected by a significantly lower mean symptom severity score compared to other subjects (median value of 0.6 and 1.1 for HCoV-HKU1-infected subjects and other subjects, respectively, Mann–Whitney $U$ test, $p$ = 0.025). Furthermore, we noticed that more people in the OC43-infected group had diarrhea (Fisher's exact test, $p < 0.001$).

When we looked at all subjects we observed that the symptom severity score was negatively associated with duration of prior illness (Spearman's rho = −0.385, $p$ = 0.006) and also with the duration of prior cough (Spearman's rho = −0.298, $p$ = 0.004). In theory, it could mean that HCoV-HKU1 infected people experienced less interference with daily activity, and therefore waited longer before seeking medical care. If this was the case, the peak in antibody levels could have been close to the date of V1 serum collection. Indeed, a high S-antibody level at V1 was found in three of the four people with a steep decrease in antibodies. This was less visible for the antibodies recognizing the NLCt or NCt (**Supplementary Figures 3**, **4** and **Supplementary Tables 1**, **2**). To test this hypothesis further, we investigated for all HCoVs whether the duration of illness or cough prior to enrollment was associated with antibody dynamics at V2. Across all subjects, we found a significant negative correlation between the duration of prior illness before visiting the GP and the fold change value using the S-Luminex assay as readout (Spearman's rho = −0.280, $p$ = 0.049). Although the number of subjects was low, we also examined three categories of the subject within the HCoV-HKU1 infections (V1–V2 antibody rise, antibody decrease, or stable antibody levels), but observed no significant link between any demographic category, or the duration of disease prior to the GP visit, and HKU1-antibody dynamics (**Table 3**).

## DISCUSSION

Here we report that a substantial portion of people infected by HCoV-HKU1 displays no rise in antibodies following infection. This unusual phenomenon makes HCoV-HKU1 noteworthy, as infections due to HCoV-OC43, HCoV-NL63, and HCoV-229E result in more typical antibody dynamics. We hypothesize that this difference is a result of lower disease severity in HCoV-HKU1 infection. We observed a less pronounced impact on daily life experienced by our HCoV-HKU1-infected subjects. A correlation between a rise in antibodies and disease severity has not been studied for the endemic HCoVs but has been reported for SARS-CoV-2. Higher neutralizing antibody titers were observed in people with more severe disease in comparison to mild cases (Brochot et al., 2020; Ren et al., 2020; Röltgen et al., 2020; Legros et al., 2021). Additionally, the presence of antibodies recognizing N protein is associated with more severe COVID-19 (Sen et al., 2021). The lack of increased antibody titer observed in half of our patients infected with HCoV-HKU1 may thus reflect the mild nature of many HCoV-HKU1 infections.

We also identified cases that showed a significant decline in the HKU1-IgG antibodies. The extended time between the onset of symptoms and GP visits observed for HCoV-HKU1 infected subjects may play a role here. In addition, it could be that HCoV-HKU1 viruses capture virus-specific HKU1-IgGs. This, in combination with a situation where HKU1-specific IgGs are not newly produced, may lead to a decreasing level of HCoV-HKU1 recognizing IgGs. In this situation, it could theoretically be that infection-induced production of secretory IgAs, instead of IgGs, is playing a role in clearing the infection (Callow, 1985; Habibi et al., 2015). Indeed, Gorse et al. found that the prevalence in which secretory IgA was found in the nasal washing of adults with seasonal coronavirus infections were higher for HCoV-HKU1 (31%) than HCoV-OC43, HCoV-229E, and HCoV-NL63 (22, 11, and 8%, respectively) (Gorse et al., 2010). Future research may be considered for testing HKU1-recognizing sIgA in nasopharyngeal samples of HCoV-HKU1-infected subjects, therefore, investigating whether higher sIgA levels are indeed found in people who display no HKU1-specific IgG rise.

By using HKU1-NLCt in our ELISA, we found that two times as many subjects had antibody fold change values above the cutoff, when compared with the previously used HKU1-NCt antigen (Dijkman et al., 2012; Edridge et al., 2020). This indicates that a limited antigenicity may play a role when NCt is used. At the same time, we did not find substantially more cross-reactivity by antibodies induced by HCoV-OC43 infections (data not shown). Since the HKU1-NLCt antigen contains one additional domain, it is tempting to suggest that using the whole N of HCoV-HKU1 may further improve the assay's sensitivity. However, due to its conserved structure, the use of whole HCoV-HKU1 N in ELISA may result in considerable cross-reactivity between HCoV-HKU1 and HCoV-OC43, as has been previously reported (Lehmann et al., 2008).

Our study does have some weaknesses. First, the PCR assay designs for HCoVs were not identical. The HCoV-HKU1 infections were identified using a commercial molecular assay that provided no information on the virus load, whereas the other HCoVs were diagnosed *via* quantitative PCRs developed in-house (Loens et al., 2012). The NL63-, OC43-, and 229E-infections all scored Ct values below 30; however, we could not identify the virus concentration in the nasopharyngeal swabs from HCoV-HKU1 infections. Secondly, we were not able to determine the HKU1 genotypes infecting our subjects. There are at least three co-circulating genotypes of HCoV-HKU1: genotypes A, B, and C (Woo et al., 2006), and it is possible that the genotypes of HCoV-HKU1 in our cohort did not match with the genotype used for the ELISA test. However, we observed similar findings for both S and N antigens, and these antigens were derived from different HCoV-HKU1 genotypes, with the NCt and NLCt antigens expressed from isolate Caen1 (genotype A), and the S antigen expressed from isolate N5 (genotype C). Furthermore, similar to HCoV-HKU1, HCoV-OC43 and HCoV-NL63 also have several co-circulating genotypes. If a mismatch between ELISA antigen and infecting genotype would result in false-negative responses, this is likely to have also occurred for HCoV-OC43 and HCoV-NL63.

In conclusion, we demonstrate that an HKU1-specific-IgG rise is a poor marker of an HCoV-HKU1 infection. These findings contribute to explaining the low detectability of HCoV-HKU1

infections by serology, and we may consider HCoV-HKU1 to be an interesting atypical endemic coronavirus.

## DATA AVAILABILITY STATEMENT

The original contributions presented in the study are included in the article/**Supplementary Material**, further inquiries can be directed to the corresponding author.

## ETHICS STATEMENT

The studies involving human participants were reviewed and approved by Cardiff and Southampton (United Kingdom): Southampton & South West Hampshire Research Ethics Committee A; Utrecht (Netherlands): Medisch Etische Toetsingcommissie Universitair Medisch Centrum Utrecht; Barcelona (Spain): Comité Étic d'Investigació Clínica Hospital Clínic de Barcelona; Mataro (Spain): Comitè d'Ètica d'Investigació Clínica (CEIC) del Consirci Sanitari del Maresme; Rotenburg (Germany): Ethik-Komission der Medizinischen Fakultät der Georg-August-Universitat Göttingen; Antwerp (Belgium): UZ Antwerpen Comité voor Medische Ethiek; Lodz, Szeczecin and Bialystok (Poland): Komisja Bioetyki Uniwersytetu Medycznego W Lodzi; Milano (Italy):IRCCS Fondazione Cà Granda Policlinico; Jonkoping (Sweden): Regionala etikprövningsnämden I Linköping; Bratislava (Slovakia): Etika Komisia Bratislavskeho; Gent (Belgium): Ethisch Comité Universitair Ziekenhuis Gent; Nice (France): Comité de Protection des Personnes Sud-Méditerranée II, Hôpital Salvator; and Jesenice (Slovenia): Komisija Republike Slovenije za Medicinsko Etiko. The patients/participants provided their written informed consent to participate in this study.

## AUTHOR CONTRIBUTIONS

FS and LH designed the research and wrote and edited the manuscript. MJ and MGi provided key antigens and methodology. KL, MI, HG, and SH-G were involved in the larger GRACE observation study, extracted clinical information from the database, and provided clinical samples. FS, MGr, and AE collected the data. FS performed the statistical analysis and visualized the data. LH supervised the experiments and validate the data. All authors contributed to manuscript revision and read and approved the submitted version.

## SUPPLEMENTARY MATERIAL

The Supplementary Material for this article can be found online at: https://www.frontiersin.org/articles/10.3389/fmicb.2022.853410/full#supplementary-material

## REFERENCES

Al-Khannaq, M. N., Ng, K. T., Oong, X. Y., Pang, Y. K., Takebe, Y., Chook, J. B., et al. (2016). Molecular epidemiology and evolutionary histories of human coronavirus OC43 and HKU1 among patients with upper respiratory tract infections in Kuala Lumpur, Malaysia. *Virol. J.* 13, 1–12. doi: 10.1186/s12985-016-0488-4

Brochot, E., Demey, B., Touzé, A., Belouzard, S., Dubuisson, J., Schmit, J. L., et al. (2020). Anti-spike, anti-nucleocapsid and neutralizing antibodies in sars-cov-2 inpatients and asymptomatic individuals. *Front. Microbiol.* 11:584251. doi: 10.3389/fmicb.2020.584251

Brouwer, P. J. M., Brinkkemper, M., Maisonnasse, P., Dereuddre-Bosquet, N., Grobben, M., Claireaux, M., et al. (2021). Two-component spike nanoparticle vaccine protects macaques from SARS-CoV-2 infection. *Cell* 184, 1188.e–1200.e. doi: 10.1016/j.cell.2021.01.035

Callow, K. A. (1985). Effect of specific humoral immunity and some non-specific factors on resistance of volunteers to respiratory coronavirus infection. *J. Hyg. Camb.* 95, 173–189. doi: 10.1017/S0022172400062410

Cui, J., Li, F., and Shi, Z. L. (2019). Origin and evolution of pathogenic coronaviruses. *Nature Rev. Microbiol.* 17, 181–192. doi: 10.1038/s41579-018-0118-9

Dijkman, R., Jebbink, M. F., El Idrissi, N. B., Pyrc, K., Müller, M. A., Kuijpers, T. W., et al. (2008). Human coronavirus NL63 and 229E seroconversion in children. *J. Clin. Microbiol.* 46, 2368–2373. doi: 10.1128/JCM.00533-08

Dijkman, R., Jebbink, M. F., Gaunt, E., Rossen, J. W. A., Templeton, K. E., Kuijpers, T. W., et al. (2012). The dominance of human coronavirus OC43 and NL63 infections in infants. *J. Clin. Virol.* 53, 135–139. doi: 10.1016/j.jcv.2011.11.011

Edridge, A. W. D., Kaczorowska, J., Hoste, A. C. R., Bakker, M., Klein, M., Loens, K., et al. (2020). Seasonal coronavirus protective immunity is short-lasting. *Nat. Med.* 26, 1691–1693. doi: 10.1038/s41591-020-1083-1

Galanti, M., and Shaman, J. (2020). Direct observation of repeated infections with endemic coronaviruses. *J. Infect. Dis.* 1–7. doi: 10.1093/infdis/jiaa392

Gorse, G. J., Patel, G. B., Vitale, J. N., and O'Connor, T. Z. (2010). Prevalence of antibodies to four human coronaviruses is lower in nasal secretions than in serum. *Clin. Vaccine Immunol.* 17, 1875–1880. doi: 10.1128/CVI.00278-10

Grobben, M., van der Straten, K., Brouwer, P. J., Brinkkemper, M., Maisonnasse, P., Dereudde-Bosquet, N., et al. (2021). Cross-reactive antibodies after SARS-CoV-2 infection and vaccination. *eLife* 10:e70330. doi: 10.7554/eLife.70330

Habibi, M. S., Jozwik, A., Makris, S., Dunning, J., Paras, A., DeVincenzo, J. P., et al. (2015). Impaired antibody-mediated protection and defective iga B-cell memory in experimental infection of adults with respiratory syncytial virus. *Am. J. Respir. Crit. Care Med*. 191, 1040–1049. doi: 10.1164/rccm.201412-2256OC

Ieven, M., Coenen, S., Loens, K., Lammens, C., Coenjaerts, F., Vanderstraeten, A., et al. (2018). Aetiology of lower respiratory tract infection in adults in primary care: a prospective study in 11 European countries. *Clin. Microbiol. Infect*. 24, 1158–1163. doi: 10.1016/j.cmi.2018.02.004

Keuning, M. W., Grobben, M., de Groen, A.-E. C., Berman-De Jong, E. P., Bijlsma, M. W., Cohen, S., et al. (2021). Saliva SARS-CoV-2 antibody prevalence in children. *Microbiol. Spectr*. 9:e0073121. doi: 10.1128/Spectrum.00731-21

Killerby, M. E., Biggs, H. M., Haynes, A., Dahl, R. M., Mustaquim, D., Gerber, S. I., et al. (2018). Human coronavirus circulation in the united states 2014–2017. *J. Clin. Virol*. 101, 52–56. doi: 10.1016/j.jcv.2018.01.019

Kirchdoerfer, R. N., Cottrell, C. A., Wang, N., Pallesen, J., Yassine, H. M., Turner, H. L., et al. (2016). Pre-fusion structure of a human coronavirus spike protein. *Nature* 531, 118–121. doi: 10.1038/nature17200

Legros, V., Denolly, S., Vogrig, M., Boson, B., Siret, E., Rigaill, J., et al. (2021). A longitudinal study of SARS-CoV-2-infected patients reveals a high correlation between neutralizing antibodies and COVID-19 severity. *Cell. Mol. Immunol*. 18, 318–327. doi: 10.1038/s41423-020-00588-2

Lehmann, C., Wolf, H., Xu, J., Zhao, Q., Shao, Y., Motz, M., et al. (2008). A line immunoassay utilizing recombinant nucleocapsid proteins for detection of antibodies to human coronaviruses. *Diagn. Microbiol. Infect. Dis*. 61, 40–48. doi: 10.1016/j.diagmicrobio.2007.12.002

Liang, F. Y., Lin, L. C., Ying, T. H., Yao, C. W., Tang, T. K., Chen, Y. W., et al. (2013). Immunoreactivity characterisation of the three structural regions of the human coronavirus OC43 nucleocapsid protein by western blot: Implications for the diagnosis of coronavirus infection. *J. Virol. Methods* 187, 413–420. doi: 10.1016/j.jviromet.2012.11.009

Liu, W. K., Liu, Q., De Chen, H., Liang, H. X., Chen, X. K., Chen, M. X., et al. (2014). Epidemiology of acute respiratory infections in children in guangzhou: a three-year study. *PLoS ONE* 9:e96674. doi: 10.1371/journal.pone.0096674

Loens, K., Van Loon, A. M., Coenjaerts, F., Van Aarle, Y., Goossens, H., Wallace, P., et al. (2012). Performance of different mono- and multiplex nucleic acid amplification tests on a multipathogen external quality assessment panel. *J. Clin. Microbiol*. 50, 977–987. doi: 10.1128/JCM.00200-11

Mackay, I. M., Arden, K. E., Speicher, D. J., O'Neil, N. T., McErlean, P. K., Greer, R. M., et al. (2012). Co-circulation of four human coronaviruses (HCoVs) in Queensland children with acute respiratory tract illnesses in 2004. *Viruses* 4, 637–653. doi: 10.3390/v4040637

Madeira, F., Park, Y. M., Lee, J., Buso, N., Gur, T., Madhusoodanan, N., et al. (2019). The EMBL-EBI search and sequence analysis tools APIs in 2019. *Nucleic Acids Res*. 47, W636–W641. doi: 10.1093/nar/gkz268

Masse, S., Capai, L., Villechenaud, N., Blanchon, T., Charrel, R., and Falchi, A. (2020). Epidemiology and clinical symptoms related to seasonal coronavirus identified in patients with. *Viruses* 12, 1–17. doi: 10.3390/v12060630

McBride, R., van Zyl, M., and Fielding, B. C. (2014). The coronavirus nucleocapsid is a multifunctional protein. *Viruses* 6, 2991–3018. doi: 10.3390/v6082991

Mourez, T., Vabret, A., Han, Y., Dina, J., Legrand, L., Corbet, S., et al. (2007). Baculovirus expression of HCoV-OC43 nucleocapsid protein and development of a western blot assay for detection of human antibodies against HCoV-OC43. *J. Virol. Methods* 139, 175–180. doi: 10.1016/j.jviromet.2006.09.024

Nickbakhsh, S., Ho, A., Marques, D. F. P., McMenamin, J., Gunson, R. N., Murcia, P. R., et al. (2020). Epidemiology of seasonal coronaviruses: establishing the context for the emergence of coronavirus disease 2019. *J. Infect. Dis*. 222, 17–25. doi: 10.1093/infdis/jiaa185

Petrie, J. G., Bazzi, L. A., McDermott, A. B., Follmann, D., Esposito, D., Hatcher, C., et al. (2021). Coronavirus occurrence in the household influenza vaccine evaluation (HIVE) cohort of michigan households: reinfection frequency and serologic responses to seasonal and severe acute respiratory syndrome coronaviruses. *J. Infect. Dis*. 1–11. doi: 10.1093/infdis/jiab161

Ren, L., Zhang, L., Chang, D., Wang, J., Hu, Y., Chen, H., et al. (2020). The kinetics of humoral response and its relationship with the disease severity in COVID-19. *Commun. Biol*. 3. doi: 10.1038/s42003-020-01526-8

Röltgen, K., Powell, A. E., Wirz, O. F., Stevens, B. A., Hogan, C. A., Najeeb, J., et al. (2020). Defining the features and duration of antibody responses to SARS-CoV-2 infection associated with disease severity and outcome. *Sci. Immunol*. 5, eabe0240. doi: 10.1126/SCIIMMUNOL.ABE0240

Sastre, P., Dijkman, R., Camuñas, A., Ruiz, T., Jebbink, M. F., Van Der Hoek, L., et al. (2011). Differentiation between human coronaviruses NL63 and 229E using a novel double-antibody sandwich enzyme-linked immunosorbent assay based on specific monoclonal antibodies. *Clin. Vaccine Immunol*. 18, 113–118. doi: 10.1128/CVI.00355-10

Sen, S. R., Sanders, E. C., Gabriel, K. N., Miller, B. M., Isoda, H. M., Salcedo, G. S., et al. (2021). Predicting COVID-19 Severity with a specific nucleocapsid antibody plus disease risk factor score. *mSphere* 6:e00203-21. doi: 10.1128/mSphere.00203-21

Severance, E. G., Bossis, I., Dickerson, F. B., Stallings, C. R., Origoni, A. E., Sullens, A., et al. (2008). Development of a nucleocapsid-based human coronavirus immunoassay and estimates of individuals exposed to coronavirus in a U.S. metropolitan population. *Clin. Vaccine Immunol*. 15, 1805–1810. doi: 10.1128/CVI.00124-08

Vabret, A., Dina, J., Gouarin, S., Petitjean, J., Tripey, V., Brouard, J., et al. (2008). Human (non-severe acute respiratory syndrome) coronavirus infections in hospitalised children in France. *J. Paediatr. Child Health* 44, 176–181. doi: 10.1111/j.1440-1754.2007.01246.x

Vos, L. M., Bruyndonckx, R., Zuithoff, N. P. A., Little, P., Oosterheert, J. J., Broekhuizen, B. D. L., et al. (2021). Lower respiratory tract infection in the community: associations between viral aetiology and illness course. *Clin. Microbiol. Infect*. 27, 96–104. doi: 10.1016/j.cmi.2020.03.023

Woo, P. C. Y., Lau, S. K. P., Chu, C., Chan, K., Tsoi, H., Huang, Y., et al. (2005). Characterization and complete genome sequence of a novel coronavirus, coronavirus HKU1, from Patients with Pneumonia. *J. Virol*. 79, 884–895. doi: 10.1128/jvi.79.2.884-895.2005

Woo, P. C. Y., Lau, S. K. P., Yip, C. C. Y., Huang, Y., Tsoi, H.-W., Chan, K.-H., et al. (2006). Comparative analysis of 22 coronavirus hku1 genomes reveals a novel genotype and evidence of natural recombination in coronavirus hku1. *J. Virol*. 80, 7136–7145. doi: 10.1128/jvi.00509-06

Yip, C. C. Y., Lam, C. S. F., Luk, H. K. H., Wong, E. Y. M., Lee, R. A., So, L. Y., et al. (2016). A six-year descriptive epidemiological study of human coronavirus infections in hospitalized patients in Hong Kong. *Virol. Sin*. 31, 41–48. doi: 10.1007/s12250-016-3714-8

Zhou, R., Zeng, R., von Brunn, A., and Lei, J. (2020). Structural characterization of the C-terminal domain of SARS-CoV-2 nucleocapsid protein. *Mol. Biomedicine* 1, 1–11. doi: 10.1186/s43556-020-00001-4

Zhou, W., Wang, W., Wang, H., Lu, R., and Tan, W. (2013). First infection by all four non-severe acute respiratory syndrome human coronaviruses takes place during childhood. *BMC Infectious Diseases* 13:433. doi: 10.1186/1471-2334-13-433

# A Mouse-Adapted Model of HCoV-OC43 and Its Usage to the Evaluation of Antiviral Drugs

Peifang Xie[1†], Yue Fang[1†], Zulqarnain Baloch[1], Huanhuan Yu[1], Zeyuan Zhao[1], Rongqiao Li[1], Tongtong Zhang[1], Runfeng Li[2], Jincun Zhao[2], Zifeng Yang[2], Shuwei Dong[1]* and Xueshan Xia[1]*

[1]The Affiliated AnNing First Hospital, Faculty of Life Science and Technology, Kunming University of Science and Technology, Kunming, China, [2]State Key Laboratory of Respiratory Disease, National Clinical Research Center for Respiratory Disease, Guangzhou Institute of Respiratory Health, The First Affiliated Hospital of Guangzhou Medical University, Guangzhou, China

The human coronavirus OC43 (HCoV-OC43) is one of the most common causes of common cold but can lead to fatal pneumonia in children and elderly. However, the available animal models of HCoV-OC43 did not show respiratory symptoms that are insufficient to assist in screening antiviral agents for respiratory diseases. In this study, we adapted the HCoV-OC43 VR-1558 strain by serial passage in suckling C57BL/6 mice and the resulting mouse-adapted virus at passage 9 (P9) contained 8 coding mutations in polyprotein 1ab, spike (S) protein, and nucleocapsid (N) protein. Pups infected with the P9 virus significantly lost body weight and died within 5 dpi. In cerebral and pulmonary tissues, the P9 virus replication induced the production of G-CSF, IFN-γ, IL-6, CXCL1, MCP-1, MIP-1α, RANTES, IP-10, MIP-1β, and TNF-α, as well as pathological alterations including reduction of neuronal cells and typical symptoms of viral pneumonia. We found that the treatment of arbidol hydrochloride (ARB) or Qingwenjiere Mixture (QJM) efficiently improved the symptoms and decreased n gene expression, inflammatory response, and pathological changes. Furthermore, treating with QJM or ARB raised the P9-infected mice's survival rate within a 15 day observation period. These findings suggested that the new mouse-adapted HCoV-OC43 model is applicable and reproducible for antiviral studies of HCoV-OC43.

Keywords: human coronavirus OC43, adaptation, mouse model, respiratory disease, model application

## INTRODUCTION

Coronaviruses (CoVs) are positive-strand RNA viruses with a genome of 30 kb in length, prone to mutation, and recombination, leading to frequent viral evolution and infecting a wide range of hosts (Lai, 1992; Woo et al., 2010). They belong to the subfamily *Orthocoronavirinae* which has been divided into four genera (*alpha, beta, delta, and gammacoronavirus*). Seven strains of CoVs known to be susceptible to humans (namely, as HCoVs) are limited to the *alpha* (HCoV-229E and HCoV-NL63) and *beta* (HCoV-OC43, HCoV-HKU1, SARS-CoV, MERS, and SARS-CoV-2) genera (Malik, 2020). Among them, HCoV-OC43 is one of the most common causes of common colds in the general population. Like other CoVs, the first two-thirds of the genome

of HCoV-OC43 contain open reading frames (ORFs) 1a and 1b, which are translated by ribosomal frameshifting to generate poly protein pp1ab, and the pp1ab is processed into non-structural proteins (NSP1-16) to form the replicasetranscriptase complex (RTC). Downstream of ORF1b, there are ORFs encoding structural and accessory proteins (Vijgen et al., 2005; Fehr and Perlman, 2015). The Spike (S) protein, one of the most important structural proteins of HCoV-OC43, is involved in virus attachment and entry processes and plays an important role in virus pathogenicity and host tropism (Peng et al., 2012; Song et al., 2020). Mutations in S protein were thought to be the primary reason for cross-species transmission and virus evolution (Peng et al., 2012). Besides, the hemagglutinin-esterase (He) specifically acts on 9-O-acetylated sialic acids to remove acetyl groups, aid in receptor binding and viral release, and promote efficient viral replication by balancing viral attachment and release (Lang et al., 2020). The nucleocapsid (N) protein, another significant structural protein, encapsulates the viral RNA and, along with NSPs, plays a crucial role in virus replication, transcriptional processes, and genome assembly (Abdel-Moneim et al., 2021). The frequent virus evolution has an impact on the adaptation of viruses to specific hosts (Coleman and Frieman, 2014).

Apart from mild upper respiratory tract symptoms, HCoV-OC43 infection in infants, the elderly, or immune-compromised adults would cause fatal encephalitis or severe lower respiratory tract illness, including bronchiolitis, asthma, and pneumonia (Vabret et al., 2003; Morfopoulou et al., 2016). It has been reported that the primary pathological mechanism of HCoV infection is the interaction between the virus and the host, which would lead to a severe immune response (de Wilde et al., 2018). The occurrence of a storm of pro-inflammatory cytokines results in tissue damage (Vabret et al., 2006; de Wilde et al., 2018). Moreover, endemic infection of HCoVs (OC43, HKU1, NL63, and 229E) caused fatalities in healthy adults and HCoV-OC43 (hazard ratio, 2.50) was substantially linked with coronavirus death (Kim et al., 2021; Veiga et al., 2021). Although there have not yet been a significant number of severe cases worldwide, the importance of including HCoVs in diagnostic panels used by official surveillance systems and the necessity of more cautious treatment for coronavirus patients has been increasingly recognized by researchers (Kim et al., 2021; Veiga et al., 2021). These studies suggest that anti-inflammatory and antiviral research are both necessary for the development of antiviral therapeutics for HCoV infections.

There are no specific antiviral therapies available for HCoV-OC43 and other HCoVs (Rajapakse and Dixit, 2021). Qingwenjiere Mixture (QJM) is a Traditional Chinese Medicine (TCM) compound with clinical efficacy against SARS-CoV-2, and we previously proved that it was effective against *in vitro* infection of SARS-CoV-2, HCoV-OC43, HCoV-229E, and HCoV-NL63

(Xie et al., 2021). Arbidol hydrochloride (ARB), a well-known broad-spectrum antiviral compound, was widely used in clinical anti-respiratory virus therapy (Blaising et al., 2014). It is effective against COVID-19 in clinical practice as well as being demonstrated to have an antiviral effect against the HCoV-OC43 virus *in vitro* (Nojomi et al., 2020; Leneva et al., 2021). However, the efficacy of QJM and ARB against *in vivo* HCoV-OC43 infection is unconfirmed. Animal models are useful for studying viral pathogenesis and evaluating antiviral and vaccine candidates. A few animal models for HCoV-OC43 infection have been developed, but it is unknown whether the infection causes lung inflammation or respiratory illness in these animals and hinders the screening of antiviral medicines (Butler et al., 2006; Keyaerts et al., 2009). Here, we made a new mouse-adapted HCoV-OC43 model with typical pulmonary disease symptoms and looked into how it could be used in pathogenesis studies and drug testing.

## MATERIALS AND METHODS

### Ethical Statement
Animal experiments were carried out in accordance with the Chinese Laboratory Animal Regulations (Ministry of Science and Technology of the People's Republic of China) and the National Laboratory Animal Standardization Technical Committee. The Animal Experiment Committee at Kunming University of Science and Technology in China approved this study, and the approval number is PZWH (Dian) K2020-0013.

### Viruses, Animals, and Drugs
The wild type of HCoV-OC43 VR-1558 was provided by Prof. Jincun Zhao (Guangzhou Medical University) and propagated in HRT-18 cells (ATCC CCL-244). The titer of viral stock was determined using the Reed–Muench method with a 50% tissue culture infective dose ($TCID_{50}$) based on cytopathic effect of HRT-18 cells. Specified pathogen-free (SPF) C57BL/6 mice were purchased from the Experimental Animal Center of Kunming Medical University. Suckling mice weighing 4–6 g within 10 days of birth with no distinction between males and females were used for subsequent viral inoculation and *in vivo* evaluation of drug efficacy. Arbidol hydrochloride tablets (ARB, 0.1 g per tablet) were purchased from CSPC Ouyi Pharmaceutical Co., Ltd. Qinwenjiere Mixture (QJM) was provided by Chinese medicine hospitals in Yunnan Province with an original concentration of 600 mg/ml. These drugs were dissolved in pure water and diluted to specific concentrations before usage.

### Serial Passage of HCoV-OC43 in Suckling C57BL/6 Mice
Suckling mice, 3–5 mice per group, were intracerebrally injected with 25 μl of the wild type of HCoV-OC43 VR-1558 virus (100$TCID_{50}$, equals to $2.5 \times 10^7$ copies), and the normal control group mice received the same volume of sterile PBS. Animals were sacrificed at 1, 2, 3, 4, and 5 days post-infection (dpi). Lung and brain tissues were collected and homogenized in sterile PBS

with a weight to volume ratio of 1:10 and clarified by centrifugation. Viral RNA was extracted from 140 μl of the supernatant with the E.Z.N.A. Viral RNA Extraction 162 R6874-02 (Omega Bio-Tek, United Kingdom) kit. The expression of OC43 nucleocapsid (*n*) genes was determined by quantitative real-time RT-PCR (qRT-PCR) as described below, followed by selecting one brain tissue filtrate that had a higher viral load at 4 dpi for further intracerebral inoculation, in which the final copy number of the inoculated virus was $10^6$ copies/μl (data not shown). Each generation of the OC43 strain was used for gene sequencing. The clarified supernatant was stored at −80°C. Partial results of this part are shown in **Figure 1** and **Supplementary Table 2**.

## Sequence Analysis

For sequence analysis of *s* and *Hemagglutinin-esterase* (*He*) genes, viral RNA from brain samples infected with WT to P9 viruses was reverse transcribed to cDNA by using the PrimeScript™ RT Master Mix Kit (Takara Bio, Japan). For genome sequence analysis, viral RNA from brain samples infected with WT and P9 viruses was transcribed *via* aforementioned method. Viral genes were amplified with the high-fidelity Taq enzyme (Vazyme) with corresponding primers (**Supplementary Table 1**). The sequences in 5′ and 3′ untranslated regions (UTR) were amplified with the SMARTer RACE 5′/3′ Kit (Takara Bio, Japan) according to the instruction. The purified PCR products with expected fragment sizes were sequenced by Tsingke Biological Technology Co., Ltd. Sequences were analyzed and assembled with SeqMan software (DNAStar Inc., Madison, WI, United States) and Mega software (Mega RAID SAS9240-8i, United States).

## Determination of the Median Lethal Dose of Suckling Mice (SMLD$_{50}$) for P9 and WT Viruses

For the P9 virus, suckling mice were randomly divided into 7 groups, including $10^{-2}$, $10^{-3}$, $10^{-4}$, $10^{-5}$, $10^{-6}$, and $10^{-7}$ and normal control group, with 10 suckling mice per group. P9 stock was successively diluted into $10^{-2}$, $10^{-3}$, $10^{-4}$, $10^{-5}$, $10^{-6}$, and $10^{-7}$ in serial log10 dilutions. In the corresponding groups, each dilution was intracerebrally inoculated with mice for 25 μl per mouse. Animals in the normal control group received the same volume of sterile PBS. The mortality rate was recorded daily for 15 consecutive days, and the SMLD50 of P9 was calculated using the Reed-Muench method. Virus titers were expressed as the reciprocal of the virus suspension's highest dilution at which 50% of inoculated suckling mice died (SMLD$_{50}$; Reed and Muench, 1938). The SMLD$_{50}$ of WT was determined by a similar procedure.

## Grouping and Modeling of Mice

Suckling mice were randomly divided into three groups: the normal control group, the wild strain group (WT), and the adapted strain group (P9) to compare the characteristics of WT and P9 viruses. Each mouse in the WT and P9 groups received 1000SMLD$_{50}$ of WT or P9 virus intracerebrally. Animals in normal control group were injected with 25 μl sterile PBS per mouse. Experiments were conducted as follows:

a. Mortality and morbidity study (10 mice per group): The symptoms, body weight, and survival time were monitored regularly for 15 days. Individuals who died within 24 h of infection were categorized as abnormal deaths, and the mean survival time (days) of each group was calculated (Smee et al., 2010).

b. The proliferation kinetics of the P9 virus in brain and lung samples (21 mice per group): After fasting for 2 h, the suckling mice were inoculated. At 12, 24, 36, 48, 72, 96, and 120 hpi, the mice were sacrificed and the copy number of OC43 *n* gene in brain and lung tissues was detected by qRT-PCR.

c. Examination of the organ index changes and OC43 *n* gene copy number at 4 dpi (4 mice per group): suckling mice were anaesthetized and sacrificed at 4 dpi to dissect the brain, heart, liver, spleen, lung, and kidney. The organ tissues and the mouse body were weighed to calculate the organ indexes. The organ tissues were, respectively, homogenized with sterile PBS for qRT-PCR detection of the copy number of OC43 *n* gene (CT value of >35 was considered negative).

d. Changes in organ index and the copy number OC43 *n* gene expression at 5 dpi (P9) and 8 dpi (WT): At 5 dpi, three mice in the normal control group and four mice in the P9 group were sacrificed, while the other three normal control mice and three WT-infected suckling mice were sacrificed at 8 dpi. The brain and lung indices and the OC43 *n* gene expression were detected.

e. OC43 N protein expression in organs and the histopathological changes of suckling mice (3–5 mice per group, but nine mice per control group): At 3 and 4 dpi, the whole tissues from the P9 group were fixed with 4% formalin for histopathological and immunohistochemical detection. The control and WT groups were analyzed by a similar procedure at 3, 4, and 8 dpi.

f. The detection of the production of inflammatory cytokines and chemokines: For the WT group, the brain and lung tissues were harvested at 0.5, 4, and 8 dpi, while the tissues of P9-infected mice were collected at 0.5 and 4 dpi. The homogenized brain and lung samples were used to detect pro-inflammatory factors produced by the Bio-plex assay.

g. The detection of P9 infection rate: suckling mice were divided into normal control group and P9 group. 80 mice were individually challenged with 1000SMLD$_{50}$ of P9 virus, while 10 mice in the control group received the same volume of sterile PBS. At 4 dpi, the entire brains and lungs from these two groups were isolated and homogenized with sterile PBS for qRT-PCR detection of the expression of OC43 *n* gene.

h. Evaluation of *in vivo* efficacy of ARB and QJM against P9 infection: the suckling mice were divided into 6 groups, including the normal control group, the P9 group, and four drug intervention groups, namely, ARB 25 mg·kg$^{-1}$·d$^{-1}$ and QJM high-, medium-, and low-dose groups (QJM 600 mg·kg$^{-1}$·d$^{-1}$, 300 mg·kg$^{-1}$·d$^{-1}$, and 150 mg·kg$^{-1}$·d$^{-1}$). Mice in P9 and drug intervention groups were individually challenged with 1000SMLD$_{50}$ of P9 virus, and the normal control group animals received the same volume of sterile PBS. At 2 hpi, P9-infected mice were, respectively, given
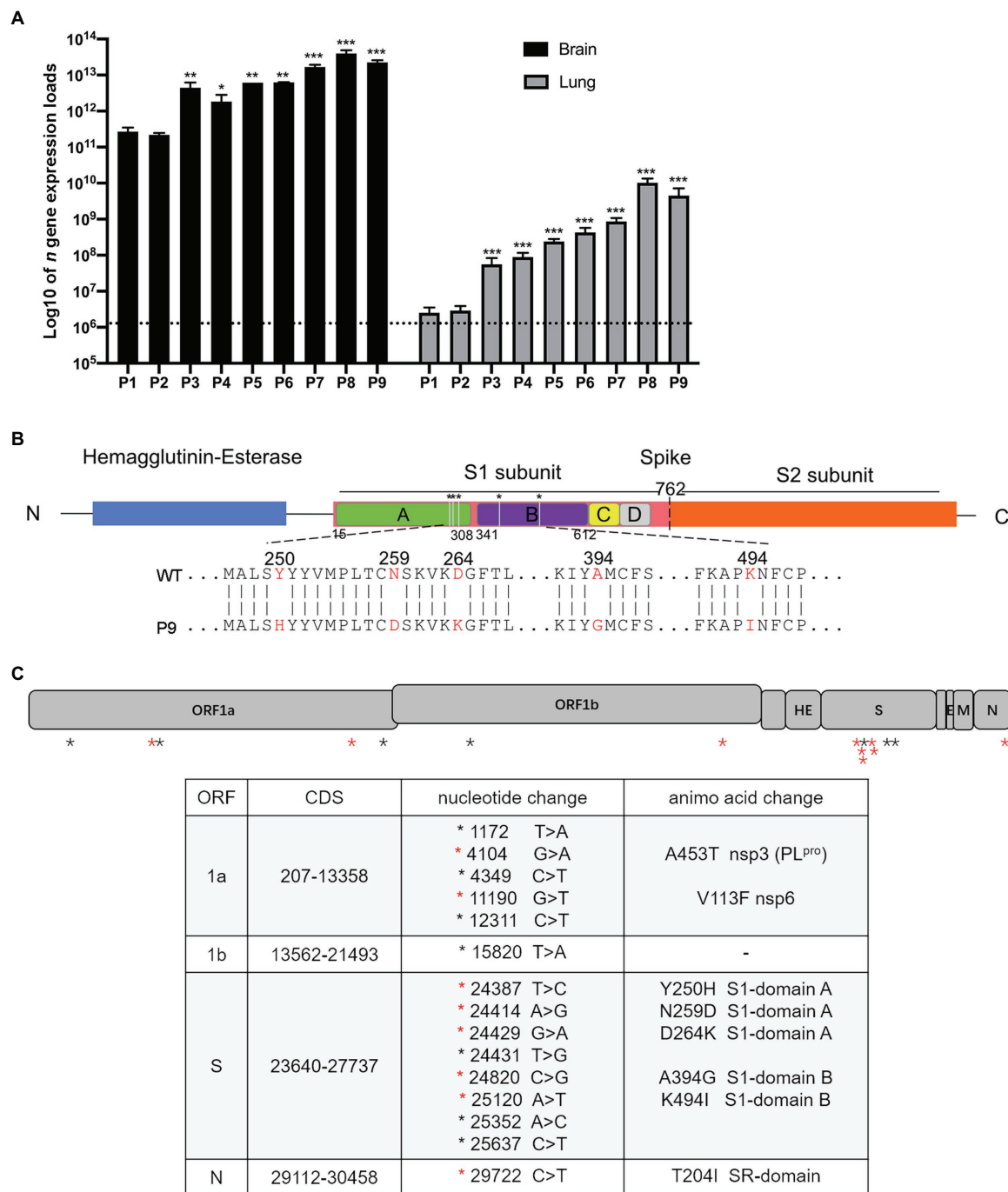
**FIGURE 1** | The expression of viral *n* gene in the brain and lungs of a series generations of mice and mutation sites between wild and adapted strains. **(A)** The expression of viral *n* gene in the brain and lung was detected at 4 dpi ($n = 3$–5). The data are presented as the log10 of the expression of viral *n* gene (copies/g), the mean and the standard error of the mean (SEM). $*p < 0.05$; $**p < 0.01$; and $***p < 0.001$; vs. P1. **(B)** A schematic representation of the HCoV-OC43-1558 HE and S proteins (drawn to scale) and the five amino acid substitutions. The hemagglutinin-esterase protein is colored in blue, the S1 subunit and S2 subunit of S protein are colored in pink and orange, respectively, and the S1 domains A, B, C, and D are colored in green, purple, yellow, and gray, respectively. The substitution of Y250H, N259D, and D264K are located in domain A of the S1 subunit, while A394G and K494I are located in domain B. **(C)** Schematic diagram of HCoV-OC43 genome indicating mutations found in P9 virus. (Top) The 30,746 nucleotide RNA genome of HCoV-OC43 is shown in this to scale drawing with ORFs indicated by gray boxes. Black asterisks indicate nucleotide mutations which did not result in coding changes. Red asterisks indicate nucleotide mutations resulting in coding changes. (Bottom) The 15 nucleotide mutations resulted in 8 coding changes in ORF1a, S, and N, respectively.

$25\,mg\cdot kg^{-1}\cdot d^{-1}$ of ARB and 600, 300, $150\,mg\cdot kg^{-1}\cdot d^{-1}$ of QJM *via* oral administration with $100\,\mu l$/mouse/day for 4 days. The examination was conducted as follows:

1. The effects of drugs on morbidity and mortality (10 mice per group): After the above-mentioned intervention procedure, the symptoms, body weight, survival time, and survival number of mice were recorded on a daily basis for 15 consecutive days. The survival curve was calculated (Smee et al., 2010).
2. At 4 dpi, the animals (10 mice per group) were sacrificed to isolate their entire brains and lungs. The organ indexes, the copy number of viral *n* gene, inflammation responses, and pathological changes of infected pups were analyzed as mentioned below.

## Organ Index Calculation and Quantitative Real-Time RT-PCR (qRT-PCR) Detection of the Expression of Viral *N* Gene

The organ indices were calculated as a ratio of organ weight (g) to body weight (g) multiplied by 100%. Viral RNA was extracted from the tissue samples as mentioned above, and $2\,\mu l$ of viral RNA was reverse transcribed and amplified using the One Step PrimeScript™ RT-PCR Kit (Takara Bio, Japan). The amplification was carried out using an Applied Biosystems 7,500 Real-Time PCR System. Data were recorded by the 7,500 Real-Time PCR software and expressed as a function of Threshold Cycle (CT). The *n* gene of HCoV-OC43 was cloned into pEASY-T1 cloning vector 165 (**Supplementary Table 1**, Trans Gen Biotech, China) and the plasmid was used to generate the standard curve to calculate the copy number of the OC43 *n* gene (Chan et al., 2020). The OC43 *n* gene expression was calculated as $copies/g = 10^{\wedge [(41.248-Ct)/3.281]} \times 0.429 \times volume/organ$ weight (g), with a CT value greater than 35 considered negative.

## Detection of the Production of Inflammatory Cytokines/Chemokines by Bio-Plex Assay

Brain and lung tissues were homogenized as mentioned above and stored at $-80°C$ before further analysis. Prior to detection, the samples were thawed on ice, clarified by centrifugation at $4°C$ for 10 min at 10,000 rpm/min, and the supernatant was collected. The protein concentration in the supernatants was measured using the Pierce BCA Protein Assay kit [Thermo Fisher Scientific (China) Co., Ltd.] according to the manufacturer's protocol. All samples were adjusted to the same concentration. The concentration of cytokines and chemokines in the supernatants of tissue homogenates was measured by the Bio-Plex Pro-Mouse Cytokine assay using the Bio-Plex 200 Multiplex Testing System (Bio-Rad, United States) according to the manufacturer's protocol. The data were analyzed using Bio-Plex Manager software (version 5.0; Bio-Rad, Labs).

## Histopathology and Immunohistochemistry

The whole brain and lung samples from each group were dissected at the indicated times and fixed with 4% paraformaldehyde for 24h, then dehydrated with ethanol, permeated with xylene, embedded with paraffin, and sectioned into $4\sim6\,\mu m$ slides. For the histopathological assay, slides were stained with hematoxylin and eosin (HE; Wuhan Google Biotechnology Co., Ltd., G1005). For immunohistochemical staining, slides were deparaffinized, rehydrated, and boiled in a citric acid (pH 6.0) antigen retrieval solution (ServiceBio, G1202). Endogenous peroxidase activity was blocked by 3% hydrogen peroxide at room temperature for 25 min. Slides were blocked with 3% BSA at room temperature for 30 min and incubated with antibody against the N protein of HCoV-OC43 (1:300, Millipore, MAB9012) overnight at $4°C$. Sections were washed three times with PBS before being incubated for 50 min at room temperature with goat anti-mouse IgG (1,200, ServiceBio, GB23301) labeled with HRP. Then, the sections were stained with 3,3′-diaminobenzidine (DAB; ServiceBio, G1211) and counterstained with hematoxylin (ServiceBio, G1004, G1309, and G1340). Images were captured using a DMI3000B Manual Inverted Microscope (Leica) and analyzed with NIS-Elements F 4.00.00 software (Leica). The staining intensity and rate of positive cells were analyzed by the software AIpathwell (Servicebio). The Histochemistry score (H-Score) was used for semi-quantitative analysis of the OC43 N protein expression level, and the H-Score was calculated as $\sum(pi \times i)$, with pi representing the ratio of positive signal pixel area to cell number and i representing staining intensity scores (no staining=0, weak staining=1, moderate staining=2, and strong staining=3). The H-Scores ranged from 0 to 300, and larger number indicated higher staining intensity. Under double-blind conditions, HE score was recorded to evaluate pathological changes in brain and lung tissues. The HE scores of brain samples were recorded as follows: 0 points, no inflammatory cell infiltration and neuronal degeneration; 1 point, 25% inflammatory cell infiltration and neuronal degeneration; 2 points, 50% inflammatory cell infiltration and neuronal cells degeneration or decrease; and 75%~100% inflammatory cell infiltration and neuronal cells degeneration or decrease. The HE scores of lung samples were described by Buchweitz et al. (2007).

## Statistical Analysis

Data analysis was performed using IBM SPSS Statistics 21.0 software. The survival curve was described by the Kaplan–Meier method and statistically analyzed by the log-rank test. One-way ANOVA was used for statistical analysis of the mean survival time, organ index, the expression of viral *n* gene, and the production of inflammatory factors. The Kruskal-Wallis test was used for the analysis of H-Scores and HE scores. $p < 0.05$ indicated a significant difference, and $p < 0.01$ and $p < 0.001$ indicated the difference was very significant.

## RESULTS

### Acquisition of an Adapted HCoV-OC43 Strain With 8 Amino Acid Mutations in the Genome

To create an HCoV-OC43 mouse adopted strain, suckling C57BL/6 mice were intracerebrally inoculated with 100 $TCID_{50}$

of wild-type virus (WT) by serial passage. Brain and lung tissue samples were collected from infected animals at 1 to 5 dpi, respectively, and brain samples with higher $n$ gene expression at 4 dpi were used for serial inoculation. The expression of viral $n$ gene in the brain and lung, respectively, approached $3.96 \times 10^{13}$ copies/g and $1.03 \times 10^{11}$ copies/g, at passage 8 (P8; **Figure 1A**). The sequences of the He and S regions from the nine generations of viruses (WT to P9) were first determined and analyzed. There were no mutations within *He* gene from WT to P9, but nine nucleic acid mutations were detected within ORF S. Among them, only six mutations resulted in five amino acid changes. Three changes (Y250H, N259D, and D264K) in the A domain of the S1 subunit and two mutations (A394G and K494I) in the B domain were detected (**Figure 1B**, **Supplementary Table 2**). In order to identify mutations associated with this adaptation, the genome sequences of WT and P9 were further investigated. Six nucleic acid mutations resulted in two amino acid changes, A453T (NSP3) and V113F (NSP6), in ORF1a (**Figure 1C**). One nucleic acid mutation leading to a T204I change was detected in ORF N (**Figure 1C**). No changes were identified in regions of 1b, ns2, ns12.9, E, and M (**Figure 1C**).

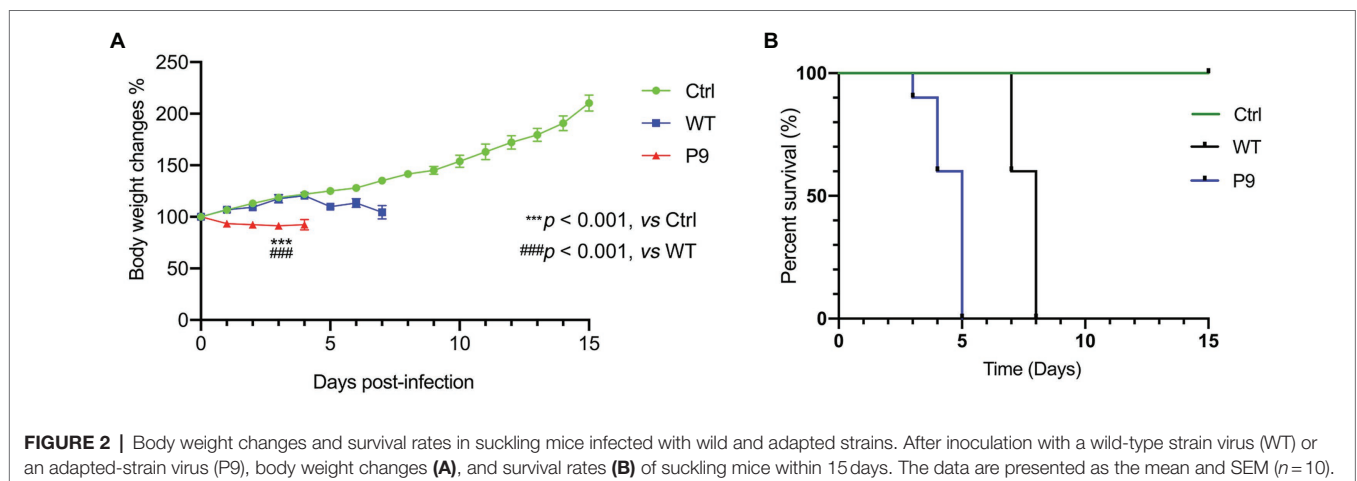**The adapted strain (P9) had increased virulence against suckling C57BL/6 mice.**

The SMLD$_{50}$ of P9 and WT in suckling mice was determined, which were $10^{-5.625}/25\,\mu l$ and $10^{-3.625}/25\,\mu l$, respectively. The disease symptoms of infected animals were recorded regularly. At 1 dpi, the mice infected with the P9 virus began to lose weight. They were reluctant to move and ingest milk at 2 dpi, with unkempt hair and poor skin, and later developed a swaggering walk and a curling tendency. The mortality rate of these mice was 100% at 5 dpi (**Figure 2B**). Body weight gain and activity of WT group animals were normal (**Figure 2A**), but later they developed disorganized hair, a swaggering stride, or curled up at 7 and 8 dpi, and then died. In the normal control group, no abnormality was found in body weight gain or regular activity (**Figure 2A**). The mean survival time in group P9 was significantly shorter than in the WT group ($4.5 \pm 0.224$ vs. $7.6 \pm 0.163$, $p < 0.001$;

**Figure 2B**, **Supplementary Table 3**). These findings indicate that both the WT and the adapted P9 viruses were fatal to suckling mice, but P9 had an earlier median lethal time, a shorter average survival period, and a lower body weight under the same infective dose.

## The Adapted Strain (P9) Was Efficiently Replicated in Brain and Lung Samples of Suckling Mice

The proliferation kinetics of the P9 virus in brain and lung samples were first investigated. The P9 virus multiplied more rapidly and greatly in brain samples than the WT virus (**Figure 3A**). The highest copy number of $n$ gene in P9 group reached $1.73 \times 10^{13}$ copies/g at 36 hpi and then kept at a higher level, whereas the replication level of the WT virus began to significantly increase from 48 hpi but was statistically lower than P9 at all indicated times (**Figure 3A**, $p < 0.01$). In lung samples, although the expression level of $n$ gene of the P9 and WT groups was comparable at 12 hpi, it increased with time in P9 and was considerably higher than that of the WT ($p < 0.05$) and control groups ($p < 0.001$; **Figure 3A**). The expression of $n$ gene in lung samples from WT-infected mice was not significantly higher than those of the normal control group (**Figure 3A**, $p > 0.05$). Since all mice in P9 group died at 5 dpi, the P9-infected mice were sacrificed and sampled at 4 dpi in subsequent experiments.

To determine the tissue infectivity of the P9 virus, brain, lung, heart, liver, spleen, and kidney samples from P9, WT, and control groups were harvested at 4 dpi to compare the organ indices and viral replication levels. The expression levels of viral $n$ gene in the brain and lung samples of the P9 group were significantly higher than those in the WT and control groups ($p < 0.001$ for the brain and $p < 0.01$ for the lung; **Figure 3B**). However, only the brain index of P9-infected mice was significantly higher than those in both the WT and control groups (**Figure 3C**, $p < 0.05$). The replication level of WT virus in the brain sample was higher than in the control group ($p < 0.001$), but the difference in



**FIGURE 2** | Body weight changes and survival rates in suckling mice infected with wild and adapted strains. After inoculation with a wild-type strain virus (WT) or an adapted-strain virus (P9), body weight changes **(A)**, and survival rates **(B)** of suckling mice within 15 days. The data are presented as the mean and SEM ($n = 10$).
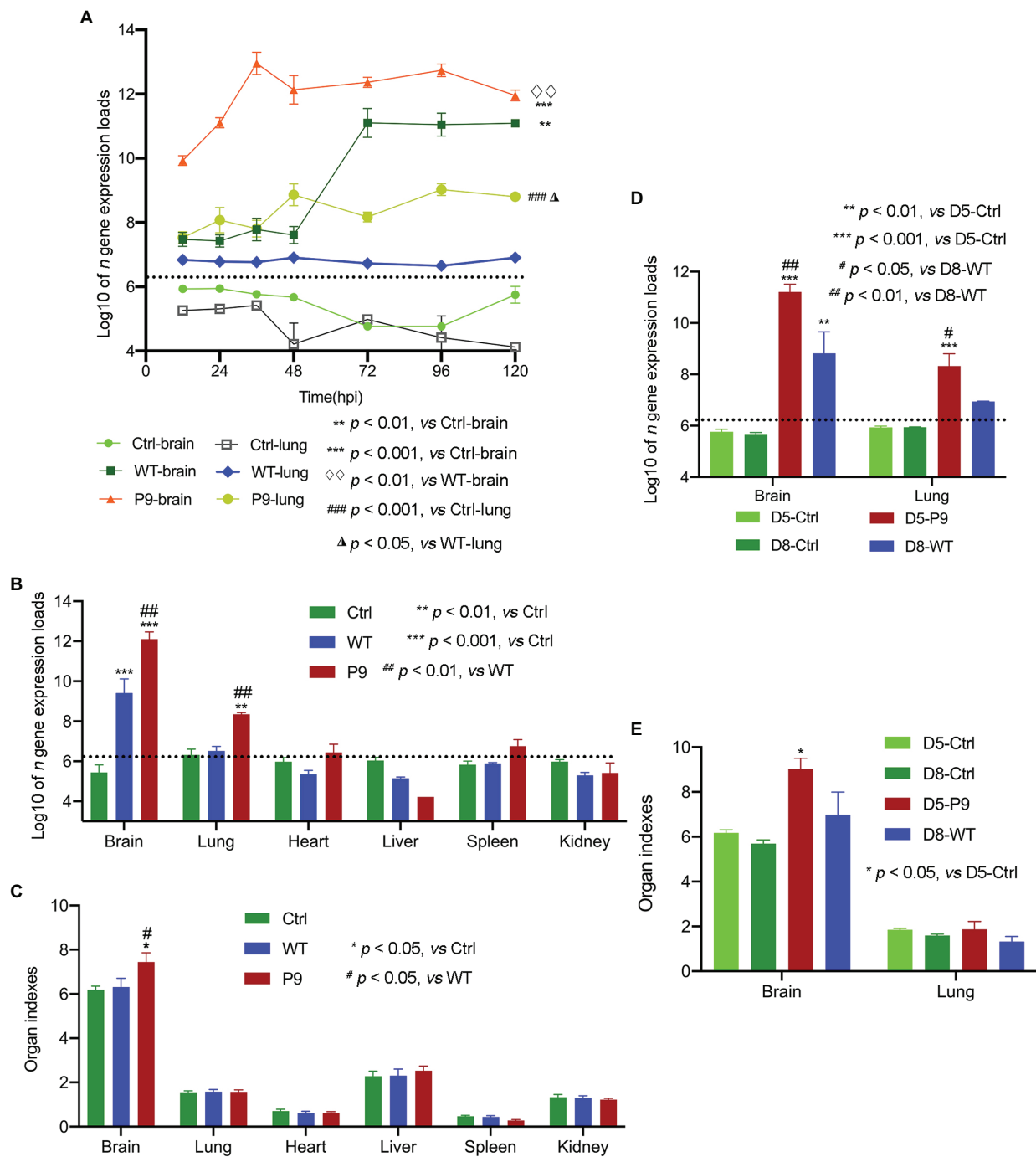
**FIGURE 3 |** Virus expression and organ indices in various organs of suckling mice. The proliferation kinetics of these viruses in the brain and lungs was analyzed ($n=3$); **(A)** Virus $n$ gene's copy number **(B)** and organ indices **(C)** in various organs of mice infected with wild-type strain viruses (WT) and adapted-strain viruses (P9) were detected at 4 dpi ($n=4$), respectively. The viral replication levels **(D)** and organ indices **(E)** in WT-infected suckling mice at 8 dpi and P9-infected at 5 dpi ($n=3–4$) were calculated. The data for viral $n$ gene (copies/g) are presented as log10, mean$\pm$SEM, and dashed lines indicate the detection limit.

the expression of viral $n$ gene was not significant in the lung samples (**Figure 3B**, $p > 0.05$). The copy number of viral $n$ gene in other organs of P9- and WT-infected mice was not significantly different from that in the control group (**Figure 3B**, $p > 0.05$). Since the mean survival time of WT group (7.6 $\pm$ 0.163 days) was longer than that of the P9 group (4.5 $\pm$ 0.224 days), the organ indices and $n$ gene expression levels between WT-infected pups at 8 dpi and P9-infected pups at 5 dpi were compared. The value of these two variables in WT group was still considerably lower than the results

in the brain ($p < 0.01$) and lung samples ($p < 0.05$) of the P9 group (**Figures 3D,E**).

Furthermore, we used immunohistochemical analysis to investigate the viral N protein expression in brain and lung tissues with DAB staining. N protein of P9 viruses was abundant in the neurons of the cerebral cortex, and the H-Score was higher than that of WT group at all indicated times (**Figure 4**). At 3 dpi, weak staining was observed in the tracheal epithelium and a few alveolar septal cells of P9 animals, while the majority of the bronchial and alveolar epithelial cells were distinctly stained at 4 dpi (**Figure 4**). The expression level of N protein in WT group was relatively lower in lung samples at 3, 4, and 8 dpi (**Figure 4**). These results indicated that the P9 virus could efficiently replicate in the lungs of suckling mice. When combined with its faster replication rate and higher replication level, the virulence of P9 virus to suckling mice was increased.

**The infection of the P9 virus caused pathological changes and upregulated the production of pro-inflammatory factors in brain and lung tissues.**

Our findings indicate that the adapted strain (P9) was efficiently replicated in the brain and lungs of suckling mice. Previous research has shown that OC43 infection could cause inflammation in the brain and involve nerve cells in the cerebral cortex (Butler et al., 2006). Therefore, we investigated the pathological and pro-inflammatory factors' changes in brain and lung tissues. Infection with the P9 virus resulted in inflammatory cell infiltration, a decrease in neuronal cells, and an increase in cell degeneration (**Figure 5A**). Similar pathological alterations were observed in the brains of WT-infected animals but not in the mock group (normal control group; **Figure 5A**). The HE scores of brain samples from the P9 group were not statistically different from those of the WT group at 3 and 4 dpi (**Figure 5A**). At 4 dpi, the expression of cytokines and chemokines G-CSF, IFN-γ, IL-6, KC, MCP-1, MIP-1α, MIP-1β, and RANTES in the brain of suckling mice was significantly upregulated after P9 infection (**Figure 5B**, $p < 0.05$, or 0.01, 0.001). Increasing expression of inflammatory cytokines was also shown in WT group at 4, 5, and 8 dpi (**Figure 5B**, $p < 0.05$, or 0.01, 0.001), but the expression level of most cytokines was lower than those in the P9-4 dpi group (**Figure 5B**, $p < 0.001$). The upregulation degree of all inflammatory factors except MIP-1β in the WT-8 dpi group was lower than that in the P9-4 dpi group (**Figure 5B**, $p < 0.001$).

In lung samples of P9-infected animals, alveolar septum widening, inflammatory cell infiltration in the alveolar septum, alveolar epithelial hyperplasia, fibrous effusion of the alveolar interstitium, concentration of inflammatory cells near the bronchus, and alveolar hyaline membrane were observed (**Figure 6A**). These changes were more severe in P9 groups at 3 and 4 dpi, but mild alveolar epithelial hyperplasia and alveolar hyaline plasma membrane were occasionally detected in WT groups at 4 and 8 dpi (**Figure 6A**, $p < 0.01$). Meanwhile, P9 infection increased the severity of the pulmonary inflammatory cytokine storm, and the chemokines and cytokines of G-CSF, IFN-γ, KC, MCP-1, MIP-1α, MIP-1β, RANTES, IP-10, and TNF-α were significantly and persistently upregulated at 0.5 and 4 dpi (**Figure 6B**). Following WT infection, G-CSF, IP-10,

and KC levels were increased at 4 dpi but decreased at 8 dpi (**Figure 6B**, $p < 0.001$). In comparison with the control group, IFN-γ, MCP-1, RANTES, and TNF-α were statistically upregulated in WT group (**Figure 6B**, $p < 0.001$). There was, however, no significant variation in MIP-1α was detected among the three groups, a protein associated with asthma and airway inflammation (**Figure 6B**, $p > 0.05$; Rojas-Dotor et al., 2013). Except for TNF-α, the other factors in the P9 group at 4 dpi were considerably higher than those of WT at 8 dpi (**Figure 6B**). These results suggest that P9 virus infection could cause pathological changes and severe cytokine storms in both their brain and lung tissues.

## The Adapted Strain (P9) Had a High Infection Rate in Brain and Lung Samples

To investigate the infection rate of P9, the entire brains and lungs were homogenized with sterile PBS with a weight to volume ratio of 1:10 (g/ml) for qRT-PCR detection of the OC43 *n* gene expression. In 80 mice infected with P9 (1000SMLD$_{50}$ per mouse) viruses, there were 67.5% of pups having CT values of less than 29% and 88.75% of pups with CT values of less than 32 in lung samples, and the *n* gene expression was detected in all brain samples (CT < 29, 100%; **Supplementary Figure 1**). When CT values of *n* gene were between 32 and 35, N protein expression was hardly detectable by the immunohistochemistry assay, but it was obviously detected when CT values were less than 29. These findings indicate that P9 had a high infection rate under 1,000 SMLD$_{50}$.

## The Adapted OC43 Model Was Useful for Evaluating the Antiviral and Anti-inflammatory Effects of Drugs

To explore the application potential of our model for evaluation of antiviral agents, the therapeutic effects of QJM and ARB on pups infected with P9 virus were analyzed. Mice were treated with high ($600\,mg\cdot kg^{-1}\cdot d^{-1}$), middle ($300\,mg\cdot kg^{-1}\cdot d^{-1}$), and low ($150\,mg\cdot kg^{-1}\cdot d^{-1}$) concentrations of QJM and with $25\,mg\cdot kg^{-1}\cdot d^{-1}$ of ARB at 2 hpi, respectively. The symptoms, including being reluctant to move and ingest milk, and the swaggering walk of suckling mice that resulted from P9 infection, were improved by drug treatments. The body weight of all infected mice decreased after viral inoculation, but all drug treatments considerably raised the body weight and survival rates to varying degrees (**Figures 7A,B**). The mice in the ARB group experienced a brief weight loss and subsequently gained weight at 4 dpi. However, one mouse in the ARB group died at 5 dpi, resulting in a 90% (9/10) survival rate (**Figures 7A,B**). The weight of mice in the high and middle doses of QJM groups began to increase at 5 dpi, and the survival rates were 100% (10/10) and 90% (9/10), whereas the weight of mice in the low-dose group began to rise at 7 dpi, but they still died at 11 dpi, with a mortality rate of 100% (**Figures 7A,B**). In the low concentration QJM group, the mean survival times were significantly increased when compared with the P9 group ($9.9 \pm 1.287$ days vs. $5.0 \pm 0.667$, $p < 0.01$; **Supplementary Table 4**). These findings suggest that both ARB and QJM treatments
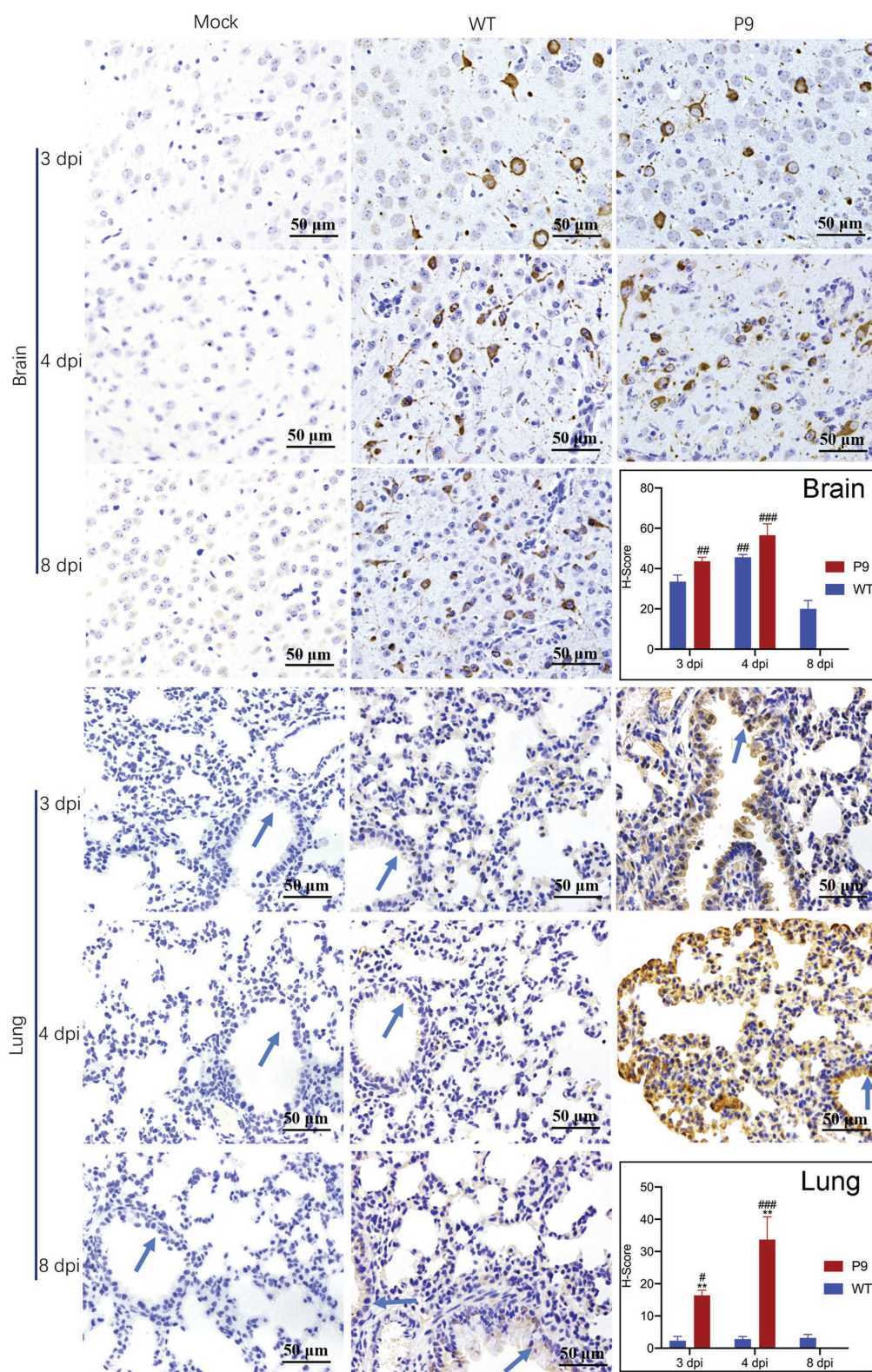
**FIGURE 4 |** Virus N protein expression and localization in organs of suckling mice. Viral nucleocapsid protein expression and localization in brain (400×) and lung (400×) tissues were examined immunohistochemically with DAB staining at the indicated times ($n = 3$–5). The OC43 N protein expression level was calculated and indicated as H-Scores. Positive expression is shown in tan. Blue arrows, bronchus. $^{\#}p < 0.05$, $^{\#\#}p < 0.01$, and $^{\#\#\#}p < 0.001$, vs. WT-8 dpi group; $^{**}p < 0.01$, vs. WT-4 dpi group.
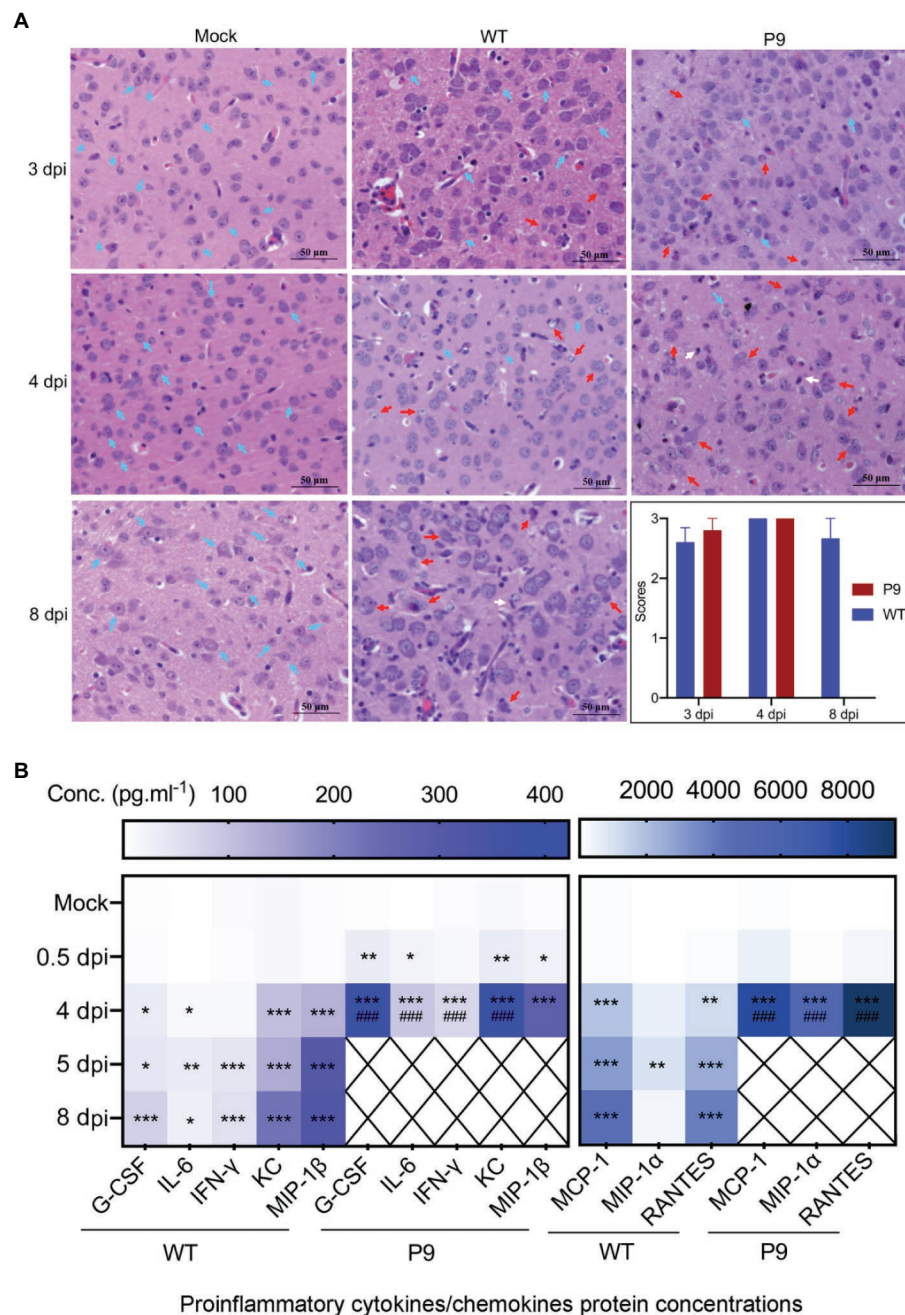
**FIGURE 5 |** Pathological changes and expression of pro-inflammatory factors in brain tissues induced by virus infection. **(A)** HE staining of brain tissue at 3, 4, and 8 dpi after virus WT or P9 infection, 400×, $n = 3$–5. HE scores were recorded for evaluation of the pathological changes. Blue arrows, normal tissue; red arrows, degenerative neurons; and white arrows, microglia. **(B)** Heat map shows the mean values of expression level of inflammatory cytokines in the brain at 0.5, 4, and 8 dpi after viral infection by the bio-plex assay, mean ($n = 5$). *$p < 0.05$, **$p < 0.01$, and ***$p < 0.001$, vs. normal control group (mock); ###$p < 0.001$, vs. WT-8 dpi group.

were able to improve symptoms and the survival rate of P9-infected mice.

Furthermore, the effect of ARB and QJM against viral replication in the brain and lung tissues of mice was detected. At 4 dpi, the expression of *n* gene in drug treatment groups was statistically different from those in the P9 group ($p < 0.01$ or 0.001). High and middle concentrations of QJM treatment

were more effective in reducing *n* gene expression levels than those of the ARB treatment ($p < 0.001$; **Figure 7C**). In addition, at 4 dpi, immunohistochemistry assays showed decreased expression of viral N protein in the neurons in the cerebral cortex of the QJM and ARB treatment groups (**Figure 8A**, $p < 0.05$ or 0.001). The effects of the high dosage of QJM treatment were better than those of the ARB group, but their

**FIGURE 6 |** Pathological changes and pro-inflammatory factor expression in lung tissues caused by virus infection. **(A)** HE staining of lung tissue after virus infection at 3, 4, and 8 dpi, 400×, $n = 3–5$. HE scores were recorded for evaluation of the pathological changes. Grey arrows, normal tissue; red arrows, alveolar septal infiltration of inflammatory cells, infiltration of inflammatory cells around the bronchus; yellow arrows, alveolar epithelial hyperplasia and alveolar septum widening; green arrows, suspected virus inclusion body; black arrows, alveolar hyaline membrane; orange arrows, trachea epithelial ulcer; and blue arrows, alveolar interstitial exudation. **$p < 0.01$, vs. WT-4 dpi group. **(B)** Heat map shows the expression of inflammatory cytokines in the lung at 0.5, 4, and 8 dpi after infection with virus by the bio-plex assay, mean (n = 3–5); *$p < 0.05$, **$p < 0.01$, and ***$p < 0.001$, vs. normal control group (mock); #$p < 0.05$, ##$p < 0.01$, and ###$p < 0.001$, vs. WT-8 dpi group.

H-Scores were not statistically different (**Figure 8A** $p > 0.5$). In lung tissues, N protein was abundantly expressed in the majority of P9-infected bronchial and alveolar epithelial cells, whereas ARB and all QJM treatments significantly lowered the H-Scores (**Figure 8B**, $p < 0.05$, 0.01, or 0.001). At 4 dpi, inflammatory cell infiltration, severe neuronal cell reduction,

and cell degeneration induced by viral infection were significantly reduced by a high dose of QJM treatment (**Figure 9A**, $p < 0.05$). ARB and the other doses of QJM treatment moderately improved the symptoms, but HE scores were not statistically different from the P9 group (**Figure 9A**, $p > 0.05$). Meanwhile, high and middle doses of QJM and ARB treatments also
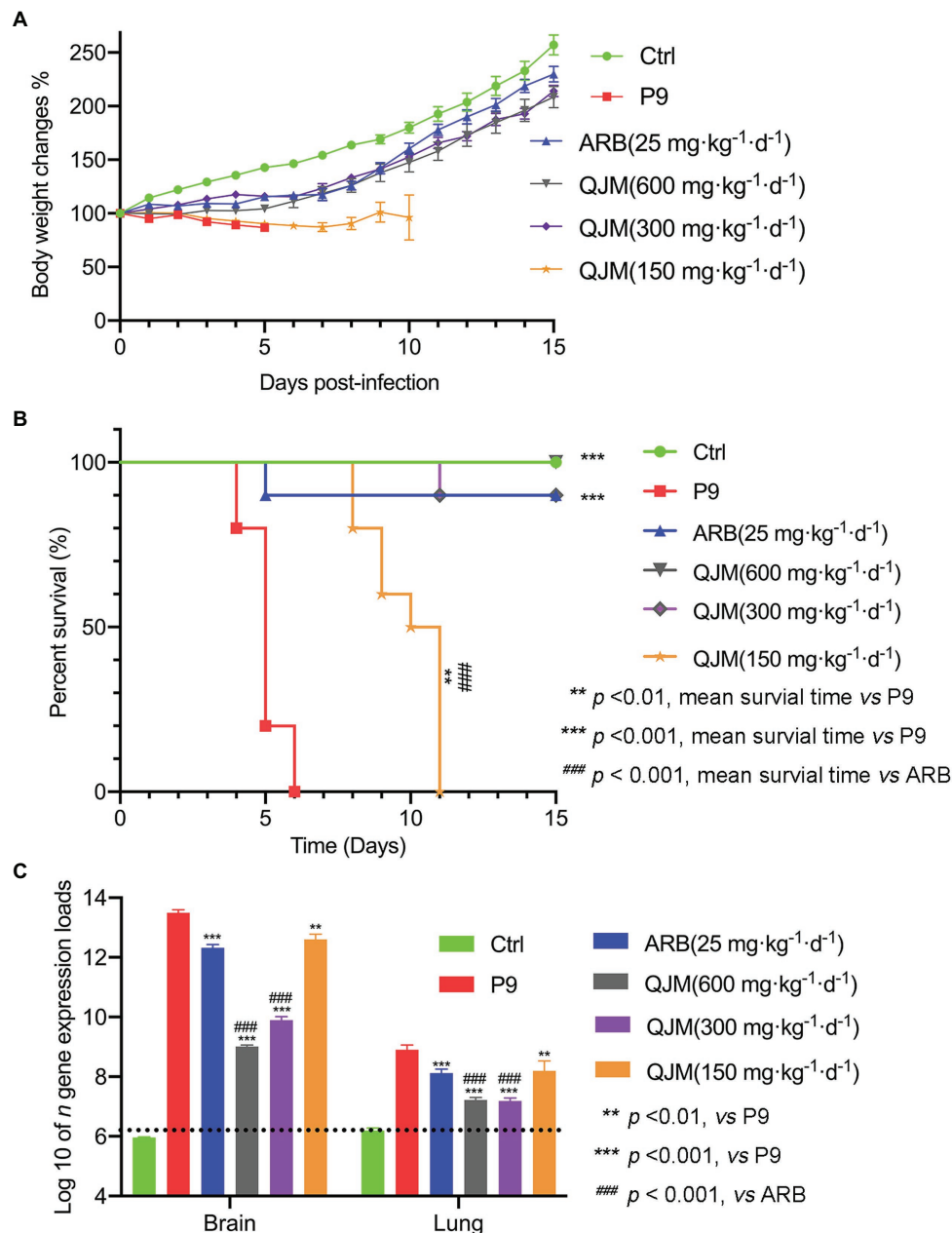
**FIGURE 7** | QJM increased the survival rate of P9-infected suckling mice and inhibited the nucleocapsid gene expression. After inoculation with an adapted-strain virus (P9) and treated with ARB and QJM, body weight change **(A)** and survival rate **(B)** of suckling mice within 15 days ($n = 10$) and the copy number of viral $n$ gene in the brain and lungs at 4 dpi (**C**; $n = 3–5$). The data for viral $n$ gene expression (copies/g) are presented as log10, mean ± SEM, and dashed lines indicate the detection limit.

significantly reversed pathological changes in lung tissues, including widened alveolar septum, infiltrated inflammatory cells, proliferated alveolar epithelium, fibrous interstitial exudation in the alveolar interstitial space, and inflammatory cells concentrated near the bronchus (**Figure 9B**, $p < 0.05$ or 0.01).

QJM and ARB interventions significantly reduced the production of pro-inflammatory cytokines and chemokines at 4 dpi in P9-infected suckling mice. In brain samples, the treatment of QJM and ARB significantly inhibited the production of G-CSF, IFN-γ, IL-6, KC, MCP-1, MIP-1α, MIP-1β, and RANTES (**Figure 10A**, $p < 0.05$). The high concentration of QJM was more effective than ARB in the suppression of all detected cytokines (**Figure 10A**, $p < 0.01$ or $p < 0.001$). In lung samples, high and middle dosage QJM treatments significantly reduced the production of G-CSF, IFN-γ, IL-6, IP-10, KC,
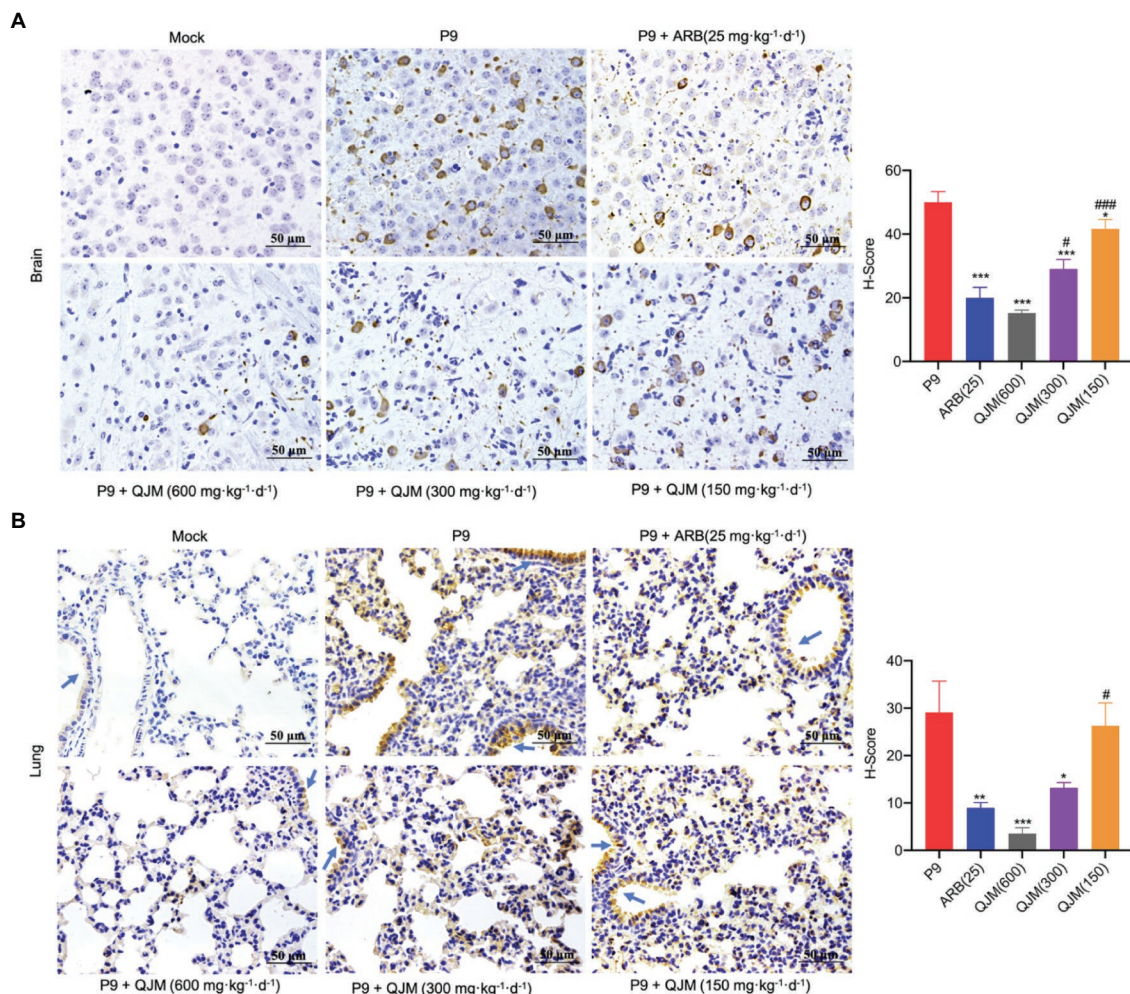
**FIGURE 8 |** QJM inhibited the N protein expression. N protein expression in brain (400×; **A)** and lung (400×; **B)** tissues (*n* = 3–5) was examined immunohistochemically with DAB staining at 4 dpi. The OC43 N protein expression level was calculated and indicated as H-Scores. Positive expression is shown in tan. Blue arrows, bronchus. *$p < 0.05$, **$p < 0.01$, and ***$p < 0.001$, vs. P9 group; #$p < 0.05$ and ###$p < 0.001$, vs. ARB group.

MCP-1, MIP-1α, MIP-1β, RANTES, and TNF-α induced by P9 infection (**Figure 10B**, $p < 0.05$, $p < 0.01$, or $p < 0.001$), and the inhibitory role was generally superior to that of ARB (**Figure 10B**). ARB played a minor role in the production of RANTES (**Figure 10B**). These results prove the efficacy of QJM and ARB against the HCoV-OC43 infection *in vivo*. Our model was useful when it came to evaluating the antiviral and anti-inflammatory effects of antiviral drugs.

## DISCUSSION

Animal models are critical in antiviral research. In this study, we developed a new mouse-adapted HCoV-OC43 that caused cerebral and pulmonary diseases in suckling C57BL/6 mice with a reduced survival period. By sequence comparison with the WT virus, 15 nucleic acid mutations resulting in 8 coding changes were detected in P9 virus, and mutations were

concentrated in the S protein. The S protein of HCoVs contains significant viral neutralisation epitopes and the interaction between this protein and its binding receptor determines the host tropism and pathogenicity of CoVs (Woo et al., 2009; Song et al., 2020). For β-CoVs, the S protein is split into S1 and S2 subunits by furin-like proteases at the conserved cleavage site of RRSRR/G. The degree of sequence variation in S1 is extremely high, whereas S2 sequences are conserved. Our result was in accordance with a previous study that 8 nucleic acid mutations in the S region of the P9 virus were all located in the S1 subunit. There are four domains in the S1 subunit, with domains A and B in OC43 serving as receptor binding domains (Peng et al., 2012; Tortorici et al., 2019). Domain A is also referred to as the N-terminal domain, which forms a complex with the glycogroup 5-N-acetyl-9-O-acetylneuraminic acid on the cell surface that allows virus invasion (Peng et al., 2012). Among 5 coding changes resulting from 8 nucleic acid mutations in P9 virus, 3 coding mutations (Y250H, N259D,
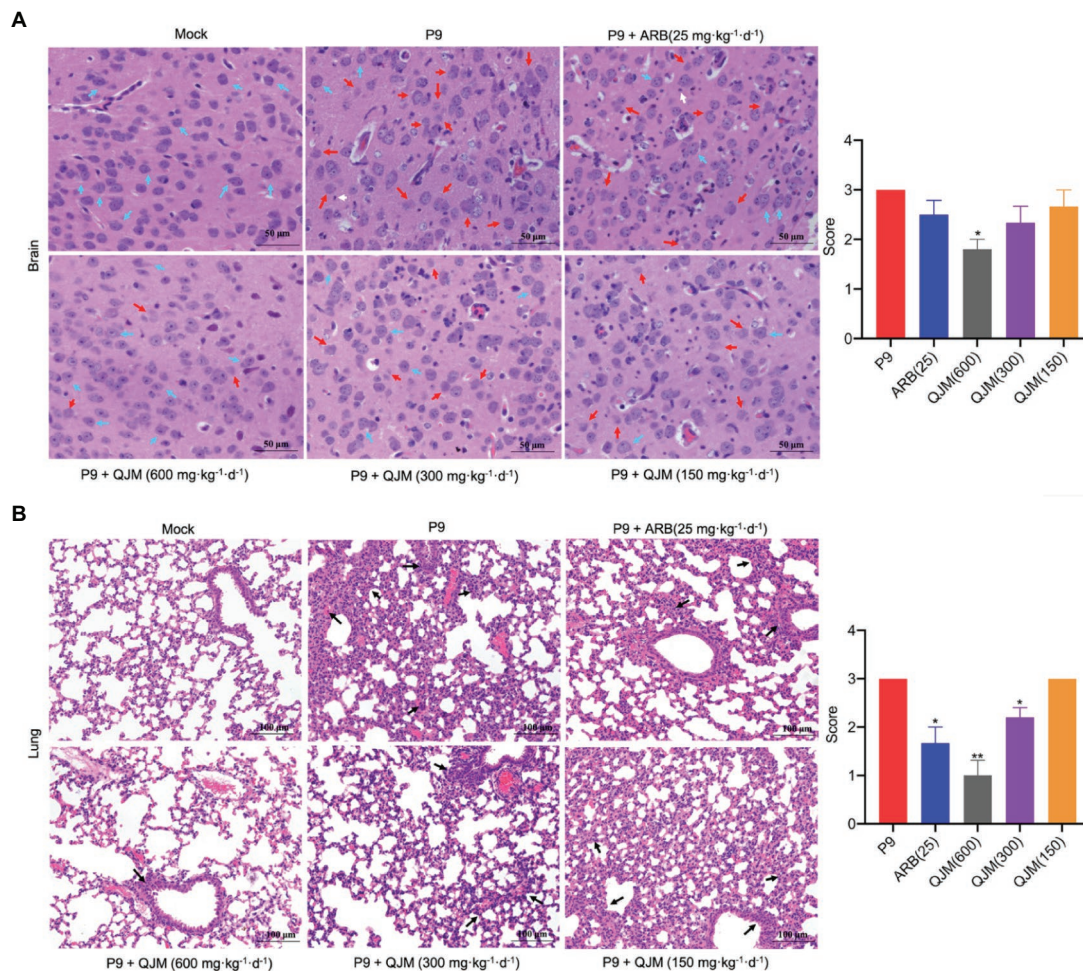
**FIGURE 9 |** QJM therapy improved the pathological changes in the brain and lungs of P9-infected suckling mice. HE staining shows the pathological changes in brain (400×; **A)** and lung (200×; **B)** tissues at 4 dpi ($n$ = 3–5). HE scores were recorded for evaluation of the pathological changes. Blue arrows, normal tissue; red arrows, progressive degeneration of neurons; white arrows, microglia; and black arrows, diseased tissue. *$p$ < 0.05 and **$p$ < 0.01, vs. P9 group.

and D264K) are located inside domain A, and a recent study indicated that numerous mutations in domain A may have a synergic effect on virus virulence (Brison et al., 2011). Another 2 mutations (A394G and K494I) were located within domain B, which was reported to have the highest variability across CoVs and correlates to the ability of different viruses to interact with distinct host receptors (Tortorici et al., 2019). Further, mutations in domain B were associated with changes in viral tropism and influenced animal-to-human transmission of SARS (Qu et al., 2005; Hulswit et al., 2016). Another 2 amino acid changes were in NSP3 and NSP6 within the ORF1a region. NSP3 is a multi-domain transmembrane protein and is responsible for cleavage of pp1ab *via* papain-like protease (PL^Pro) and block host innate immune response (Serrano et al., 2009). It has been reported that the synonymous mutation in NSP3 (F106F) could affect the fitness of the virus (Tomaszewski et al., 2020). NSP6 decreases the autophagic capacity of infected cells, which provides an innate defense against viral infections (Mercatelli and Giorgi, 2020). Most recently, the accumulation of mutations

in S1 subunit of S protein was found to be associated with ORF1a: 3,675–3,677 deletion and this deletion was indicated as an adaptive mutation that facilitates the process of SARS-CoV-2 evolution (Kistler et al., 2022). One coding mutation was found in N protein. The *n* gene mutation was positively correlated with the severity of coronavirus cases and a high number of deaths seen in South American countries like Brazil (Burki, 2020; Vahed et al., 2021). Besides, the mutations R203K and G204R in the N protein contributed to the improved viral fitness of the COVID-19 B.1.298 variant (Plante et al., 2021). Since viral infection is a game between the virus and the host cells, the influence of the identified coding mutations on expanded tropism and enhanced virulence of P9 viruses should be verified in future work.

An ideal animal model for infectious diseases should exhibit similarities to humans in terms of symptoms, infection routes, and the link between viral replication level and disease severity, as well as practical advantages such as low cost, a clear genetic background, and ease of manipulation (Gretebeck and Subbarao,
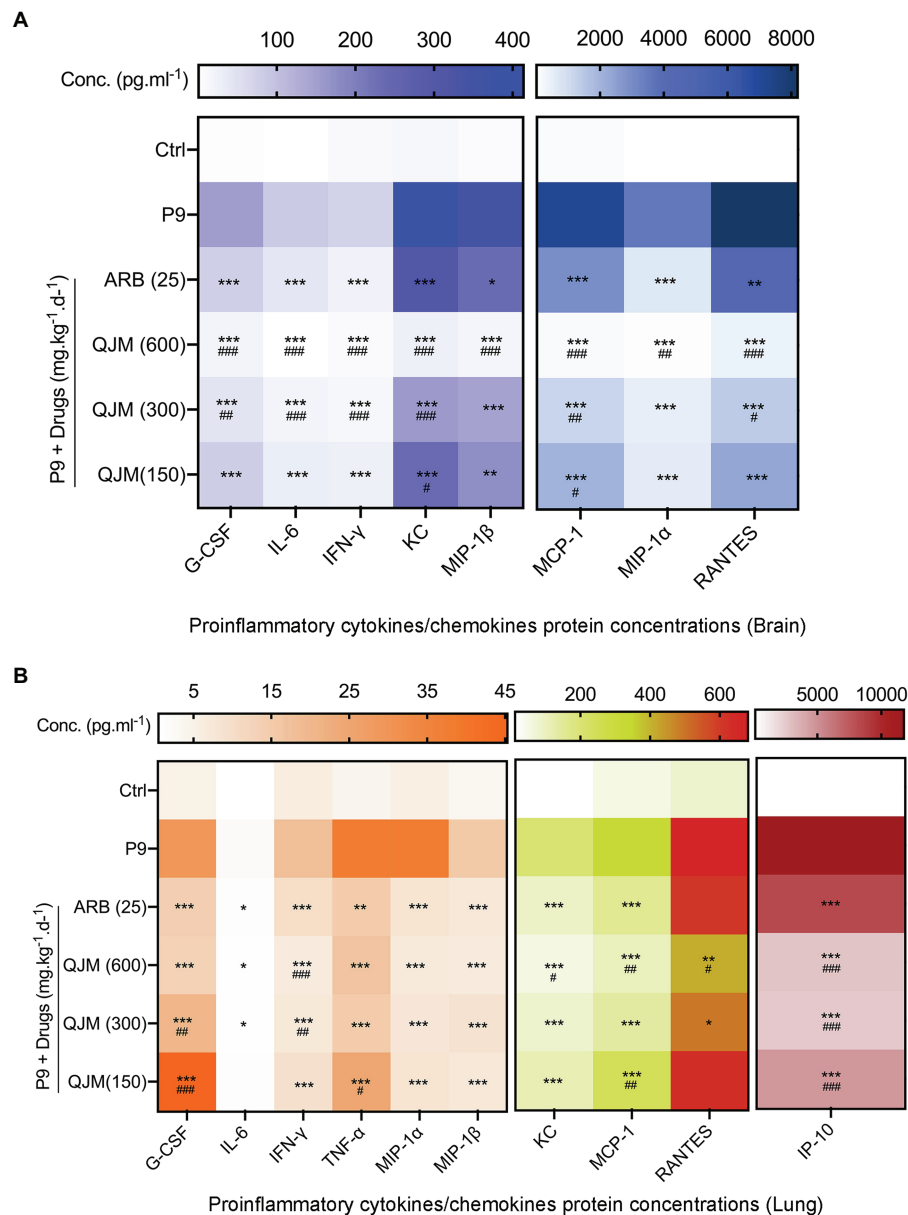
**FIGURE 10 |** QJM therapy modulated the expression of inflammatory/chemokines in the brain and lungs of P9-infected suckling mice. Heat map: The expression of inflammatory cytokines in the brain **(A)** and lung **(B)** at 4 dpi after treating with ARB and QJM by the bio-plex method, mean ($n = 3–5$); $*p < 0.05$, $**p < 0.01$, and $***p < 0.001$, vs. P9 group; and $\#p < 0.05$, $\#\#p < 0.01$, and $\#\#\#p < 0.001$, vs. ARB group.

2015). The laboratory mouse is a useful and affordable model that has been developed for HCoV-OC43 infection since the distribution of 9-O-acetylated sialic acid receptors, the attachment receptor for this virus, in mice is most similar to that of humans (Wasik et al., 2017; Lang et al., 2020). However, as one of the most common respiratory pathogens, the viral replication level in pulmonary tissues and the occurrence of lung inflammation and respiratory illness in reported HCoV-OC43 mouse models were not determined (Jacomy and Talbot, 2001, 2003; Jacomy et al., 2006). In present study, the infected mice presented lethargy and stooped posture, which were similar to some symptoms of human beings. Besides cerebral infectivity, the pulmonary invasiveness of P9 virus was demonstrated by qRT-PCR detection of viral replication in lung tissues, and the expression of the viral *n* gene increased with time. Histopathological and immunohistochemical examinations confirmed the occurrence of pneumonia. In addition, compared with WT infection, the P9 virus resulted in lower body weight and shorter survival time, as well as a higher viral multiplication level in brain samples. The copy numbers of viral *n* gene reached $3.96 \times 10^{13}$ copies/g and $1.03 \times 10^{11}$ copies/g in brain and lung samples,

respectively. This viral replication level was comparable with 2 reported fatal cases associated with this virus, and the viral loads were $3.49 \times 10^6$ to $1.10 \times 10^{10}$ copies/ml in the respiratory tract specimens of a 75-year-old patient with fatal pneumonia, and Ct values ranged from 22 to 24 in an immunocompromised child with fatal encephalitis (Nilsson et al., 2020; Lau et al., 2021). It should be noted that the infection was conducted by intracerebral inoculation, which was different from the natural route of infection. We tried intranasal inoculation and found that it was easy to cause asphyxia in suckling mice, whereas intracerebral inoculation of suckling mice benefited the success rate of modeling. Although the infection method did not mimic natural infection way, our adapted OC43 model developed encephalitis and pneumonia and exhibited similar tissue tropism, symptoms, and inflammation response to humans. Compared to reported mouse models, this model provides a useful tool for pathogenesis studies of respiratory and brain diseases caused by HCoV infection.

Besides the association of the severity and mortality of HCoV infection with a high viral replication level, the pathological role of the immune response triggered by infection has been increasingly recognized (Zhang et al., 2020). Tissue injury and inflammatory alterations are required phenotypes for lung disease in animal models (Wong et al., 2004; Channappanavar and Perlman, 2017; Mahallawi et al., 2018). In this study, P9 infection led to the occurrence of typical viral pneumonia symptoms (**Figure 4**). It also resulted in a large decrease in neuronal cells, which was consistent with previous studies (Jacomy and Talbot, 2003; Butler et al., 2006). Moreover, it stimulated the expression of inflammatory cytokine storms in brain and lung samples, such as G-CSF, IFN-γ, KC, MCP-1, MIP-1α, MIP-1β, RANTES, IP-10, and TNF-α, which were similar to the inflammation response induced by HCoV-infected patients (Wong et al., 2004; Channappanavar and Perlman, 2017; Mahallawi et al., 2018). A previous study found that the S1 subunit of SARS-CoV-2 interacted with the human ACE2 receptor to activate the NF-κB pathway, which upregulated the expression of pro-inflammatory cytokines and chemokines (IL-1β, TNF-α, IL-6, and MCP-1) and resulted in epithelial damage in human bronchial epithelial cells (Hsu et al., 2020a). Over-expression of a range of pro-inflammatory cytokines and chemokines would cause inflammatory cell activation and infiltration, increase vascular permeability, and, eventually, lead to pulmonary edema and pneumonia (Kircheis et al., 2020). For instance, during the acute inflammatory response to a virus infection, the body releases the cytokines TNF-α, IL-1, and IL-6, which act on fibroblasts and endothelial cells, hence increasing vascular permeability (Gulati et al., 2016; Kawano et al., 2017). Further, the expression of MIP-1α and MCP-1 by macrophages, T cells, monocytes, and other inflammatory cells enhanced the release of IL-6 or IL-8, which contributed to the pathogenic process of bronchiectasis (Barnes, 2008; Rui Jin and Miao, 2017; Yibing Niu, 2018). IP-10 is thought to be a biomarker for the severity of COVID-19 (Chen et al., 2020). Following virus infection, alveolar macrophages and neutrophils can emit a substantial amount

of IP-10 to attract T cells that express the IP-10 receptor CXCR3 to the infected region, accelerating the onset, and progression of lung tissue inflammation (Liangdi Hu et al., 2019). Meanwhile, inflammatory factors expressed in the brain, such as IL-6 and IFN-γ in the cerebral white matter, can activate inflammatory responses, leading to neurodegeneration and the onset of multiple sclerosis (Gulati et al., 2016). These findings may help to explain the degenerative changes in nerve cells and the development of neuropathic gait in suckling mice following P9 infection. Based on previous studies, our results suggested that P9 infection partially mimicked the clinical symptoms, viral replication, and pathological features observed in HCoV patients. Therefore, this model is valuable for elucidating the mechanisms of tissue damage and inflammation induced by viral infection.

Mice infected with adapted viruses have been proven to be accessible and reproducible for evaluating the efficacy and safety of antiviral therapies for viral infections (Day et al., 2009; Dinnon et al., 2020). The death rates, body weight loss, viral replication level, production of pro-inflammatory factors, and pathogenic alterations in the brain and lung tissues of P9-infected pups might be useful indicators for antiviral and anti-inflammatory drug screening. We employed the model to look into the pharmacology of QJM and ARB in vivo. Previous study found that QJM and ARB showed a strong antiviral and anti-inflammatory effect of OC43 in vitro (Xie et al., 2021). In this study, QJM and ARB treatment raised the survival rates and suppressed the expression of OC43 nucleocapsid protein genes and their proteins, while decreasing G-CSF, IFN-γ, IP-10, KC, MCP-1, MIP-1α, RANTES, and TNF-α. In combination of our previous study, we proved that QJM and ARB have both in vivo and in vitro antiviral and anti-inflammatory effects against HCoV-OC43 infection. This model was useful for assessing the efficacy of antiviral drugs.

This study established a novel mouse-adapted OC43 model that is practical and repeatable for antiviral research and successfully used it to evaluate the efficacy of QJM, which demonstrated this TCM had antiviral and anti-inflammatory activities against OC43 in vivo. In addition, the amino acid mutations discovered in ORF1ab, ORFS, and ORFN may be required for the adapted virus to become more virulent. Future research may investigate whether these mutations are linked to the extended lung tissue tropism. Furthermore, because of the difference in immune responses between suckling mice and adult mice, our model is suitable for drug research at a young age stage. Our model provides a choice for future anti-coronavirus drug screening and vaccine evaluation.

## DATA AVAILABILITY STATEMENT

The datasets presented in this study can be found in online repositories. The names of the repository/repositories and accession number(s) can be found in the article/ **Supplementary Material**.

## AUTHOR CONTRIBUTIONS

XX and SD conceived and designed the study, are responsible for study coordination, and obtained funding and ethical approval. PX and YF developed the study design, revised the protocol, and wrote the original draft. ZB revised the manuscript. PX, YF, HY, ZZ, RL, and TZ conducted the experiment. RL performed the data curation, review, and editing the manuscript. ZY and JZ obtained the resources. All authors contributed to the article and approved the submitted version.

## FUNDING

## ACKNOWLEDGMENTS

## SUPPLEMENTARY MATERIAL

The Supplementary Material for this article can be found online at: https://www.frontiersin.org/articles/10.3389/fmicb.2022.845269/full#supplementary-material. The GenBank accession numbers for genome sequences of WT and P9 viruses discussed in this paper are HCoV-OC43 WT sequence (ON376724) and HCoV-OC43 P9 sequence (ON376725).

**Supplementary Figure 1 |** The infection rate of P9 virus in brains and lung samples. The copy number of OC43 $n$ gene was detected by qRT-PCR at 4 dpi in brain and lung samples of suckling mice infected with P9 virus ($n = 80$).

**Supplementary Figure 2 |** Graphical abstract of this study.

## REFERENCES

Abdel-Moneim, A. S., Abdelwhab, E. M., and Memish, Z. A. (2021). Insights into SARS-CoV-2 evolution, potential antivirals, and vaccines. *Virology* 558, 1–12. doi: 10.1016/j.virol.2021.02.007

Barnes, P. J. (2008). The cytokine network in asthma and chronic obstructive pulmonary disease. *J. Clin. Invest.* 118, 3546–3556. doi: 10.1172/jci36130

Blaising, J., Polyak, S. J., and Pécheur, E. I. (2014). Arbidol as a broad-spectrum antiviral: an update. *Antivir. Res.* 107, 84–94. doi: 10.1016/j.antiviral.2014.04.006

Brison, E., Jacomy, H., Desforges, M., and Talbot, P. J. (2011). Glutamate excitotoxicity is involved in the induction of paralysis in mice after infection by a human coronavirus with a single point mutation in its spike protein. *J. Virol.* 85, 12464–12473. doi: 10.1128/jvi.05576-11

Buchweitz, J. P., Karmaus, P. W., Harkema, J. R., Williams, K. J., and Kaminski, N. E. (2007). Modulation of airway responses to influenza A/PR/8/34 by Delta9-tetrahydrocannabinol in C57BL/6 mice. *J. Pharmacol. Exp. Ther.* 323, 675–683. doi: 10.1124/jpet.107.124719

Burki, T. (2020). COVID-19 in Latin America. *Lancet Infect. Dis.* 20, 547–548. doi: 10.1016/s1473-3099(20)30303-0

Butler, N., Pewe, L., Trandem, K., and Perlman, S. (2006). Murine encephalitis caused by HCoV-OC43, a human coronavirus with broad species specificity, is partly immune-mediated. *Virology* 347, 410–421. doi: 10.1016/j.virol.2005.11.044

Chan, J. F., Yip, C. C., To, K. K., Tang, T. H., Wong, S. C., Leung, K. H., et al. (2020). Improved molecular diagnosis of COVID-19 by the novel, highly sensitive and specific COVID-19-RdRp/Hel real-time reverse transcription-PCR assay validated In vitro and with clinical specimens. *J. Clin. Microbiol.* 58, e00310–20. doi: 10.1128/jcm.00310-20

Channappanavar, R., and Perlman, S. (2017). Pathogenic human coronavirus infections: causes and consequences of cytokine storm and immunopathology. *Semin. Immunopathol.* 39, 529–539. doi: 10.1007/s00281-017-0629-x

Chen, Y., Wang, J., Liu, C., Su, L., Zhang, D., Fan, J., et al. (2020). IP-10 and MCP-1 as biomarkers associated with disease severity of COVID-19. *Mol. Med.* 26, 97. doi: 10.1186/s10020-020-00230-x

Coleman, C. M., and Frieman, M. B. (2014). Coronaviruses: important emerging human pathogens. *J. Virol.* 88, 5209–5212. doi: 10.1128/jvi.03488-13

Day, C. W., Baric, R., Cai, S. X., Frieman, M., Kumaki, Y., Morrey, J. D., et al. (2009). A new mouse-adapted strain of SARS-CoV as a lethal model for evaluating antiviral agents in vitro and in vivo. *Virology* 395, 210–222. doi: 10.1016/j.virol.2009.09.023

de Wilde, A. H., Snijder, E. J., Kikkert, M., and van Hemert, M. J. (2018). Host factors in coronavirus replication. *Curr. Top. Microbiol. Immunol.* 419, 1–42. doi: 10.1007/82_2017_25

Dinnon, K. H. 3rd, Leist, S. R., Schäfer, A., Edwards, C. E., Martinez, D. R., Montgomery, S. A., et al. (2020). A mouse-adapted model of SARS-CoV-2 to test COVID-19 countermeasures. *Nature* 586, 560–566. doi: 10.1038/s41586-020-2708-8

Fehr, A. R., and Perlman, S. (2015). Coronaviruses: an overview of their replication and pathogenesis. *Methods Mol. Biol.* 1282, 1–23. doi: 10.1007/978-1-4939-2438-7_1

Gretebeck, L. M., and Subbarao, K. (2015). Animal models for SARS and MERS coronaviruses. *Curr. Opin. Virol.* 13, 123–129. doi: 10.1016/j.coviro.2015.06.009

Gulati, K. G. S., Joshi, J., Rai, N., and Ray, A. (2016). cytokines and their role in health and disease: a brief overview. *MOJ Immunol.* 4, 1–9. doi: 10.15406/moji.2016.04.00121

Hsu, A. C.-Y., Wang, G., Reid, A. T., Veerati, P. C., Pathinayake, P. S., Daly, K., et al. (2020a). SARS-CoV-2 spike protein promotes hyper-inflammatory response that can be ameliorated by spike-antagonistic peptide and FDA-approved ER stress and MAP kinase inhibitors. *bioRxiv*, 2020.2009.2030.317818. doi: 10.1101/2020.09.30.317818

Hulswit, R. J., de Haan, C. A., and Bosch, B. J. (2016). Coronavirus spike protein and tropism changes. *Adv. Virus Res.* 96, 29–57. doi: 10.1016/bs.aivir.2016.08.004

Jacomy, H., Fragoso, G., Almazan, G., Mushynski, W. E., and Talbot, P. J. (2006). Human coronavirus OC43 infection induces chronic encephalitis leading to disabilities in BALB/C mice. *Virology* 349, 335–346. doi: 10.1016/j.virol.2006.01.049

Jacomy, H., and Talbot, P. J. (2001). Susceptibility of murine CNS to OC43 infection. *Adv. Exp. Med. Biol.* 494, 101–107. doi: 10.1007/978-1-4615-1325-4_16

Jacomy, H., and Talbot, P. J. (2003). Vacuolating encephalitis in mice infected by human coronavirus OC43. *Virology* 315, 20–33. doi: 10.1016/s0042-6822(03)00323-4

Kawano, Y., Fukui, C., Shinohara, M., Wakahashi, K., Ishii, S., Suzuki, T., et al. (2017). G-CSF-induced sympathetic tone provokes fever and primes antimobilizing functions of neutrophils via PGE2. *Blood* 129, 587–597. doi: 10.1182/blood-2016-07-725754

Keyaerts, E., Li, S., Vijgen, L., Rysman, E., Verbeeck, J., Van Ranst, M., et al. (2009). Antiviral activity of chloroquine against human coronavirus OC43 infection in newborn mice. *Antimicrob. Agents Chemother.* 53, 3416–3421. doi: 10.1128/aac.01509-08

Kim, T., Choi, H., Shin, T. R., Ko, Y., Park, Y. B., Kim, H. I., et al. (2021). Epidemiology and clinical features of common community human coronavirus disease. *J. Thorac. Dis.* 13, 2288–2299. doi: 10.21037/jtd-20-3190

Kircheis, R., Haasbach, E., Lueftenegger, D., Heyken, W. T., Ocker, M., and Planz, O. (2020). NF-κB pathway as a potential target for treatment of critical stage COVID-19 patients. *Front. Immunol.* 11:598444. doi: 10.3389/fimmu.2020.598444

Kistler, K. E., Huddleston, J., and Bedford, T. (2022). Rapid and parallel adaptive mutations in spike S1 drive clade success in SARS-CoV-2. *Cell Host Microbe.* 30, 545–555.e4. doi: 10.1016/j.chom.2022.03.018

Lai, M. M. (1992). RNA recombination in animal and plant viruses. *Microbiol. Rev.* 56, 61–79. doi: 10.1128/mr.56.1.61-79.1992

Lang, Y., Li, W., Li, Z., Koerhuis, D., van den Burg, A. C. S., Rozemuller, E., et al. (2020). Coronavirus hemagglutinin-esterase and spike proteins coevolve for functional balance and optimal virion avidity. *Proc. Natl. Acad. Sci. U. S. A.* 117, 25759–25770. doi: 10.1073/pnas.2006299117

Lau, S. K. P., Li, K. S. M., Li, X., Tsang, K.-Y., Sridhar, S., and Woo, P. C. Y. (2021). Fatal pneumonia associated With a novel genotype of human coronavirus OC43. *Front. Microbiol.* 12:795449. doi: 10.3389/fmicb.2021.795449

Leneva, I., Kartashova, N., Poromov, A., Gracheva, A., Korchevaya, E., Glubokova, E., et al. (2021). Antiviral activity of Umifenovir In vitro against a broad Spectrum of coronaviruses, including the novel SARS-CoV-2 virus. *Viruses* 13:1665. doi: 10.3390/v13081665

Liangdi Hu, X. W., Chen, X., and Zhang, P. (2019). Research progress in IP-10-mediated inflammation in viral infectious diseases. *Chin. J. Virol* 35, 672–678. doi: 10.13242/j.cnki.bingduxuebao.003568

Mahallawi, W. H., Khabour, O. F., Zhang, Q., Makhdoum, H. M., and Suliman, B. A. (2018). MERS-CoV infection in humans is associated with a pro-inflammatory Th1 and Th17 cytokine profile. *Cytokine* 104, 8–13. doi: 10.1016/j.cyto.2018.01.025

Malik, Y. A. (2020). Properties of coronavirus and SARS-CoV-2. *Malays. J. Pathol.* 42, 3–11.

Mercatelli, D., and Giorgi, F. M. (2020). Geographic and genomic distribution of SARS-CoV-2 mutations. *Front. Microbiol.* 11:1800. doi: 10.3389/fmicb.2020.01800

Morfopoulou, S., Brown, J. R., Davies, E. G., Anderson, G., Virasami, A., Qasim, W., et al. (2016). Human coronavirus OC43 associated with fatal encephalitis. *N. Engl. J. Med.* 375, 497–498. doi: 10.1056/NEJMc1509458

Nilsson, A., Edner, N., Albert, J., and Ternhag, A. (2020). Fatal encephalitis associated with coronavirus OC43 in an immunocompromised child. *Infect Dis.* 52, 419–422. doi: 10.1080/23744235.2020.1729403

Nojomi, M., Yassin, Z., Keyvani, H., Makiani, M. J., Roham, M., Laali, A., et al. (2020). Effect of Arbidol (Umifenovir) on COVID-19: a randomized controlled trial. *BMC Infect. Dis.* 20:954. doi: 10.1186/s12879-020-05698-w

Peng, G., Xu, L., Lin, Y. L., Chen, L., Pasquarella, J. R., Holmes, K. V., et al. (2012). Crystal structure of bovine coronavirus spike protein lectin domain. *J. Biol. Chem.* 287, 41931–41938. doi: 10.1074/jbc.M112.418210

Plante, J. A., Mitchell, B. M., Plante, K. S., Debbink, K., Weaver, S. C., and Menachery, V. D. (2021). The variant gambit: COVID-19's next move. *Cell Host Microbe.* 29, 508–515. doi: 10.1016/j.chom.2021.02.020

Qu, X. X., Hao, P., Song, X. J., Jiang, S. M., Liu, Y. X., Wang, P. G., et al. (2005). Identification of two critical amino acid residues of the severe acute respiratory syndrome coronavirus spike protein for its variation in zoonotic tropism transition via a double substitution strategy. *J. Biol. Chem.* 280, 29588–29595. doi: 10.1074/jbc.M500662200

Rajapakse, N., and Dixit, D. (2021). Human and novel coronavirus infections in children: a review. *Paediatr. Int. Child Health* 41, 36–55. doi: 10.1080/20469047.2020.1781356

Reed, L. J., and Muench, H. (1938). A simple method of estimating fifty per cent endpoints12. *Am. J. Epidemiol.* 27, 493–497. doi: 10.1093/oxfordjournals.aje.a118408

Rojas-Dotor, S., Segura-Méndez, N. H., Miyagui-Namikawa, K., and Mondragón-González, R. (2013). Expression of resistin, CXCR3, IP-10, CCR5 and MIP-1α in obese patients with different severity of asthma. *Biol. Res.* 46, 13–20. doi: 10.4067/s0716-97602013000100002

Rui Jin, J. T., and Miao, S. (2017). Expression and clinical significance of macrophage inflammatory protein-1 in serum of patients with asthma. *J. Crit. Care Inter. Med.* 23, 362–364.

Serrano, P., Johnson, M. A., Chatterjee, A., Neuman, B. W., Joseph, J. S., Buchmeier, M. J., et al. (2009). Nuclear magnetic resonance structure of the nucleic acid-binding domain of severe acute respiratory syndrome coronavirus nonstructural protein 3. *J. Virol.* 83, 12998–13008. doi: 10.1128/jvi.01253-09

Smee, D. F., Hurst, B. L., Wong, M. H., Bailey, K. W., Tarbet, E. B., Morrey, J. D., et al. (2010). Effects of the combination of favipiravir (T-705) and oseltamivir on influenza A virus infections in mice. *Antimicrob. Agents Chemother.* 54, 126–133. doi: 10.1128/aac.00933-09

Song, Y., Song, J., Wei, X., Huang, M., Sun, M., Zhu, L., et al. (2020). Discovery of Aptamers targeting the receptor-binding domain of the SARS-CoV-2 spike glycoprotein. *Anal. Chem.* 92, 9895–9900. doi: 10.1021/acs.analchem.0c01394

Tomaszewski, T., DeVries, R. S., Dong, M., Bhatia, G., Norsworthy, M. D., Zheng, X., et al. (2020). New pathways of mutational change in SARS-CoV-2 proteomes involve regions of intrinsic disorder important for virus replication and release. *Evol. Bioinformatics Online* 16:1176934320965149. doi: 10.1177/1176934320965149

Tortorici, M. A., Walls, A. C., Lang, Y., Wang, C., Li, Z., Koerhuis, D., et al. (2019). Structural basis for human coronavirus attachment to sialic acid receptors. *Nat. Struct. Mol. Biol.* 26, 481–489. doi: 10.1038/s41594-019-0233-y

Vabret, A., Dina, J, Gouarin, S., Petitjean, J., Corbet, S., and Freymuth, F. (2006). Detection of the new human corona virus HKU1: a report of 6 cases. *Clin. Infect. Dis.* 42, 634–639. doi: 10.1086/500136

Vabret, A., Mourez, T., Gouarin, S., Petitjean, J., and Freymuth, F. (2003). An outbreak of coronavirus OC43 respiratory infection in Normandy, France. *Clin. Infect. Dis.* 36, 985–989. doi: 10.1086/374222

Vahed, M., Calcagno, T.M., Quinonez, E., and Mirsaeidi, M. (2021). *Impacts of 203/204: RG> KR Mutation in the N Protein of SARS-CoV-2.* BioRxiv. doi: 10.1101/2021.01.14.426726

Veiga, A., Martins, L. G., Riediger, I., Mazetto, A., Debur, M. D. C., and Gregianini, T. S. (2021). More than just a common cold: endemic coronaviruses OC43, HKU1, NL63, and 229E associated with severe acute respiratory infection and fatality cases among healthy adults. *J. Med. Virol.* 93, 1002–1007. doi: 10.1002/jmv.26362

Vijgen, L., Keyaerts, E., Moës, E., Thoelen, I., Wollants, E., Lemey, P., et al. (2005). Complete genomic sequence of human coronavirus OC43: molecular clock analysis suggests a relatively recent zoonotic coronavirus transmission event. *J. Virol.* 79, 1595–1604. doi: 10.1128/jvi.79.3.1595-1604.2005

Wasik, B. R., Barnard, K. N., Ossiboff, R. J., Khedri, Z., Feng, K. H., Yu, H., et al. (2017). Distribution of O-acetylated sialic acids among target host tissues for Influenza virus. *mSphere* 2, e00379–16. doi: 10.1128/mSphere.00379-16

Wong, C. K., Lam, C. W., Wu, A. K., Ip, W. K., Lee, N. L., Chan, I. H., et al. (2004). Plasma inflammatory cytokines and chemokines in severe acute respiratory syndrome. *Clin. Exp. Immunol.* 136, 95–103. doi: 10.1111/j.1365-2249.2004.02415.x

Woo, P. C., Huang, Y., Lau, S. K., and Yuen, K. Y. (2010). Coronavirus genomics and bioinformatics analysis. *Viruses* 2, 1804–1820. doi: 10.3390/v2081803

Woo, P. C., Lau, S. K., Huang, Y., and Yuen, K. Y. (2009). Coronavirus diversity, phylogeny and interspecies jumping. *Exp. Biol. Med. (Maywood)* 234, 1117–1127. doi: 10.3181/0903-mr-94

Xie, P., Fang, Y., Shen, Z., Shao, Y., Ma, Q., Yang, Z., et al. (2021). Broad antiviral and anti-inflammatory activity of Qingwenjiere mixture against SARS-CoV-2 and other human coronavirus infections. *Phytomedicine* 93:153808. doi: 10.1016/j.phymed.2021.153808

Yibing Niu, S. H. (2018). Advances in the relationship between monocyte chemoattractant protein-1 and pulmonary diseases. *Int. J. Respir.* 38, 1406–1409.

Zhang, Y. Y., Li, B. R., and Ning, B. T. (2020). The comparative immunological characteristics of SARS-CoV, MERS-CoV, and SARS-CoV-2 coronavirus infections. *Front. Immunol.* 11:2033. doi: 10.3389/fimmu.2020.02033

or those of the publisher, the editors and the reviewers. Any product that may be evaluated in this article, or claim that may be made by its manufacturer, is not guaranteed or endorsed by the publisher.

# SARS-CoV-2 Nucleocapsid Protein Has DNA-Melting and Strand-Annealing Activities With Different Properties From SARS-CoV-2 Nsp13

Bo Zhang[1]*[†], Yan Xie[2†], Zhaoling Lan[1†], Dayu Li[1], Junjie Tian[1], Qintao Zhang[1], Hongji Tian[1], Jiali Yang[1], Xinnan Zhou[1], Shuyi Qiu[3], Keyu Lu[1]* and Yang Liu[2,3]*

[1]College of Basic Medicine, Zunyi Medical University, Zunyi, China, [2]School of Public Health, Zunyi Medical University, Zunyi, China, [3]Key Laboratory of Plant Resource Conservation and Germplasm Innovation in Mountainous Region (Ministry of Education), College of Life Sciences/Institute of Agro-bioengineering, Guizhou University, Guiyang, China

Since December 2019, severe acute respiratory syndrome coronavirus 2 (SARS-CoV-2) has spread throughout the world and has had a devastating impact on health and economy. The biochemical characterization of SARS-CoV-2 proteins is important for drug design and development. In this study, we discovered that the SARS-CoV-2 nucleocapsid protein can melt double-stranded DNA (dsDNA) in the 5′-3′ direction, similar to SARS-CoV-2 nonstructural protein 13. However, the unwinding activity of SARS-CoV-2 nucleocapsid protein was found to be more than 22 times weaker than that of SARS-CoV-2 nonstructural protein 13, and the melting process was independent of nucleoside triphosphates and $Mg^{2+}$. Interestingly, at low concentrations, the SARS-CoV-2 nucleocapsid protein exhibited a stronger annealing activity than SARS-CoV-2 nonstructural protein 13; however, at high concentrations, it promoted the melting of dsDNA. These findings have deepened our understanding of the SARS-CoV-2 nucleocapsid protein and will help provide novel insights into antiviral drug development.

Keywords: SARS-CoV-2, Nsp13, nucleocapsid protein, unwinding, helicase

## INTRODUCTION

Since December 2019, the coronavirus disease 2019 (COVID-19) pandemic caused by severe acute respiratory syndrome coronavirus 2 (SARS-CoV-2) has spread throughout the world and caused damage to the global economy and individual health. SARS-CoV-2 is an airborne virus (Jiang et al., 2020) and humans are primarily infected by oral and nasal inhalation. Following SARS-CoV-2 infection, typical clinical symptoms include headache, cough, fever, sore throat, fatigue, myalgia and dyspnea, which may result in death (Jiang et al., 2020; Singhal, 2020). Compared with severe acute respiratory syndrome coronavirus (SARS-CoV) and Middle East respiratory syndrome coronavirus (MERS-CoV), SARS-CoV-2 is highly infectious, and people are generally susceptible to infection by this virus. Although mortality associated with COVID-19 is low, this virus still poses a significant threat to human health (Reynolds et al., 2021). As of July 2021, it has infected over 195 million people and caused over 4.2 million deaths

worldwide (Zhou et al., 2020). Therefore, there is an urgent need to understand the molecular mechanisms underlying SARS-CoV-2 pathogenesis, immune evasion, and disease progression.

SARS-CoV-2 is a beta coronavirus that belongs to the Coronaviridae family (Wu et al., 2020). It is a spherical, encapsulated, positive-sense single-stranded RNA virus. The total length of the genome is approximately 30 kb and the open reading frame (ORF) is predicted to contain 11 genes, encoding approximately 20 functional proteins (Wu et al., 2020). The genomic sequence of SARS-CoV-2 exhibits the typical structural characteristics of coronaviruses, including a 5′ untranslated region, 5′ replicase polysaccharide protein gene (ORF1/ab), spike glycoprotein gene (S), envelope glycoprotein gene (E), membrane glycoprotein gene (M), nucleocapsid protein gene (N), and 3′ untranslated region (Zhou et al., 2020; Thye et al., 2021). Among the different mutants of SARS-CoV-2 and even among different coronaviruses, the SARS-CoV-2 nonstructural protein 13 (CoV-2 Nsp13) and SARS-CoV-2 nucleocapsid protein (CoV-2 N) sequences are highly conserved (**Supplementary Figure 1**). Elucidating the structure and function of CoV-2 Nsp13 and CoV-2 N will be useful for the development of anti-SARS-CoV-2 drugs (Gurung, 2020; Gussow et al., 2020; Mirza and Froeyen, 2020).

CoV-2 Nsp13 is predicted to contain 596 amino acids (located in the ORF1ab polyprotein from amino acids 5,325 to 5,925; Gurung, 2020). Similar to SARS-CoV and MERS-CoV Nsp13, CoV-2 Nsp13 has a triangular, pyramid shape that consists of five domains. The structure of the pyramid-shaped CoV-2 Nsp13 consists of two RecA-like helicase subdomains (1A and 2A), which form the triangular base, an N-terminal zinc-binding domain, a helical "stalk" domain, and a beta-barrel 1B domain (Mirza and Froeyen, 2020; Newman et al., 2021). The same structural characteristics were previously reported for the SARS-CoV and MERS-CoV Nsp13 proteins (Mirza and Froeyen, 2020; Newman et al., 2021). CoV-2 Nsp13 is important for viral replication as a helicase that unwinds duplex RNA and a 5′-triphosphatase that is likely involved in the 5′-capping of viral mRNA (Min et al., 2021). Studies have found that CoV-2 Nsp13 strongly inhibits type I interferon signaling (Lei et al., 2020; Xia et al., 2020), highlighting the versatile activities of CoV-2 Nsp13 during viral infection. Another study reported that SARS-CoV-2 blocks immune activation during infection, suggesting that CoV-2 Nsp13 plays a role in blocking IFN and NF-κB activation and acts as an immune regulator (Vazquez et al., 2021). Studies have indicated that CoV-2 Nsp13 exhibits 5′-3′ unwinding activity on double-stranded DNA (dsDNA) and double-stranded RNA (Mickolajczyk et al., 2021).

CoV-2 N consists of 413 amino acid residues and is the only protein that binds to genomic RNA in the nucleocapsid (Kang et al., 2020). It is involved in viral replication and cell signaling pathway regulation (Carlson et al., 2020). CoV-2 N is one of the most conserved proteins in coronaviruses (**Supplementary Figure 1**; McBride et al., 2014). CoV-2 N of various coronaviruses exhibits high immunogenicity, which can induce the body to produce a robust immune response (Aboagye et al., 2018; Smits et al., 2021). CoV-2 N has been repeatedly proposed as a vaccine candidate, suggesting that it has the potential to induce an immune response capable of preventing infection from various strains of

human coronaviruses (Yang et al., 2009; Shi et al., 2015). To develop drug targets for COVID-19, Gussow et al. used a novel approach combining advanced machine learning methods and traditional genome comparison technology to screen four potential key regions in coronavirus strains that result in high mortality rates and identify potential genomic determinants, three of which are located in CoV-2 N. Thus, CoV-2 N may be a key target in combating the COVID-19 pandemic (Gussow et al., 2020). Therefore, it is particularly important to study the biochemical function of CoV-2 N, which will provide insights on future vaccine research.

Initially, the N protein was known as an RNA-binding protein critical for viral genome packaging. Owing to its distinct RNA-binding activity, it was recently reported to bind to host mRNAs and further interfere with the normal functioning of the host (Nabeel-Shah et al., 2022). Because this protein can also bind to DNA nonspecifically (Tang et al., 2005; Zhao et al., 2021), it may also perform specific functions by binding to DNA in cells. Interestingly, the N protein of human immunodeficiency virus, also a positive-sense single-stranded RNA virus, performs cellular functions by binding to DNA (Gien et al., 2022). However, little is known about the dynamics of the interaction between the N protein and DNA.

The ORF of SARS-CoV-2 is predicted to encode approximately 20 functional proteins. Among these, only CoV-2 Nsp13 has been reported to exhibit helicase activity. Surprisingly, we found that the SARS-CoV-2 N protein (a structural protein) can open double-stranded nucleic acids. However, the two proteins differ to a considerable extent in sequence and structure, which suggests that their mechanisms of opening nucleic acid substrates are different (**Supplementary Figure 2**). This biochemical characteristic of CoV-2 N is similar to that of single-stranded binding proteins, which exist widely. In prokaryotes, the representative protein is *Escherichia coli* single-stranded DNA (ssDNA)-binding protein (SSB), whereas in eukaryotes, the representative protein is replication protein A (RPA), both of which exhibit dsDNA unwinding activity (Wang et al., 2004; Safa et al., 2016). Of these, RPA, which is an essential factor in DNA metabolism, can unwind dsDNA directly or initially combine with dsDNA and recruit other proteins to unwind dsDNA (Fan et al., 2009).

To gain insights on the various functions of CoV-2 N, we expressed and purified full-length CoV-2 N protein and compared the dsDNA unwinding activities of CoV-2 N and CoV-2 Nsp13. We demonstrated that recombinant CoV-2 N exhibits efficient unwinding activity with several DNA substrates involved in DNA replication, repair, and recombination. Although CoV-2 N can unwind dsDNA, it does not possess the characteristics of a typical helicase. Interestingly, CoV-2 N strongly promotes ssDNA annealing at low concentrations, whereas it exhibits unwinding activity at high concentrations.

# MATERIALS AND METHODS

## Reagents and Buffers

All chemicals were of reagent grade. Buffers were prepared using high-quality deionized water from a Milli-Q ultrapure

water purification system (Millipore, Burlington, MA, United States) with a resistivity greater than 18.2 MΩ·cm and further filtered through a 2-μm filter before use. All chemicals were purchased from Sigma (St. Louis, MO, United States) unless otherwise indicated. All solutions were filtered and extensively degassed immediately before use.

## Preparation of DNA

The DNA substrates used in unwinding and annealing experiments as well as the primers were purchased from Shanghai Sangon Biological Engineering Technology & Services Co., Ltd. (Shanghai, China). Various substrate structures were designed such as DNA with different 5′ and 3′ overhang lengths and various nucleotide length internal bubbles. The 3′ or 5′ end of one of the ssDNAs was fluorescence (FAM) labeled so that single- and double-stranded changes could be observed at a wavelength of 560 nM. Details of the structures and sequences of unlabeled or FAM-labeled DNA substrates are shown in **Table 1**. Duplex substrates were annealed by incubating at 95°C for 5 min, followed by cooling to 25°C for approximately 7 h [annealing buffer: 25 mM Tris–HCl (pH 7.5) and 50 mM NaCl]. The various duplex substrates were stored at −20°C.

## Recombinant Plasmids

Plasmid pET-28a-2019-nCoV-N was obtained from Guangdong Laboratory Animal Monitoring and contained the CoV-2 N coding sequence (CoV-2 N GenBank accession: NC_045512.2), which has a 6xHis-tag cloned downstream of the AUG promoter. pSmart-I-CoV-2 Nsp13 contained the CoV-2 Nsp13 coding sequence (CoV-2 Nsp13 GenBank accession: OM019196.1) with a 6-his tag and an in-frame N-terminal SUMO fusion tag cloned downstream of the AUG promoter in the pSmart-I expression vector (Jing et al., 2016). The latter is a SUMO protease-cleavage site between the SUMO tag and the expressed protein. The pSmart-I-CoV-2 Nsp13 was synthesized by General Biosystems Co., Ltd. (Anhui, China).

## Protein Expression and Purification

The pET28a-CoV-2 N and pSmart-I-CoV-2 Nsp13 vectors were transformed into *E. coli* 2,566 for protein expression. The cells were grown in LB medium and the proteins were expressed overnight at 18°C after induction with 0.3 mM and 0.6 mM isopropyl β-d-1-thiogalactopyranoside (IPTG), respectively. All media contained 50 μg/ml kanamycin. The supernatant containing CoV-2 N was precipitated with 3.5 M ammonium sulfate for 3 h. After removing the supernatant, the precipitate was redissolved in a buffer containing 20 mM Tris–HCl (pH 7.5) and 300 mM NaCl. The supernatant was loaded onto Ni-NTA Sepharose beads (GE Healthcare, Boston, United States). The protein was eluted with 200 mM imidazole, followed by reducing the concentration of NaCl to 50 mM by dialysis. The protein was further purified on the SP Sepharose 6 Fast Flow column (GE Healthcare, Boston, United States). The eluted fractions were collected and concentrated, following which 5% glycerol (v/v) was added to them. The preparation was subsequently stored at −80°C.

The cleared lysate containing CoV-2 Nsp13 with a SUMO tag was loaded onto Ni-NTA Sepharose beads (GE Healthcare, Boston, United States). The protein was eluted with 200 mM imidazole. Fractions containing the proteins of interest were pooled and dialyzed overnight at 4°C against a buffer containing 25 mM Tris–HCl (pH 7.5) and 500 mM NaCl. The constructs were cleaved with SUMO protease [1:100 SUMO protease: protein (molar ratio)] to remove the SUMO tag. After dialysis, the samples were reapplied to Ni-NTA Sepharose beads using the same purification buffers. The solution containing CoV-2 Nsp13 was precipitated using 3.5 M ammonium sulfate for 3 h. After removing the supernatant, the precipitate was redissolved in a buffer containing 20 mM Tris–HCl (pH 7.5) and 300 mM NaCl. After redissolving, the supernatant was further purified by gel filtration chromatography using a SuperDeX 200 10/300 GL column (GE Healthcare, Boston, United States) and a buffer containing 20 mM Tris–HCl (pH 7.5), 300 mM NaCl, 10% glycerol (v/v), and 2 mM dithiothreitol (DTT). The eluted fractions were collected, concentrated, and stored at −80°C.

## Unwinding and Annealing Assays

CoV-2 N was incubated with dsDNA in unwinding buffer A [25 mM Tris–HCl (pH 7.5) and 300 mM NaCl] at 30°C for 10 min. CoV-2 Nsp13 was incubated with dsDNA in unwinding buffer B [25 mM Tris–HCl (pH 7.5), 50 mM NaCl, 1.5 mM MgCl_2, and 1 mM DTT], and 10 mM adenosine triphosphate (ATP) was added to initiate the reaction at 30°C for 10 min. The reactions were quenched by the addition of 5× stop loading buffer (150 mM EDTA, 2% SDS, 30% glycerol, and 0.1% bromophenol blue). The products of the DNA unwinding reactions were resolved on native 12% PAGE gels (Acr:Bis = 39:1) at 100 V for 80 min. The DNA in the polyacrylamide gels was visualized using ChemiDoc MP and quantitated using Image Lab software (Bio-Rad, California, United States).

Two DNA substrates were used for the DNA annealing assays. Substrate S1 was 43 nt (nucleotide) and substrate S2 was 21 nt (nucleotide). CoV-2 N was incubated with the two single DNAs in buffer A (the same as unwinding buffer A) at 30°C for 10 min. CoV-2 Nsp13 was incubated with two the single DNAs in buffer B (the same as unwinding buffer B) at 30°C for 10 min. The reactions were quenched by the addition of 5 × stop loading buffer. The products of the DNA annealing reactions were then resolved on native 12% PAGE gels (Acr:Bis = 39:1) at 100 V for 80 min. The DNA in the polyacrylamide gels was visualized using ChemiDoc MP (Bio-Rad).

## Binding Assay

The fluorescently labeled DNA substrate can rotate freely when it is not bound to the enzyme molecule (i.e., showing low fluorescence anisotropy). When the substrate binds to the enzyme molecule to form a complex, its free rotation is significantly reduced, resulting in a significant increase in fluorescence anisotropy. Therefore, changes in anisotropy

**TABLE 1** | Sequences and structure information of the unwinding and annealing substrates.

| Name | Structure | Sequence(F,Fluorescein) | Comment |
|---|---|---|---|
| 5′-OhS22D21 | 5′ 22n / 21bp 3′ | 5′-CTGTAGGAATGTGAAATAAAAACGATGTTTTATTTACATTGTA-3′-F<br>3′-GCTACAAAATAAATGTAACAT-5′ | 5′-22 nt-Overhanged-21 bp |
| S43 | 5′ 43nt 3 | 5′-CTGTAGGAATGTGAAATAAAAACGATGTTTTATTTACATTGTA-3′-F | 43 nt ssDNA |
| S21 | 5′ 21nt 3 | 3′-GCTACAAAATAAATGTAACAT-5′ | 21 nt ssDNA |
| 3′-OhS22D21 | 21bp / 22nt 3′ 5′ | 3′-CTGTAGGAATGTGAAATAAAAACGATGTTTTATTTACATTGTA-5′<br>5′-GCTACAAAATAAATGTAACAT-3′-F | 3′-22 nt-Overhanged-21 bp |
| S43-a | 3′ 43nt 5′ | 3′-CTGTAGGAATGTGAAATAAAAACGATGTTTTATTTACATTGTA-5′ | 43 nt ssDNA |
| S21-a | 5′ 21nt 3 | 5′-GCTACAAAATAAATGTAACAT-3′-F | 21 nt ssDNA |
| DS32 | 5′ 32bp 3′ | 5′-TATCGAAGAATGTTATGTCATTCCGGCAGATG-3′-F<br>3′-ATAGCTTCTTACAATACAGTAAGGCCGTCTAC-5′ | 32 bp dsDNA |
| 5′-OhS4D20 | 5′ 4nt / 20bp 3′ p | 5′-AATGTTATGTCATTCCGGCAGATG-3′-F<br>3′-AATACAGTAAGGCCGTCTAC-5′ | 5′-4 nt-Overhanged-20 bp |
| 5′-OhS12D20 | 5′ 12nt / 20bp 3′ | 5′-TATCGAAGAATGTTATGTCATTCCGGCAGATG-3′-F<br>3′-AATACAGTAAGGCCGTCTAC-5′ | 5′-12 nt-Overhanged-20 bp |
| 5′-OhS14D20 | 5′ 14nt / 20bp 3′ | 5′-CCTATCGAAGAATGTTATGTCATTCCGGCAGATG-3′-F<br>3′-AATACAGTAAGGCCGTCTAC-5′ | 5′-14 nt-Overhanged-20 bp |
| 5′-OhS15D20 | 5′ 15nt / 20bp 3′ | 5′-TCCTATCGAAGAATGTTATGTCATTCCGGCAGATG-3′-F<br>3′-AATACAGTAAGGCCGTCTAC-5′ | 5′-15 nt-Overhanged-20 bp |
| 5′-OhS16D20 | 5′ 16nt / 20bp 3′ p | 5′-ATCCTATCGAAGAATGTTATGTCATTCCGGCAGATG-3′-F<br>3′-AATACAGTAAGGCCGTCTAC-5′ | 5′-16 nt-Overhanged-20 bp |
| BS4 | 4nt / 18b 18bp 3′ | 5′-CCATGCAGCTGTCAGTCCATTGTCATGCTAGGCCTACTGC-3′-F<br>3′-GGTACGTCGACAGTCAGGATTGAGTACGATCCGGATGACG-5′ | Bubble-4 nt |
| BS12 | 12nt / 5′ 14bp 14bp 3′ | 5′-CCATGCAGCTGTCAGTCCATTGTCATGCTAGGCCTACTGC-3′-F<br>3′-GGTACGTCGACAGTGTCCATTGTCATCGATCCGGATGACG-5′ | Bubble-12 nt |
| BS14 | 14nt / 5′ 13bp 13bp 3′ | 5′-CCATGCAGCTGTCAGTCCATTGTCATGCTAGGCCTACTGC-3′-F<br>3′-GGTACGTCGACAGAGTCCATTGTCATGGATCCGGATGACG-5′ | Bubble-14 nt |
| BS15 | 15nt / 5′ 13bp 12bp 3′ | 5′-CCATGCAGCTGTCAGTCCATTGTCATGCTAGGCCTACTGC-3′-F<br>3′-GGTACGTCGACAGAGTCCATTGTCATGCATCCGGATGACG-5′ | Bubble-15 nt |
| BS16 | 16nt / 5′ 12bp 12bp 3′ | 5′-CCATGCAGCTGTCAGTCCATTGTCATGCTAGGCCTACTGC-3′-F<br>3′-GGTACGTCGACACAGTCCATTGTCATGC ATCCGGATGACG-5′ | Bubble-16 nt |

indirectly reflect the combined state of the DNA substrate and protein. The fluorescently labeled DNA substrate was complexed with varying amounts of protein in binding buffer [CoV-2 N: 50 mM Tris–HCl and 300 mM NaCl (pH 7.0); Nsp13: 50 mM Tris–HCl and 20 mM NaCl (pH 7.0)]. Each sample was allowed to equilibrate in solution for 5 min, following which steady-state fluorescence anisotropy was measured. A second reading was taken after 10 min to ensure that the mixture was well equilibrated and stable. As detected using the SpectraMax iD3 microplate reader (Molecular Devices, LLC, United States), the rotation decreases as its anisotropy increases. The equilibrium dissociation constant was determined by fitting the binding curves using Equation 1:

$$\Delta r = \Delta r_{max} \times P \div \left(k_d + P\right) \qquad (1)$$

where $\Delta r_{max}$ is the maximal amplitude of anisotropy ($=r_{max}$, RNA/DNA–protein complex$-r_{free}$ RNA/DNA), $P$ is protein concentration, and $K_d$ represents the equilibrium dissociation constant, which is the corresponding protein concentration when it reaches half of the maximum anisotropy in the fitted curve.
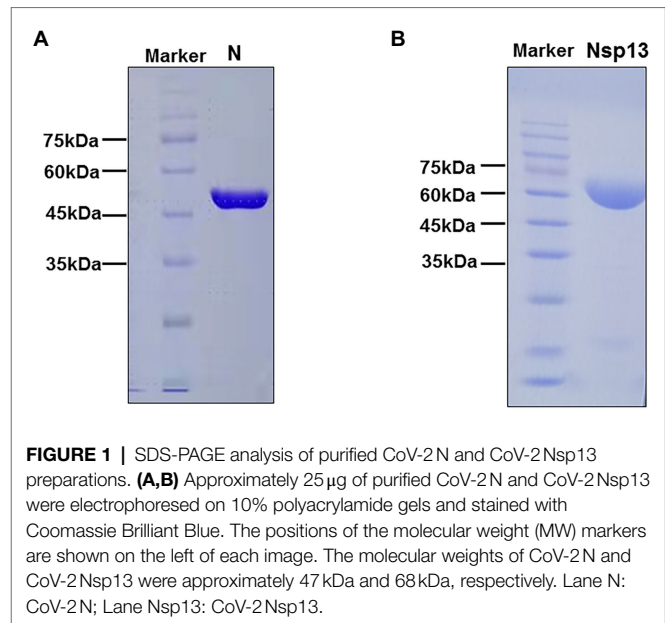
## RESULTS

## Expression and Purification of CoV-2 N and CoV-2 Nsp13

To analyze the biochemical characteristics of recombinant CoV-2 N and CoV-2 Nsp13, we first constructed and purified them. SDS-PAGE revealed that the molecular weights of CoV-2 N and CoV-2 Nsp13 were 47 kDa and 68 kDa, respectively, which are consistent with the theoretical molecular weights (**Figures 1A,B**).

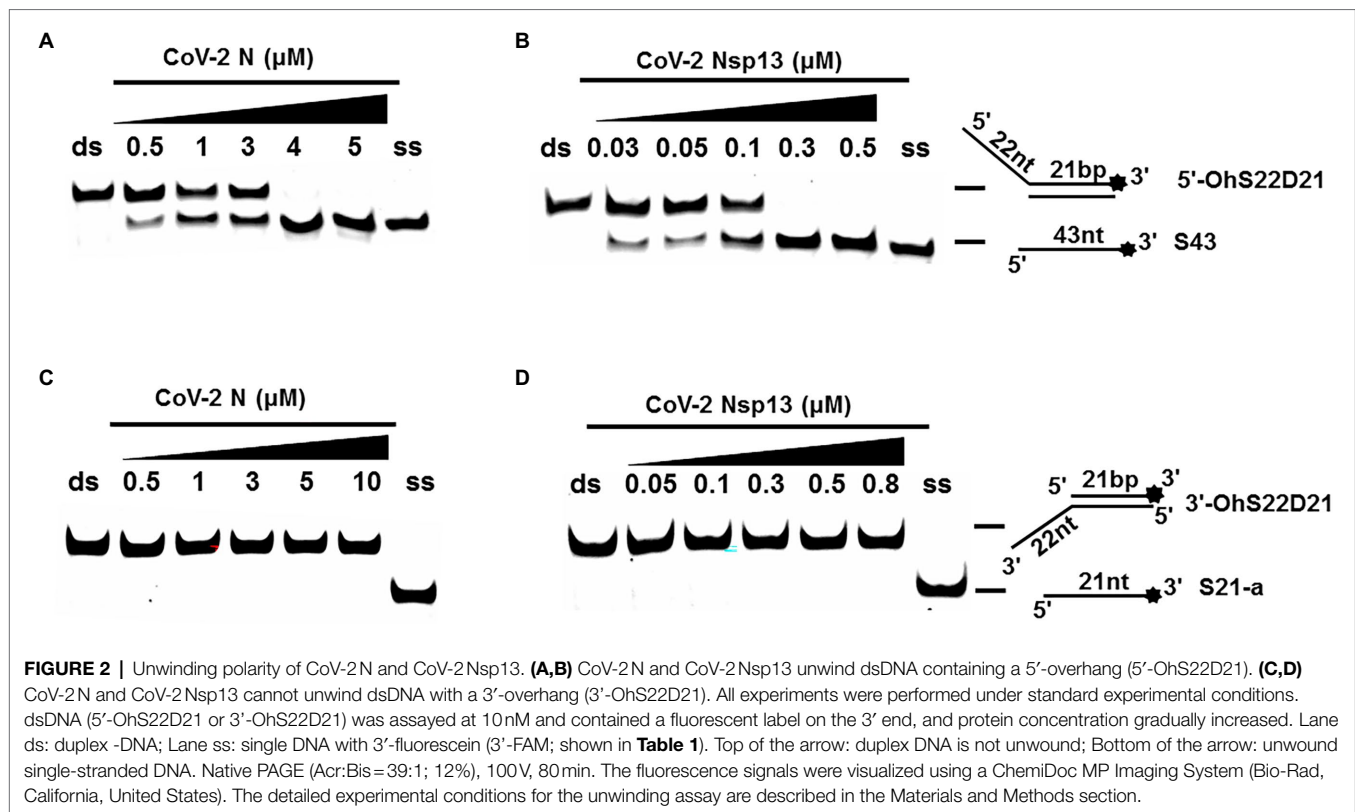## CoV-2 N Unwinding Has a Polarity of 5′–3′

One of the important characteristics of dsDNA unwinding is the unwinding polarity, which is defined by the backbone polarity of the flanking ssDNA that promotes the initiation of unwinding and defines, in turn, the direction of helicase movement along the strand. To determine and compare the polarity of CoV-2 N and CoV-2 Nsp13, partial dsDNA substrates with either a 5′ or 3′ single-stranded overhang were used (5'-Oh S22D21 and 3'-OhS22D21, respectively, **Table 1**). The results clearly showed that CoV-2 N and CoV-2 Nsp13 had similar unwinding polarities. They unwound the 5′ single-stranded overhang–containing substrate only (**Figures 2A,B**) and not the 3′ single-stranded overhang–containing substrate (**Figures 2C,D**).

Complete unwinding of the dsDNA required 5 μM CoV-2 N but only 0.3 μM CoV-2 Nsp13 (**Figures 2A,B**). Thus, the unwinding activity of CoV-2 N was more than 22 times weaker than that of CoV-2 Nsp13 (**Supplementary Figures 3A–C**). We also compared the Km value of the unwinding reaction, which is one of the most important parameters for evaluating the activity of helicases (**Supplementary Figure 3D**).



**FIGURE 1 |** SDS-PAGE analysis of purified CoV-2 N and CoV-2 Nsp13 preparations. **(A,B)** Approximately 25 μg of purified CoV-2 N and CoV-2 Nsp13 were electrophoresed on 10% polyacrylamide gels and stained with Coomassie Brilliant Blue. The positions of the molecular weight (MW) markers are shown on the left of each image. The molecular weights of CoV-2 N and CoV-2 Nsp13 were approximately 47 kDa and 68 kDa, respectively. Lane N: CoV-2 N; Lane Nsp13: CoV-2 Nsp13.

## CoV-2 N Is Not a Helicase

Using an *in vitro* gel assay system, the unwinding activity of recombinant CoV-2 N and CoV-2 Nsp13 was examined. To determine and compare the conditions for optimal nucleotide unwinding activity, we evaluated different concentrations of protein, NaCl, DTT, and divalent cations ($Mg^{2+}$), and compared the unwinding temperature and time using a substrate containing a 5′ single-stranded overhang (5′-OhS22D21, **Table 1**). A typical helicase usually binds more efficiently to nucleic acid substrates at low salt concentrations, which also promote the activity of the helicase. CoV-2 N showed a better ratio of unwinding at 100–300 mM NaCl, whereas CoV-2 Nsp13 exhibited a stronger unwinding ability as NaCl concentration decreased, causing complete unwinding at 50 mM NaCl (**Figures 3A,B**). Helicases are motor proteins that hydrolyze ATP for energy in a process that requires divalent metal ions, such as $Mg^{2+}$. We adjusted the protein concentration to 3 μM, and the ratio of unwinding at this concentration in the reaction without $Mg^{2+}$ was approximately 50% (**Figure 3C**). The addition of $Mg^{2+}$ did not considerably inhibit or promote the unwinding activity of CoV-2 N, and the unwinding ratio was similar to that in the reaction without $Mg^{2+}$, indicating that CoV-2 N does not require $Mg^{2+}$ to unwind dsDNA (**Figure 3C**). However, CoV-2 Nsp13 showed a strong dependence on $Mg^{2+}$ for dsDNA unwinding (**Figure 3D**). Notably, the unwinding activity of CoV-2 N was independent of DTT as the addition of DTT to the reaction mixture had no obvious effects on unwinding (**Figure 3E**). However, CoV-2 Nsp13 showed dependence on DTT, exhibiting an optimum response at 1–3 mM DTT (**Figure 3F**). Temperature is also a crucial factor that affects unwinding activity. Assays for *in vitro* helicase activity are usually performed at 4–30°C. The dsDNA was completely unwound by CoV-2 N when the reaction was performed at 25°C–30°C (**Figure 3G**), whereas it was unwound by CoV-2 Nsp13 only at 30°C (**Figure 3H**). Finally, we analyzed the time required for CoV-2 N and CoV-2 Nsp13 to completely unwind the dsDNA (5′-OhS22D21). Similar to the

**FIGURE 2 |** Unwinding polarity of CoV-2 N and CoV-2 Nsp13. **(A,B)** CoV-2 N and CoV-2 Nsp13 unwind dsDNA containing a 5′-overhang (5′-OhS22D21). **(C,D)** CoV-2 N and CoV-2 Nsp13 cannot unwind dsDNA with a 3′-overhang (3′-OhS22D21). All experiments were performed under standard experimental conditions. dsDNA (5′-OhS22D21 or 3′-OhS22D21) was assayed at 10 nM and contained a fluorescent label on the 3′ end, and protein concentration gradually increased. Lane ds: duplex -DNA; Lane ss: single DNA with 3′-fluorescein (3′-FAM; shown in **Table 1**). Top of the arrow: duplex DNA is not unwound; Bottom of the arrow: unwound single-stranded DNA. Native PAGE (Acr:Bis = 39:1; 12%), 100 V, 80 min. The fluorescence signals were visualized using a ChemiDoc MP Imaging System (Bio-Rad, California, United States). The detailed experimental conditions for the unwinding assay are described in the Materials and Methods section.

temperature experiment, the whole reaction process was performed at low temperature. The samples were removed at the corresponding reaction times (**Figures 3I,J**), and stop buffer was added immediately. The results indicated that the unwinding rate of the two was similar. After 5 min of initiating the reaction, CoV-2 N and CoV-2 Nsp13 had almost completely unwound the dsDNA (**Figures 3I,J**).

## CoV-2 N Unwinding Activity Does Not Depend on Nucleoside Triphosphates

A typical helicase usually not only relies on ATP but also utilizes other nucleoside triphosphates (NTPs), such as cytidine triphosphate (CTP), guanine triphosphate (GTP), and uridine triphosphate (UTP). To determine the effect of NTPs on the unwinding activity of CoV-2 N, we set the final concentration of the reaction of CoV-2 N to 3 μM in the reaction. At this concentration, dsDNA was unwound to approximately 50% in the absence of NTPs (**Figure 2A**).

The results showed that CoV-2 N could still unwind the dsDNA (5′-Oh S22D21) in reaction buffer A, which did not contain NTP, and a gradual increase in NTP concentration had no obvious effect on the promotion or inhibition of unwinding (**Figure 4A**). The opening of double-stranded nucleic acids by CoV-2 N does not appear to be dependent on the energy provided by ATP hydrolysis. It is more likely that CoV-2 N binds to the transiently opened single-stranded nucleic acid (similar to SSB and RPA) to prevent complementary base repairing.

Unlike CoV-2 N, CoV-2 Nsp13 is a typical helicase, and ATP usually participates in the unwinding process. Therefore, we set the final concentration of CoV-2 Nsp13 to 0.3 μM, which was sufficient to fully unwind the double-strand nucleic acid present in the reaction mixture at saturation concentration. The results indicated that although CoV-2 Nsp13 could still partially unwind dsDNA in reaction buffer B, we observed that in samples containing ATP and GTP, the unwinding ratio increased with increasing concentrations of ATP and GTP (**Figure 4B**). We compared the unwinding ratios of NTPs at 10 μM and 50 μM, respectively, to demonstrate the ability of CoV-2 Nsp13 (0.3 μM) to utilize the four NTPs (**Supplementary Figure 4**).

## Unwinding Activity of CoV-2 N and CoV-2 Nsp13

To determine the physiological functions of CoV-2 N and CoV-2 Nsp13 during viral replication, various nucleotides (D32, OhS4D20, OhS12D20, OhS14D20, OhS15D20 and OhS16D20 in **Table 1**) were fluorescently labeled to determine the unwinding activity of the two proteins in an *in vitro* gel assay. Neither CoV-2 N nor CoV-2 Nsp13 could unwind blunt dsDNA (**Figures 5A,B**). This suggests that CoV-2 N and CoV-2 Nsp13 require a 5′-ss tail to effectively unwind dsDNA.

Examining the effect of single-stranded overhang length on the unwinding abilities of CoV-2 N and CoV-2 Nsp13 indicated that the overhang length of the dsDNA substrate should be at least 16 nucleotides for CoV-2 N to unwind it (**Figure 5C**). However, CoV-2 Nsp13 was able to unwind
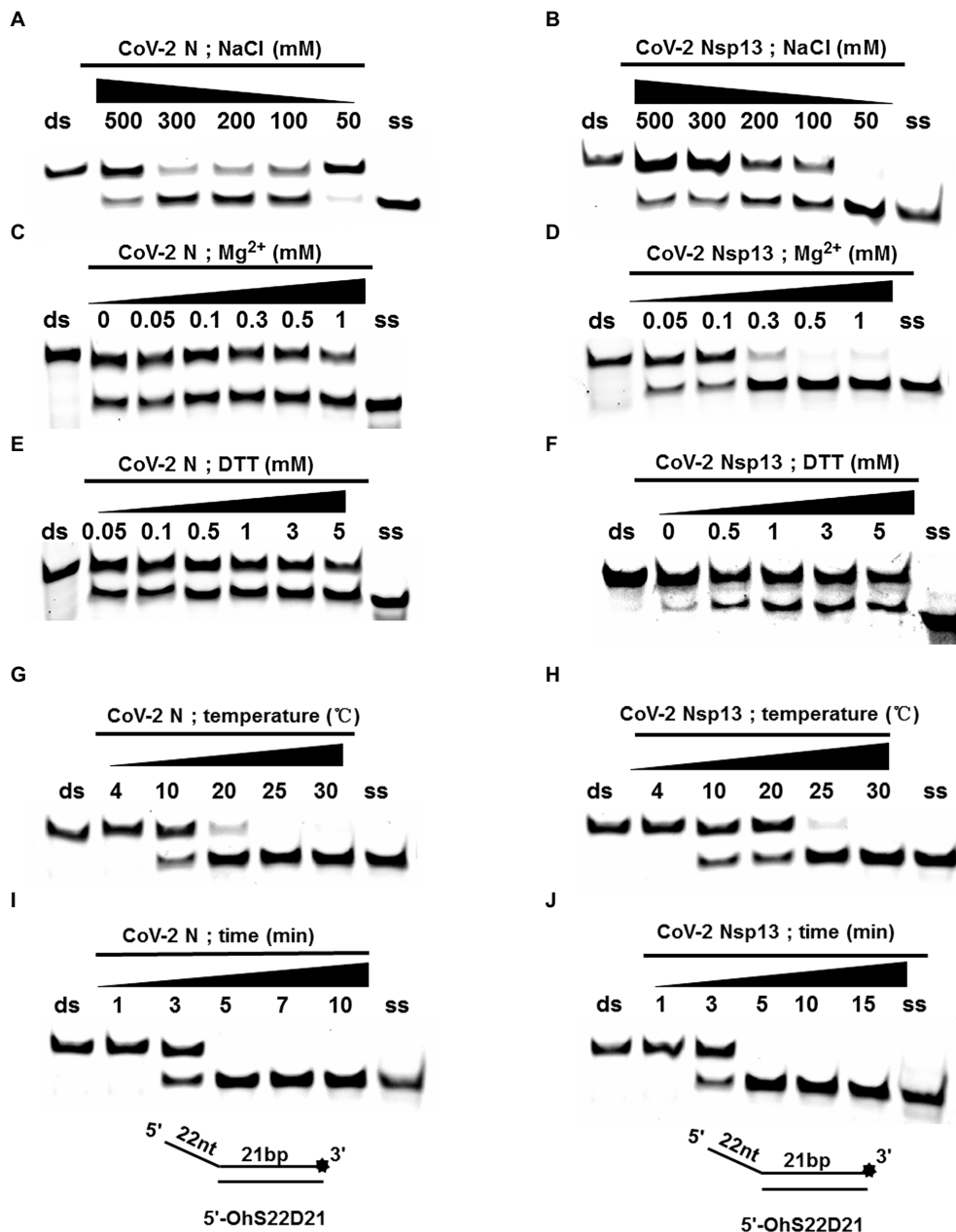
**FIGURE 3 |** Determination and comparison of optimal buffer compositions for CoV-2 N and CoV-2 Nsp13 unwinding. **(A–F)** Protein concentrations of CoV-2 N and CoV-2 Nsp13 were 3 μM (note: the protein concentration is 5 μM in **A**) and 0.3 μM (note: the protein concentration is 0.1 μM in **F**), respectively, and the reactions were performed in buffer A and buffer B (removing the single-factor NaCl, $Mg^{2+}$, DTT shown in **A–F**). **(G–J)** The protein concentrations of CoV-2 N and CoV-2 Nsp13 were saturating concentrations of 5 μM and 0.3 μM, respectively. All solutions used were kept on ice for precooling. Samples were placed on ice before reactions were initiated. A water bath of the corresponding temperature was used immediately after reactions were started, and stop buffer was added at appropriate times to terminate reactions. All used substrates were 5′-overhang DNA (5'-OhS22D21) at 10 nM.

substrates with overhangs of ≤16 nucleotides in length, with the efficacy increasing with increasing overhang length increased; however, no obvious difference was observed when the overhang length exceeded 14 nucleotides (**Figure 5D** and **Supplementary Figure 5**).

When different concentrations of CoV-2 N and CoV-2 Nsp13 were incubated with dsDNA containing various bubble structures (BS4, BS12, BS14, BS15, and BS16), CoV-2 N could

not alter the structure of the dsDNA (**Figure 6A**); however, CoV-2 Nsp13 was able to unwind it. When the bubble spanned 12 nucleotides, the unwinding ratio improved with the length of the single-stranded (**Figure 6B** and **Supplementary Figure 6**). The dsDNA containing bubble structures is similar to a two-linked, forked substrates. Each fork structure contains a 3′ single-stranded tail. Therefore, CoV-2 Nsp13 was able to unwind both strands, which did not involve polarity.
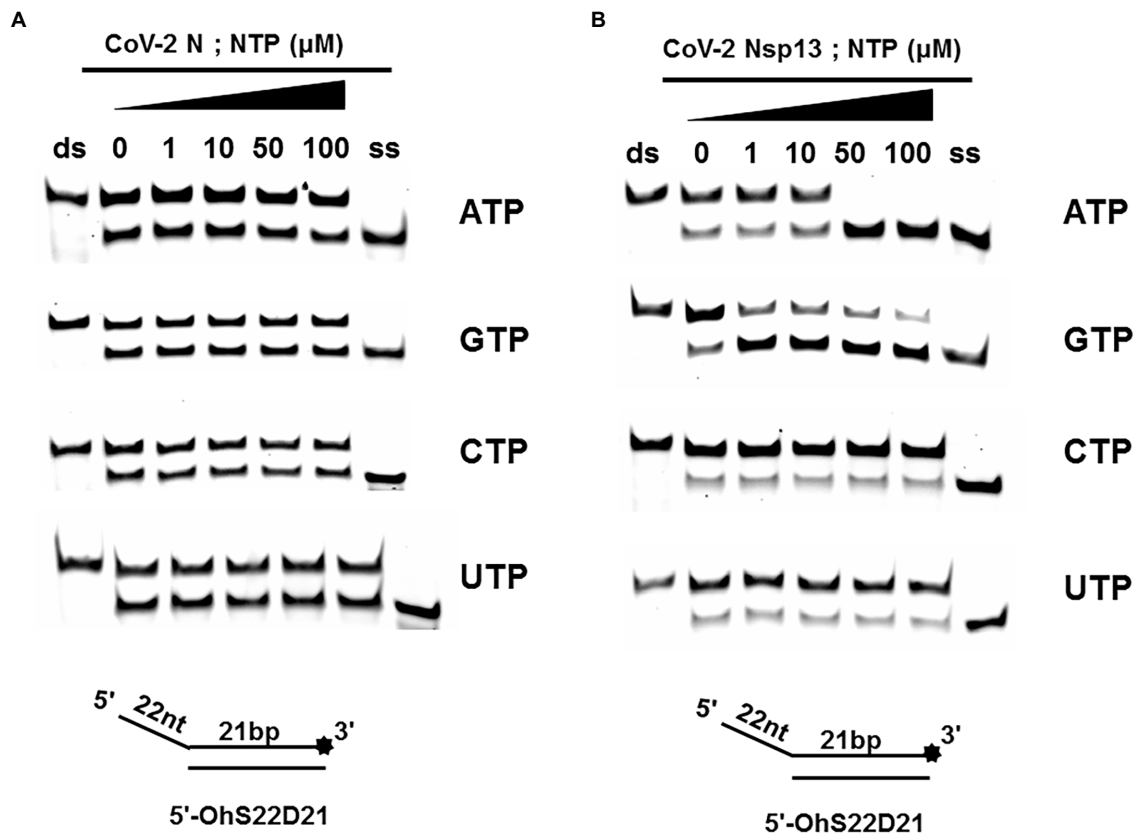
**FIGURE 4 |** Unwinding activities of CoV-2 N and CoV-2 Nsp13 in the presence of different nucleoside triphosphates at different concentrations. **(A,B)** The 5′-overhang DNA substrate at 10 nM (5′-OhS22D21). CoV-2 N concentration was 3 μM in buffer A and CoV-2 Nsp13 was 0.3 μM in buffer B, respectively. For a clearer analysis of the propensity of CoV-2 Nsp13 to NTP species, we performed comparisons by scanning gray values using Image Lab software (**Supplementary Figure 4**). All experiments were performed under experimental conditions described in "Materials and Methods."
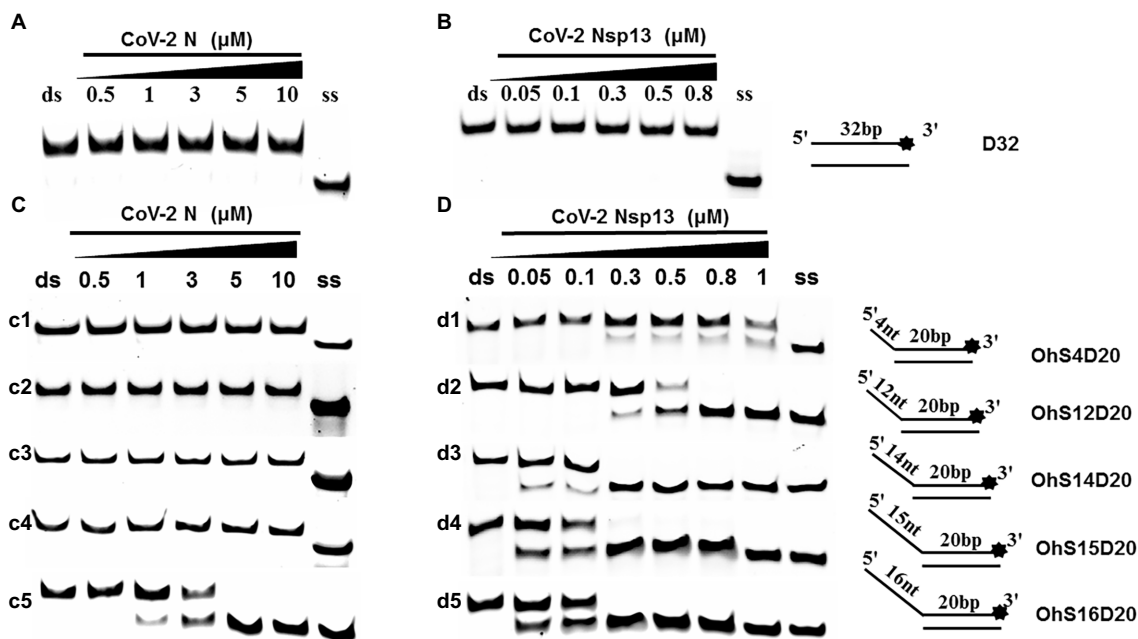
## Annealing Activity of CoV-2 N and CoV-2 Nsp13

Both CoV-2 N and CoV-2 Nsp13 exhibit strong binding activity to ssDNA, and this activity can often promote the annealing of two complementary ssDNA molecules (**Figures 7A,B**). The substrates used in **Figures 2A,B** were dsDNA molecules, which had been successfully annealed before the reaction, and the unwinding process was observed. To gain insights on the annealing properties of CoV-2 N and CoV-2 Nsp13, the nucleic acid substrates used in **Figures 7C,D** were two partially complementary paired ssDNAs (S43 and S21) that did not exhibit annealing. The experiments were performed in buffer A and buffer B using an *in vitro* gel assay system. Typical helicase-dependent unwinding requires ATP hydrolysis, whereas DNA annealing usually does not require ATP. This is one of the reasons why no ATP was included in the reaction. Another important factor is that annealing and unwinding are performed simultaneously after the addition of ATP; thus, the annealing activity cannot be observed. Gradually increasing concentrations of CoV-2 N and CoV-2 Nsp13 were added in the reaction solution containing two partially complementary ssDNAs (S43 and S21). The

optimal annealing concentration of CoV-2 Nsp13 was markedly different from that of CoV-2 N (**Figures 7C,D**). The annealing ratio of CoV-2 N at the optimum concentration reached 59.4%, whereas that of CoV-2 Nsp13 was only 6.5%. The annealing activity of CoV-2 N was almost 10 times that of CoV-2 Nsp13 (**Supplementary Figure 7**). Our results demonstrated that CoV-2 N does not need to hydrolyze ATP during dsDNA unwinding. Thus, CoV-2 N exhibits the two opposite activities of unwinding and annealing at different concentrations in the same reaction buffer. However, considering that the concentration of CoV-2 N required for annealing is much lower than that required for unwinding, the main function of CoV-2 N is likely annealing.
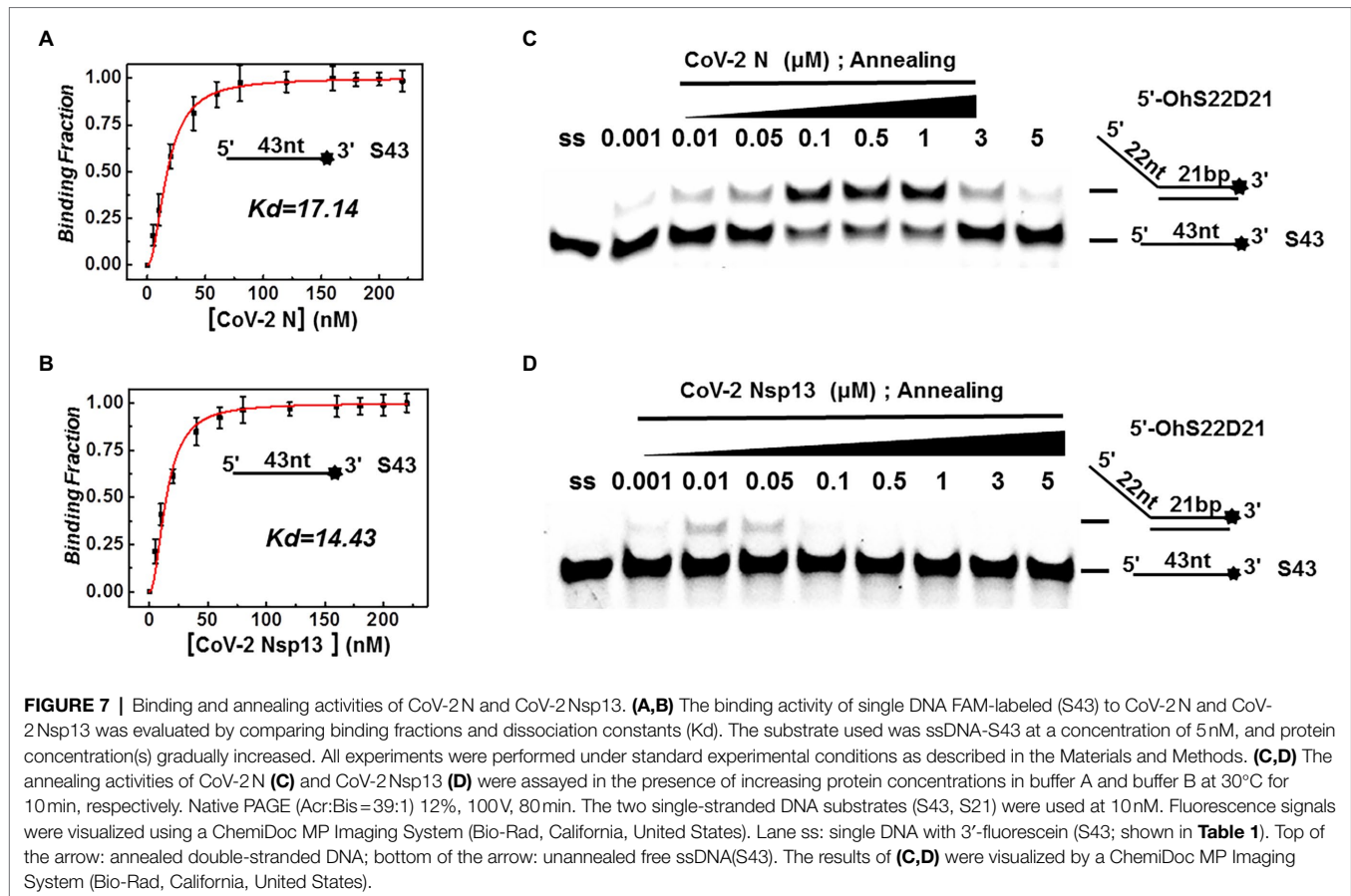
## DISCUSSION

CoV-2 N is the only protein that binds to genomic RNA in the nucleocapsid. It is closely related to gene replication and cell signaling pathway regulation. The N protein is one of the most conserved proteins of coronaviruses (Zhou et al., 2020; Thye et al., 2021). CoV-2 Nsp13 significantly contributes to viral

**FIGURE 5 |** Comparison of the effect of single-strand overhang length on the unwinding ability of CoV-2 N and CoV-2 Nsp13. **(A,B)** Blunt-end dsDNA substrate (DS32). **(C,D)** Comparison of the effect of single-strand overhang length (4 nt–16 nt) on the unwinding activities of CoV-2 N and CoV-2 Nsp13. (c1, d1) 5'-OhS4D20; (c2, d2) 5'-OhS12D20; (c3, d3) 5'-OhS14D20; (c4, d4) 5'-OhS15D20; (c5, d5) 5'-OhS16D20. The unwinding activities of CoV-2 N and CoV-2 Nsp13 were assayed in the presence of increasing protein concentrations in buffer A and buffer B, respectively. All 5'-overhang dsDNA substrates used at 10 nM.
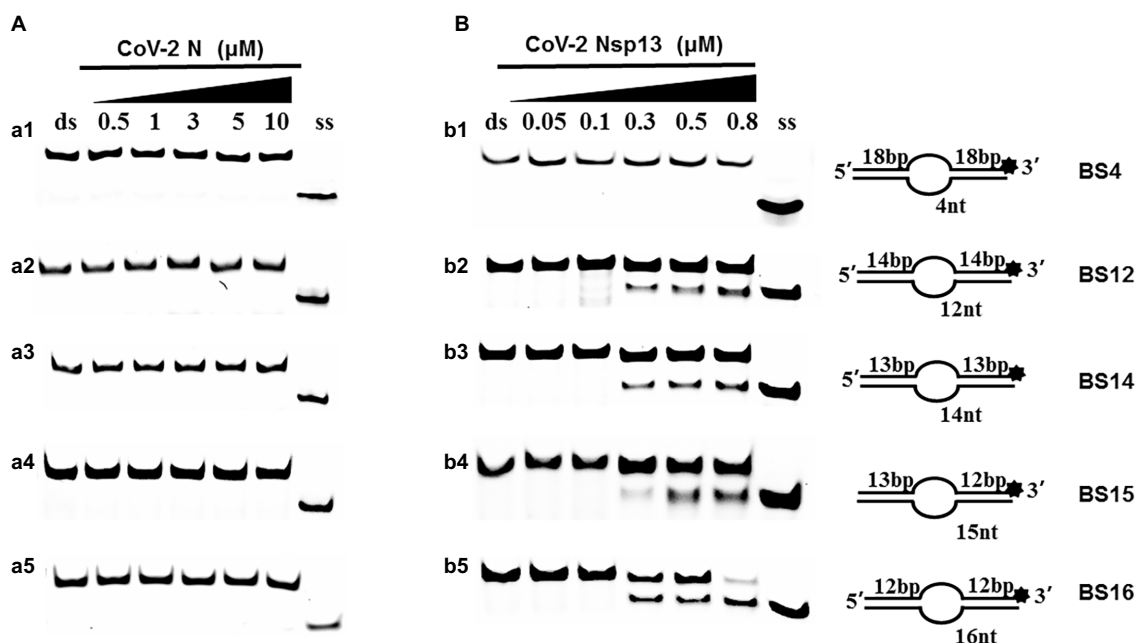


**FIGURE 6 |** Comparison of the effect of the dsDNA bubble structure on the unwinding ability of CoV-2 N and CoV-2 Nsp13. (a1, b1) BS4; (a2, b2) BS12; (a3, b3) BS14; (a4, b4) BS15; and (a5, b5) BS16. All experiments were performed using a series of dsDNA bubble substrates (shown in **Table 1**), The unwinding activities of CoV-2 N and CoV-2 Nsp13 were assayed in the presence of increasing protein concentrations in buffer A and buffer B, respectively. All the bubble dsDNA substrates fixed at 10 nM. All experiments were performed under standard experimental conditions as described in "Materials and Methods." **(A,B)** Comparison of dsDNA bubble structure (4 nt -16 nt) on the unwinding activities of CoV-2 N and CoV-2 Nsp13.

**FIGURE 7 |** Binding and annealing activities of CoV-2 N and CoV-2 Nsp13. **(A,B)** The binding activity of single DNA FAM-labeled (S43) to CoV-2 N and CoV-2 Nsp13 was evaluated by comparing binding fractions and dissociation constants (Kd). The substrate used was ssDNA-S43 at a concentration of 5 nM, and protein concentration(s) gradually increased. All experiments were performed under standard experimental conditions as described in the Materials and Methods. **(C,D)** The annealing activities of CoV-2 N **(C)** and CoV-2 Nsp13 **(D)** were assayed in the presence of increasing protein concentrations in buffer A and buffer B at 30°C for 10 min, respectively. Native PAGE (Acr:Bis = 39:1) 12%, 100 V, 80 min. The two single-stranded DNA substrates (S43, S21) were used at 10 nM. Fluorescence signals were visualized using a ChemiDoc MP Imaging System (Bio-Rad, California, United States). Lane ss: single DNA with 3'-fluorescein (S43; shown in **Table 1**). Top of the arrow: annealed double-stranded DNA; bottom of the arrow: unannealed free ssDNA(S43). The results of **(C,D)** were visualized by a ChemiDoc MP Imaging System (Bio-Rad, California, United States).

replication and exhibits the highest sequence conservation among coronaviruses, highlighting its importance in viral viability (Adedeji et al., 2012; Yu et al., 2012). This enzyme represents a promising target for the development of drugs against coronaviruses (Adedeji and Sarafianos, 2014). Therefore, it is necessary to systematically analyze the biochemical characteristics of CoV-2 N and CoV-2 Nsp13 *in vitro*. Based on the published sequences, we successfully expressed and purified two proteins, corroborating the findings of previous reports (Zeng et al., 2020; Newman et al., 2021).

The results of this and previous studies indicate that CoV-2 Nsp13 exhibits unwinding activity (Mickolajczyk et al., 2021). However, no specific reports indicate that CoV-2 N or other coronavirus nucleocapsid proteins exhibit unwinding activity. The two proteins exhibited little similarity in their primary sequences. CoV-2 Nsp13 contains structurally conserved domains of typical helicases, such as ATP-binding and ATP-hydrolysis sites, whereas CoV-2 N does not contain any domain with predicted unwinding function (**Supplementary Figures 1** and **2**). This suggests that the N protein, which resembles a single-strand binding protein, opens duplexes via a mechanism that is different to typical helicases (**Figure 8**; McBride et al., 2014; Kang et al., 2020; Zeng et al., 2020).

An *in vitro* gel assay system was established for the first time to determine the effect of the unwinding activity of CoV-2 N *in vitro*. Unlike CoV-2 Nsp13, we found that CoV-2 N

was not a helicase. CoV-2 N does not require $Mg^{2+}$, DTT, or NTP to unwind dsDNA. CoV-2 N unwound dsDNA in the presence of 100–300 mM NaCl. Conversely, CoV-2 Nsp13 exhibited superior unwinding activity at low NaCl concentrations. Our binding experiments revealed that concentrations of NaCl of >400 mM inhibited CoV-2 N binding to ssDNA (the result is not show). This may explain why the unwinding ability of CoV-2 N becomes weaker at high salt concentrations (**Figure 3A**). Low salt concentration is known to affect the binding of N protein to ssDNA, possibly due to charge effects. It is worth noting that the unwinding activity of CoV-2 N protein does not require ATP and $Mg^{2+}$, two essential cofactors for helicases. Therefore, the unwinding properties of CoV-2 N are probably similar to those of RPA owing to its helix-destabilizing activity, rather than helicase activity. However, CoV-2 N does not unwind dsDNA in the same way as typical SSB proteins, which require a specific temperature (Wang et al., 2004; Safa et al., 2016). Our results indicated that CoV-2 N completely unwound dsDNA at 25°C and 30°C. RPA is extremely heat-labile and very sensitive to freezing and thawing. Compared with CoV-2 N and CoV-2 Nsp13, the effect of temperature and time was somewhat consistent. Both proteins can unwind dsDNA, but they require very different unwinding environments. CoV-2 Nsp13, the only protein with an unwinding domain in the SARS-CoV-2 genome, is very important for viral replication and recombination. The
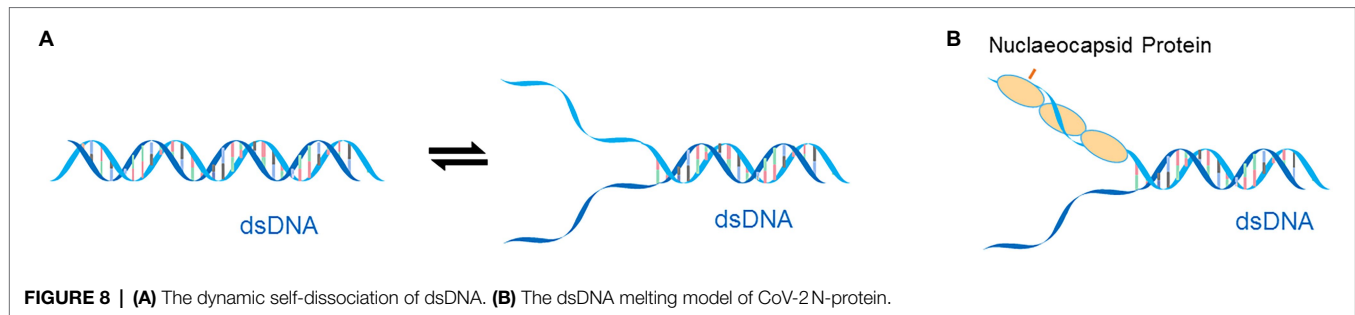
**FIGURE 8 |** **(A)** The dynamic self-dissociation of dsDNA. **(B)** The dsDNA melting model of CoV-2 N-protein.

properties of DNA and RNA are similar, and CoV-2 N may also act on viral RNA in a similar manner. CoV-2 N is more likely a supplement for CoV-2 Nsp13 under the conditions of stress, such as a lack of ATP. However, the mode of their action is very different, and it is possible that the two function independently at different stages of viral replication.

Our findings demonstrated that the concentration of N protein required for dsDNA unwinding was much higher (4 μM) than that of Nsp13 (0.3 μM) (**Figures 2A,B**). This is clearly applicable for CoV-2 N, which is a multifunctional protein and not a typical helicase, and may mean that multifunctional proteins should be present at higher concentrations in vivo to perform this function. For example, telomerase, which is essentially a polymerase but not a typical polymerase, is irreplaceable in all organisms. Compared with typical reverse transcriptases and polymerases, the polymerization activity of telomerase is only 1/10,000. In addition, nucleocapsid protein is the most abundant viral protein, with concentrations of up to $10^8$ molecules in an infected cell (Tugaeva et al., 2021). Considering that the volume of human lung cells is approximately $170\,\mu m^3$, the concentration of nucleocapsid protein can reach nearly 1 mM, which is much higher than the concentrations used in our unwinding experiments.

Although CoV-2 N and CoV-2 Nsp13 exhibit the same unwinding polarity, they show differences in unwinding substrates. The present study demonstrates that CoV-2 N has strict requirements for tail-chain length, only unwinding substrates with a 5′ overhang of 16 nucleotides. This suggests that similar to RPA, the unwinding activity of CoV-2 N depends on ssDNA length. CoV-2 Nsp13 showed properties similar to typical helicases—its unwinding activity was exhibited only when the single-stranded bubble structure was at least 12 nucleotides in length and activity increased with increased tail length (**Figure 6B**). However, CoV-2 N could not open substrates with bubble structures of any length (**Figure 6A**).

Our findings of the difference in CoV-2 N and CoV-2 Nsp13 annealing activities at equivalent and increasing concentrations indicate that the annealing activity of CoV-2 N is active at low concentrations, whereas the unwinding activity predominates at high concentrations. This may be because high amounts of CoV-2 N can saturate ssDNA and eliminate the secondary structure, so that the ssDNA is in a simple state that is conducive

to binding by other proteins. The proteins bound to the nucleic acid protect the ssDNA. It is also possible that CoV-2 N regulates the transition between annealing and unwinding based on its concentration. Thus, annealing is likely to be the primary function of CoV-2 N.

The role of the unwinding function of CoV-2 N in viruses and host cells remains unclear, and further studies are needed. A reasonable hypothesis regarding its function may relate to the different subcellular localization of the N protein in host cells. The N protein of coronavirus may be localized in the cytoplasm and nucleus of host cells (Rowland et al., 1999; Hiscox et al., 2001; Wurm et al., 2001; Timani et al., 2005). In the cytoplasm, this protein participates in viral genome replication, transcription, and packaging through its RNA-binding and -annealing activities (McBride et al., 2014). In the nucleus, this protein delays the cell cycle in the G2/M phase by relocalizing into the nucleus through its nuclear localization sequence (Wurm et al., 2001). Early studies on SARS-CoV N protein showed the protein also exhibits high nucleolar localization in the G2/M phase in SARS-CoV–infected cells (Cawood et al., 2007). In contrast, recent studies on SARS-CoV-2 transfection revealed that the N protein was also apparent in the G1/S phase of the cell cycle (Gao et al., 2021). The S phase of the cell cycle represents the DNA replication phase. Thus, the ssDNA binding activity and dsDNA unwinding activity of the SARS-CoV-2 N protein observed in this study indicate that this protein binds to the host's genomic ssDNA during replication and affects host cell replication. This creates favorable conditions for the packaging of SARS-CoV-2.

## DATA AVAILABILITY STATEMENT

The original contributions presented in the study are included in the article/**Supplementary Material**; further inquiries can be directed to the corresponding authors.

## AUTHOR CONTRIBUTIONS

BZ and YL are responsible for the experiments design. BZ, YX, and ZL performed experiments. BZ, DL, and QZ compiled figures. BZ, KL, and YL wrote and edited the manuscript. BZ, YX, ZL, DL, JT, QZ, HT, JY,

XZ, SQ, and YL analyzed and interpreted the data. All authors contributed to the article and approved the submitted version.

## SUPPLEMENTARY MATERIAL

The Supplementary Material for this article can be found online at: https://www.frontiersin.org/articles/10.3389/fmicb.2022.851202/full#supplementary-material

## REFERENCES

Aboagye, J. O., Yew, C. W., Ng, O. -W., Monteil, V. M., Mirazimi, A., and Tan, Y. -J. (2018). Overexpression of the nucleocapsid protein of Middle East respiratory syndrome coronavirus up-regulates CXCL10. *Biosci. Rep.* 38:1059. doi: 10.1042/BSR20181059

Adedeji, A. O., and Sarafianos, S. G. (2014). Antiviral drugs specific for coronaviruses in preclinical development. *Curr. Opin. Virol.* 8, 45–53. doi: 10.1016/j.coviro.2014.06.002

Adedeji, A. O., Singh, K., Calcaterra, N. E., DeDiego, M. L., Enjuanes, L., Weiss, S., et al. (2012). Severe acute respiratory syndrome coronavirus replication inhibitor that interferes with the nucleic acid unwinding of the viral helicase. *Antimicrob. Agents Chemother.* 56, 4718–4728. doi: 10.1128/AAC.00957-12

Carlson, C. R., Asfaha, J. B., Ghent, C. M., Howard, C. J., Hartooni, N., Safari, M., et al. (2020). Phosphoregulation of phase separation by the SARS-CoV-2 N protein suggests a biophysical basis for its dual functions. *Mol. Cell* 80, 1092–1103. doi: 10.1016/j.molcel.2020.11.025

Cawood, R., Harrison, S. M., Dove, B. K., Reed, M. L., and Hiscox, J. A. (2007). Cell cycle dependent nucleolar localization of the coronavirus nucleocapsid protein. *Cell Cycle* 6, 863–867. doi: 10.4161/cc.6.7.4032

Fan, J. -H., Bochkareva, E., Bochkarev, A., and Gray, D. M. (2009). Circular dichroism spectra and electrophoretic mobility shift assays show that human replication protein A binds and melts intramolecular G-quadruplex structures. *Biochemistry* 48, 1099–1111. doi: 10.1021/bi801538h

Gao, T., Gao, Y., Liu, X., Nie, Z., Sun, H., Lin, K., et al. (2021). Identification and functional analysis of the SARS-COV-2 nucleocapsid protein. *BMC Microbiol.* 21, 1–10. doi: 10.1186/s12866-021-02107-3

Gien, H., Morse, M., McCauley, M. J., Kitzrow, J. P., Musier-Forsyth, K., Gorelick, R. J., et al. (2022). HIV-1 Nucleocapsid protein binds double-stranded DNA in multiple modes to regulate compaction and capsid Uncoating. *Viruses* 14:235. doi: 10.3390/v14020235

Gurung, A. B. (2020). In silico structure modelling of SARS-CoV-2 Nsp13 helicase and Nsp14 and repurposing of FDA approved antiviral drugs as dual inhibitors. *Gene rep.* 21:100860. doi: 10.1016/j.genrep.2020.100860

Gussow, A. B., Auslander, N., Faure, G., Wolf, Y. I., Zhang, F., and Koonin, E. V. (2020). Genomic determinants of pathogenicity in SARS-CoV-2 and other human coronaviruses. *Proc. Natl. Acad. Sci.* 117, 15193–15199. doi: 10.1073/pnas.2008176117

Hiscox, J. A., Wurm, T., Wilson, L., Britton, P., Cavanagh, D., and Brooks, G. (2001). The coronavirus infectious bronchitis virus nucleoprotein localizes to the nucleolus. *J. Virol.* 75, 506–512. doi: 10.1128/JVI.75.1.506-512.2001

Jiang, F., Deng, L., Zhang, L., Cai, Y., Cheung, C. W., and Xia, Z. (2020). Review of the clinical characteristics of coronavirus disease 2019 (COVID-19). *J. Gen. Intern. Med.* 35, 1545–1549. doi: 10.1007/s11606-020-05762-w

Jing, H., Hu, J., He, B., Abril, Y. L. N., Stupinski, J., Weiser, K., et al. (2016). A SIRT2-selective inhibitor promotes c-Myc oncoprotein degradation and exhibits broad anticancer activity. *Cancer Cell* 29, 297–310. doi: 10.1016/j.ccell.2016.02.007

Kang, S., Yang, M., Hong, Z., Zhang, L., Huang, Z., Chen, X., et al. (2020). Crystal structure of SARS-CoV-2 nucleocapsid protein RNA binding domain reveals potential unique drug targeting sites. *Acta Pharm. Sin. B* 10, 1228–1238. doi: 10.1016/j.apsb.2020.04.009

Lei, X., Dong, X., Ma, R., Wang, W., Xiao, X., Tian, Z., et al. (2020). Activation and evasion of type I interferon responses by SARS-CoV-2. *Nat. Commun.* 11, 1–12. doi: 10.1038/s41467-020-17665-9

McBride, R., Van Zyl, M., and Fielding, B. C. (2014). The coronavirus nucleocapsid is a multifunctional protein. *Viruses* 6, 2991–3018. doi: 10.3390/v6082991

Mickolajczyk, K. J., Shelton, P. M., Grasso, M., Cao, X., Warrington, S. E., Aher, A., et al. (2021). Force-dependent stimulation of RNA unwinding by SARS-CoV-2 nsp13 helicase. *Biophys. J.* 120, 1020–1030. doi: 10.1016/j.bpj.2020.11.2276

Min, Y.-Q., Huang, M., Sun, X., Deng, F., Wang, H., and Ning, Y.-J. (2021). Immune evasion of SARS-CoV-2 from interferon antiviral system. *Comput. Struct. Biotechnol. J.* 19, 4217–4225. doi: 10.1016/j.csbj.2021.07.023

Mirza, M. U., and Froeyen, M. (2020). Structural elucidation of SARS-CoV-2 vital proteins: computational methods reveal potential drug candidates against main protease, Nsp12 polymerase and Nsp13 helicase. *J. pharmaceutical analys.* 10, 320–328. doi: 10.1016/j.jpha.2020.04.008

Nabeel-Shah, S., Lee, H., Ahmed, N., Burke, G. L., Farhangmehr, S., Ashraf, K., et al. (2022). SARS-CoV-2 nucleocapsid protein binds host mRNAs and attenuates stress granules to impair host stress response. *iScience* 25:103562. doi: 10.1016/j.isci.2021.103562

Newman, J. A., Douangamath, A., Yadzani, S., Yosaatmadja, Y., Aimon, A., Brandão-Neto, J., et al. (2021). Structure, mechanism and crystallographic fragment screening of the SARS-CoV-2 NSP13 helicase. *Nat. Commun.* 12, 1–11. doi: 10.1038/s41467-021-25166-6

Reynolds, D., Huesemann, M., Edmundson, S., Sims, A., Hurst, B., Cady, S., et al. (2021). Viral inhibitors derived from macroalgae, microalgae, and cyanobacteria: A review of antiviral potential throughout pathogenesis. *Algal Res.* 57:102331. doi: 10.1016/j.algal.2021.102331

Rowland, R., Kervin, R., Kuckleburg, C., Sperlich, A., and Benfield, D. A. (1999). The localization of porcine reproductive and respiratory syndrome virus nucleocapsid protein to the nucleolus of infected cells and identification of a potential nucleolar localization signal sequence. *Virus Res.* 64, 1–12. doi: 10.1016/S0168-1702(99)00048-9

Safa, L., Gueddouda, N. M., Thiébaut, F., Delagoutte, E., Petruseva, I., Lavrik, O., et al. (2016). 5′ to 3′ unfolding directionality of DNA secondary structures by replication protein A: G-quadruplexes and duplexes. *J. Biol. Chem.* 291, 21246–21256. doi: 10.1074/jbc.M115.709667

Shi, J., Zhang, J., Li, S., Sun, J., Teng, Y., Wu, M., et al. (2015). Epitope-based vaccine target screening against highly pathogenic MERS-CoV: an in silico approach applied to emerging infectious diseases. *PLoS One* 10:e0144475. doi: 10.1371/journal.pone.0144475

Singhal, T. (2020). A review of coronavirus disease-2019 (COVID-19). *The Indian J. pediatrics* 87, 281–286. doi: 10.1007/s12098-020-03263-6

Smits, V. A., Hernández-Carralero, E., Paz-Cabrera, M. C., Cabrera, E., Hernández-Reyes, Y., Hernández-Fernaud, J. R., et al. (2021). The Nucleocapsid protein triggers the main humoral immune response in COVID-19 patients. *Biochem. Biophys. Res. Commun.* 543, 45–49. doi: 10.1016/j.bbrc.2021.01.073

Tang, T. K., Wu, M. P. J., Chen, S. T., Hou, M. H., Hong, M. H., Pan, F. M., et al. (2005). Biochemical and immunological studies of nucleocapsid proteins of severe acute respiratory syndrome and 229E human coronaviruses. *Proteomics* 5, 925–937. doi: 10.1002/pmic.200401204

Thye, A. Y.-K., Law, J. W.-F., Pusparajah, P., Letchumanan, V., Chan, K.-G., and Lee, L.-H. (2021). Emerging SARS-CoV-2 variants of concern (VOCs): An impending global crisis. *Biomedicine* 9:1303. doi: 10.3390/biomedicines9101303

Timani, K. A., Liao, Q., Ye, L., Zeng, Y., Liu, J., Zheng, Y., et al. (2005). Nuclear/nucleolar localization properties of C-terminal nucleocapsid protein of SARS coronavirus. *Virus Res.* 114, 23–34. doi: 10.1016/j.virusres.2005.05.007

Tugaeva, K. V., Hawkins, D. E., Smith, J. L., Bayfield, O. W., Ker, D.-S., Sysoev, A. A., et al. (2021). The mechanism of SARS-CoV-2 nucleocapsid protein recognition by the human 14-3-3 proteins. *J. Mol. Biol.* 433:166875. doi: 10.1016/j.jmb.2021.166875

Vazquez, C., Swanson, S. E., Negatu, S. G., Dittmar, M., Miller, J., Ramage, H. R., et al. (2021). SARS-CoV-2 viral proteins NSP1 and NSP13 inhibit interferon activation through distinct mechanisms. *PLoS One* 16:e0253089. doi: 10.1371/journal.pone.0253089

Wang, X., Haber, J. E., and West, S. (2004). Role of Saccharomyces single-stranded DNA-binding protein RPA in the strand invasion step of double-strand break repair. *PLoS Biol.* 2:e21. doi: 10.1371/journal.pbio.0020021

Wu, F., Zhao, S., Yu, B., Chen, Y.-M., Wang, W., Song, Z.-G., et al. (2020). A new coronavirus associated with human respiratory disease in China. *Nature* 579, 265–269. doi: 10.1038/s41586-020-2008-3

Wurm, T., Chen, H., Hodgson, T., Britton, P., Brooks, G., and Hiscox, J. A. (2001). Localization to the nucleolus is a common feature of coronavirus nucleoproteins, and the protein may disrupt host cell division. *J. Virol.* 75, 9345–9356. doi: 10.1128/JVI.75.19.9345-9356.2001

Xia, H., Cao, Z., Xie, X., Zhang, X., Chen, J. Y.-C., Wang, H., et al. (2020). Evasion of type I interferon by SARS-CoV-2. *Cell Rep.* 33:108234. doi: 10.1016/j.celrep.2020.108234

Yang, K., Sun, K., Srinivasan, K., Salmon, J., Marques, E., Xu, J., et al. (2009). Immune responses to T-cell epitopes of SARS CoV-N protein are enhanced by N immunization with a chimera of lysosome-associated membrane protein. *Gene Ther.* 16, 1353–1362. doi: 10.1038/gt.2009.92

Yu, M.-S., Lee, J., Lee, J. M., Kim, Y., Chin, Y.-W., Jee, J.-G., et al. (2012). Identification of myricetin and scutellarein as novel chemical inhibitors of the SARS coronavirus helicase, nsP13. *Bioorg. Med. Chem. Lett.* 22, 4049–4054. doi: 10.1016/j.bmcl.2012.04.081

Zeng, W., Liu, G., Ma, H., Zhao, D., Yang, Y., Liu, M., et al. (2020). Biochemical characterization of SARS-CoV-2 nucleocapsid protein. *Biochem. Biophys. Res. Commun.* 527, 618–623. doi: 10.1016/j.bbrc.2020.04.136

Zhao, H., Wu, D., Nguyen, A., Li, Y., Adão, R. C., Valkov, E., et al. (2021). Energetic and structural features of SARS-CoV-2 N-protein co-assemblies with nucleic acids. *IScience* 24:102523. doi: 10.1016/j.isci.2021.102523

Zhou, P., Yang, X.-L., Wang, X.-G., Hu, B., Zhang, L., Zhang, W., et al. (2020). A pneumonia outbreak associated with a new coronavirus of probable bat origin. *Nature* 579, 270–273. doi: 10.1038/s41586-020-2012-7

# Advantages of publishing in Frontiers

**OPEN ACCESS**
Articles are free to read for greatest visibility and readership

**FAST PUBLICATION**
Around 90 days from submission to decision

**HIGH QUALITY PEER-REVIEW**
Rigorous, collaborative, and constructive peer-review

**TRANSPARENT PEER-REVIEW**
Editors and reviewers acknowledged by name on published articles

**Frontiers**
Avenue du Tribunal-Fédéral 34
1005 Lausanne | Switzerland

**Visit us:** www.frontiersin.org
**Contact us:** frontiersin.org/about/contact

**REPRODUCIBILITY OF RESEARCH**
Support open data and methods to enhance research reproducibility

**DIGITAL PUBLISHING**
Articles designed for optimal readership across devices

**FOLLOW US**
@frontiersin

**IMPACT METRICS**
Advanced article metrics track visibility across digital media

**EXTENSIVE PROMOTION**
Marketing and promotion of impactful research

**LOOP RESEARCH NETWORK**
Our network increases your article's readership